DOKUZ EYLÜL UNIVERSITY

GRADUATE SCHOOL OF NATURAL AND APPLIED SCIENCES

CLUSTER SHIFT KEYING: A NOVEL CHAOTIC COMMUNICATION SCHEME

by

Zekeriya Sarı

March, 2024

İZMİR

CLUSTER SHIFT KEYING: A NOVEL CHAOTIC COMMUNICATION SCHEME

A Thesis Submitted to the
Graduate School of Natural And Applied Sciences of Dokuz Eylül University
In Partial Fulfillment of the Requirements for the Degree of Doctor of Philosophy in Department of Electrical and Electronics Engineering

by

Zekeriya Sarı

March, 2024

İZMİR

Ph.D. THESIS EXAMINATION RESULT FORM

We have read the thesis entitled "**CLUSTER SHIFT KEYING: A NOVEL CHAOTIC COMMUNICATION SCHEME**" completed by **ZEKERİYA SARI** under supervision of **ASSOC. PROF. DR. SERKAN GÜNEL** and we certify that in our opinion it is fully adequate, in scope and in quality, as a thesis for the degree of Doctor of Philosophy.

.....

Assoc. Prof. Dr. Serkan GÜNEL

Supervisor

.....	.....
Prof. Dr. Mustafa Alper Selver	Prof. Dr. Cem Civelek
Thesis Committee Member	Thesis Committee Member
.....	.....
Prof. Dr. Berna Özbek	Prof. Dr. Mustafa A. Altınkaya
Examining Committee Member	Examining Committee Member

Prof. Dr. Okan FISTIKOĞLU
Director
Graduate School of Natural and Applied Sciences

ACKNOWLEDGEMENTS

I am immensely grateful for the opportunity to embark on this academic journey and successfully complete my Ph.D. thesis. It would not have been possible without the guidance, support, and encouragement of several individuals and institutions whom I would like to acknowledge with deep appreciation.

First and foremost, I owe my heartfelt gratitude to my supervisor, Assoc. Prof. Dr. Serkan Günel, for all of his support, invaluable guidance, and continuous motivation throughout this research. His expertise, insightful feedback, and dedication to excellence have shaped my work and helped me grow both as a researcher and as an individual.

I would also like to express my sincere thanks to the members of my thesis committee for their invaluable contributions and constructive feedback on this research. Their expertise and diverse perspectives have greatly enriched the quality and scope of my study.

Furthermore, I am deeply grateful to my friends and family for their continuous support, patience, and understanding throughout this demanding journey. Their constant encouragement, and belief in my abilities have been my motivation to persevere during challenging times.

Finally, this work was supported by Dokuz Eylül University Scientific Research Projects (DEU BAP) under Grant 2021.KB.FEN.007. Besides, the numerical calculations reported in this thesis were fully/partially performed at TUBITAK ULAKBIM, High Performance and Grid Computing Center (TRUBA resources). I would like to acknowledge the financial and technical support I received from the institutions that provided me with the necessary resources to conduct my research.

Completing this Ph.D. thesis has been a challenging but immensely rewarding experience, and I am indebted to all the individuals and institutions who have played a

crucial role in my academic journey. This accomplishment would not have been possible without their support and guidance.

Zekeriya SARI

CLUSTER SHIFT KEYING: A NOVEL CHAOTIC COMMUNICATION SCHEME

ABSTRACT

A network of chaotic systems can be designed in such a way that the cluster patterns formed by synchronous nodes can be controlled through the coupling parameters. This thesis presents a novel approach to exploiting such a network for covert communication, where controlled clusters encode symbols spatiotemporally. The cluster synchronization network is divided into two subnetworks: transmitter and receiver. First, a network with controlled parameters in the transmitter is designed specifically. Second, it is ensured that the nodes of the links connecting the transmitter and receiver are not in the same clusters for all the control parameters. The former condition ensures that the control parameters changed at the transmitter change the whole clustering scheme. The second condition enforces that the transmitted signals are always continuous and chaotic. Hence, the transmitted signals are not modulated by the information directly but distributed over the links connecting the subnetworks. The information cannot be deciphered by eavesdropping on the channel links without knowing the network topology. The performance has been assessed by extensive simulations of bit error rates under noisy channel conditions.

Keywords: Cluster shift keying, chaos based communications, covert communication, cluster synchronization, chaotic systems

KÜME ANAHTARLAMA: YENİ BİR KAOTİK İLETİŞİM TEKNİĞİ

ÖZ

Kaotik sistemlerden oluşan bir ağ, eşzamanlı düğüm gruplarının bağlantı parametreleri aracılığıyla kontrol edilebileceği şekilde tasarlanabilir. Bu çalışamada, kontrol edilebilen öbeklerin sembolleri uzay-zamansal olarak kodladığı böyle bir ağın örtülü haberleşme amacıyla kullanılması için yeni bir yaklaşım sunulmaktadır. Öbek eşzamanlılığı sergileyebilen ağ, verici ve alıcı olarak iki alt ağa bölünür. İlk olarak, kontrol parametreleri vericide bulunan ağın tasarımı yapılır. İkinci olarak, vericiyi ve alıcıyı birbirine bağlayan bağlantıların düğümlerinin tüm kontrol parametreleri için aynı öbeklerde olmaması sağlanır. İlk koşul, vericide değiştirilen kontrol parametrelerinin tüm öbek şemasını değiştirmesini sağlar. İkinci koşul, iletilen işaretlerin her zaman sürekli ve kaotik olmasını sağlar. Dolayısıyla, iletilen işaretler doğrudan bilgi tarafından kiplenmez, alt ağları birbirine bağlayan bağlantılar üzerinden dağıtılır. Ağ topolojisi bilinmeden kanal bağlantılarının dinlenilmesi ile bilgilerin deşifre edilmesi mümkün değildir. Önerilen haberleşme sisteminin gürültü performansı, gürültülü kanal koşulları altında bit hata oranlarının kapsamlı benzetimleri ile elde edilmiştir.

Anahtar kelimeler: Öbek kaydırmalı kipleme, kaos tabanlı haberleşme, örtülü haberleşme, öbek eşzamanlılığı, kaotik sistemler

CONTENTS

Page

Ph.D. THESIS EXAMINATION RESULT FORM ii
ACKNOWLEDGEMENTS iii
ABSTRACT v
ÖZ vi
LIST OF FIGURES xv
LIST OF TABLES xvi

CHAPTER ONE – INTRODUCTION 1

1.1 Chaotic Synchronization in Networks 1
1.2 Chaotic Communication Methods and Their Common Weakness 3
1.3 Thesis Statement 5
1.4 Aims and Objectives 8
1.5 Significance of Research 10
1.6 Outline 11

CHAPTER TWO – DEFINITIONS AND PRELIMINARIES 12

2.1 Definitions 12
2.2 Mathematical Preliminaries 15
2.3 Variational Equations 18
2.4 Lyapunov Exponents 19
2.5 Master Stability Function 21

CHAPTER THREE – PINNING CONTROL 26

3.1 Introduction to Pinning Control 26
3.2 Cluster Synchronization in Undirected Networks 28
3.3 Cluster Synchronization in Directed Networks 34
3.4 Illustrative Examples 37

3.4.1 Cluster Synchronization in Undirected Networks 37
3.4.2 Cluster Synchronization in Directed Networks 40

CHAPTER FOUR – TOPOLOGICAL CONTROL OF CLUSTERS 43

4.1 Controlling Synchronous Patterns 43
4.2 Illustrative Examples 48
4.2.1 Without Control Network 48
4.2.1.1 Changing Coupling Strength 51
4.2.1.2 Removing Links 54
4.2.1.3 Rewiring Links 60
4.2.1.4 Removing and Rewiring Links 61
4.2.2 With Control Network 67
4.2.2.1 Inducing Cluster Synchronization 67
4.2.2.2 Controlling Cluster Synchronization 71

CHAPTER FIVE – CHAOTIC COMMUNICATION SYSTEMS 75

5.1 Spread Spectrum Communications 75
5.2 Chaos Based Modulation Schemes 76
5.2.1 Chaos Shift Keying 77
5.2.2 Differential Chaos Shift Keying 80
5.3 Detection Performances 82
5.3.1 Detection Performance of Chaos Shift Keying 82
5.3.2 Detection Performance of Differential Chaos Shift Keying 90
5.4 Numerical Simulations 94
5.4.1 Chaos Shift Keying Performance 94
5.4.2 Differential Chaos Shift Keying Performance 95

CHAPTER SIX – NETWORK DESIGN 97

6.1 Network Design Using Pinning Control 97
6.2 Network Design Using Topological Control 104
6.2.1 Design without Control Network 104

6.2.2 Design with Control Network 128
6.2.2.1 Conceptual Design 128
6.2.2.2 Network Design Approach Disconnected Subnetworks 130
6.2.2.3 Network Design Approach Connected Subnetworks 141
6.2.2.4 Splitting Nodes 150

CHAPTER SEVEN – CLUSTER SHIFT KEYING 153

7.1 Quantifying Noise 153
7.1.1 Quantifying Noise in terms of E_b/N_0 153
7.1.2 SNR 158
7.2 The Type of Coupling 158
7.2.1 Unidirectional Coupling 159
7.2.2 Bidirectional Coupling 163
7.3 Noise Model 168
7.4 Detection Rule 169
7.5 Illustrative Examples 171
7.5.1 Example I: Design without Control Network 171
7.5.1.1 The Network 171
7.5.1.2 Signalling 176
7.5.1.3 Detection Performance 179
7.5.2 Example II: Design with Control Network 180
7.5.2.1 The Network 180
7.5.2.2 Signalling 184
7.5.2.3 Detection Performance 186

CHAPTER EIGHT – CONCLUSION 191

REFERENCES 195

LIST OF FIGURES

Page

Figure 1.1 Spatio-temporal status of the network when symbol (a) s_j and (b) s_k are being transmitted. $s_j \neq s_k$. 7

Figure 3.1 An undirected network. Nodes $1, 2, 3$ are wanted to be pinned to node $1'$ while the nodes $4, 5, 6$ are wanted to be pinned to node $2'$. 37

Figure 3.2 Simulation results of network in Figure 3.1 39

Figure 3.3 A directed network. The nodes $1, 2, 8, 11$ are wanted to be pinned to node $1'$, the nodes $3, 4, 6, 7$ are wanted to be pinned to node $2'$, and nodes $5, 9, 10$ are wanted to be pinned to node $3'$. 40

Figure 3.4 Simulation results of network in Figure 3.3 42

Figure 4.1 (a) A simple network possessing reflection symmetry $\mathcal{S}_1$. (b) The cluster synchronization pattern $\mathscr{C}_1$ corresponding to symmetry $\mathcal{S}_1$. The nodes in the same cluster are shown with the same color. 48

Figure 4.2 The distribution of the eigenvalues $\lambda_i^t, i = 1, 2$ of $\mathbf{\Omega}$ and $\lambda_i^s, i = 1, 2, 3$ of $\mathbf{\Theta}$. Here $\eta = \epsilon\lambda$. The dashed vertical line shows the boundary between the stable and unstable modes. i.e, the mode corresponding to λ is stable if $\eta = \epsilon\lambda < \tilde{\eta}$. 51

Figure 4.3 The change of the distribution of the eigenvalues $\lambda_i^t, i = 1, 2$ of $\mathbf{\Omega}$ and $\lambda_i^s, i = 1, 2, 3$ of $\mathbf{\Theta}$ 51

Figure 4.4 Plots of the master stability function for the Lorenz dynamics for various inner coupling matrix schemes $\boldsymbol{P}$. The notation $i \rightarrow j$ corresponds to unique nonzero element p_{ij} of element of $\boldsymbol{P} = [p_{ij}]$. 52

Figure 4.5 The simulation of the network in Figure 4.1.....55

Figure 4.6 The spatiotemporal view of the network in Figure 4.1. 56

Figure 4.7 (a) A simple network with possessing symmetry $\mathcal{S}_2$. (b) The cluster synchronization pattern $\mathscr{C}_2$ corresponding to symmetry $\mathcal{S}_2$. The nodes in the same cluster are shown with the same color. 56

Figure 4.8 The simulation of the network in Figure 4.7. 58

Figure 4.9 The spatiotemporal view of the network in Figure 4.7. 59

Figure 4.10 (a) A simple network with possessing symmetry $\mathcal{S}_3$. (b) The cluster synchronization pattern $\mathscr{C}_3$ corresponding to symmetry $\mathcal{S}_3$. The nodes in the same cluster are shown with the same color. 59

Figure 4.11 The simulation of the network in Figure 4.10. 62

Figure 4.12 The spatiotemporal view of the network in Figure 4.10.$\epsilon = 11.5$ 63

Figure 4.13 The simulation of the network in Figure 4.10. 64

Figure 4.14 The spatiotemporal view of the network in Figure 4.11. $\epsilon = 11.5$ (a) $0 \leq t < 1000$, (b) $1000 \leq t < 2000$, (c) $2000 \leq t \leq 3000$. 65

Figure 4.15 (a) An example network having the rotation symmetries (b) $\mathcal{S}_1$ and (c) $\mathcal{S}_2$, and (d) a rotation symmetry $\mathcal{S}_3$. 66

Figure 4.16 The change of the spatiotemporal status of the original (unpinned) network. 67

Figure 4.17 Controlled network. 68

Figure 4.18 The change of spatiotemporal status of the network for changing control strength α. 69

Figure 4.19 The numerical simulation of the network. 74

Figure 5.1 Block diagram for chaos shift keying. 78

Figure 5.2 Block diagram for differential chaos shift keying. 81

Figure 5.3 Block diagram of single user chaos shift keying. 83

Figure 5.4 Block diagram of multiple access chaos shift keying. 87

Figure 5.5 Block diagram of single user differential chaos shift keying. 89

Figure 5.6 Block diagram of multiple access differential chaos shift keying (MA-DCSK) 91

Figure 5.7 Detection performance of single user CSK with logistic map..... 94

Figure 5.8 Detection performance of single user DCSK with logistic map 95

Figure 5.9 Comparison of detection performances of single user CSK and DCSK with logistic map. 96

Figure 6.1 An example network..... 98

Figure 6.2 The network in Figure 6.1 with the nodes 1 and 6 are coupled to each other. 98

Figure 6.3 The network in Figure 6.2 with nodes 1 and 6 are decoupled, and the nodes 1 and 4 are coupled. 99

Figure 6.4 The network in Figure 6.3 with the nodes 3 and 4 are coupled. 100

Figure 6.5 The network in Figure 6.4 with the nodes 3 and 4 are coupled. 100

Figure 6.6 The first cluster pattern with the clusters $\mathscr{G}_1 = \{1, 2, 3\}$ and $\mathscr{G}_2 = \{4, 5, 6\}$. The nodes in the same cluster is shown with the same color..... 101

Figure 6.7 The second cluster pattern with the clusters $\mathscr{G}_1 = \{1, 2, 3\}$ and $\mathscr{G}_2 = \{4, 5, 6\}$. 101

Figure 6.8 The network to be used in the proposed communication system. 102

Figure 6.9 The distribution of the nodes in the network in Figure 6.8 between the transmitter and the receiver. 103

Figure 6.10 The cluster pattern of the network during symbol 0 transmission..... 103

Figure 6.11 The cluster pattern during symbol 1 transmission. 103

Figure 6.12 (a) A network that can be programmed to exhibit three different cluster patterns. (b) The pattern corresponding to the symmetry $\mathcal{S}_1$. (c) The pattern corresponding to the symmetry $\mathcal{S}_2$. (d) The pattern corresponding to the symmetry $\mathcal{S}_3$..... 105

Figure 6.13 (a) A network that can be programmed to exhibit three different cluster patterns. (b) The pattern corresponding to the symmetry $\mathcal{S}_1$. (c) The pattern corresponding to the symmetry $\mathcal{S}_2$.(d) The pattern corresponding to the symmetry $\mathcal{S}_3$..... 106

Figure 6.14 The change of eigenvalues in response to the change of the weight between the nodes 1 and 4. (a) The change of the eigenvalue distribution for the symmetry $\mathcal{S}_1$. (b) The change of the eigenvalue distribution for the symmetry $\mathcal{S}_2$. 110

Figure 6.15 Plot of the master stability function for the Lorenz dynamics given in (4.22) and the inner coupling matrix $\boldsymbol{P} = [p_{ij}]$ with only nonzero element $p_{21} = 0$..... 111

Figure 6.16 The simulation of the network in Figure 6.13a. $e_{ij} = |x_i - x_j|$ where $\boldsymbol{x}_i = [x_i, y_i, z_i]$. 113

Figure 6.17 The spatiotemporal view of the network in Figure 6.13. $\epsilon = 10.5$ (a) $0 \leq t < 1000$, (b) $1000 \leq t < 2000$, ... 114

Figure 6.18 Using the network in Figure 6.13a in a binary communication system in which the symbols are s_1, s_2. The cluster pattern is controlled via the weight w_{14}. (a)Spatiotemporal status of the network during s_1 transmission. (b) Spatiotemporal status of the network during s_2 transmission. $\epsilon = 10.5$ 115

Figure 6.19 A network that can be programmed to possessing different topological symmetries. (a), (c) The symmetry $\mathcal{S}_1$ its corresponding pattern, respectively. (c), (d) The symmetry $\mathcal{S}_2$ its corresponding pattern, respectively.(e), (f) The symmetry $\mathcal{S}_3$ its corresponding pattern, respectively. 116

Figure 6.20 The change of eigenvalues for the symmetry $\mathcal{S}_1$ 120

Figure 6.21 The change of eigenvalues for the symmetry $\mathcal{S}_2$ 121

Figure 6.22 The change of eigenvalues for the symmetry $\mathcal{S}_2$ 122

Figure 6.23 The change of eigenvalues for the symmetry $\mathcal{S}_3$ 123

Figure 6.24 The simulation of the network in Figure 6.19. $e_{ij} = |x_i - x_j|$ where $\boldsymbol{x}_i = [x_i, y_i, z_i]$. 125

Figure 6.25 The spatiotemporal view of the network in Figure 6.19. $\epsilon = 15$. (a) $0 \leq t < 1000$, ()b) $1000 \leq t < 2000$, ... 126

Figure 6.26 Using the network in Figure 6.19 in a binary communication system in which the symbols are s_1, s_2. The cluster pattern is controlled via the weight w_{58}. (a) Spatiotemporal status of the network during s_1 transmission. (b) Spatiotemporal status of the network during s_2 transmission. $\epsilon = 20$..... 127

Figure 6.27 Conceptual network design. 130

Figure 6.28 The cluster pattern 1. 131

Figure 6.29 Error waveforms $e_{ij}(t)$ for $i, j = 1, 2, \ldots, 9$..... 132

Figure 6.30 (a) Time waveform and (b) the chaotic attractor of the node 1..... 133

Figure 6.31 The cluster pattern 2 133

Figure 6.32 Error waveforms $e_{ij}(t)$ for $i, j = 1, 2, \ldots, 9$..... 134

Figure 6.34 The cluster pattern 3 136

Figure 6.35 Error waveforms $e_{ij}(t)$ for $i, j = 1, 2, \ldots, 9$..... 137

Figure 6.36 (a) Time waveform and (b) the chaotic attractor of the node 1..... 138

Figure 6.37 The cluster pattern 4 138

Figure 6.38 Error waveforms $e_{ij}(t)$ for $i, j = 1, 2, \ldots, 6$..... 139

Figure 6.39 (a) Time waveform and (a) the chaotic attractor of the node 1. 140

Figure 6.41 The change of the spatiotemporal status of the original (unpinned) network. 142

Figure 6.46 The change of the spatiotemporal status of the original (unpinned) network. 147

Figure 6.47 The change of spatiotemporal status of the network for changing control strength. 149

Figure 6.49 The change of spatiotemporal status of the network for changing control strength α. 151

Figure 6.50 Symbol 0 transmission 152

Figure 6.51 Symbol 1 transmission 152

Figure 7.7 (a) and (b) are the cluster patterns in the illustrative network. (c) and (d) are the split of the nodes of the network in (a) and (b) between the transmitter and receiver, respectively. 172

Figure 7.15 The change of spatiotemporal status of the network with respect to a coupling strength ϵ, and b and c control strength α corresponding to the cluster patterns in 7.14a and 7.14b, respectively. 182

Figure 7.16 (a) and (b) The split of nodes of the network in Figure 7.14a and Figure 7.14b, respectively. 184

Figure 7.18 BER performances (plotted by solid lines with markers) obtained by numerical simulations and curves (plotted by dashed lines) fitted to the BER performances to represent the trends of the noise performances. BER performances in terms of noise level σ and probability of making a detection error P_e of the network in Figure 7.16 for $\epsilon = 3$ and different values of α and s_f. 187

Figure 7.19 BER performances (plotted by solid lines with markers) obtained by numerical simulations and curves (plotted by dashed lines) fitted to the BER performances to represent the trends of the noise performances. BER performances of a single user CSK, DCSK, and CLSK scheme for $\epsilon = 3, \alpha = 10, s_f = 1000$ in terms of the ratio of average symbol energy to noise power spectral density E_b/N_0 versus the probability of making a detection error P_e. 188

LIST OF TABLES

Page

Table 5.1 Classification of chaotic communication systems 77

Table 7.1 Number of bits used for different noise levels in 7.13. 180

Table 7.2 Number of bits used for different values of σ, α and s_f in Figure 7.18. 186

CHAPTER ONE
INTRODUCTION

As a communication system based on the cluster synchronization of chaotic systems is proposed in this thesis, a brief introduction about the chaotic systems and available chaos communication systems will be insightful before further progress. For this purpose, chaotic synchronization in networks of chaotic systems will be introduced briefly in this chapter. The chaos communication methods will be outlined next, with a particular emphasis on their common weakness. Then, the central hypothesis of the study is presented. The chapter concludes with the aims, objectives, and significance of the study.

1.1 Chaotic Synchronization in Networks

Despite their intrinsically simple and deterministic structures, chaotic dynamical systems are characterized by their sensitive dependencies on initial conditions and parameter changes (Shilnikov et al., 1998; Wiggins, 2003). Predicting the outputs of these systems in terms of their past values is only possible for a short period. Their signals have characteristically high bandwidth (Abarbanel, 1996).

The phenomenon of chaotic synchronization is as old as the discovery of the existence of these systems. Since the observation that two identical chaotic systems with different initial conditions can synchronize (Pecora & Carroll, 1990; Strogatz, 2001), the questions of what types of synchronization are possible and under what conditions these different types of synchronization are ensured for a network consisting of chaotic systems coupled to each other have been actively studied. For the smallest network consisting of two systems, the phenomenon of chaotic synchronization has been enriched to phase (Rosenblum et al., 1996), lag (Rosenblum et al., 1997), complete (Pecora & Carroll, 1990), anticipating (Voss, 2000), generalized (Rulkov et al., 1995) synchronization. Depending on the network topology, the number of nodes, and the strength and type of the couplings in the network, it is known that coupled chaotic systems exhibit richer dynamics than each node of the network does. Suppose the individual nodes capable of exhibiting

periodic, quasi-periodic, or chaotic dynamics are properly coupled. In that case, all the nodes can wholly synchronize, each can continue evolving independently with separate dynamics, or they can synchronize in groups, i.e., they can form clusters. The case in which all the nodes are completely synchronized is called *full synchronization*, while the case in which the nodes are synchronized in groups but there is no synchronization among the groups is called *cluster synchronization*. Numerous studies have shown that a network of continuous-time chaotic systems with a predetermined topology can be forced to exhibit full synchronization or cluster synchronization if the coupling strengths between the nodes in the network exceed certain thresholds. If not, the nodes having individual dynamics continue their independent evolution. Depending on the network topology, number of nodes, and coupling type, the thresholds that make full (Pecora & Carroll, 1998; Belykh et al., 2006; Porfiri & di Bernardo, 2008; Li et al., 2009; Yu et al., 2009) or cluster (Pecora & Carroll, 1998; Belykh et al., 2000, 2003) synchronization possible can be found using the techniques available in Lyapunov stability theory, graph theory and control theory. Arbitrarily-selected cluster patterns in diffusively-coupled undirected networks can be realized by using coupling schemes with cooperative and competitive weights (Ma et al., 2006), pinning control strategy (Wu et al., 2009), graph theory (Schaub et al., 2016) or topological sensitivity (Fu et al., 2013; Lin et al., 2016b,a; Gambuzza et al., 2021). A desired cluster pattern can also be realized in heterogeneous (Lu et al., 2010; Wang et al., 2019), adaptive(Wu et al., 2009; Wu & Lu, 2011), fractional-order (Chen et al., 2012), directed (Liu & Chen, 2011), multiplex (Jalan & Singh, 2014; Sevilla-Escoboza et al., 2016), and delayed (Singh et al., 2017; **?**) networks. In (Pecora et al., 2014), a framework that shows the connection between network symmetries and cluster formation is presented. In (Sorrentino et al., 2016), a method is proposed to find and analyze all possible cluster synchronization patterns. In (Khanra et al., 2022), a method to identify a network's clusters without the need to explore its symmetry group is introduced.

In addition to the problem of investigation of full or cluster synchronization that can be observed in the networks with a given topology, the problem of designing a

network that enables the stable realizations of *desired* cluster synchronizations has been studied extensively. Answers to how and how much strength the systems must be coupled to each other have been sought, and the corresponding necessary and sufficient conditions have been investigated. It has been shown that it is possible to ensure synchronization of different clusters in a network consisting of chaotic systems by changing the network parameters. For instance, by changing the coupling strengths between the nodes (Belykh et al., 2000; Hillier et al., 2006; Ma et al., 2006) or coefficients of the control signals acting on some particular nodes (Wu et al., 2009; Lin et al., 2016a; Wang et al., 2019), one can control which clusters of nodes synchronize to each other. This very particular ability lies at the heart of the method proposed in this study.

1.2 Chaotic Communication Methods and Their Common Weakness

The transmission of information that third parties can access poses a security problem, even if the information is encrypted. The problem can be overcome physically by using specifically designed transmission channels that are not publicly accessible. On the other hand, such specific physical channels are i) not generally economic, ii) areas where they can access are limited, iii) are direct targets because they can be accessed maliciously. Often, information having strategic importance and secrecy is required to be transmitted from publicly available physical mediums. In particular, recent advances in wireless communication necessitate—to ensure transmission security—encryption of information transmitted through publicly-available channels so that its content cannot be understood even if third parties access it. This type of encryption algorithm assumes that the hardware and software used to decipher the encrypted data cannot respond at a rate that produces results within an acceptable period. For this reason, more and more complex numerical encryption/decryption algorithms are needed to cope with rapidly developing hardware and software capabilities. Thus, it is also necessary for the systems employing these complex algorithms to become increasingly complex (Christine et al., 2015).

Precautions to prevent physical listening of signals transmitted from public or private channels provide an additional layer of security to those provided by encryption/decryption systems. In private channels, preventing the channel signals from being listened to can be achieved by physically isolating the channel (for example, by using deeply embedded fiber cables in a hidden route) and, thus, restricting physical access to the channel. Alternative precautions for public channels are required because such a measure is impossible for them. Carefully-determined modulation techniques can ensure that the signal is buried into other signals so that it cannot be detected easily. Transmitting signals at randomly changing frequency bands and at discrete time instants are among these frequently used techniques. These types of techniques require a wide frequency band during transmission. Hence, they are generally preferred in secure communication as they allow only partial access to the transmitted signals when listening to a narrow band (Cook, 1983; Simon, 2002).

Owing to their inherent characteristics, the chaotic systems can be thought to be used for data encryption (Dachselt et al., 1997; Dachselt & Schwarz, 2001; Kocarev, 2001; Amigó, 2009) and secure communication (Bohme & Schwarz, 1986; Parlitz et al., 1992; Kennedy & Hasler, 1993; Kolumban et al., 1996; Feldmann et al., 1996; Chua, 1997). Chaotic communication methods are based on synchronizing chaotic systems in the receiver and the transmitter. They can generally be grouped as chaotic masking, chaos shift keying, or chaotic parameter modulation Cuomo & Oppenheim (1993); Kennedy & Hasler (1993); Xiang-Jun (2006); Yang et al. (2017); Tan et al. (2018); Herceg et al. (2018); Cai et al. (2019); Zhang et al. (2019); Tan et al. (2019); Lu et al. (2020); Cai et al. (2021). In the chaotic masking method, the signal to be transmitted is directly added to a chaotic carrier signal. This direct addition can make the systems in the receiver, and the transmitter loses their chaotic behaviors unless the power of the message signal is sufficiently small compared to that of the chaotic carrier signal. The chaos shift keying method requires that the outputs of the chaotic systems be switched over a symbol duration according to the message signal and that the switching time is long enough to ensure the synchronization of the chaotic systems in the receiver and transmitter. This requirement makes its effectiveness

controversial in modern applications that require high data transmission rates. In the chaotic modulation method, the message signal changes the system parameters. However, the sensitive dependence of chaotic systems on initial conditions also reduces noise immunity (Abel & Schwarz, 2002).

Furthermore, various signal analysis techniques, such as time-frequency analysis and parameter estimation, have shown that these chaotic communication methods alone cannot prevent third parties' retrieval of the message signal. The performances of these methods are unfortunately not comparable to those of the classical modulation methods, despite their elegant formulation of the problem and implementation simplicity. Ultimately, the interest in chaotic communication and signal processing methods remained at the academic level.

The primary common weakness of the chaotic communication systems explained above is their attempt to modulate the message signal in such a way as to change the chaotic dynamics of the systems, which may lead—depending on whether the power of the message signal is dominant to those of the chaotic systems—to the destruction of the chaotic dynamics that carry the message signal in chaotic masking and chaotic modulation methods. Likewise, the modulation methods based on chaos shift keying cannot prevent data retrieval through secondary means, such as signal analysis methods like time-frequency analysis and parameter estimation, because of discontinuities in the transmitted signal. To overcome the vulnerabilities mentioned above, modulation of the message signal into the *spatio-temporal synchronization* status of a network consisting of chaotic systems so that the chaotic dynamics of the systems in the network is *not directly affected* constitutes the main idea of the study. At this very point, the proposed method differs from the chaotic modulation methods explained above.

1.3 Thesis Statement

The central hypothesis of this thesis is that it is possible to design a communication scheme, namely cluster shift keying (CLSK), based on cluster synchronization in

networks of chaotic systems in which we encode symbols into the *spatiotemporal synchronization status of the network*. In our approach, the network is explicitly designed to be in several cluster synchronization modes depending on coupling parameters. The cluster synchronization of the network is divided into two subnetworks, transmitter and receiver, and control of particular coupling strengths between the nodes at the transmitter subnetwork switches the synchronization pattern of the structure. The transmitter and receiver subnetworks are not necessarily in drive-response mode (Parlitz et al., 1992; Kennedy & Hasler, 1993). The presence of a particular symbol is detected by the presence of the particular cluster pattern at the receiver subnetwork (Figure 1.1). We choose the cluster patterns such that the nodes connecting the transmitter and receiver are never in the same cluster. Hence, the signals transmitted always remain chaotic regardless of the symbols sent, effectively masking the information. The error signals between the nodes at the receiver subnetwork represent the symbols. A symbol is detected over the nodes at the receiver, and the signals received through the channel links are not directly involved. As a result, one needs complete knowledge of the network topology to decipher the symbols, rendering the communication immune to eavesdropping. Besides, the scheme tends to be robust against channel noise due to the guaranteed asymptotic stability of the network by construction.

In the chaotic communication methods outlined in §1.2, the modulation is performed directly on the chaotic carrier signal in the time-frequency domain, which leads to the retrieval of the message signal via time-frequency analysis methods. In the proposed method, however, performing the modulation in the spatiotemporal domain by exploiting the synchronization of clusters of nodes in the transmitter and the receiver makes the signals transmitted through the channel always remain chaotic regardless of the symbol being sent. This ensures that even if the signals transmitted through the channel are listened to by third parties, the information being sent from the transmitter to the receiver cannot be deciphered by signal analysis methods such as time-frequency analysis or parameter estimation without the exact knowledge of the transmitter and receiver network topologies, directly.

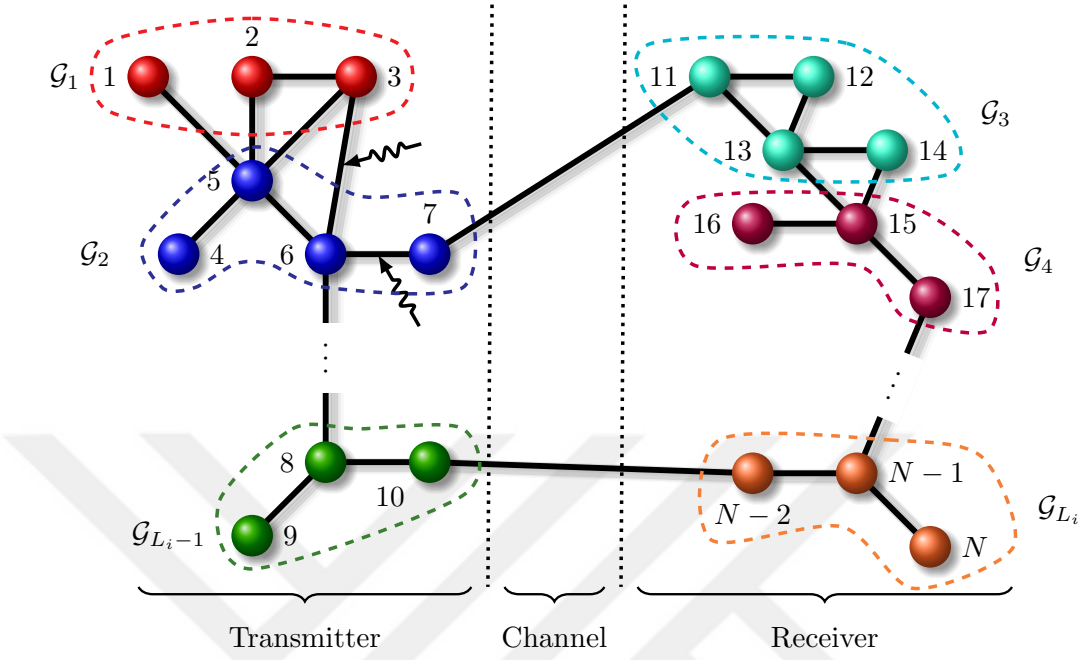

(a)

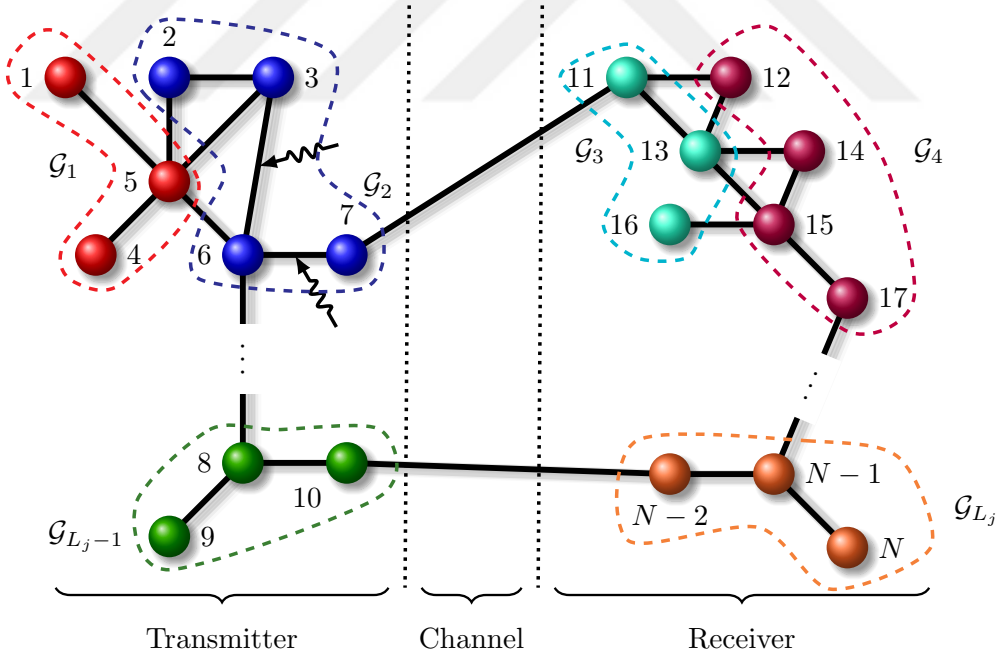

(b)

Figure 1.1 Spatio-temporal status of the network when symbol (a) s_j and (b) s_k are being transmitted. $s_j \neq s_k$.

1.4 Aims and Objectives

Throughout the study, we have reached the intermediate aims outlined below.

1. Our first goal is to design a chaotic network that enables us to control the synchronization of desired node clusters through network control parameters. The methods reported on the problem of cluster synchronization (Ma et al. (2006); Fu et al. (2013); Lin et al. (2016a)) in networks of chaotic systems have suited our network design problem. Inspired by the methods outlined in these studies, we have designed numerous networks whose cluster patterns can be controlled by parameters such as the coupling strengths or the feedback coefficients.

2. Most of these networks could not meet the specific requirements that

   (a) when the network is divided into two as transmitter and receiver, the control parameters must reside at the transmitter side only,

   (b) the nodes of the links connecting the transmitter and the receiver must never be in the same cluster for all values of the control parameters.

   We have continuously revised our network design methods to meet these requirements.

3. Once the networks that meet all the basic requirements of the proposed communication system have been designed, the networks have been optimized further. For example, our earlier designs have bidirectional signal transmission between the transmitter and receiver, resulting in a full-duplex signal transmission. In such a configuration, we had difficulties quantifying the amount of channel noise to get the performance of the communication system. For a fair noise performance comparison of the proposed communication system and the available chaos communication methods in the literature, we have devised networks in which the signal transmission is unidirectional, i.e., from the transmitter to the receiver only.

Further optimization of the network design regarding bandwidth usage has been done. When the network nodes are split between the transmitter and the receiver, the number of links in the channel directly affects the bandwidth usage. The higher the number of links in the channel, the larger the bandwidth usage of the communication system. In order to efficiently use system resources, the fewer links in the channel, the better we are. Hence, after our preliminary designs, we have revised our methods to design networks with fewer links to the channel.

4. We must ensure the specific cluster pattern corresponds to the sent symbol. Thus, we must ensure that the nodes in the same clusters are synchronized while those in different clusters are definitely out of synchronization. Initially, we have designed networks based on the methods that ensure synchronization of nodes in the same cluster while not being able to guarantee that the nodes in different clusters are out of synchronization. This design may result in networks causing incorrect detection. To overcome this problem, we have adopted methods based on pinning control. In the pinning control approach, the clusters of nodes in the network are pinned to control nodes, each of which follows different trajectories. Each node in the cluster is synchronized with the pinned node. Hence, synchronizing with different trajectories enforces that the nodes in different clusters are out of synchronization.

5. Once the conceptual design of the proposed communication system has been completed, we have obtained its bit error rate (BER) performance through extensive numerical simulations. Then, we have compared its performance to the available chaos communication systems. Additionally, we have investigated how the BER performance of the proposed communication system reacts to changes in parameters such as coupling strengths, feedback coefficients, or spreading factors.

6. The claim that the covertness of the communication system is ensured by transmitting chaotic signals having no relation to the information being sent has been justified numerically by investigating the spectrograms of the transmitted signals. No apparent correlation has been observed between the transmitted

signals and the symbols being sent.

1.5 Significance of Research

This study proposes a novel chaotic communication method based on cluster synchronization in a network of chaotic systems. In this context, the study distinguishes from already available ones in the literature by the following points:

1. This study puts forth a novel method based on cluster synchronization of chaotic systems for covert transmission of signals. Let alone the details, the idea that cluster synchronization can be used for covert communication is already a novelty in its own right. One of the major distinctions of the proposed method is that it modulates the data being sent into the cluster synchronization pattern, i.e., the *spatio-temporal status*, of the network, unlike the ones available in the literature that modulate the data *into the chaotic carrier signal directly*. It is crucially important that the method modulates the data sent in the space-time domain but not in the time-frequency domain. This ensures that the nodes in the network always stay in their chaotic regimes and overcome the problems seen in the chaotic communication systems described before, such as the destruction of the chaotic dynamics or retrieval of the message signal by secondary means.

2. To the author's knowledge, almost all the schemes proposed in the chaos communication literature formulate the noise performance problem from the communication system point of view. The BER performances of those systems have been derived without using the system-theoretical details. In this study, however, we approach the problem from the system-theoretical view. In particular, the channel noise is involved in our analysis by formulating the network dynamics in stochastic differential equations (SDEs), not in the form of ordinary differential equations (ODEs) as in most available chaos communication schemes.

3. A new and realistic application has been proposed for the chaotic systems that

cannot find enough engineering application areas despite their being elegantly formulated and easy to implement.

4. A new relation between cluster synchronization in chaotic systems and communication theory has been established. It is also possible that this may have significant consequences, including the case of biological neural networks.

1.6 Outline

Following this introductory Chapter, we revisit the necessary and sufficient conditions to design networks that ensure different cluster patterns for different values of control parameters in the following two chapters. In particular, the pinning control method is outlined in Chapter 2, while the cluster control using the network topology is presented in Chapter 3. Next, in Chapter 4, available chaos communication methods are briefed to help us comment on the distinguishing points of the proposed communication system. The details of network design using different approaches outlined in Chapters 2 and 3 are explained in Chapter 5. This Chapter also explains how to optimize the designed networks, explicitly focusing on effectively utilizing communication system resources. Chapter 6 presents the details of the proposed communication system, including its conceptual design, symbol encoding and decoding, signaling, security, and noise performance. First, the requirements of the networks to be used in the communication systems are outlined. Then, the principles behind the symbol encoding are explained. The derivation of a detection rule to recover the symbols from the cluster pattern in the receiver is described. The network dynamics under noise have been modeled, and the BER performance of the proposed communication system has been obtained and compared to well-known chaos communication schemes. Chapter 7 concludes the thesis with remarks and future works.

CHAPTER TWO
DEFINITIONS AND PRELIMINARIES

2.1 Definitions

Definition 2.1.1 (Diffusively Coupled Matrix)**.** For real matrix $\boldsymbol{C} = [c_{ij}] \in \mathbb{R}^{N\times N}$ if the sum of each row is equal to zero, that is, $\sum_{j=1}^{'N} c_{ij} = 0,\ i = 1, \ldots, N$, then the matrix $\boldsymbol{C}$ is called a diffusively coupled matrix. In addition, if all the off-diagonal elements of $\boldsymbol{C}$ are nonnegative, that is, $c_{ij} \geq 0,\ i \neq j$, then the matrix $\boldsymbol{C}$ is called as a nonnegative diffusively coupled matrix.

Definition 2.1.2 (Diffusively-Coupled Network)**.** The network of linearly coupled continuous time identical dynamical systems whose dynamics evolves by

$$\dot{\boldsymbol{x}}_i = f(\boldsymbol{x_i}) + \sum_{i=1}^{N} \epsilon_{ij} \boldsymbol{P} \boldsymbol{x}_j \quad i = 1, \ldots, N, \tag{2.1}$$

is called a diffusively coupled network. Here, $\boldsymbol{x}_i = [x_{i,1}, \ldots, x_{i,d}] \in \mathbb{R}^d$ is the state vector of node i. $f : \mathbb{R}^d \mapsto \mathbb{R}^d$ is the vector-valued function corresponding to the dynamics of identical nodes. ϵ_{ij} is the coupling strength between node i and j. $\epsilon_{ij} > 0$ if there exists a coupling from j to i; otherwise, $\epsilon_{ij} = 0$. The nonnegative diffusively-coupled matrix $\boldsymbol{E} = [\epsilon_{ij}] \in \mathbb{R}^{N\times N}$ denotes the coupling configuration of the network. The eigenvalues of $\boldsymbol{E}$ satisfy $0 = \lambda_1 > \lambda_2 \geq \lambda_3 \geq \ldots \geq \lambda_N$. The matrix $\boldsymbol{P} \in \mathbb{R}^{d\times d}$ determines by which variables the nodes are coupled. Associated with the topology of the network in 2.1, an undirected graph $\mathscr{G} = \{\mathcal{N}, \mathcal{L}\}$ can be constructed, where $\mathcal{N} = \{1, 2, \ldots, N\}$ is the set of nodes, and $\mathcal{L} = \{\ell_{ij} = (i, j) \mid i, j \in \mathcal{N}, i < j\}$ is the set of links ℓ_{ij} that connects the nodes i and j.

Definition 2.1.3 (Undirected Diffusively-Coupled Network)**.** A network defined in Definition 2.1.2 is an undirected diffusively coupled network if $\epsilon_{ij} = \epsilon_{ji}, \forall i = 1, 2, \ldots, N$. An undirected graph can be associated with an undirected network.

Definition 2.1.4 (Directed Diffusively-Coupled Network)**.** A network defined in Definition 2.1.2 is a directed diffusively coupled network if $\epsilon_{ij} \neq \epsilon_{ji}, \exists i = 1, 2, \ldots, N$. A directed graph can be associated with a directed network.

Definition 2.1.5 (Full Synchronization)**.** Consider the network in (2.1). Let $\boldsymbol{s}(t)$ be a solution of individual node dynamics, i.e. $\dot{\boldsymbol{s}}(t) = f(\boldsymbol{s}(t))$. The network in (2.1) achieves full synchronization if $\lim_{t\mapsto\infty} |\boldsymbol{x}_i(t) - \boldsymbol{s}(t)|,\ i = 1, 2, \ldots, N$. In the case of full synchronization, all the nodes synchronize to a common dynamics.

Definition 2.1.6 (Full Synchronization Manifold)**.** The full synchronization is associated to full synchronization manifold

$$\mathcal{M}_f = \{\boldsymbol{x}_1 = \boldsymbol{x}_2 = \ldots = \boldsymbol{x}_N \triangleq \boldsymbol{s}\} \tag{2.2}$$

Definition 2.1.7 (Cluster Synchronization)**.** Let $\{\mathcal{G}_1, \mathcal{G}_2, \ldots, \mathcal{G}_L\}$ be the partition of $\mathcal{N}$ into L nonempty subsets such that $\cup_{k=1}^{L} \mathcal{G}_k = \mathcal{N}$ where $\mathcal{G}_l \neq \emptyset, \forall l$, and $\mathcal{G}_i \cap \mathcal{G}_j = \emptyset, i \neq j$, and $\mathcal{G}_l$ represents the node indices in cluster l. A network is said to realize L-cluster synchronization with the partition $\{\mathcal{G}_1, \mathcal{G}_2, \ldots, \mathcal{G}_l\}$ if, for any initial values,

$$\lim_{t\mapsto\infty} \|\boldsymbol{e}_{ij}(t)\| = 0, \qquad i, j \in \mathcal{G}_k, i \neq j \tag{2.3}$$

$$\lim_{t\mapsto\infty} \|\boldsymbol{e}_{ij}(t)\| \neq 0, \qquad i \in \mathcal{G}_k, j \in \mathcal{G}_l, k \neq l, i \neq j \tag{2.4}$$

are satisfied. When cluster synchronization is achieved, the nodes in the same cluster synchronize, while there is no synchronization between the nodes in different clusters.

Definition 2.1.8 (Cluster Synchronization Manifold)**.** Let $\hat{i}$ denote the subscript of the subset in which node i is, i.e., $i \in \mathcal{G}_{\hat{i}}$. Let the special solutions $\boldsymbol{s}_1, \boldsymbol{s}_2, \ldots, \boldsymbol{s}_L$ of the individual node dynamics $\dot{\boldsymbol{x}} = f(\boldsymbol{x})$ be associated to $\mathcal{G}_1, \mathcal{G}_2, \ldots, \mathcal{G}_L$, respectively, such that $\boldsymbol{s}_i \not\equiv \boldsymbol{s}_j$ for $i \neq j$. The cluster synchronization can be represented by the cluster synchronization manifold

$$\mathcal{M} = \{\boldsymbol{x}_i = \boldsymbol{s}_{\hat{i}} \mid i = 1, 2, \ldots, L\} \tag{2.5}$$

Definition 2.1.9 (Cluster Synchronization Pattern)**.** The spatial status of the network corresponding to a cluster synchronization is called a *cluster pattern* represented by $\mathscr{C} = \{\mathcal{G}_1, \mathcal{G}_2, \ldots, \mathcal{G}_L\}$.

Definition 2.1.10 (Cluster Pattern Set)**.** $\mathscr{P} = \{\mathscr{C}_1, \mathscr{C}_2, \ldots, \mathscr{C}_M\}$ is called the cluster pattern set where $\mathscr{C}_m = \{\mathcal{G}_{1,m}, \mathcal{G}_{2,m}, \ldots, \mathcal{G}_{L_m,m}\}, m = 1, 2, \ldots, M$, L_m is the number of clusters in $\mathscr{C}_m$, and $\mathcal{N} = \cup_{l=1}^{L_m} \mathcal{G}_{l,m},\ \forall m$.

Definition 2.1.11 (Cluster Pattern Capacity)**.** The number M of the cluster pattern set $\mathcal{P}$ is called the cluster pattern capacity.

Definition 2.1.12 (Inter-act and Intra-act Node)**.** Let $\mathcal{G}_i^{inter}$ is subset of $\mathcal{G}_i$ such that for any node j in $\mathcal{G}_i$ there exists at least one node $k \in \mathcal{G}_m,\ m \neq i$ from which there exists a directed path to j, i.e., $\epsilon_{kj} \neq 0$. A node $j \in \mathcal{G}_i$ is called an inter-act node if $i \in \mathcal{G}_i^{inter}$; otherwise it is an intra-act node. $\mathcal{G}_i^{intra}$ is the subset of all intra-act nodes of $\mathcal{G}_i$. In other words, an inter-act node receives information from the nodes in other clusters, while an intra-act node can receive and transmit information from the nodes in the same cluster.

Definition 2.1.13 (Symmetric Node Pair)**.** Consider the network in (2.1). Let $\mathcal{S}$ be the topological symmetry (e.g., reflection, rotation) of the network. A node pair (i, j) is a symmetric pair if the exchange of nodes i and j does not change the topological structure, i.e., after exchange operation, the network dynamics evolved by (2.1) again.

Definition 2.1.14 (QUAD Function)**.** Let $\boldsymbol{\Delta} = diag(\delta_1, \ldots, \delta_d)$ be a diagonal matrix and $\boldsymbol{P} = diag(p_1, \ldots, p_d)$ be a positive definite diagonal matrix. Then, $QUAD(\boldsymbol{\Delta}, \boldsymbol{P})$ denotes the set of continuous functions $f : \mathbb{R}^d \mapsto \mathbb{R}^d$ satisfying

$$(\boldsymbol{x}-\boldsymbol{y})^T \boldsymbol{P}(f(\boldsymbol{x}) - f(\boldsymbol{y}) - \boldsymbol{\Delta}(\boldsymbol{x}-\boldsymbol{y})) \leq -\omega(\boldsymbol{x}-\boldsymbol{y})^T(\boldsymbol{x}-\boldsymbol{y}),\ \omega > 0,\ \forall \boldsymbol{x}, \boldsymbol{y} \in \mathbb{R}^d. \quad (2.6)$$

Definition 2.1.15 (Irreducible Matrix)**.** A square matrix $\boldsymbol{E}$ is said to be reducible if there exists a permutation matrix $\boldsymbol{Q}$ such that $\boldsymbol{Q}^T\boldsymbol{E}\boldsymbol{Q} = \begin{bmatrix} \boldsymbol{E}_{11} & \boldsymbol{E}_{12} \\ 0 & \boldsymbol{E}_{22} \end{bmatrix}$ where $\boldsymbol{E}_{11}$ and $\boldsymbol{E}_{22}$ are square matrices. The matrix $\boldsymbol{E}$ is irreducible if it is not reducible.

Definition 2.1.16 ($\mathbb{E}_1$ Matrix Class)**.** Suppose that $\boldsymbol{E} = [\epsilon_{ij}] \in \mathbb{R}^{N\times N}$ If $\epsilon_{ij} = \epsilon_{ji} \geq 0,\ i \neq j,\ \epsilon_{ii} = -\sum_{j=1}^{n} \epsilon_{ij},\ i = 1, \ldots, n$ and $\boldsymbol{E}$ is irreducible, then we say that $\boldsymbol{E} \in \mathbb{E}_0$

Definition 2.1.17 ($\mathbb{E}_2$ Matrix Class)**.** For a symmetric matrix $\boldsymbol{E} = [\epsilon_{ij}] \in \mathbb{R}^{N\times N}$ can be partitioned into

$$\boldsymbol{E} = \begin{bmatrix} \boldsymbol{E}_{11} & \boldsymbol{E}_{12} & \cdots & \boldsymbol{E}_{1L} \\ \boldsymbol{E}_{21} & \boldsymbol{E}_{22} & \cdots & \boldsymbol{E}_{2L} \\ \vdots & \vdots & \ddots & \vdots \\ \boldsymbol{E}_{L1} & \boldsymbol{E}_{L2} & \cdots & \boldsymbol{E}_{LL} \end{bmatrix} \tag{2.7}$$

where $\boldsymbol{E}_{ij} \in \mathbb{R}^{k_i \times k_j},\ i, j = 1, \ldots, L$ if each block $\boldsymbol{E}_{ij}$ is a zero-row-matrix, then $\boldsymbol{E} \in \mathbb{E}_1$. Furthermore, if $\boldsymbol{E}_{ii} \in \mathbb{E}_0,\ i = 1, \ldots, L$, then we say that $\boldsymbol{E} \in \mathbb{E}_2$

Definition 2.1.18 (Gershgorin Disks)**.** Let $\boldsymbol{C} \in \mathbb{R}^{N\times N}$ be a square complex matrix A Gershgorin disk is the set of points such that $\{z \mid \|z - c_{ii}\| \leq \sum_{j=1, j\neq i}^{n} |c_{ij}|\}$

2.2 Mathematical Preliminaries

Lemma 2.2.1. *Every eigenvalue of nonnegative diffusively coupled matrix $\boldsymbol{C}$ lies in one of the Gershgorin disks.*

Proof. See (Lü et al., 2004). □

Lemma 2.2.2. *If $\boldsymbol{C}$ is a diffusively coupled matrix, then the following results hold*

i) 0 *is and eigenvalue of the matrix $\boldsymbol{C}$, associated with the eigenvector $\boldsymbol{\nu} = [1, \ldots, 1] \in \mathbb{R}^n$.*

ii) If $\boldsymbol{C}$ is a nonnegative diffusively coupled matrix, then the real parts of all eigenvalues of $\boldsymbol{C}$ are less than or equal to 0*, and all eigenvalues with zero real part are the real eigenvalue* 0*.*

iii) If $\boldsymbol{C}$ is nonnegative diffusively coupled matrix and is irreducible, then 0 *is its eigenvalue of multiplicity* 1*.*

Proof. See (Lü et al., 2004). □

Corollary 2.2.3. *Let $\boldsymbol{A} > 0$ denote that the matrix $\boldsymbol{A} \in \mathbb{R}^{N\times N}$ is positive definite, and $\boldsymbol{M} = \mathbb{R}^{N\times N}$ be a block matrix such that*

$$\boldsymbol{M} = \begin{bmatrix} \boldsymbol{A} & \boldsymbol{B} \\ \boldsymbol{C} & \boldsymbol{D} \end{bmatrix} \tag{2.8}$$

where $\boldsymbol{A} \in \mathbb{R}^{K\times K}, \boldsymbol{B} \in \mathbb{R}^{K\times M}, \boldsymbol{C} \in \mathbb{R}^{M\times K}, \boldsymbol{D} \in \mathbb{R}^{M\times M}$, and $K + M = N$. If $\boldsymbol{D}$ is non-singular, we have the following:

- $\boldsymbol{M} > 0 \Leftrightarrow \boldsymbol{D} > 0$ *and* $\boldsymbol{A} - \boldsymbol{B}\boldsymbol{D}^{-1}\boldsymbol{B}^T > 0$
- $\boldsymbol{M} > 0 \Leftrightarrow \boldsymbol{A} > 0$ *and* $\boldsymbol{C} - \boldsymbol{B}^T\boldsymbol{A}^{-1}\boldsymbol{B} > 0$

Proof. See (Zhang, 2006). □

Proposition 2.2.4. *If $\boldsymbol{A} = [a_{ij}] \in \mathbb{R}^{N\times N}$ is an irreducible matrix with rank $N - 1$ and $a_{ij} = a_{ji} \geq 0$ if $i \neq j$ and $\sum_{j=1}^{N} a_{ij} = 0$ for $i = 1, 2, \ldots, N$. Then, the eigenvalues of the matrix*

$$\tilde{\boldsymbol{A}} = \begin{bmatrix} a_{11} - \epsilon & a_{12} & \ldots & a_{1n} \\ a_{21} & a_{22} & \ldots & a_{2n} \\ \vdots & \vdots & \ddots & \vdots \\ a_{n1} & a_{n2} & \ldots & a_{nn} \end{bmatrix} \tag{2.9}$$

is negative for any $\epsilon > 0$.

Proof. See (Chen et al., 2007). □

Theorem 2.2.5 (Courant-Fisher Theorem)**.** *Let $\boldsymbol{A} \in \mathbb{R}^{n\times n}$ be a symmetric matrix with eigenvalues $\lambda_1 \leq \ldots \leq \lambda_n$ and corresponding eigenvectors $\boldsymbol{\nu}_1, \ldots, \boldsymbol{\nu}_n$. Then,*

$$\begin{aligned}
\lambda_1 &= \min_{\|\boldsymbol{x}\|=1} \boldsymbol{x}^T \boldsymbol{A}\boldsymbol{x} = \min_{\boldsymbol{x}\neq 0} \frac{\boldsymbol{x}^T \boldsymbol{A}\boldsymbol{x}}{\boldsymbol{x}^T \boldsymbol{x}} \\
\lambda_2 &= \min_{\|\boldsymbol{x}\|=1, \boldsymbol{x}\perp \boldsymbol{\nu}_1} \boldsymbol{x}^T \boldsymbol{A}\boldsymbol{x} = \min_{\boldsymbol{x}\neq 0, \boldsymbol{x}\perp \boldsymbol{\nu}_1} \frac{\boldsymbol{x}^T \boldsymbol{A}\boldsymbol{x}}{\boldsymbol{x}^T \boldsymbol{x}} \\
\lambda_n &= \lambda_{max} = \max_{\|\boldsymbol{x}\|=1} \boldsymbol{x}^T \boldsymbol{A}\boldsymbol{x} = \min_{\boldsymbol{x}\neq 0} \frac{\boldsymbol{x}^T \boldsymbol{A}\boldsymbol{x}}{\boldsymbol{x}^T \boldsymbol{x}}
\end{aligned} \tag{2.10}$$

In general, for $1 \leq k \leq n$*, let* S_k *denote the span of* $\boldsymbol{\nu}_1, \ldots, \boldsymbol{\nu}_k$ *(with* $S_0 = 0$*), and let* $S_k^{\perp}$ *denote the orthogonal complement of* S_k*. Then,*

$$\lambda_k = \min_{\|\boldsymbol{x}\|=1, \boldsymbol{x}\in S_{k-1}^{\perp}} \boldsymbol{x}^T \boldsymbol{A}\boldsymbol{x} = \min_{\boldsymbol{x}\neq 0, \boldsymbol{x}\in S_{k-1}^{\perp}} \boldsymbol{x}^T \boldsymbol{A}\boldsymbol{x}. \tag{2.11}$$

Proof. See (Bhatia, 2013). □

Corollary 2.2.6. *Since the network in (2.1) is diffusively-coupled, when the full synchronization is achieved, the coupling term drops for each of the node i, and each node dynamics evolves by* $\dot{\boldsymbol{x}}_i(t) = f(\boldsymbol{s}),\ i = 1, 2, \ldots, N$ *for some* $\boldsymbol{s}(t)$ *where* $\dot{\boldsymbol{s}} = f(\boldsymbol{s})$*.*

Proof. Diffusive coupling implies,

$$\sum_{i=1}^{N} \epsilon_{ij} = 0. \tag{2.12}$$

From Definition 2.1.5, there exist some $T > 0$ such that $\boldsymbol{x}_1(t) = \boldsymbol{x}_2(t) = \ldots = \boldsymbol{x}_n(t) \equiv \boldsymbol{s}(t),\ \forall t \geq T$. Using (2.12), when the synchronization manifold is achieved, the network evolves by

$$\dot{\boldsymbol{s}} = f(\boldsymbol{s}) + \sum_{i=1}^{N} \epsilon_{ij} \boldsymbol{P}\boldsymbol{s} = f(\boldsymbol{s}) + \boldsymbol{P}\boldsymbol{s} \sum_{i=1}^{N} \epsilon_{ij} = f(\boldsymbol{s}). \tag{2.13}$$

□

2.3 Variational Equations

Consider the following differential equation

$$\dot{\boldsymbol{x}} = f(\boldsymbol{x}), \quad t > t_0, \quad \boldsymbol{x}(t_0) = \boldsymbol{x}_0 \tag{2.14}$$

Let $\boldsymbol{\phi}(t, t_0, \boldsymbol{\phi}_0)$ denote the solution of (2.14) with initial condition $\boldsymbol{\phi}_0$, i.e.

$$\dot{\boldsymbol{\phi}}(t, t_0, \boldsymbol{\phi}_0) = f(\boldsymbol{\phi}(t, t_0, \boldsymbol{\phi}_0), \quad t > t_0, \quad \boldsymbol{\phi}(t_0, t_0, \boldsymbol{\phi}_0) = \boldsymbol{\phi}_0 \tag{2.15}$$

$\boldsymbol{\psi}(t, t_0, \boldsymbol{\psi}_0)$ denote the solution of (2.14) with initial condition $\boldsymbol{\psi}_0$, i.e.

$$\dot{\boldsymbol{\psi}}(t, t_0, \boldsymbol{\psi}_0) = f(\boldsymbol{\psi}(t, t_0, \boldsymbol{\psi}_0), \quad t > t_0, \quad \boldsymbol{\psi}(t_0, t_0, \boldsymbol{\psi}_0) = \boldsymbol{\psi}_0 \tag{2.16}$$

Here, we assume that $\boldsymbol{\psi}_0 = \boldsymbol{\phi}_0 + \boldsymbol{\delta}_0$ for some $\boldsymbol{\delta}_0 \in \mathbb{R}$ and $\boldsymbol{\psi}_(t, t_0, \boldsymbol{\psi}_0) = \boldsymbol{\phi}_(t, t_0, \boldsymbol{\phi}_0) + \boldsymbol{\delta}(t, t_0, \boldsymbol{\delta}_0)$. $\boldsymbol{\delta}(t_0, t_0, \boldsymbol{\delta}_0) = \boldsymbol{\delta}_0$ and $\boldsymbol{\delta}_0$ is the initial perturbation given to $\boldsymbol{\phi}_0$, and the $\boldsymbol{\psi}(t, t_0, \boldsymbol{\psi}_0)$ is the perturbed solution. The problem is how the initial perturbation $\boldsymbol{\delta}_0$ evolves ad $\boldsymbol{\delta}(t, t_0, \boldsymbol{\delta}_0$. To this end, we start with,

$$\dot{\boldsymbol{\psi}}(t, t_0, \boldsymbol{\psi}_0) = \dot{\boldsymbol{\phi}}(t, t_0, \boldsymbol{\phi}_0) + \dot{\boldsymbol{\delta}}(t, t_0, \boldsymbol{\delta}_0) = f(\boldsymbol{\psi}(t, t_0, \boldsymbol{\psi}_0)) = f(\boldsymbol{\phi}(t, t_0, \boldsymbol{\phi}_0) + \boldsymbol{\delta}(t, t_0, \boldsymbol{\delta}_0)) \tag{2.17}$$

Using the Taylor series expansion of $f(\boldsymbol{\psi}(t, t_0, \boldsymbol{\psi}_0)) = f(\boldsymbol{\phi}(t, t_0, \boldsymbol{\phi}_0) + \boldsymbol{\delta}(t, t_0, \boldsymbol{\delta}_0))$ near the solution $\boldsymbol{\phi}(t, t_0, \boldsymbol{\phi}_0)$,

$$\begin{aligned} \dot{\boldsymbol{\phi}}(t, t_0, \boldsymbol{\phi}_0) + \dot{\boldsymbol{\delta}}(t, t_0, \boldsymbol{\delta}_0) &= f(\boldsymbol{\phi}(t, t_0, \boldsymbol{\phi}_0) + \boldsymbol{\delta}(t, t_0, \boldsymbol{\delta}_0)) \\ &= f(\boldsymbol{\phi}(t, t_0, \boldsymbol{\phi}_0)) + \nabla^T f(\boldsymbol{\phi}(t, t_0, \boldsymbol{\phi}_0))(\boldsymbol{\delta}(t, t_0, \boldsymbol{\delta}_0) \\ &= \dot{\boldsymbol{\phi}}(t, t_0, \boldsymbol{\phi}_0) + Df(\boldsymbol{\phi}(t, t_0, \boldsymbol{\phi}_0))(\boldsymbol{\delta}(t, t_0, \boldsymbol{\delta}_0) \end{aligned} \tag{2.18}$$

which implies

$$\dot{\boldsymbol{\delta}}(t, t_0, \boldsymbol{\delta}_0) = Df(\boldsymbol{\phi}(t, t_0, \boldsymbol{\phi}_0))(\boldsymbol{\delta}(t, t_0, \boldsymbol{\delta}_0) \tag{2.19}$$

2.4 Lyapunov Exponents

Lyapunov exponents quantify the average rate of convergence or divergence of two trajectories that start infinitesimally close. As such, they play a crucial role in the stability analysis of dynamical systems and the quantification of the sensitive dependence of dynamical systems on the initial conditions. For most dynamical systems, we must resort to numerical methods to obtain the Lyapunov exponents.

Let $\boldsymbol{s}$ be a special solution of the system

$$\dot{\boldsymbol{x}} = f(\boldsymbol{x}), \quad \boldsymbol{x}(t_0) = \boldsymbol{x}_0 \in \mathbb{R}^d, \tag{2.20}$$

with the initial condition $\boldsymbol{s}_0$. The matrix variational equation of the system in (2.20) corresponding to $\boldsymbol{s}(t)$ is

$$\dot{\boldsymbol{\Delta}}(t) = Df(\boldsymbol{s})\boldsymbol{\Delta}, \quad \boldsymbol{\Delta}(t_0) = \boldsymbol{\Delta}_0 = \boldsymbol{I}_d, \tag{2.21}$$

where $\boldsymbol{I}_d$ is $d \times d$ identity matrix. The Lyapunov exponent $\mu_i,\ i = 1, 2, \ldots, d$ is defined as (Geist et al., 1990)

$$\mu_i = \ln \lambda_i, \tag{2.22}$$

where λ_i is the eigenvalue of the matrix

$$\mathbf{\Gamma} = \lim_{t \mapsto \infty} (\mathbf{\Delta}^T(t)\mathbf{\Delta}(t))^{1/2t}. \tag{2.23}$$

Geometric interpretation of the Lyapunov spectrum $\{\mu_i | i = 1, 2, \ldots, d\}$ can be associated with the change of the volume V_k a parallelepiped P_k in the tangent space $T_{\boldsymbol{s}}M$ [2] The axis of the parallelepipeds are given by $\tilde{\boldsymbol{e}}_1, \tilde{\boldsymbol{e}}_2, \ldots, \tilde{\boldsymbol{e}}_d$ where $\tilde{\boldsymbol{e}}_l = Df(\boldsymbol{s})\boldsymbol{e}_l,\ l = 1, 2, \ldots, d$ where $\{\boldsymbol{e}_l | l = 1, 2, \ldots, d\}$ is an orthonormal basis for $\mathbb{R}^d$. Let $\mu_1 \leq \mu_2 \leq \ldots \leq \mu_d$. Then, sum of the first k Lyapunov exponents is

$$S_k = \sum_{i=1}^{k} \mu_i = \lim_{t \mapsto \infty} \frac{1}{t} \ln V_k. \tag{2.24}$$

Let k dimensional parallelepiped P be represented by $d \times k$ matrix $\boldsymbol{P} = \begin{bmatrix} \tilde{\boldsymbol{e}}_1 & \tilde{\boldsymbol{e}}_2 & \ldots & \tilde{\boldsymbol{e}}_k \end{bmatrix}$. Then, the volume V_k is (Geist et al., 1990)

$$V_k = \prod_{i=1}^{k} R_{ii}, \tag{2.25}$$

where $\boldsymbol{P} = \boldsymbol{Q}\boldsymbol{R}$ where $\boldsymbol{Q}$ is an orthogonal matrix and $\boldsymbol{R}$ is an upper triangular matrix and R_{ii} is the diagonal elements of $\boldsymbol{R}$. Substituting (2.25) into (2.24),

$$S_k = \sum_{i=1}^{k} \mu_i = \lim_{t \mapsto \infty} \frac{1}{t} \ln V_k = \lim_{t \mapsto \infty} \frac{1}{t} \ln \left(\prod_{i=1}^{k} R_{ii} \right) = \lim_{t \mapsto \infty} \frac{1}{t} \left(\sum_{i=1}^{k} \ln R_{ii} \right) \tag{2.26}$$

which implies

$$\mu_i = \lim_{t \mapsto \infty} \frac{1}{t} \ln R_{ii}. \tag{2.27}$$

[2] Let M be a k times differentiable manifold in $\mathbb{R}^d$ and let $\boldsymbol{x} \in M$. Tangent space of M at $\boldsymbol{x}$, denoted by $T_{\boldsymbol{x}}M$, is the set of all tangent vectors at $\boldsymbol{x}$.

We need to solve the differential equations

$$\dot{\boldsymbol{s}} = f(\boldsymbol{s}), \quad \boldsymbol{s}(t_0) = \boldsymbol{s}_0 \in \mathbb{R}^d \tag{2.28}$$

$$\dot{\boldsymbol{\Delta}} = Df(\boldsymbol{s})\boldsymbol{\Delta}, \quad \boldsymbol{\Delta}(t_0) = \boldsymbol{\Delta}_0 = \boldsymbol{I}_d \tag{2.29}$$

numerically to obtain the Lyapunov exponents. Let the system be solved for a time duration $(0, T)$ with a step size of δt seconds where $T = n\delta t$ and let $t_j = j\delta t$. Thus, R_{ii} in (2.27) can be found as

$$R_{ii} = \prod_{j=0}^{n-1} R_{ii}^j \tag{2.30}$$

where $\boldsymbol{P}^j = \boldsymbol{Q}^j\boldsymbol{R}^j$ is the parallelepiped at time t_j, and R_{ii}^j is the diagonal elements of $\boldsymbol{R}^j$. Substituting (2.30) into (2.27), we have

$$\mu_i = \frac{1}{\delta t} \lim_{n\mapsto\infty} \frac{1}{n} \sum_{j=0}^{n-1} \ln R_{ii}^j \tag{2.31}$$

Obviously, we need to compute (2.31) for a finite interval of $(0, T)$. Thus, we have

$$\mu_i \approx \frac{1}{\delta t} \frac{1}{n} \sum_{j=0}^{n-1} \ln R_{ii}^j. \tag{2.32}$$

2.5 Master Stability Function

The network in (2.1) can be represented more compactly as

$$\dot{\boldsymbol{X}} = F(\boldsymbol{X}) + (\boldsymbol{E} \otimes \boldsymbol{P})\boldsymbol{X}, \tag{2.33}$$

where $\boldsymbol{X} = [\boldsymbol{x}_1^T, \boldsymbol{x}_2^T \ldots, \boldsymbol{x}_N^T]T$, $F(\boldsymbol{X}) = [f(\boldsymbol{x}_1)^T, f(\boldsymbol{x}_2)^T, \ldots, f(\boldsymbol{x}_N)^T]^T$. Here, $\boldsymbol{x}^T$

denotes the transpose of $\boldsymbol{x}$ and $\otimes$ denotes the Kronecker product of two matrices.

Let $\boldsymbol{S} = [\boldsymbol{s}^T, \boldsymbol{s}^T, \ldots, \boldsymbol{s}^T]^T \in \mathbb{R}^{Nd}$. The variational equation for (2.33) with respect to $\boldsymbol{S}$ is

$$\dot{\boldsymbol{\Delta}} = (DF(\boldsymbol{S}) + (\boldsymbol{E} \otimes \boldsymbol{P}))\boldsymbol{\Delta}, \tag{2.34}$$

where $\boldsymbol{\Delta} = [\boldsymbol{\delta_1}^T, \boldsymbol{\delta_2}^T, \ldots, \boldsymbol{\delta_N}^T]$, and $DF(\boldsymbol{S}) = \nabla^T F(\boldsymbol{S})$ where $F(\boldsymbol{X}) = [F_1(\boldsymbol{X}), F_2(\boldsymbol{X}), \ldots, F_N(\boldsymbol{X})]^T = [f(\boldsymbol{x}_1), f(\boldsymbol{x}_2), \ldots, f(\boldsymbol{x}_N)]^T$. Thus,

$$\nabla F(\boldsymbol{X}) = \begin{bmatrix} \frac{\partial F_1(\boldsymbol{X})}{\partial \boldsymbol{x}_1} & \frac{\partial F_2(\boldsymbol{X})}{\partial \boldsymbol{x}_1} & \cdots & \frac{\partial F_N(\boldsymbol{X})}{\partial \boldsymbol{x}_1} \\ \frac{\partial F_1(\boldsymbol{X})}{\partial \boldsymbol{x}_2} & \frac{\partial F_2(\boldsymbol{X})}{\partial \boldsymbol{x}_2} & \cdots & \frac{\partial F_N(\boldsymbol{X})}{\partial \boldsymbol{x}_2} \\ \vdots & \vdots & \ddots & \vdots \\ \frac{\partial F_1(\boldsymbol{X})}{\partial \boldsymbol{x}_N} & \frac{\partial F_2(\boldsymbol{X})}{\partial \boldsymbol{x}_N} & \cdots & \frac{\partial F_N(\boldsymbol{X})}{\partial \boldsymbol{x}_N}, \end{bmatrix} \tag{2.35}$$

where $\boldsymbol{x}_j = [x_j^{(1)}, \ldots, x_j^{(d)}]$, and

$$\frac{\partial F_i(\boldsymbol{X})}{\partial \boldsymbol{x}_j} = \begin{bmatrix} \frac{\partial f(\boldsymbol{x}_i)}{\partial x_j^{(1)}} & \cdots & \frac{\partial f(\boldsymbol{x}_i)}{\partial x_j^{(d)}} \end{bmatrix}^T. \tag{2.36}$$

We have

$$j \neq i \quad \Rightarrow \quad \frac{\partial f(x_i)}{\partial x_j^{(1)}} = [0, \ldots, 0]^T. \tag{2.37}$$

From (2.36) and (2.37), (2.35) can be written in block diagonal form

$$\nabla F(\boldsymbol{X}) = \begin{bmatrix} \frac{\partial F_1(\boldsymbol{X})}{\partial \boldsymbol{x}_1} & 0 & \dots & 0 \\ 0 & \frac{\partial F_2(\boldsymbol{X})}{\partial \boldsymbol{x}_2} & \dots & 0 \\ \vdots & \vdots & \ddots & \vdots \\ 0 & 0 & \dots & \frac{\partial F_n(\boldsymbol{X})}{\partial \boldsymbol{x}_N} \end{bmatrix} = \begin{bmatrix} \frac{\partial f(\boldsymbol{x}_1)}{\partial \boldsymbol{x}_1} & 0 & \dots & 0 \\ 0 & \frac{\partial f(\boldsymbol{x}_2)}{\partial \boldsymbol{x}_2} & \dots & 0 \\ \vdots & \vdots & \ddots & \vdots \\ 0 & 0 & \dots & \frac{\partial f(\boldsymbol{x}_N)}{\partial \boldsymbol{x}_N} \end{bmatrix}$$
$$= \begin{bmatrix} \nabla f(\boldsymbol{x}_1) & 0 & \dots & 0 \\ 0 & \nabla f(\boldsymbol{x}_2) & \dots & 0 \\ \vdots & \vdots & \ddots & \vdots \\ 0 & 0 & \dots & \nabla f(\boldsymbol{x}_N) \end{bmatrix}. \tag{2.38}$$

Thus,

$$DF(\boldsymbol{X}) = \nabla^T F(\boldsymbol{X}) = \begin{bmatrix} Df(\boldsymbol{x}_1) & 0 & \dots & 0 \\ 0 & Df(\boldsymbol{x}_2) & \dots & 0 \\ \vdots & \vdots & \ddots & \vdots \\ 0 & 0 & \dots & Df(\boldsymbol{x}_N) \end{bmatrix}, \tag{2.39}$$

which implies

$$DF(\boldsymbol{S}) = \begin{bmatrix} Df(\boldsymbol{s}) & 0 & \dots & 0 \\ 0 & Df(\boldsymbol{s}) & \dots & 0 \\ \vdots & \vdots & \ddots & \vdots \\ 0 & 0 & \dots & Df(\boldsymbol{s}) \end{bmatrix} = \boldsymbol{I}_N \otimes Df(\boldsymbol{s}), \tag{2.40}$$

where $\boldsymbol{I}_N$ is $N \times N$ identity matrix. Substituting (2.40) into (2.34),

$$\dot{\boldsymbol{\Delta}} = (\boldsymbol{I}_N \otimes Df(\boldsymbol{s}) + \boldsymbol{E} \otimes \boldsymbol{P})\boldsymbol{\Delta}. \tag{2.41}$$

Let $\boldsymbol{L}$ be the diagonalizing matrix for $\boldsymbol{E}$ such that $\boldsymbol{L}\boldsymbol{E}\boldsymbol{L}^{-1} = diag(\lambda_1, \ldots, \lambda_n) = \boldsymbol{\Lambda}$. Multiplying both sides of (2.41) by $\boldsymbol{L}^{-1} \otimes \boldsymbol{I}_d$, we have

$$\begin{aligned}
(\boldsymbol{L}^{-1} \otimes \boldsymbol{I}_d)\dot{\boldsymbol{\Delta}} &= (\boldsymbol{L}^{-1} \otimes \boldsymbol{I}_d)(\boldsymbol{I}_N \otimes Df(\boldsymbol{s}) + \boldsymbol{E} \otimes \boldsymbol{P})\boldsymbol{\Delta} \\
&= (\boldsymbol{L}^{-1} \otimes \boldsymbol{I}_d)(\boldsymbol{I}_N \otimes Df(\boldsymbol{s}))\boldsymbol{\Delta} + (\boldsymbol{L}^{-1} \otimes \boldsymbol{I}_d)(\boldsymbol{E} \otimes \boldsymbol{P})\boldsymbol{\Delta} \\
&= (\boldsymbol{I}_N \otimes Df(\boldsymbol{s}))(\boldsymbol{L}^{-1} \otimes \boldsymbol{I}_d)\boldsymbol{\Delta} + (\boldsymbol{L}^{-1}\boldsymbol{E}) \otimes (\boldsymbol{I}_d\boldsymbol{P})\boldsymbol{\Delta} \\
&= (\boldsymbol{I}_N \otimes Df(\boldsymbol{s}))(\boldsymbol{L}^{-1} \otimes \boldsymbol{I}_d)\boldsymbol{\Delta} + (\boldsymbol{L}^{-1}\boldsymbol{L}\boldsymbol{\Lambda}\boldsymbol{L}^{-1}) \otimes (\boldsymbol{P}\boldsymbol{I}_d)\boldsymbol{\Delta} \\
&= (\boldsymbol{I}_N \otimes Df(\boldsymbol{s}))(\boldsymbol{L}^{-1} \otimes \boldsymbol{I}_d)\boldsymbol{\Delta} + (\boldsymbol{\Lambda}\boldsymbol{L}^{-1}) \otimes (\boldsymbol{P}\boldsymbol{I}_d)\boldsymbol{\Delta} \\
&= (\boldsymbol{I}_N \otimes Df(\boldsymbol{s}))(\boldsymbol{L}^{-1} \otimes \boldsymbol{I}_d)\boldsymbol{\Delta} + (\boldsymbol{\Lambda} \otimes \boldsymbol{P})(\boldsymbol{L}^{-1} \otimes \boldsymbol{I}_d)\boldsymbol{\Delta}.
\end{aligned} \tag{2.42}$$

Using the change of variable $(\boldsymbol{L}^{-1} \otimes \boldsymbol{I}_d)\boldsymbol{\Delta} = \boldsymbol{\Xi}$, we have

$$\dot{\boldsymbol{\Xi}} = (\boldsymbol{I}_N \otimes Df(\boldsymbol{s}) + \boldsymbol{\Lambda} \otimes \boldsymbol{P})\boldsymbol{\Xi}, \tag{2.43}$$

where $\boldsymbol{\Xi} = [\boldsymbol{\xi}_1, \ldots, \boldsymbol{\xi}_N]^T$. The block (2.43) can be written as

$$\dot{\boldsymbol{\xi}}_k = (Df(\boldsymbol{s}) + \lambda_k \boldsymbol{P})\boldsymbol{x}_k, \quad k = 1, \ldots, N, \tag{2.44}$$

where λ_k, $k = 1, \ldots, N$ are the eigenvalues of $\boldsymbol{E}$. $\lambda_1 = 0$ is an eigenvalue of $\boldsymbol{E}$ corresponding to eigenvector $\boldsymbol{\nu}_1 = [1, \ldots, 1]^T$. To see this, let $\boldsymbol{e}_1, \boldsymbol{e}_2, \ldots, \boldsymbol{e}_N$ be the columns of $\boldsymbol{E}$. Then,

$$\boldsymbol{E}\boldsymbol{\nu}_1 = \begin{bmatrix} \boldsymbol{e}_1 & \boldsymbol{e}_2 & \ldots & \boldsymbol{e}_N \end{bmatrix} \begin{bmatrix} 1 & 1 & \ldots & 1 \end{bmatrix}^T = \boldsymbol{e}_1 + \boldsymbol{e}_2 + \ldots + \boldsymbol{e}_N \tag{2.45}$$

$$= \begin{bmatrix} \sum_{i=1}^{N} \epsilon_{1j} & \sum_{i=1}^{N} \epsilon_{2j} & \ldots & \sum_{i=1}^{n} \epsilon_{Nj} \end{bmatrix} = 0\boldsymbol{\nu}_1. \tag{2.46}$$

$\lambda_1 = 0$ corresponds the longitudinal direction along the synchronization manifold since $\dot{\boldsymbol{\xi}}_1 = Df(\boldsymbol{s})\boldsymbol{\xi}_1$. Other modes corresponding to $\lambda_k,\ k = 2, \ldots, N$ corresponds to the transversal modes and the synchronization manifold is asymptotically stable if the maximum Lyapunov exponents μ_k of the systems

$$\dot{\boldsymbol{\xi}}_k = (Df(\boldsymbol{s}) + \lambda_k \boldsymbol{P})\boldsymbol{\xi}_k, \quad k = 2, \ldots, N, \tag{2.47}$$

satisfies $\mu_k \leq 0$ implying that $\|\boldsymbol{\xi}_k\| = 0$ as $t \mapsto \infty$ for $k = 2, \ldots, N$.

The synchronization condition depends on the calculation of the Lyapunov exponents of the variational equation, which depends on the node dynamics and the calculation of the eigenvalues of the connectivity matrix of the network and, therefore, depends on the network topology.

The systems in (2.47) are completely identical apart from the eigenvalue λ_k. Therefore, given that the node dynamics f, the inner coupling matrix $\boldsymbol{P}$, we can define the master stability function $\mu = g(\lambda)$ where μ is the maximum Lyapunov exponents using the generic system (Huang et al., 2009)

$$\dot{\boldsymbol{\xi}} = (Df(\boldsymbol{s}) + \lambda \boldsymbol{P})\boldsymbol{\xi}. \tag{2.48}$$

CHAPTER THREE
PINNING CONTROL

In this chapter, the pinning control techniques have been presented. Since the literature on pinning control is too extensive to be explained in detail in a single chapter, the material presented in this chapter has been kept to include the ones focused on directed and undirected networks to achieve cluster synchronization.

3.1 Introduction to Pinning Control

In the real world, the systems do not exist in isolation. Instead, they interact with each other, forming interconnected networks. Examples of these complex networks include biological neural networks, computer networks, social relations networks, electrical power grids, and the Internet. Complex networks can be described as networks comprised of numerous high-dimensional nodes connected to each other through a multitude of edges. The connections between these nodes can be infinite or irregular and may exhibit nonlinear and time-varying behavior. While simple networks with regular topologies, such as lattice, ring, star, or fully-connected structures, provide researchers with a platform to explore complexities arising from node dynamics, they fail to model many real-world networks accurately. Consequently, the emergence of random graphs, small-world networks, and scale-free networks has fueled interest in network science. Researchers from various fields of science and engineering are increasingly drawn to network science due to its remarkable properties and potential applications in various scientific realms.

Concurrent with the advancements in network science, control theory, which is a well-established field within systems theory, has also made significant strides. Controllability, in particular, focuses on determining whether a system is controllable and, if not, under what conditions it may become controllable. However, classical control theory has traditionally centered on individual systems and their dynamics, mostly overlooking the inherent complexities and directionalities intrinsic to their topologies. While this may not pose a significant issue for small networks with simple topologies, as the complexity of the network increases, achieving individual control

over all nodes becomes prohibitively expensive or even practically infeasible. In such cases, leveraging the network's topological properties explicitly can enhance the practical feasibility of control solutions. To this end, pinning control has emerged as an effective control strategy that uniquely addresses node dynamics and network topology.

Pinning control has been inspired by biological observations, such as the remarkable behavior of the worm C. elegans, which only needs to activate less than 17% of its neurons to elicit a response in its entire body. Additionally, in fish schools, a small group of informed individuals play a significant role in determining the foraging behavior of the entire group. Similarly, within honeybee swarms, a mere 5% of specialized individuals can guide the group towards a new nest site (Chen, 2014).

These examples prove that a few individuals can effectively control a complex network's collective behavior. Utilizing this control strategy is more efficient and practical than attempting to control each individual within the network. However, several unanswered questions persist in this context: What is the optimal number of these specialized individuals, and how should they be chosen from the entire network? To address these questions, pinning control was introduced (Chen, 2014).

To formally present the concept of pinning control, it is necessary to establish a well-defined framework within the domain of control theory. In this regard, let us consider a network that consists of high-dimensional nonlinear dynamical systems as its nodes. The network can have either a directed or an undirected nature, and it possesses a specific topology, such as regular, random, small-world, or scale-free.

Assuming that the control objective is defined over the network nodes, for instance, achieving synchronization, it is crucial to ascertain the requirements associated with this objective. These requirements may involve achieving synchronization within a finite time frame or minimizing control energy expenditure.

The present framework aims to ascertain the optimal number and placement of controllers within a network to achieve the desired control objective. This particular

problem is known as pinning control. The overall performance can be optimized by strategically determining the number and locations of the controllers. The solution to this problem is contingent upon the individual nodes' dynamics and the underlying network topology.

3.2 Cluster Synchronization in Undirected Networks

Consider an undirected network defined in Definition 2.1.3. When the pinning control is introduced, the controlled network evolves by

$$\begin{aligned} \dot{\boldsymbol{x}}_i &= f(\boldsymbol{x}_i) + \sum_{j=1}^{N} \epsilon_{ij} \boldsymbol{P} \boldsymbol{x}_j + \boldsymbol{u}_i, \quad i \in \mathcal{J}, \\ \dot{\boldsymbol{x}}_i &= f(\boldsymbol{x}_i) + \sum_{j=1}^{N} \epsilon_{ij} \boldsymbol{P} \boldsymbol{x}_j, \quad i \notin \mathcal{J}. \end{aligned} \tag{3.1}$$

where $\mathcal{J} \subset \mathcal{N} = \{1, \ldots, N\}$ denotes the set of pinned (controlled) nodes, and $\boldsymbol{u}_i$ is the control on the i-th node. Let $\mathcal{G}_1 = \{1, \ldots, k_1\}, \mathcal{G}_2 = \{k_1 + 1, \ldots, k_1 + k_2\}, \ldots, \mathcal{G}_L = \{k_1 + \cdots + k_{L-1} + 1, \ldots, k_1 + \cdots + k_L\}$ such that $\mathcal{G}_i \neq \mathcal{G}_j$ if $i \neq j$, $\cup_{l=1}^{L} \mathcal{G}_l = \mathcal{N}$ and $\sum_{i=1}^{L} k_l = N$. Assume L special solutions $\boldsymbol{s}_1, \boldsymbol{s}_2, \ldots, \boldsymbol{s}_L$ where $\dot{\boldsymbol{s}}_i = f(\boldsymbol{s}_i),\ i = 1, 2, \ldots, L$, and $\lim_{t \mapsto \infty} \|\boldsymbol{s}_i(t) - \boldsymbol{s}_j(t)\| \neq 0$ for $i \neq j$. Let $\boldsymbol{P} = \boldsymbol{I}_d$, $\mathcal{J} = \{k_1, k_1 + k_2, \ldots, k_1 + \cdots + k_L\}$, and

$$\boldsymbol{u}_{k_1 + k_2 + \cdots + k_l} = -\alpha_l (\boldsymbol{x}_{k_1 + k_2 + \cdots + k_l} - \boldsymbol{s}_l), \quad l = 1, 2, \ldots, L \tag{3.2}$$

where $\boldsymbol{I}_d$ is $d \times d$ dimensional identity matrix, and $\alpha_l,\ l = 1, 2, \ldots, L$ are control strengths. Then, we can define the following pinned network

$$\begin{aligned}\dot{\boldsymbol{x}}_i &= f(\boldsymbol{x}_i) + \sum_{j=1}^{N} \epsilon_{ij}\boldsymbol{x}_j - \alpha_{\hat{i}}(\boldsymbol{x}_i - \boldsymbol{s}_{\hat{i}}) \quad i \in \mathcal{J}, \\ \dot{\boldsymbol{x}}_i &= f(\boldsymbol{x}_i) + \sum_{j=1}^{N} \epsilon_{ij}\boldsymbol{x}_j \quad i \notin \mathcal{J}.\end{aligned} \tag{3.3}$$

The problem is finding the sufficient conditions to ensure the cluster synchronization represented by the manifold in (2.5).

Theorem 3.2.1. *(Wu et al., 2009) Suppose the coupling matrix $\boldsymbol{E} = [\epsilon_{ij}]$ in (3.3) satisfies $\boldsymbol{E} \in \mathbb{E}_1$. Let $\boldsymbol{\Delta} = diag(\delta_1, \delta_2, \ldots, \delta_d)$ be a diagonal matrix and $\boldsymbol{P} = diag(p_1, p_2, \ldots, p_d)$ be a positive definite matrix such that $f \in QUAD(\boldsymbol{\Delta}, \boldsymbol{P})$. If*

$$\boldsymbol{E} + \delta_i \boldsymbol{I}_N - \boldsymbol{A} \leq 0, \quad i = 1, 2, \ldots, d, \tag{3.4}$$

where $\boldsymbol{I}_N \in \mathbb{R}^{N\times N}$ is the identity matrix, $\boldsymbol{A} = diag(a_1, a_2, \ldots, a_N) \in \mathbb{R}^{N\times N}$ is the diagonal matrix with entries $a_{k_1} = \alpha_1,\ a_{k_1+k_2} = \alpha_2, \ldots, a_{k_1+k_2+\cdots+k_L} = \alpha_L$ and $a_i = 0$ if $i \notin \mathcal{J}$, then for any initial values cluster synchronization represented by the manifold in (2.5) can be realized in the network in (3.3).

Proof. See Wu et al. (2009). □

From Theorem (3.2.1),

1. Under the assumption of $\boldsymbol{E} \in \mathbb{E}_1$, the cluster synchronization manifold $\mathcal{M}$ in (2.5) is an invariant manifold of the coupled system. In addition, it is clear that when $\boldsymbol{E} \in \mathbb{E}_1$, each block $\boldsymbol{E}_{ij}$ in block form in (2.7) has nonzero elements or is a zero matrix. For $i \neq j$, if $\epsilon_{\tilde{i}\tilde{j}} \leq 0$ with $\tilde{i} \in \mathcal{G}_i$ and $\tilde{j} \in \mathcal{G}_j$, then the coupling between $\tilde{i}$ and $\tilde{j}$ is called inhibitory coupling, which can be regarded a mechanism to desynchronize $\tilde{i}$ and $\tilde{j}$.

2. It can be seen that, in order to realize cluster synchronization, we should

(a) construct a coupling matrix $\boldsymbol{E} \in \mathbb{E}_1$,

(b) select control strengths $\alpha_1, \alpha_2, \ldots, \alpha_L > 0$ such that the matrix inequality in (3.4) is satisfied.

In the following, an efficient construction method to ensure the matrix inequality in (3.4) is given.

Lemma 3.2.2. *Suppose that $\boldsymbol{B} \in \mathbb{E}_1$ and $\boldsymbol{E} = diag(0, 0, \ldots, 0, \epsilon)$ with $\epsilon > 0$ are two matrices of size $N \times N$. Then, $\boldsymbol{B} - \boldsymbol{E}$ is negative definite.*

Proof. See Proposition 2.2.4 □

Lemma 3.2.3. *For a matrix $\boldsymbol{\Phi} = [\phi_{ij}] \in \mathbb{R}^{M \times N}$, let*

$$\mu(\boldsymbol{\Phi}) \triangleq \frac{1}{2} \max\{M, N\} \max_{i,j} |\phi_{ij}|, \tag{3.5}$$

and $\lambda_{max}(\boldsymbol{\Phi})$ denote the maximal eigenvalue of $\boldsymbol{\Phi}$. Then,

$$\boldsymbol{x}^T \boldsymbol{\Phi} \boldsymbol{y} \leq \mu(\boldsymbol{\Phi})(\boldsymbol{x}^T \boldsymbol{x} + \boldsymbol{y}^T \boldsymbol{y}) \quad \forall \boldsymbol{x} \in \mathbb{R}^M, \quad \forall \boldsymbol{y} \in \mathbb{R}^N \tag{3.6}$$

Proof. Denote $\boldsymbol{x} = [x_1, x_2 \ldots, x_M]$, $\boldsymbol{y} = [y_1, y_2, \ldots, y_N]$, $\boldsymbol{B} = [b_{ij}] \in \mathbb{R}^{M \times N}$

$$\boldsymbol{x}^T \boldsymbol{B} \boldsymbol{y} = \sum_{i=1}^{M} \sum_{j=1}^{N} x_i b_{ij} y_j \leq \sum_{i=1}^{M} \sum_{j=1}^{N} |x_i y_j| |b_{ij}| \leq \max_{i,j} b_{ij} \sum_{i=1}^{M} \sum_{j=1}^{N} |x_i y_j|. \tag{3.7}$$

We have

$$\begin{aligned} 0 \leq (x_i + y_j)^2 &= \left(x_i^2 + y_i^2 + 2x_i y_j\right) \quad \Rightarrow \quad 2x_i y_j \leq -\left(x_i^2 + y_j^2\right), \\ 0 \leq (x_i - y_j)^2 &= \left(x_i^2 + y_i^2 - 2x_i y_j\right) \quad \Rightarrow \quad 2x_i y_j \leq \left(x_i^2 + y_j^2\right). \end{aligned} \tag{3.8}$$

Hence,

$$|x_i y_j| \leq \frac{1}{2}|\left(x_i^2 + y_j^2\right)| = \frac{1}{2}\left(x_i^2 + y_j^2\right). \tag{3.9}$$

Therefore, (3.7) can be rewritten as

$$\begin{aligned}
\boldsymbol{x}^T \boldsymbol{B}\boldsymbol{y} &\leq \max_{i,j} b_{ij} \sum_{i=1}^{M}\sum_{j=1}^{N} \frac{1}{2}\left(x_i^2 + y_j^2\right) = \frac{1}{2}\max_{i,j} b_{ij}\left(\sum_{i=1}^{M}\sum_{j=1}^{N} x_i^2 + \sum_{i=1}^{M}\sum_{j=1}^{N} y_j^2\right) \\
&= \frac{1}{2}\max_{i,j} b_{ij}\left(N\sum_{i=1}^{M} x_i^2 + M\sum_{j=1}^{N} y_j^2\right) \leq \frac{1}{2}\max\{M,N\}\max_{i,j} b_{ij}\left(\sum_{i=1}^{M} x_i^2 + \sum_{j=1}^{N} y_j^2\right) \\
&= \frac{1}{2}\max\{M,N\}\max_{i,j} b_{ij}\left(\boldsymbol{x}^T\boldsymbol{x} + \boldsymbol{y}^T\boldsymbol{y}\right) = \mu(\boldsymbol{B})\left(\boldsymbol{x}^T\boldsymbol{x} + \boldsymbol{y}^T\boldsymbol{y}\right).
\end{aligned} \tag{3.10}$$

□

Theorem 3.2.4. *(Wu et al., 2009) Suppose that γ_i, $i = 1, 2, \ldots, L$ are L positive constants and that*

$$\boldsymbol{\Phi} = \begin{bmatrix} \boldsymbol{\Phi}_{11} & \boldsymbol{\Phi}_{12} & \ldots & \boldsymbol{\Phi}_{1L} \\ \boldsymbol{\Phi}_{21} & \boldsymbol{\Phi}_{22} & \ldots & \boldsymbol{\Phi}_{2L} \\ \vdots & \vdots & \ddots & \vdots \\ \boldsymbol{\Phi}_{L1} & \boldsymbol{\Phi}_{L2} & \ldots & \boldsymbol{\Phi}_{LL} \end{bmatrix} \in \mathbb{E}_2, \tag{3.11}$$

where $\boldsymbol{\Phi}_{ij} \in \mathbb{R}^{k_i \times k_j}$, $i, j = 1, \ldots, L$. Denote $\boldsymbol{\Gamma}_i = diag(0, 0, \ldots, 0, \gamma_i) \in \mathbb{R}^{k_i \times k_i}$, $i = 1, 2, \ldots, L$. We pick the coupling matrix

$$\boldsymbol{E} = \begin{bmatrix} \beta\boldsymbol{\Phi}_{11} & \boldsymbol{\Phi}_{12} & \ldots & \boldsymbol{\Phi}_{1L} \\ \boldsymbol{\Phi}_{21} & \beta\boldsymbol{\Phi}_{22} & \ldots & \boldsymbol{\Phi}_{2L} \\ \vdots & \vdots & \ddots & \vdots \\ \boldsymbol{\Phi}_{L1} & \boldsymbol{\Phi}_{L2} & \ldots & \beta\boldsymbol{\Phi}_{LL} \end{bmatrix}, \tag{3.12}$$

and the control strengths

$$\alpha_i = \beta\gamma_i \quad i = 1, 2, \ldots, L, \tag{3.13}$$

where β is a positive constant. For a diagonal matrix $\boldsymbol{\Delta} = diag(\delta_1, \delta_2, \ldots, \delta_d)$ if the coupling strength β satisfies,

$$\beta \geq \max_{1 \leq i \leq L} \beta_i, \tag{3.14}$$

where

$$\beta_i \triangleq \frac{\max\limits_{1 \leq k \leq d} \delta_k + 2(L-1) \max\limits_{u \neq v} \mu(\boldsymbol{\Phi}_{uv})}{-\lambda_{max}(\boldsymbol{\Phi}_{ii} - \boldsymbol{\Gamma}_i)}, \tag{3.15}$$

then the matrix inequality in (3.4) is satisfied.

Proof. See Wu et al. (2009) □

Based on Theorem 3.2.4, the construction method to achieve the desired cluster pattern can be divided into three steps:

1. Arbitrarily choose a matrix $\boldsymbol{\Phi} \in \mathbb{E}_2$ and L positive constants $\gamma_1, \gamma_2, \ldots, \gamma_L$.
2. Construct the coupling matrix $\boldsymbol{E}$ as in (3.12) and select the control strengths as in (3.13). Since $\boldsymbol{\Phi} \in \mathbb{E}_2$, it is clear that $\boldsymbol{E} \in \mathbb{E}_1$
3. Pick a coupling strength β as in (3.14).

Theorem 3.2.5. *(Wu et al., 2009) Suppose that $\gamma_i,\ i = 1, 2, \ldots, L$ positive constants and that*

$$\boldsymbol{\Phi} = \begin{bmatrix} \boldsymbol{\Phi}_{11} & \boldsymbol{\Phi}_{12} & \ldots & \boldsymbol{\Phi}_{1L} \\ \boldsymbol{\Phi}_{21} & \boldsymbol{\Phi}_{22} & \ldots & \boldsymbol{\Phi}_{2L} \\ \vdots & \vdots & \ddots & \vdots \\ \boldsymbol{\Phi}_{L1} & \boldsymbol{\Phi}_{L2} & \ldots & \boldsymbol{\Phi}_{LL} \end{bmatrix} \in \mathbb{E}_2, \tag{3.16}$$

where $\mathbf{\Phi}_{ij} \in \mathbb{R}^{k_i \times k_j},\ i, j = 1, \ldots, L$. *We pick the coupling matrix*

$$\boldsymbol{E}(t) = \begin{bmatrix} \beta(t)\mathbf{\Phi}_{11} & \mathbf{\Phi}_{12} & \ldots & \mathbf{\Phi}_{1L} \\ \mathbf{\Phi}_{21} & \beta(t)\mathbf{\Phi}_{22} & \ldots & \mathbf{\Phi}_{2L} \\ \vdots & \vdots & \ddots & \vdots \\ \mathbf{\Phi}_{L1} & \mathbf{\Phi}_{L2} & \ldots & \beta(t)\mathbf{\Phi}_{LL} \end{bmatrix}, \tag{3.17}$$

and the control strengths

$$\alpha_i(t) = \beta(t)\gamma_i \quad i = 1, 2, \ldots, L, \tag{3.18}$$

where $\beta(t)$ *is the adaptive coupling strength. Let* $\mathbf{\Delta} = diag(\delta_1, \delta_2, \ldots, \delta_d)$ *be diagonal matrix and* $\boldsymbol{P} = diag(p_1, p_2, \ldots, p_d) \in \mathbb{R}^{d \times d}$ *be positive definite diagonal matrix such that* $f \in QUAD(\boldsymbol{P}, \mathbf{\Delta})$. *Then, the coupled system*

$$\begin{aligned} \dot{\boldsymbol{x}}_i(t) &= f(\boldsymbol{x}_i(t)) + \sum_{j=1}^{N} \epsilon_{ij}(t)\boldsymbol{x}_j(t) - \alpha_{\hat{i}}(t)(\boldsymbol{x}_i(t) - \boldsymbol{s}_{\hat{i}}(t)), \quad i \in J, \\ \dot{\boldsymbol{x}}_i(t) &= f(\boldsymbol{x}_i(t)) + \sum_{j=1}^{N} \epsilon_{ij}(t)\boldsymbol{x}_j(t), \quad i \notin J, \\ \dot{\beta}(t) &= \frac{\eta}{2} \sum_{i=1}^{N} \boldsymbol{e}_i^T \boldsymbol{P} \boldsymbol{e}_i, \end{aligned} \tag{3.19}$$

where $\beta(0) \geq 0$ *and* $\eta > 0$, *can achieve the cluster synchronization represented by the manifold (2.5).*

Proof. See Wu et al. (2009) □

With the material presented in this section, it is possible to design a network in which some controllable cluster patterns are ensured. However, the main drawback of this method is that it requires the outer coupling matrix $\boldsymbol{E}$ to be partitioned into sub-blocks, each of which is zero-row-sums. This constitutes quite a restriction on

controlling a network to manifest various cluster patterns because the zero-row-sum property of each block is challenging to satisfy for all desired cluster patterns.

3.3 Cluster Synchronization in Directed Networks

Consider a directed network defined in Definition 2.1.4 where $\epsilon > 0$ and $\boldsymbol{E} = \epsilon\boldsymbol{\Xi} = \epsilon[\xi_{ij}]$. The problem is to find appropriate controllers such that the cluster synchronization represented by the manifold in Definition 2.1.8 is achieved in the network.

If pinning controllers are applied, we have,

$$\dot{\boldsymbol{x}}_i = f(\boldsymbol{x}_i) + \epsilon \sum_{j=1}^{N} \xi_{ij} \boldsymbol{P} \boldsymbol{x}_j + \boldsymbol{u}_i, \quad i = 1, \ldots, N, \tag{3.20}$$

where the form of the pinning controllers is to be determined. The dynamics of the error $\boldsymbol{e}_i(t) = \boldsymbol{x}_i(t) - \boldsymbol{s}_{\hat{i}}(t)$ is found as

$$\begin{aligned} \dot{\boldsymbol{e}}_i &= f(\boldsymbol{x}_i) + \epsilon \sum_{j=1}^{N} \xi_{ij} \boldsymbol{P} \boldsymbol{x}_j + \boldsymbol{u}_i - f(\boldsymbol{x}_{\hat{i}}) \\ &= f(\boldsymbol{x}_i) - f(\boldsymbol{x}_{\hat{i}}) + \epsilon \sum_{j=1}^{N} \xi_{ij} \boldsymbol{P} \boldsymbol{x}_j + \boldsymbol{u}_i \pm \epsilon \sum_{j=1}^{N} \xi_{ij} \boldsymbol{P} \boldsymbol{s}_{\hat{j}} \\ &= f(\boldsymbol{x}_i) - f(\boldsymbol{x}_{\hat{i}}) + \epsilon \sum_{j=1}^{N} \xi_{ij} \boldsymbol{P} \boldsymbol{e}_j + \epsilon \sum_{j=1}^{N} \xi_{ij} \boldsymbol{P} \boldsymbol{s}_{\hat{j}} + \boldsymbol{u}_i. \end{aligned} \tag{3.21}$$

Lemma 3.3.1. *(Ma & Lu, 2013) If node i is an intra-act node, i.e., $i \in \mathcal{G}_{\hat{i}}^{intra}$, then the following holds*

$$\epsilon \sum_{j=1}^{n} \xi_{ij} \boldsymbol{P} s_{\hat{j}} = 0. \tag{3.22}$$

Proof. See (Ma & Lu, 2013) □

Inspired by the concept of inter-act and intra-act nodes defined in Definition 2.1.12, consider the following pinning controllers are used (Ma & Lu, 2013)

$$\boldsymbol{u}_i = \begin{cases} -\epsilon\alpha_i \boldsymbol{P}(\boldsymbol{x}_i - \boldsymbol{s}_{\hat{i}}) - \epsilon \sum_{j=1}^{N} \xi_{ij} \boldsymbol{P} \boldsymbol{s}_{\hat{j}}, & i \in \mathcal{G}_{\hat{i}}^{inter}, \\ \epsilon\alpha_i \boldsymbol{P}(\boldsymbol{x}_i - \boldsymbol{s}_{\hat{i}}), & \in \mathcal{G}_{\hat{i}}^{intra} \wedge DegIn(i) = 0, \\ 0, & otherwise. \end{cases} \tag{3.23}$$

where $DegIn(i)$ denotes the number of links that start from j and ends in i where $j \neq i$.

Remark 3.3.2. The strategy for determining the controllers in (3.23) is as follows:

- If node i is an inter-act node, the first term of controllers is employed to synchronize the nodes in the same cluster. Meanwhile, the second one is utilized to counteract the interaction among clusters.
- If node i is an intra-act node with zero in-degree, it means that there is not any node that can influence the node i so that it is very difficult to make the trajectories of the node i reach $s_{\hat{i}}$ by self-synchronization. Therefore, the negative feedback controller is designed to achieve the synchronization.

Without loss of generality, the network nodes can be rearranged so that the first L nodes are pinned.

Theorem 3.3.3. *(Ma & Lu, 2013) Let $f \in QUAD(\boldsymbol{\Delta}, \boldsymbol{P})$. The controlled network can achieve cluster synchronization if the following condition holds:*

$$\omega \boldsymbol{I}_N + \epsilon \frac{\boldsymbol{\Xi} + \boldsymbol{\Xi}^T}{2} - \epsilon \boldsymbol{A} < 0, \tag{3.24}$$

where $\boldsymbol{A} = diag(\alpha_1, \alpha_2, \ldots, \alpha_L, 0, \ldots, 0) \in \mathbb{R}^{N \times N}$ and ω is given in (2.6).

Proof. See (Ma & Lu, 2013). □

Let

$$\boldsymbol{\Omega} = \omega \boldsymbol{I}_N + \epsilon \frac{\boldsymbol{\Xi} + \boldsymbol{\Xi}^T}{2} = \begin{bmatrix} \boldsymbol{\Omega}_{11} & \boldsymbol{\Omega}_{12} \\ \boldsymbol{\Omega}_{12}^T & \boldsymbol{\Omega}_{22} \end{bmatrix} \tag{3.25}$$

where $\boldsymbol{\Omega}_{11} \in \mathbb{R}^{K \times K},\ \boldsymbol{\Omega}_{12} \in \mathbb{R}^{K \times M},\ \boldsymbol{\Omega}_{22} \in \mathbb{R}^{M \times M},\ K + M = N$. Similarly, let

$$\boldsymbol{A} = \begin{bmatrix} \boldsymbol{A}_{11} & \boldsymbol{0} \\ \boldsymbol{0} & \boldsymbol{0} \end{bmatrix} \tag{3.26}$$

where $\boldsymbol{A}_{11} \in \mathbb{R}^{K \times K}$ and

$$\boldsymbol{\Xi} = \begin{bmatrix} \boldsymbol{\Xi}_{11} & \boldsymbol{\Xi}_{12} \\ \boldsymbol{\Xi}_{12}^T & \boldsymbol{\Xi}_{22} \end{bmatrix} \tag{3.27}$$

where $\boldsymbol{\Xi}_{11} \in \mathbb{R}^{K \times K},\ \boldsymbol{\Xi}_{12} \in \mathbb{R}^{K \times M},\ \boldsymbol{\Xi}_{22} \in \mathbb{R}^{M \times M},\ K + M = N$.

Corollary 3.3.4. *Let $f \in QUAD(\boldsymbol{\Delta}, \boldsymbol{P})$. The controlled network can achieve cluster synchronization if the following two conditions hold:*

$$\lambda_{max}\left(\frac{\boldsymbol{\Xi}_{22} + \boldsymbol{\Xi}_{22}^T}{2}\right) < -\frac{\omega}{\epsilon}, \tag{3.28a}$$

$$\alpha_i > \frac{\lambda_{max}(\boldsymbol{\Omega}_{11} - \boldsymbol{\Omega}_{12}\boldsymbol{\Omega}_{22}^{-1}\boldsymbol{\Omega}_{12}^T)}{\epsilon} \quad i = 1, 2, \ldots, L. \tag{3.28b}$$

Proof. See (Ma & Lu, 2013) □

One of the main contributions of the work presented in this section is that it makes it possible to construct a network capable of achieving a determined cluster pattern

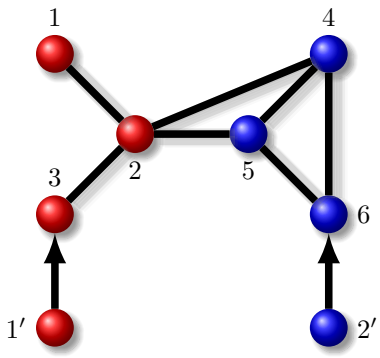

Figure 3.1 An undirected network. Nodes $1, 2, 3$ are wanted to be pinned to node $1'$ while the nodes $4, 5, 6$ are wanted to be pinned to node $2'$.

without considering the zero-row-sum sub-block partitioning of the outer coupling matrix. On the other hand, the number of pinning controllers is fixed: the inter-act nodes and the intra-act nodes with zero in-degrees have to be pinned. Therefore, it does not provide any flexibility to minimize the number of pinning controllers.

3.4 Illustrative Examples

3.4.1 Cluster Synchronization in Undirected Networks

Consider the network given in Figure 3.1 whose dynamics is

$$\begin{aligned} \dot{\boldsymbol{x}}_i &= f(\boldsymbol{x}_i) + \sum_{j=6}^{n} \epsilon_{ij} \boldsymbol{P} \boldsymbol{x}_j - \alpha_i \boldsymbol{P}(\boldsymbol{x}_i - \boldsymbol{s}_{\hat{i}}), \quad i \in \mathcal{J} i, \\ \dot{\boldsymbol{x}}_i &= f(\boldsymbol{x}_i) + \sum_{j=6}^{n} \epsilon_{ij} \boldsymbol{P} \boldsymbol{x}_j, \quad i \notin \mathcal{J}, \end{aligned} \tag{3.29}$$

where $\mathcal{J} = \{3, 6\}$, $L = 2$, $\boldsymbol{x}_i = [x_{i,1}, x_{i,2}, x_{i,3}] \in \mathbb{R}^3$, $f : \mathbb{R}^3 \mapsto \mathbb{R}^3$ is the Chua dynamics given by,

$$f(\boldsymbol{x}_i) = \begin{bmatrix} k_1(x_{i,2} - h(x_{i,1}) \\ x_{i,1} - x_{i,2} + x_{i,3} \\ -k_2 x_{i,2} \end{bmatrix}, \tag{3.30}$$

where $h(x_{i,1}) = bx_{i,1} + 1/2(a-b)(|x_{i,1}+1| - |x_{i,1}-1|)$ for $k_1 = 9, k_2 = 100/7, a = -1/7, b = 2/7$. Our objective to construct the clusters $\mathcal{G}_1 = \{1,2,3\}$ and $\mathcal{G}_2 = \{4,5,6\}$, corresponding to the special solutions $\boldsymbol{s}_1$ and $\boldsymbol{s}_2$, respectively, where $\dot{\boldsymbol{s}}_i = f(\boldsymbol{s}_i),\ i = 1,2$. The inner coupling matrix $\boldsymbol{P} = diag(1,1,1)$. For the individual node dynamics, it can be shown that (Wu et al., 2009) $f \in QUAD(10\boldsymbol{I}_3, \boldsymbol{I}_3)$. The missing part at this point is the determination of outer coupling matrix $\boldsymbol{E}$ and of control strengths $\alpha_i,\ i = 1,2,\ldots,L$ of the network, which are going to be determined following the steps in Theorem 3.2.4. We start with $\gamma_i = 200,\ i = 1,2,\ldots,L$ and

$$\boldsymbol{\Phi} = \begin{bmatrix} -1 & 1 & 0 & 0 & 0 & 0 \\ 1 & -2 & 1 & 0 & -1 & 1 \\ 0 & 1 & -1 & 0 & 1 & -1 \\ 0 & 0 & 0 & -1 & 1 & 0 \\ 0 & -1 & 1 & 1 & -2 & 1 \\ 0 & 1 & -1 & 0 & 1 & -1 \end{bmatrix}. \tag{3.31}$$

$\boldsymbol{\Phi} \in \mathbb{E}_2$. Next, we find

$$\begin{aligned} &\max_{1\le k\le 3} \delta_k = 10 \\ &\max_{u\neq v, 1\le u\le 2, 1\le v\le 2} \mu(\boldsymbol{\Phi}_{uv}) = 1.5 \\ &\max_{1\le i\le 2} \left(\frac{\max_k \delta_k + 2(l-1)\max_{u\neq v} \mu(\boldsymbol{\Phi}_{uv})}{-\lambda_{max}(\boldsymbol{\Phi}_{ii} - \boldsymbol{\Gamma}_i)} \right) = 34.1578. \end{aligned} \tag{3.32}$$

Thus, we choose $\beta = 34.1578$. Then, we constructed the coupling matrix $\boldsymbol{E}$ and control strengths $\alpha_i\ , i = 1,2$ as in (3.12) and (3.13),

$$\boldsymbol{E} = \begin{bmatrix} -34.2 & 34.2 & 0.0 & 0.0 & 0.0 & 0.0 \\ 34.2 & -68.3 & 34.2 & 0.0 & -1.0 & 1.0 \\ 0.0 & 34.2 & -34.2 & 0.0 & 1.0 & -1.0 \\ 0.0 & 0.0 & 0.0 & -34.2 & 34.2 & 0.0 \\ 0.0 & -1.0 & 1.0 & 34.2 & -68.3 & 34.2 \\ 0.0 & 1.0 & -1.0 & 0.0 & 34.2 & -34.2 \end{bmatrix}, \tag{3.33}$$

and

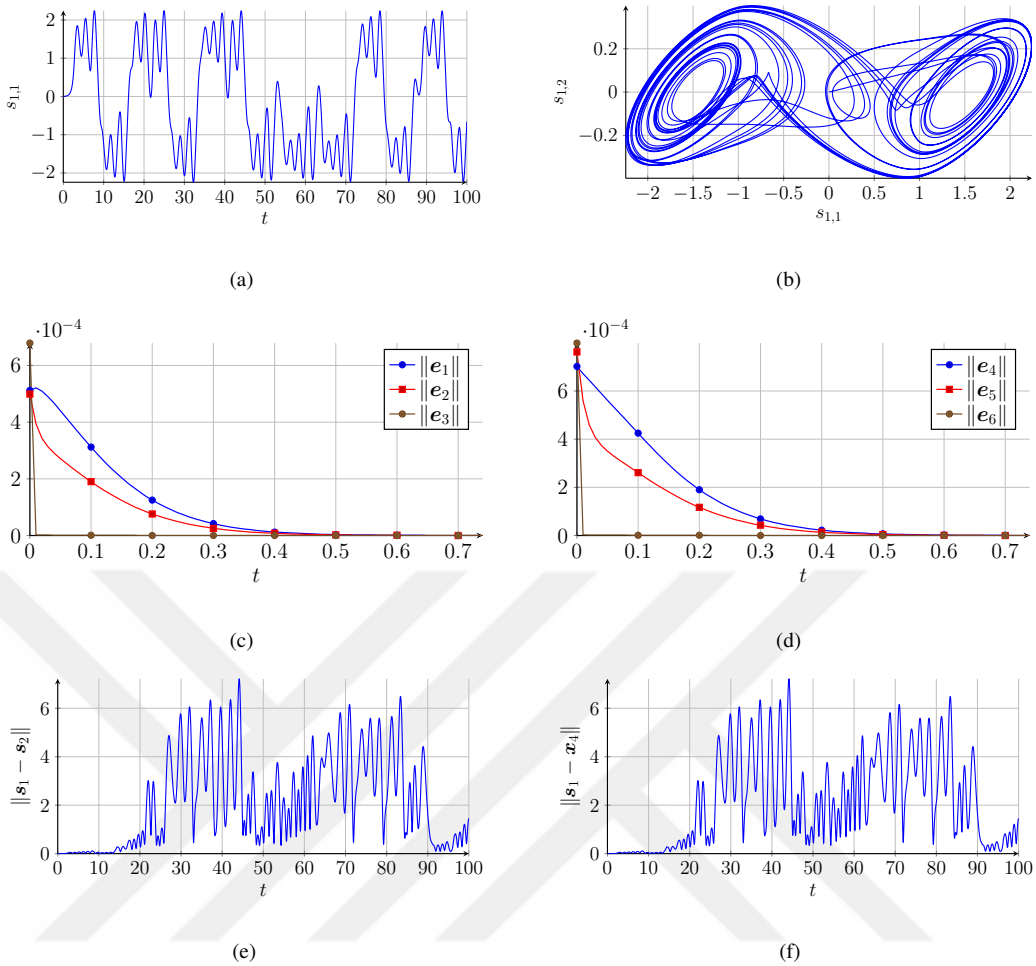

Figure 3.2 Simulation results of network in Figure 3.1

$$\alpha_i = 6831.5687, \quad i = 1, 2. \tag{3.34}$$

After the construction, the network is simulated. In Figure 3.2 are shown the simulation results from which the construction of the clusters $G_1 = \{1, 2, 3\}$ and $G_2 = \{3, 4, 5\}$ is apparent. The time waveform and trajectory in Figure 3.2a and 3.2b show that the nodes are chaotic. Figure 3.2c and 3.2d shows that the nodes in the same clusters synchronize while Figure 3.2e and 3.2f shows that there is no synchronization between the nodes in different clusters.

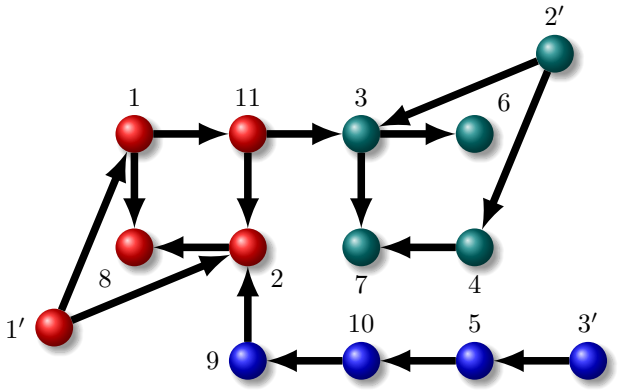

Figure 3.3 A directed network. The nodes $1, 2, 8, 11$ are wanted to be pinned to node $1'$, the nodes $3, 4, 6, 7$ are wanted to be pinned to node $2'$, and nodes $5, 9, 10$ are wanted to be pinned to node $3'$.

3.4.2 Cluster Synchronization in Directed Networks

Consider the network in Figure 3.3 whose dynamics is given by,

$$\begin{aligned}
&\dot{\boldsymbol{x}}_i = f(\boldsymbol{x}_i) + \epsilon \sum_{j=1}^{N} \xi_{ij} \boldsymbol{P} \boldsymbol{x}_j + \boldsymbol{u}_i \quad i = 1, 2, \ldots, N, \\
&\boldsymbol{u}_i = \begin{cases} -\epsilon\alpha_i \boldsymbol{P}(\boldsymbol{x}_i - \boldsymbol{s}_{\hat{i}}) - \epsilon \sum_{j=1}^{N} \xi_{ij} \boldsymbol{P} \boldsymbol{s}_{\hat{j}}, & i \in G_{\hat{i}}^{inter}, \\ -\epsilon\alpha_i \boldsymbol{P}(\boldsymbol{x}_i - \boldsymbol{s}_{\hat{i}}), & i \in G_{\hat{i}}^{intra} \wedge DegIn(i) = 0, \\ 0, & otherwise, \end{cases}
\end{aligned} \tag{3.35}$$

where $\boldsymbol{x}_i = [x_{i,1}, x_{i,2}, x_{i,3}] \in \mathbb{R}^3$, $f : \mathbb{R}^3 \mapsto \mathbb{R}^3$ is the Lü system with the dynamics,

$$f(\boldsymbol{x}_i) = \begin{bmatrix} k_1(x_{i,2} - x_{i,1}) \\ k_2 x_{i,2} - x_{i,1} x_{i,3} \\ x_{i,1} x_{i,2} - k_3 x_{i,2} \end{bmatrix} \tag{3.36}$$

for $k_1 = 36, k_2 = 20, k_3 = 3$. The inner coupling matrix $\boldsymbol{P} = diag(1, 1, 1)$ and the coupling strength $\epsilon = 80$. The nodes 2 and 3 are inter-act nodes and the nodes $1, 4, 5$ are intra-act nodes with zero in-degree. Thus, according to the control strategy outlined in Remark 3.3.2, the nodes $1, 2, \ldots, 5$ are the controlled nodes. Now, the problem is determinining control strengths $\alpha_i,\ i = 1, 2, 3$. For the individual node dynamics, one

can show that (Ma & Lu, 2013),

$$(\boldsymbol{x}-\boldsymbol{y})^T(f(\boldsymbol{x})-f(\boldsymbol{y})) \leq 37.8(\boldsymbol{x}-\boldsymbol{y})^T(\boldsymbol{x}-\boldsymbol{y}), \tag{3.37}$$

which implies $\omega = 38.8$ can be chosen. The outer coupling matrix of the network is

$$\boldsymbol{\Xi} = \begin{bmatrix} 0 & -2 & 0 & 0 & 0 & 0 & 0 & 0 & 1 & 0 & 1 \\ 0 & 0 & -1 & 0 & 0 & 0 & 0 & 0 & 0 & 0 & 1 \\ 0 & 0 & 0 & 0 & 0 & 0 & 0 & 0 & 0 & 0 & 0 \\ 0 & 0 & 0 & 0 & 0 & 0 & 0 & 0 & 0 & 0 & 0 \\ 0 & 0 & 1 & 0 & 0 & -1 & 0 & 0 & 0 & 0 & 0 \\ 0 & 0 & 1 & 1 & 0 & 0 & -2 & 0 & 0 & 0 & 0 \\ 1 & 1 & 0 & 0 & 0 & 0 & 0 & -2 & 0 & 0 & 0 \\ 0 & 0 & 0 & 0 & 0 & 0 & 0 & 0 & -1 & 1 & 0 \\ 0 & 0 & 0 & 0 & 1 & 0 & 0 & 0 & 0 & -1 & 0 \\ 1 & 0 & 0 & 0 & 0 & 0 & 0 & 0 & 0 & 0 & -1 \end{bmatrix} \tag{3.38}$$

from which we have,

$$\alpha > \frac{1}{\epsilon}\lambda_{max}\left(\boldsymbol{\Gamma}_{11} - \boldsymbol{\Gamma}_{12}\boldsymbol{\Gamma}_{22}^{-1}\boldsymbol{\Gamma}_{12}^T\right) = 8.9697, \tag{3.39}$$

where

$$\boldsymbol{\Gamma} = \omega \boldsymbol{I}_n + \frac{\epsilon}{2}(\boldsymbol{\Xi} + \boldsymbol{\Xi}^T) = \begin{bmatrix} \boldsymbol{\Gamma}_{11} & \boldsymbol{\Gamma}_{12} \\ \boldsymbol{\Gamma}_{12}^T & \boldsymbol{\Gamma}_{22} \end{bmatrix}. \tag{3.40}$$

Thus, $\alpha_1 = \alpha_2 = \alpha_3 = 8.9697$.

The simulation results performed under these configurations are given in Figure 3.3. From the results, it is clear that the construction of the clusters $\mathcal{G}_1 = \{1, 2, 8, 11\}$, $\mathcal{G}_2 = \{3, 4, 6, 7\}$, $\mathcal{G}_3 = \{5, 9, 10\}$ is achieved. The node dynamics are chaotic, as seen from Figure 3.4a and 3.2b. Figure 3.4c - 3.4e shows the nodes in the same clusters synchronize, and Figure 3.4f shows that the nodes in different clusters do not synchronize.

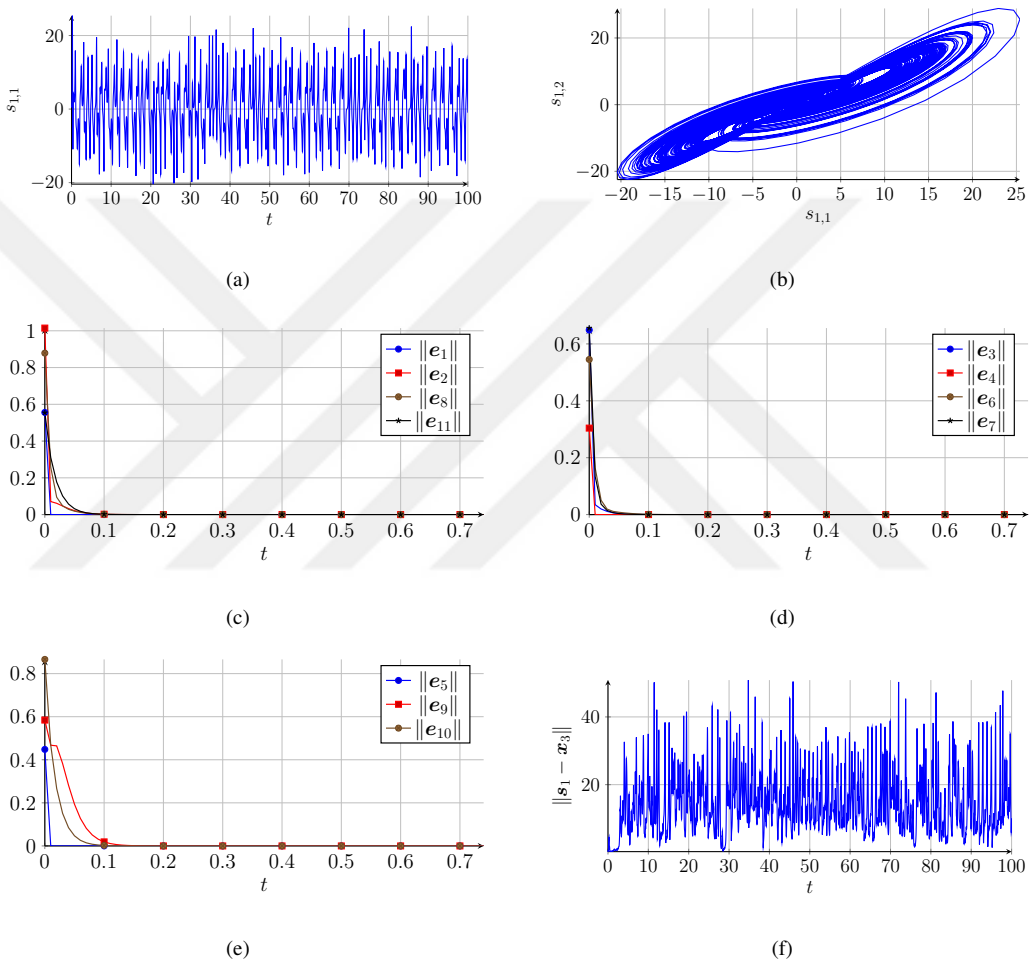

Figure 3.4 Simulation results of network in Figure 3.3

.

CHAPTER FOUR
TOPOLOGICAL CONTROL OF CLUSTERS

When appropriately coupled, the dynamical systems can exhibit a wealthy class of collective behaviors, which has been well-known since the 1990s (Pecora & Carroll, 1990). The concept of synchronization can be cited as one of the most interesting among those collective behaviors (Pecora & Carroll, 2015). Although the type of synchronization to be considered here is complete synchronization, various types of synchronization have been reported, such as phase synchronization, frequency synchronization, lag synchronization, generalized synchronization, etc., in the case of two coupled systems. Informally, two dynamical systems exhibit complete synchronization when following the same trajectory in their phase spaces. If we go beyond tiny networks consisting of just two nodes, we can come across much more enriched types of synchronization. Full synchronization, in which all the nodes synchronize with each other, is one such possibility (Pecora & Carroll, 1990; Yu et al., 2009). More interestingly, we have cluster synchronization when the nodes synchronize in different groups without synchronization among the groups (Ma et al., 2006; Fu et al., 2013, 2014). The individual node dynamics and configuration, i.e., topology and coupling strength, determine the type of synchronization observed in the network. The conditions under which different types of synchronization are ensured can be obtained via the tools from the dynamical system theory, control theory, and graph theory. In the remaining part of this chapter, we will derive one such condition that ensures full synchronization in diffusively coupled networks. The conditions to be obtained in this chapter for the full synchronization will be enlarged for the case of cluster synchronization in the networks of diffusively coupled networks.

4.1 Controlling Synchronous Patterns

Theorem 4.1.1. *Consider an undirected network given in Definition 2.1.3 where* $\epsilon > 0$ *and* $\boldsymbol{E} = \epsilon\boldsymbol{\Xi} = \epsilon[\xi_{ij}]$. *Let* $g(\cdot)$ *be the master stability function corresponding to the network, and* $\tilde{\eta} < 0$ *be the threshold such that* $\mu = g(\eta) < 0$ *for* $\eta < \tilde{\eta}$. *Then, the eigenvalue condition*

$$|\lambda_2^s| < \lambda_{min}, \tag{4.1}$$

and the coupling strength condition

$$\epsilon \in [\tilde{\eta}/\lambda_{min},\ \tilde{\eta}/\lambda_2^s] \tag{4.2}$$

are the necessary conditions for the cluster synchronization represented by the manifold in (2.1.8).

Proof. For a network consisting of N nodes, each topological symmetry $\mathcal{S}$ of the network can be associated with a permutation matrix $\boldsymbol{\Delta} = [\hat{\delta}_{ij}] \in \mathbb{R}^{N\times N}$ where $\hat{\delta}_{ij} = 1$ if (i, j) is a symmetric pair; otherwise, $\hat{\delta}_{ij} = 0$. A cluster pattern $\mathscr{C}$ can be constructed by grouping the nodes forming the symmetric pairs into the same clusters.

Although different cluster patterns are obtained for different topological symmetries, the cluster synchronizations corresponding to these cluster patterns may be either dynamically or topologically unstable (Lin et al., 2016a). To make the cluster pattern stable, consider a control network whose dynamics evolves by

$$\dot{\boldsymbol{s}}_k = f(\boldsymbol{s}_k) + \sum_{l=1}^{L} \omega_{kl} \boldsymbol{P} \boldsymbol{s}_l, \quad k = 1, 2, \ldots, L, \tag{4.3}$$

and

$$\omega_{kl} = \sum_{j\in\mathcal{G}_k} \sum_{j\in\mathcal{G}_l} \xi_{ij}/N_k, \tag{4.4}$$

with N_k is the number of nodes in $\mathcal{G}_k$. The original network in (2.1) is controlled by pinning each node $\boldsymbol{s}_k$ to all nodes of $\mathcal{G}_k$. Thus, the dynamics of the controlled network take the form

$$\dot{\boldsymbol{x}}_i = f(\boldsymbol{x}_i) + \epsilon \sum_{j=1}^{N} \xi_{ij} \boldsymbol{P} \boldsymbol{x}_j + \alpha\epsilon \sum_{k=1}^{L} \delta_{ik} \boldsymbol{P} \boldsymbol{s}_k, \quad i = 1, 2, \ldots, N, \tag{4.5}$$

where $\alpha > 0$ is the control strength where $\delta_{ik} = 1$ if i-th node is pinned to k-th pinning node; otherwise $\delta_{ik} = 0$.

Let us assume the control network is deactivated first, i.e., $\alpha = 0$, and investigate the stability of the cluster pattern $\mathscr{C}$ corresponding to a topological symmetry $\mathcal{S}$. Consider the special solution $\boldsymbol{v}_k$ on the cluster synchronization manifold $\mathcal{M}$ in (2.5) associated to cluster $\mathcal{G}_k$ for $k = 1, 2, \ldots, L$. The perturbation $\boldsymbol{e}_i = \boldsymbol{x}_i - \boldsymbol{v}_k$ where $i \in \mathcal{G}_k$ evolves by

$$\dot{\boldsymbol{e}}_i = Df(\boldsymbol{v}_k)\boldsymbol{e}_i + \epsilon \sum_{j \in \mathcal{G}_k} \xi_{ij} \boldsymbol{P} \boldsymbol{e}_j + \epsilon \sum_{l \neq k} \sum_{m \in \mathcal{G}_l} \xi_{im} \boldsymbol{P} (\boldsymbol{e}_m - \boldsymbol{e}_i), \tag{4.6}$$

where Df is the Jacobian of $f(\cdot)$.

Denoting $\boldsymbol{\mathscr{E}} = [\boldsymbol{\mathscr{E}}_1, \boldsymbol{\mathscr{E}}_2, \ldots, \boldsymbol{\mathscr{E}}_L]^T$, where $\boldsymbol{\mathscr{E}}_k = [\boldsymbol{e}_1, \boldsymbol{e}_2, \ldots, \boldsymbol{e}_{N_k}]^T$ is the error vector corresponding to k-th cluster, (4.6) can be written as,

$$\dot{\boldsymbol{\mathscr{E}}} = \left[\sum_{k=1}^{L} \boldsymbol{\Gamma}_k \otimes Df(\boldsymbol{v}_k) + \epsilon \Xi \sum_{k=1}^{L} \boldsymbol{\Gamma}_k \otimes \boldsymbol{P} \right] \boldsymbol{\mathscr{E}}, \tag{4.7}$$

where $\boldsymbol{\Gamma}_k = [\gamma_{ik}]$, $\gamma_{ik} = 1$ if $i \in \mathcal{G}_k$; $\gamma_{ik} = 0$, otherwise. Let $\boldsymbol{\Delta}$ be the permutation matrix corresponding to $\mathcal{S}$. $\boldsymbol{\Delta}^2 = \boldsymbol{I}_{N \times N}$ by construction, therefore $\boldsymbol{\Delta}$ is diagonalizable. Thus, there exist $\boldsymbol{\Psi} = [\boldsymbol{\psi}_1, \boldsymbol{\psi}_2, \ldots, \boldsymbol{\psi}_N]^T \in \mathbb{R}^{N \times N}$ such that $\mathrm{diag}(\zeta_1, \zeta_2, \ldots, \zeta_N) = \boldsymbol{\Psi}^{-1} \boldsymbol{\Delta} \boldsymbol{\Psi}$ where ζ_k is the eigenvalue corresponding to the eigenvector $\boldsymbol{\psi}_k$ of $\boldsymbol{\Delta}$. Using the transformation $\boldsymbol{Y} = h(\boldsymbol{E}) = \boldsymbol{\Psi} \boldsymbol{E}$, (4.7) can be transformed into

$$\dot{\boldsymbol{Y}} = \left[\sum_{k=1}^{L} \boldsymbol{\Gamma}_k \otimes Df(\boldsymbol{v}_k) + \epsilon \boldsymbol{\Theta} \sum_{k=}^{L} \boldsymbol{\Gamma}_k \otimes \boldsymbol{P} \right] \boldsymbol{Y}, \tag{4.8}$$

where $\boldsymbol{Y} = [\boldsymbol{Y}_1, \boldsymbol{Y}_2, \ldots, \boldsymbol{Y}_L]^T$,

$$\boldsymbol{\Theta} = \boldsymbol{\Psi}^{-1}\boldsymbol{\Xi}\boldsymbol{\Psi} = \begin{bmatrix} \boldsymbol{\Omega} & \boldsymbol{0} \\ \boldsymbol{0} & \boldsymbol{\Phi} \end{bmatrix} \tag{4.9}$$

with $\boldsymbol{\Omega} = \text{diag}(\boldsymbol{\Omega}_1, \boldsymbol{\Omega}_2, \ldots, \boldsymbol{\Omega}_L)$, $\boldsymbol{\Omega}_k \in \mathbb{R}^{(N_k-1)\times(N_k-1)}$ and $\boldsymbol{\Gamma} \in \mathbb{R}^{L\times L}$. $\boldsymbol{\Omega}_k$ characterizes the motion transverse to the synchronization manifold of k-th cluster, and the subspace spanned by the eigenvectors of $\boldsymbol{\Omega}_k$ is called transversal subspace of k-th cluster. Since $\boldsymbol{\Phi}$ characterizes the motion parallel to the synchronization manifolds of the clusters, the subspace spanned by the eigenvectors of $\boldsymbol{\Phi}$ is called synchronous subspace.

The transformation h decouples the dynamics of the perturbations corresponding to each cluster. Hence, the stability of the k-th cluster can be determined from the decoupled dynamics

$$\dot{\boldsymbol{Y}}_k = [Df(\boldsymbol{\upsilon}_k) + \epsilon\boldsymbol{\Omega}_{\boldsymbol{k}}\boldsymbol{P}]\boldsymbol{Y}_k, \tag{4.10}$$

where $\boldsymbol{Y}_k = [\boldsymbol{y}_1, \boldsymbol{y}_2, \ldots, \boldsymbol{y}_{N_k}]$, and $\boldsymbol{I}_k$ is $N_k - 1$ dimensional identity matrix. Let $0 > \lambda^t_{k,1} \geq \lambda^t_{k,2} \geq \ldots \geq \lambda^t_{N_k}$ be eigenvalues, and $\boldsymbol{\rho}_{k,1}, \boldsymbol{\rho}_{k,2}, \ldots, \boldsymbol{\rho}_{k,N_k}$ be the corresponding eigenvectors of $\boldsymbol{\Omega}_{\boldsymbol{k}}$. Using the transformation $\boldsymbol{Z}_k = q(\boldsymbol{R}^{-1}\boldsymbol{Y}_k)$ where $\boldsymbol{R} = [\boldsymbol{\rho}_{k,1}, \boldsymbol{\rho}_{k,2}, \ldots, \boldsymbol{\rho}_{k,N_k}]$ and $\text{diag}(\lambda^t_{k,1}, \lambda^t_{k,2}, \ldots, \lambda^t_{k,N_k}) = \boldsymbol{R}^{-1}\boldsymbol{\Omega}_k\boldsymbol{R}$, the dynamics of l-th transverse mode $\boldsymbol{z}_{k,l}$ can be obtained as

$$\dot{\boldsymbol{z}}_{k,l} = [Df(\boldsymbol{\upsilon}_k) + \epsilon\lambda^t_{k,l}\boldsymbol{P}]\boldsymbol{z}_{k,l}, \quad l = 1, 2, \ldots, N_k. \tag{4.11}$$

Dropping the subscripts and superscripts, and letting $\eta = \epsilon\lambda$ in (4.11), we obtain the generic system

$$\dot{\boldsymbol{z}} = (Df(\boldsymbol{\upsilon}) + \eta\boldsymbol{P})\boldsymbol{z}. \tag{4.12}$$

The master stability function $\mu = g(\eta)$ maps η to the system's maximum Lyapunov exponent μ in 4.12. If $\mu_{k,l} = g(\epsilon\lambda_{k,l}^t) \leq 0$, then l-th mode is stable, i.e., $\lim_{t\mapsto\infty} \|\boldsymbol{z}_{k,l}\| = 0$; otherwise it is unstable.

Let $0 = \lambda_1^s > \lambda_2^s \geq \ldots \geq \lambda_L^s$ be eigenvalues of $\boldsymbol{\Phi}$. Then, the following conditions must be necessarily satisfied for a cluster synchronization manifold to be stable (Lin et al., 2016a):

i) All the transverse modes in the transverse subspace must be stable, i.e., $\mu_{k,l}^t = g(\epsilon\lambda_{k,l}^t) \leq 0,\ \forall k, l.$

ii) At least one of nontrivial modes in the synchronous subspace be unstable, i.e., $\mu_k^s = g(\epsilon\lambda_k^s) > 0, \exists k \in \{2, 3, \ldots, L\}$ to avoid full synchronization.

There exists a threshold $\tilde{\eta} < 0$ such that $\mu = g(\eta) < 0$ for $\eta < \tilde{\eta}$ for most of the well-known dynamical systems (Huang et al., 2009). Denoting $\lambda_{min} = \min\{|\lambda_{k,1}^t|, k = 1, 2, \ldots, L\}$, the necessary conditions for the cluster synchronization are satisfied if

$$|\lambda_2^s| < \lambda_{min} \tag{4.13}$$

and

$$\epsilon \in [\tilde{\eta}/\lambda_{min},\ \tilde{\eta}/\lambda_2^s]. \tag{4.14}$$

When the control network is activated, it can be seen that the matrix in (4.9) takes the form

$$\boldsymbol{\Theta} = \boldsymbol{\Psi}^{-1}\boldsymbol{\Xi}\boldsymbol{\Psi} = \begin{bmatrix} \boldsymbol{\Omega} - \alpha I_{N'} & \boldsymbol{0} & \boldsymbol{0} \\ \boldsymbol{0} & \boldsymbol{\Phi} - \alpha I_L & \alpha \boldsymbol{I}_L \\ \boldsymbol{0} & \boldsymbol{0} & \boldsymbol{A} \end{bmatrix} \tag{4.15}$$

where $\boldsymbol{A} = [\alpha_{kl}] \in \mathbb{R}^{L\times L}$ is the control matrix in (4.3) (Lin et al., 2016a).

Correspondingly, the condition for inducing cluster synchronization is $\alpha > \alpha_1 = \bar{\eta}/\epsilon - \lambda_{min}$. In the case of induced cluster synchronization, the nodes in the same cluster in the original network in (4.5) are synchronized. At the same time, there is no synchronization between a control node $\boldsymbol{s}_k$ and its associated controlled nodes $\boldsymbol{x}_i,\ i \in \mathcal{G}_k$. Hence, the synchronization is *induced*, not enforced, by the control node. If the control strength α satisfies $\alpha > \alpha_2 = \bar{\eta}/\epsilon$, the control node $\boldsymbol{s}_k$ and all its associated controlled nodes $\boldsymbol{x}_i,\ i \in \mathcal{G}_k$ are synchronized. Thus, the cluster synchronization is *controlled* by the control node if $\alpha > \alpha_2$. □

4.2 Illustrative Examples

4.2.1 Without Control Network

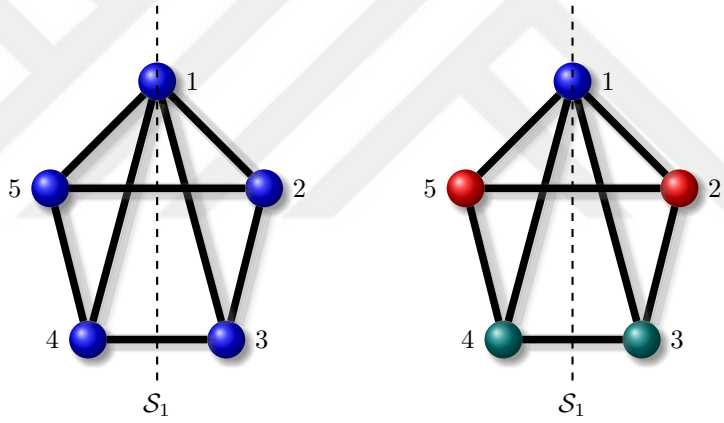

(a) (b)

Figure 4.1 (a) A simple network possessing reflection symmetry $\mathcal{S}_1$. (b) The cluster synchronization pattern $\mathscr{C}_1$ corresponding to symmetry $\mathcal{S}_1$. The nodes in the same cluster are shown with the same color.

Consider the network shown in Figure 4.1a. The network possesses $\mathcal{S}_1$ reflection symmetry. The change of nodes 2 and 5 and nodes 3 and 4 does not change the network topology. If the initial conditions of the nodes 2 and 5, and the nodes 3 and 4 were the same, then during the network evolution, the spatiotemporal status of the network would always stay in the cluster synchronization pattern, as shown in Figure 4.1b. That is, the nodes 2 and 5; and the nodes 3 and 4 would always be synchronized, forming the clusters $\mathcal{G}_1 = \{1\}, \mathcal{G}_2 = \{2, 5\}, \mathcal{G}_3 = \{3, 4\}$. Because the nodes 2 and 5, and the nodes

3 and 4 receive the same coupling signals. However, since the nodes in the network are chaotic systems, any minute differences in the initial conditions of the systems may result in different spatiotemporal behaviors. In other words, the system must meet certain specifications for the cluster pattern in Figure 4.1b to become stable.

Using the analysis presented in the previous section, we now investigate the stability of the cluster pattern corresponding to reflection symmetry $\mathcal{S}_1$. The permutation matrix corresponding to $\mathcal{S}_1$ is

$$\mathbf{\Delta} = \begin{bmatrix} 1 & 0 & 0 & 0 & 0 \\ 0 & 0 & 0 & 0 & 1 \\ 0 & 0 & 0 & 1 & 0 \\ 0 & 0 & 1 & 0 & 0 \\ 0 & 1 & 0 & 0 & 0 \end{bmatrix}. \tag{4.16}$$

From the eigendecomposition of $\mathbf{\Delta}$, the transformation matrix $\mathbf{\Psi}$ is

$$\mathbf{\Psi} = \begin{bmatrix} 0.00 & 0.00 & 0.00 & 1.00 & 0.00 \\ 0.00 & -0.71 & 0.00 & 0.00 & 0.71 \\ 0.71 & 0.00 & 0.71 & 0.00 & 0.00 \\ -0.71 & 0.00 & 0.71 & 0.00 & 0.00 \\ 0.00 & 0.71 & 0.00 & 0.00 & 0.71 \end{bmatrix}. \tag{4.17}$$

Let $\boldsymbol{W} = [w_{ij}]$ be the weight matrix where w_{ij} is the weight of the coupling between the nodes i and j. If we adopt the normalized coupling scheme such that $\xi_{ij} = w_{ij} / \sum_{j=1}^{N} w_{ij}$ and $w_{ij} = 1,\ i, j = 1, 2, \ldots, N$, we have

$$\mathbf{\Xi} = \begin{bmatrix} -1.00 & 0.25 & 0.25 & 0.25 & 0.25 \\ 0.33 & -1.00 & 0.33 & 0.00 & 0.33 \\ 0.33 & 0.33 & -1.00 & 0.33 & 0.00 \\ 0.33 & 0.00 & 0.33 & -1.00 & 0.33 \\ 0.33 & 0.33 & 0.00 & 0.33 & -1.00 \end{bmatrix}. \tag{4.18}$$

Using the transformation in (4.9), we have

$$\Theta = \begin{bmatrix} -1.33 & -0.33 & 0.00 & 0.00 & 0.00 \\ -0.33 & -1.33 & 0.00 & 0.00 & 0.00 \\ 0.00 & 0.00 & -0.67 & 0.47 & 0.33 \\ 0.00 & 0.00 & 0.35 & -1.00 & 0.35 \\ 0.00 & 0.00 & 0.33 & 0.47 & -0.67 \end{bmatrix}. \tag{4.19}$$

Thus, the block matrices Ω and Φ are

$$\Omega = \begin{bmatrix} -1.33 & -0.33 \\ -0.33 & -1.33 \end{bmatrix}, \tag{4.20}$$

$$\Phi = \begin{bmatrix} -0.67 & 0.47 & 0.33 \\ 0.35 & -1.00 & 0.35 \\ 0.33 & 0.47 & -0.67 \end{bmatrix}. \tag{4.21}$$

The eigenvalues of Ω are $\lambda_1^t = -1 > \lambda_2^t = -1.67$, and the eigenvalues of Φ are $\lambda_1^s = 0 > \lambda_2^s = -1 > \lambda_3^s = -1.33$. Let $\eta = \epsilon\lambda$, then $\mu = g(\eta) < 0$ if $\eta < \tilde{\eta}$, where $\tilde{\eta}$ is determined by the node dynamics f and the coupling matrix $\boldsymbol{P}$. The distribution of the eigenvalues of the matrices Ω and Φ is shown in Figure 4.2. The eigenvalue condition is not satisfied for the symmetry $\mathcal{S}_1$ since λ_1^t is in the unstable regime. Since the transversal mode corresponding to λ_1^t is ustable, the cluster synchronization pattern corresponding to the symmetry $\mathcal{S}_1$ is also not stable. Since $\eta = \epsilon\lambda$, one may make the mode corresponding to λ_1^t stable by scaling the uniform coupling strength ϵ. However, if the mode corresponding to λ_1^t is shifted into the stable region by adjusting the uniform coupling strength ϵ, then all the nontrivial modes of Ξ reside in the stable region, which implies full synchronization. Nevertheless, full synchronization is not the desired synchronization pattern required by the symmetry $\mathcal{S}_1$. Thus, changing the strengths of all the couplings in the network by scaling the uniform coupling strength ϵ does not suffice to make the cluster synchronization pattern corresponding to the symmetry $\mathcal{S}_1$.

The problem with the stability of the cluster synchronization pattern corresponding to the symmetry $\mathcal{S}$ is that the eigenvalues $\lambda_1^t = \lambda_s^2$. To make the cluster pattern stable, we need to satisfy the condition $\lambda_1^t > \lambda_2^s$ For this inequality to be satisfied, we need to

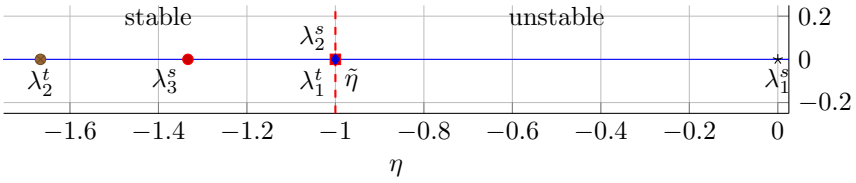

Figure 4.2 The distribution of the eigenvalues $\lambda_i^t, i = 1, 2$ of $\mathbf{\Omega}$ and $\lambda_i^s, i = 1, 2, 3$ of $\mathbf{\Theta}$. Here $\eta = \epsilon\lambda$. The dashed vertical line shows the boundary between the stable and unstable modes. i.e, the mode corresponding to λ is stable if $\eta = \epsilon\lambda < \tilde{\eta}$.

modify the distribution of the eigenvalues of the outer coupling matrix $\mathbf{\Xi}$. Naturally, changing the uniform coupling strength ϵ_1 does not affect the distribution of the eigenvalues of $\mathbf{\Xi}$. We need to change elements of $\mathbf{\Xi}$ directly, which implies modifications in the network topology. This modification may be in the form of changing the weight of a link, adding or deleting new links, or rewiring the links between specific pairs of nodes between different pairs of nodes. To the effect of the network modification on the distribution of the eigenvalues of $\mathbf{\Xi}$, we will investigate the case of changing the weight of a link in the network first. The change of network modification in the form of adding a new link and rewiring a link will come next.

4.2.1.1 Changing Coupling Strength

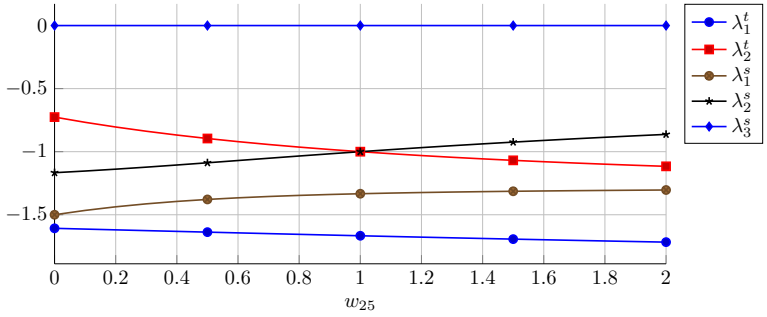

Figure 4.3 The change of the distribution of the eigenvalues $\lambda_i^t, i = 1, 2$ of $\mathbf{\Omega}$ and $\lambda_i^s, i = 1, 2, 3$ of $\mathbf{\Theta}$

We will go on the analysis with the network shown in Figure 4.1. In the network, $w_{ij} = 1,\ i, j \in \{1, 3, 4\}$ and $w_{25} = w_{52}$ will be changed in the interval $[0, 2]$. Figure 4.3 shows the change of the distribution of the eigenvalues of $\mathbf{\Omega}$ and $\mathbf{\Phi}$ when the weight of the coupling between the nodes w_{25} changes. Note from the Figure 4.3, the eigenvalue

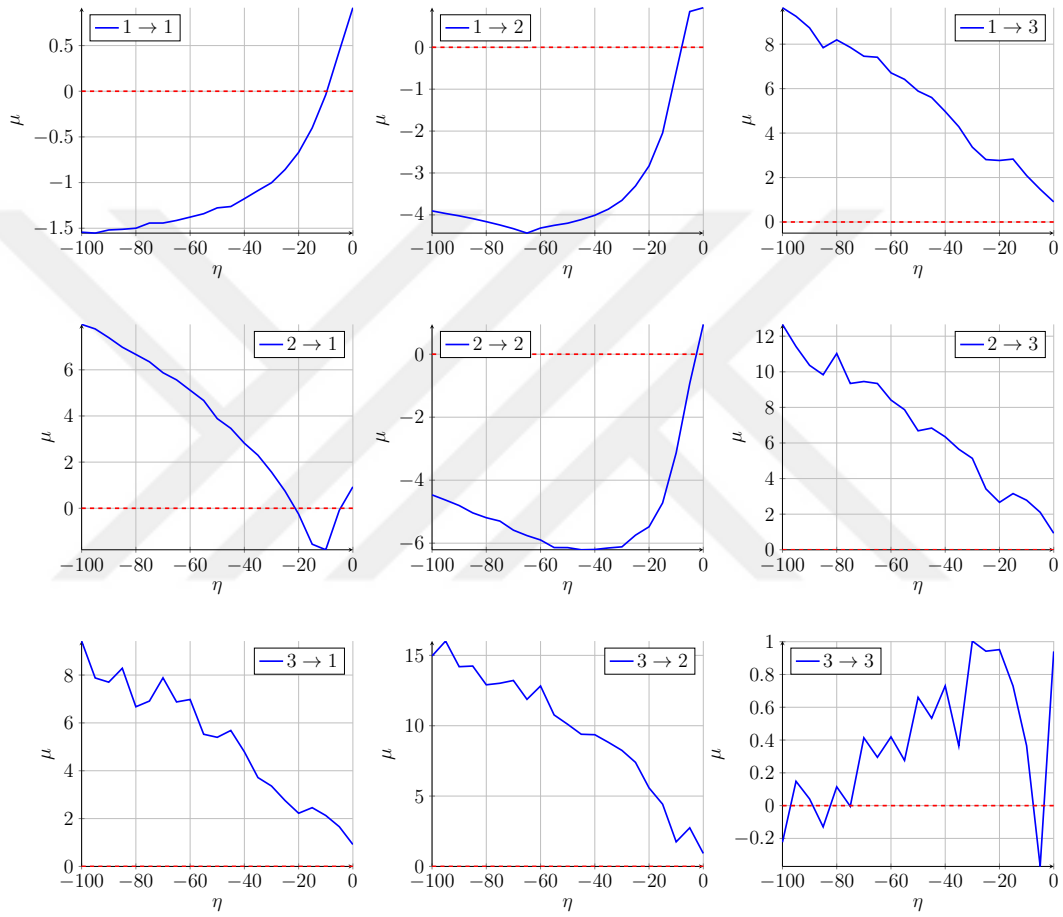

Figure 4.4 Plots of the master stability function for the Lorenz dynamics for various inner coupling matrix schemes $\boldsymbol{P}$. The notation $i \rightarrow j$ corresponds to unique nonzero element p_{ij} of element of $\boldsymbol{P} = [p_{ij}]$.

condition $\lambda_1^t > \lambda_2^s$ is not satisfied for $w_{25} \leq 1$, and is satisfied for $w_{2,5} > 1$. Let us choose $w_{25} = 1.5$. Then the eigenvalue of $\mathbf{\Omega}$ and $\mathbf{\Phi}$ are found to be $\lambda_1^t = -1.06 > \lambda_2^t = -1.69$ and $\lambda_1^s = 0 > \lambda_2^s = -0.92 > \lambda_3^s = -1.31$. The next step is to determine the range $[\epsilon_1, \epsilon_2]$ for ϵ such that transverse mode corresponding to λ_1^t is stable, i.e. $\epsilon_1 \lambda_1^t < \tilde{\eta}$. At the same time, to avoid the full synchronization state, we need to satisfy $\epsilon_2 \lambda_2^s > \tilde{\eta}$. Thus, the range of ϵ is $[\tilde{\eta}/\lambda_1^t, \tilde{\eta}/\lambda_2^s]$. The parameter $\tilde{\eta}$ depends on the individual nodes dynamics and the inner coupling matrix $\boldsymbol{P}$ (Huang et al., 2009). We need to find $\tilde{\eta}$, which depends on the individual nodes dynamics and inner coupling matrix $\boldsymbol{P}$. Let us choose the Lorenz system as the node dynamics, which is defined as

$$\begin{aligned} \dot{x} &= \sigma(y - x) \\ \dot{y} &= x(\rho - z) - y \\ \dot{z} &= xy - \beta z \end{aligned} \tag{4.22}$$

where $\boldsymbol{x} = [x, y, z]$. The Lorenz system shows chaotic dynamics for the parameter values $\sigma = 10, \beta = 8/3, \rho = 35$. The plots of the master stability functions are plotted in Figure 4.4 for different inner coupling matrices $\boldsymbol{P}$. Note from that for the $1 \rightarrow 1$ configuration that corresponds to the inner coupling matrix $\boldsymbol{P} = \text{diag}(1, 0, 0)$, the critical value $\eta < \tilde{\eta} \approx -10$, the master stability function is negative, which implies stability. Thus, the lower and upper thresholds for the uniform coupling are $\epsilon_1 = -10/-1.06 = 9.43$ and $\epsilon_2 = -10/-0.92 = 10.87$. Let us choose $\epsilon = 9.6 \in [\epsilon_1, \epsilon_2]$ and simulate the system. In Figure 4.5 are shown $\|\boldsymbol{x}_i - \boldsymbol{x}_j\|$ for $i, j = 1, 2, \ldots, N$ where $\|\boldsymbol{x}\|$ denotes the norm of $\boldsymbol{x}$. From Figure 4.5, it is clear that the cluster pattern corresponding to the symmetry $\mathcal{S}_1$ is achieved since $\lim_{t \mapsto \infty} \|\boldsymbol{x}_2 - \boldsymbol{x}_5\| = 0, \lim_{t \mapsto \infty} \|\boldsymbol{x}_3 - \boldsymbol{x}_4\| = 0$, and $\lim_{t \mapsto \infty} \|\boldsymbol{x}_1 - \boldsymbol{x}_j\| \neq 0, j = 2, 3, 4, 5$. Thus, the cluster pattern $\mathcal{G}_1 = \{1\}, \mathcal{G}_2 = \{2, 5\}, \mathcal{G}_3 = \{3, 4\}$ is apparent. The spatiotemporal view of the network is shown in Figure 4.6, where

$$\|\boldsymbol{x}\|_{rms} = \sqrt{\frac{1}{T} \int_0^T \|\boldsymbol{x}(t)\|^2 dt} \tag{4.23}$$

with T being the total simulation duration.

4.2.1.2 Removing Links

We now investigate cases where the cluster pattern can be controlled by removing or rewiring a link. For this case, consider that the link between the nodes 1 and 4 is removed in the network shown in Figure 4.1. The network is shown in Figure 4.7a when this link is removed. Since the network's topological structure is changed due to link removal, the symmetry and the corresponding cluster pattern to be observed in the network in Figure 4.7a are changed, too. As shown in Figure 4.7b, now the cluster pattern to be observed is $\mathcal{G}_1 = \{1, 5\}, \mathcal{G}_2 = \{2, 4\}, \mathcal{G}_3 = \{3\}$. The permutation matrix corresponding to this symmetry in Figure 4.7b is

$$\mathbf{\Delta} = \begin{bmatrix} 0 & 0 & 0 & 0 & 1 \\ 0 & 0 & 0 & 1 & 0 \\ 0 & 0 & 1 & 0 & 0 \\ 0 & 1 & 0 & 0 & 0 \\ 1 & 0 & 0 & 0 & 0 \end{bmatrix}, \tag{4.24}$$

and the corresponding transformation matrix $\mathbf{\Psi}$ is

$$\mathbf{\Psi} = \begin{bmatrix} 0.00 & -0.71 & 0.00 & 0.00 & 0.71 \\ 0.71 & 0.00 & 0.00 & 0.71 & 0.00 \\ 0.00 & 0.00 & 1.00 & 0.00 & 0.00 \\ -0.71 & 0.00 & 0.00 & 0.71 & 0.00 \\ 0.00 & 0.71 & 0.00 & 0.00 & 0.71 \end{bmatrix}. \tag{4.25}$$

The weight w_{ij} between all the nodes are chosen to be $w_{ij} = 1,\ i, j = 1, 2, \ldots, 5$. Thus, the outer coupling matrix $\mathbf{\Xi}$ is

$$\mathbf{\Xi} = \begin{bmatrix} -1.00 & 0.33 & 0.00 & 0.33 & 0.33 \\ 0.33 & -1.00 & 0.33 & 0.00 & 0.33 \\ 0.00 & 0.50 & -1.00 & 0.50 & 0.00 \\ 0.33 & 0.00 & 0.33 & -1.00 & 0.33 \\ 0.33 & 0.33 & 0.00 & 0.33 & -1.00 \end{bmatrix}. \tag{4.26}$$

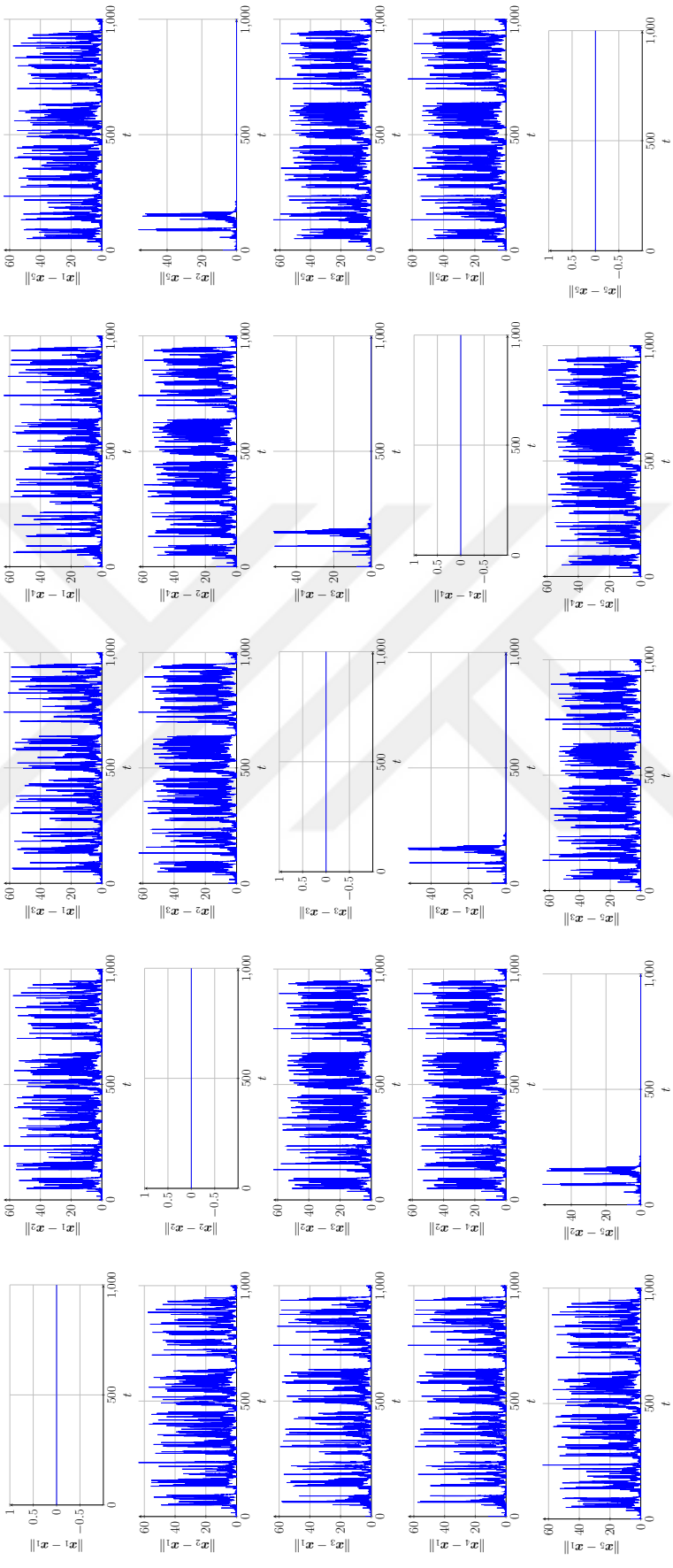

Figure 4.5 The simulation of the network in Figure 4.1.

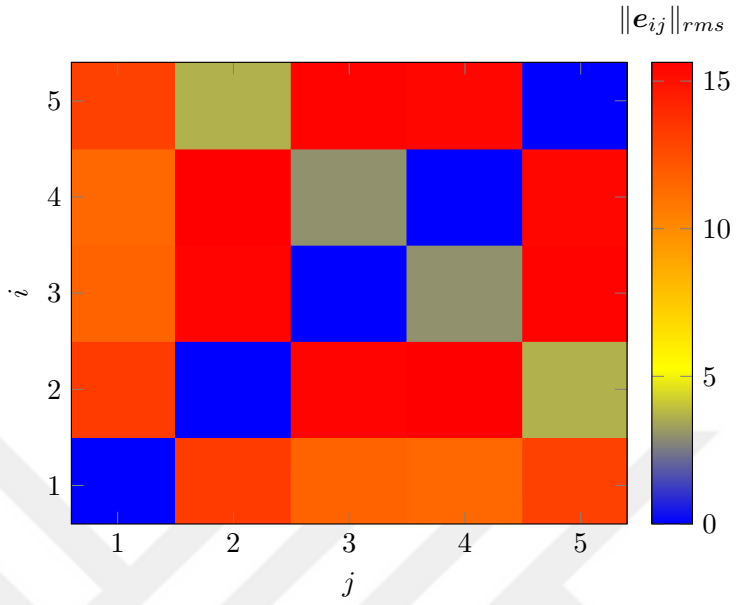

Figure 4.6 The spatiotemporal view of the network in Figure 4.1.

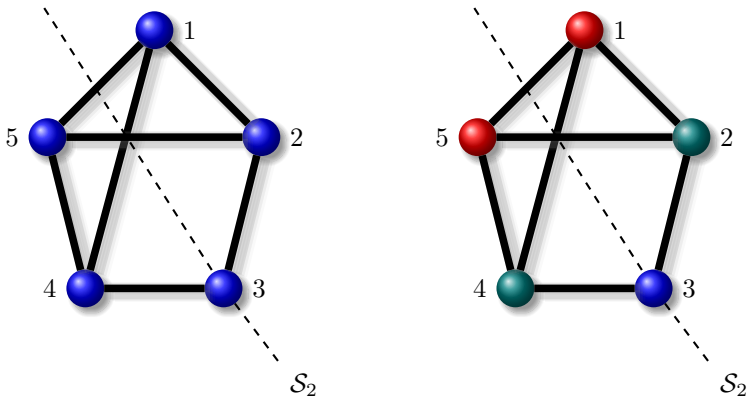

(a) (b)

Figure 4.7 (a) A simple network with possessing symmetry $\mathcal{S}_2$. (b) The cluster synchronization pattern $\mathscr{C}_2$ corresponding to symmetry $\mathcal{S}_2$. The nodes in the same cluster are shown with the same color.

When we transform Ξ using Ψ, we get

$$\Theta = \begin{bmatrix} -1.00 & 0.00 & 0.00 & 0.00 & 0.00 \\ 0.00 & -1.33 & 0.00 & 0.00 & 0.00 \\ 0.00 & 0.00 & -1.00 & 0.71 & 0.00 \\ 0.00 & 0.00 & 0.47 & -1.00 & 0.67 \\ 0.00 & 0.00 & 0.00 & 0.67 & -0.67 \end{bmatrix}, \tag{4.27}$$

which implies

$$\Omega = \begin{bmatrix} -1.00 & 0.00 \\ 0.00 & -1.33 \end{bmatrix}, \tag{4.28}$$

and

$$\Phi = \begin{bmatrix} -1.00 & 0.71 & 0.00 \\ 0.47 & -1.00 & 0.67 \\ 0.00 & 0.67 & -0.67 \end{bmatrix}. \tag{4.29}$$

The eigenvalues of Ω and Φ are found to be $\lambda_1^t = -1. > \lambda_2^t = -1.33$ and $\lambda_1^s = 0 > \lambda_2^s = -0.86 > \lambda_3^s = -1.80$. Since $\lambda_1^t < \lambda_2^s$, the eigenvalue condition is satisfied. The nodes in the network are Lorenz dynamics defined in (4.22) and the inner coupling matrix $\boldsymbol{P} = \text{diag}(1, 0, 0)$, which implies threshold for the stability is $\tilde{\eta} \approx -10$. Hence, the range for uniform coupling strength ϵ is $[\epsilon_1, \epsilon_2]$ where $\epsilon_1 = \tilde{\eta}/\lambda_1^t = -10/-1 = 10$ and $\epsilon_2 = \tilde{\eta}/\lambda_2^s = -10/-0.86 = 11.6$. Suppose we choose $\epsilon = 11.5$. In that case, we can see from time waveforms of the errors shown in Figure 4.8 that the cluster pattern corresponding to symmetry in Figure 4.7b is achieved since the node 1 synchronize to node 5, node 2 synchronize to node 4 and node 3 is out of synchronization with all remaining nodes in the network.

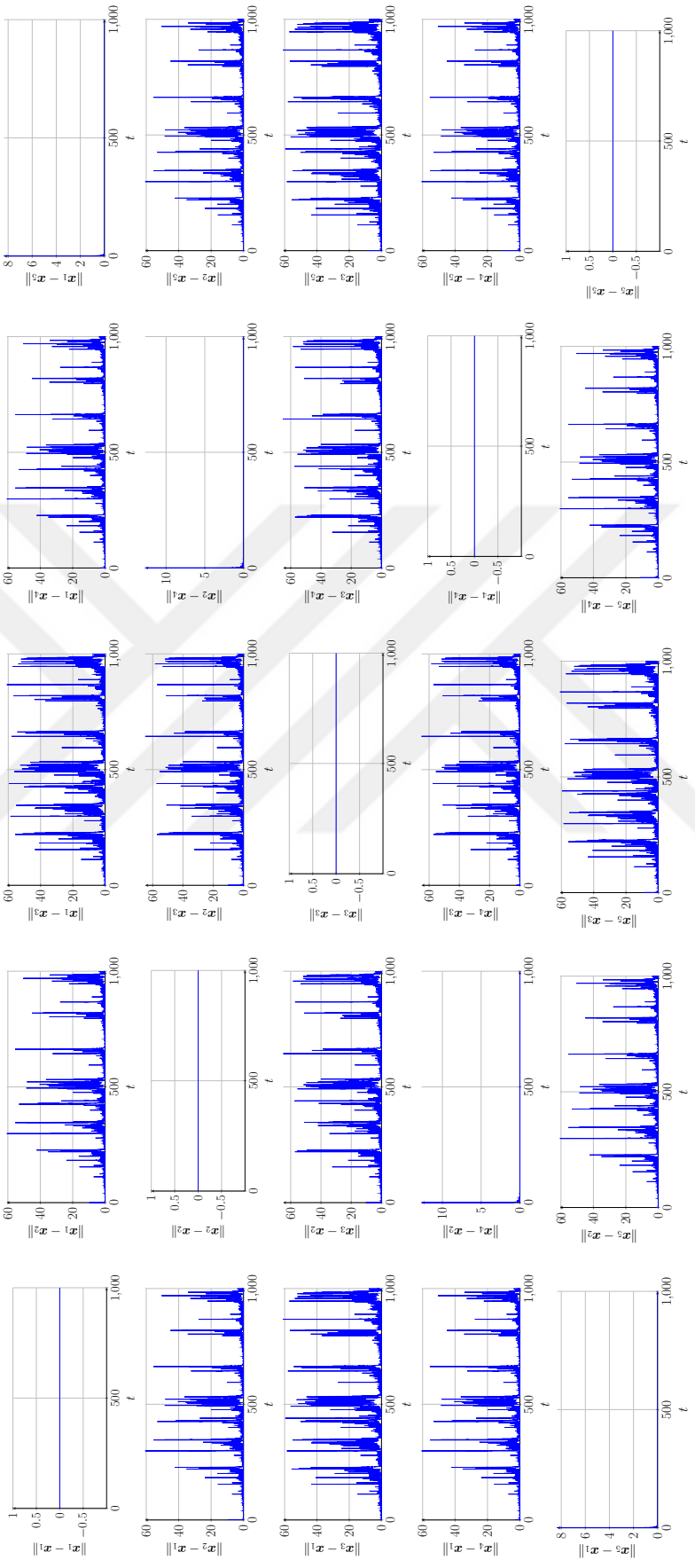

Figure 4.8 The simulation of the network in Figure 4.7.

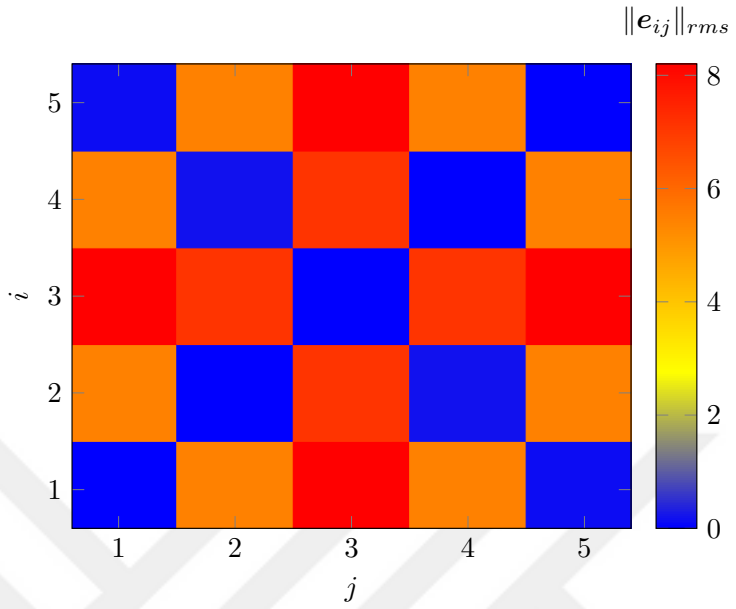

Figure 4.9 The spatiotemporal view of the network in Figure 4.7.

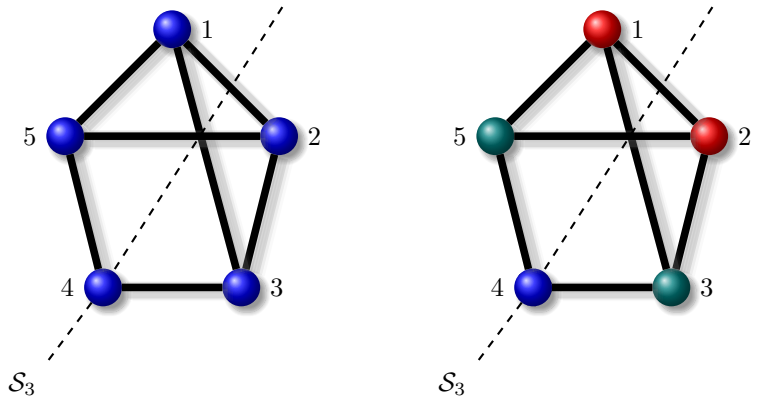

(a) (b)

Figure 4.10 (a) A simple network with possessing symmetry $\mathcal{S}_3$. (b) The cluster synchronization pattern $\mathscr{C}_3$ corresponding to symmetry $\mathcal{S}_3$. The nodes in the same cluster are shown with the same color.

4.2.1.3 Rewiring Links

Let us consider how the cluster pattern changes in response to link rewiring. For this purpose, consider that the link between the node 1 and 4 in the network Figure 4.7a is removed and rewired between the nodes 1 and 3. The resulting network is shown in Figure 4.10a. Again, the change in the topological structure of the network results in a change in the symmetry that the network possesses. Note how the symmetry axis of the network changes. We go from the network in Figure 4.7a to the network in Figure 4.10a. The cluster pattern to be observed in the network in Figure 4.10a is shown in Figure 4.10b. The permutation matrix corresponding to the symmetry in Figure 4.10b is

$$\mathbf{\Delta} = \begin{bmatrix} 0 & 1 & 0 & 0 & 0 \\ 1 & 0 & 0 & 0 & 0 \\ 0 & 0 & 0 & 0 & 1 \\ 0 & 0 & 0 & 1 & 0 \\ 0 & 0 & 1 & 0 & 0 \end{bmatrix}, \tag{4.30}$$

and the corresponding transformation matrix $\mathbf{\Psi}$ is

$$\mathbf{\Psi} = \begin{bmatrix} 0.71 & 0.00 & 0.00 & 0.71 & 0.00 \\ -0.71 & 0.00 & 0.00 & 0.71 & 0.00 \\ 0.00 & -0.71 & 0.00 & 0.00 & 0.71 \\ 0.00 & 0.00 & -1.00 & 0.00 & 0.00 \\ 0.00 & 0.71 & 0.00 & 0.00 & 0.71 \end{bmatrix}. \tag{4.31}$$

The weight w_{ij} between all the nodes are chosen to be $w_{ij} = 1,\ i, j = 1, 2, \ldots, 5$. Thus, the outer coupling matrix $\mathbf{\Xi}$ is

$$\mathbf{\Xi} = \begin{bmatrix} -1.00 & 0.33 & 0.33 & 0.00 & 0.33 \\ 0.33 & -1.00 & 0.33 & 0.00 & 0.33 \\ 0.33 & 0.33 & -1.00 & 0.33 & 0.00 \\ 0.00 & 0.00 & 0.50 & -1.00 & 0.50 \\ 0.33 & 0.33 & 0.00 & 0.33 & -1.00 \end{bmatrix}, \tag{4.32}$$

When we transform $\mathbf{\Xi}$ using $\mathbf{\Psi}$, we get

$$\boldsymbol{\Theta} = \begin{bmatrix} -1.33 & 0.00 & 0.00 & 0.0 & 0.0 \\ 0.00 & -1.00 & 0.0 & 0.0 & 0.0 \\ 0.00 & 0.00 & -1.00 & 0.00 & 0.71 \\ 0.00 & 0.00 & 0.00 & -0.67 & 0.67 \\ 0.00 & 0.00 & 0.47 & 0.67 & -1.00 \end{bmatrix}, \tag{4.33}$$

which implies

$$\boldsymbol{\Omega} = \begin{bmatrix} -1.33 & 0.00 \\ 0.00 & -1.00 \end{bmatrix}, \tag{4.34}$$

and

$$\boldsymbol{\Phi} = \begin{bmatrix} -1.00 & 0.00 & 0.71 \\ 0.00 & -0.67 & 0.67 \\ 0.47 & 0.67 & -1.00 \end{bmatrix}. \tag{4.35}$$

The eigenvalues of $\boldsymbol{\Omega}$ and $\boldsymbol{\Phi}$ is found to be $\lambda_1^t = -1 > \lambda_2^t = -1.33$ and $\lambda_1^s = 0 > \lambda_2^s = -0.86 > \lambda_3^s = -1.80$. Since $\lambda_1^t < \lambda_2^s$, the eigenvalue condition is satisfied. The nodes in the network are Lorenz dynamics defined in (4.22) and the inner coupling matrix $\boldsymbol{P} = \text{diag}(1, 0, 0)$, which implies threshold for the stability is $\tilde{\eta} \approx -10$. Hence, the range for uniform coupling strength ϵ is $[\epsilon_1, \epsilon_2]$ where $\epsilon_1 = \tilde{\eta}/\lambda_1^t = -10/-1 = 10$ and $\epsilon_2 = \tilde{\eta}/\lambda_2^s = -10/-0.86 = 11.6$. Suppose we choose $\epsilon = 11.5$. In that case, we can see from time waveforms of the errors shown in Figure 4.11 that the cluster pattern corresponding to symmetry in Figure 4.10b is achieved since the node 1 synchronizes to node 2, node 3 synchronize to node 5 and node 4 is out of synchronization with all remaining nodes in the network.

4.2.1.4 Removing and Rewiring Links

Finally, we connect the pieces to illustrate that the control of the topological structure of the network can control the cluster pattern. Figure 4.13 shows the change of the cluster patterns of the network in response to the change in the network

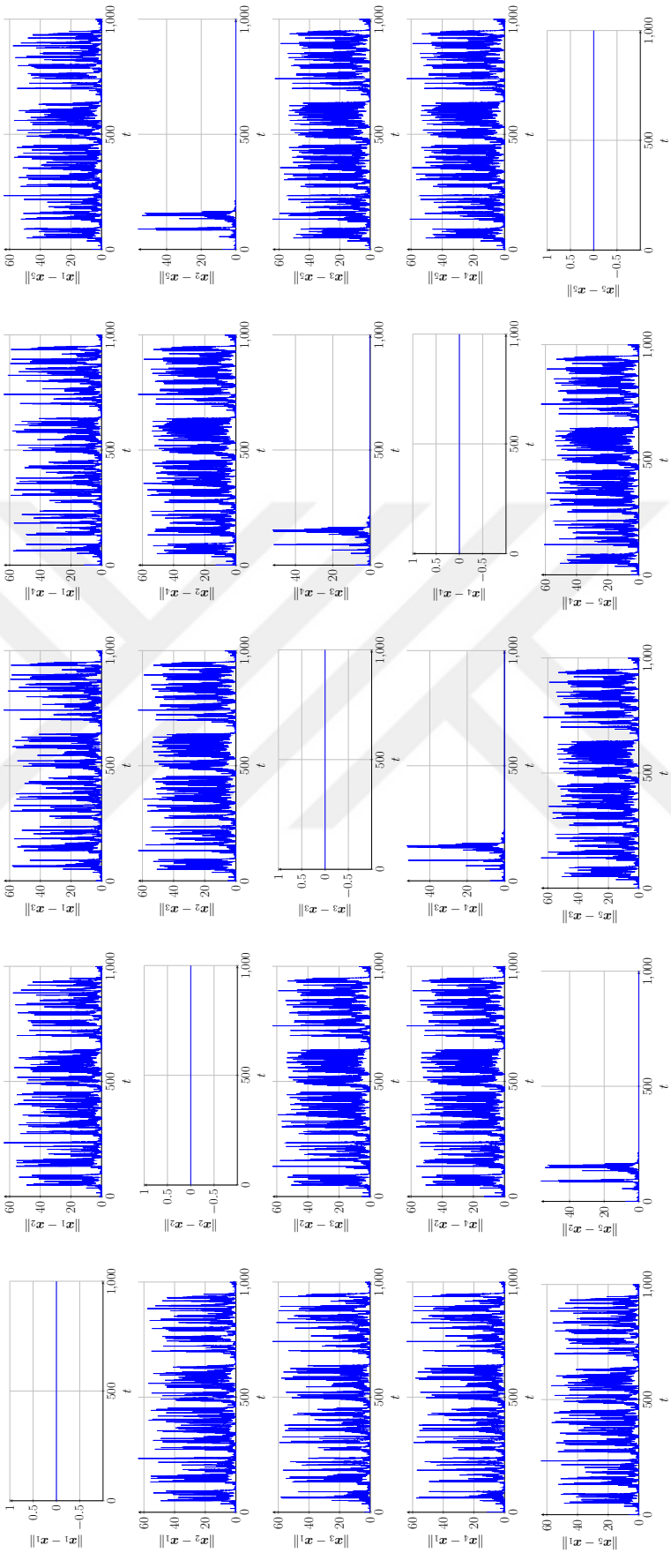

Figure 4.11 The simulation of the network in Figure 4.10.

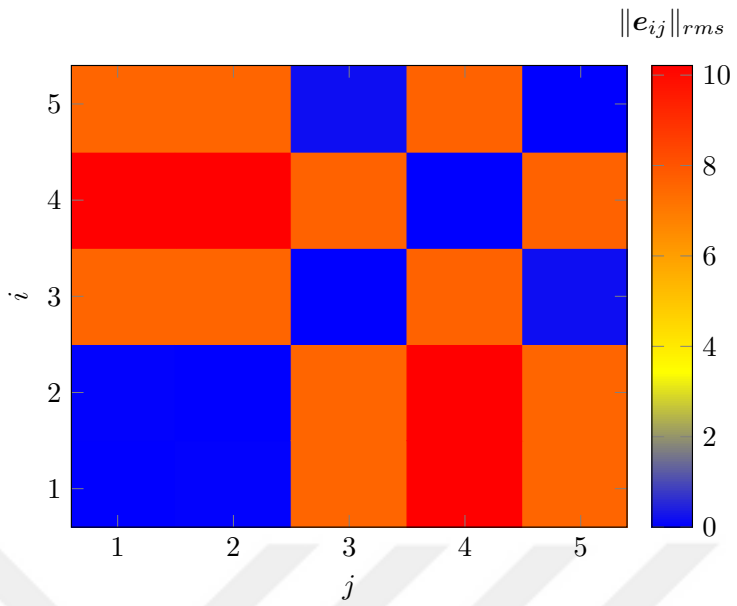

Figure 4.12 The spatiotemporal view of the network in Figure 4.10.$\epsilon = 11.5$

topological structure. We start from the unweighted network in Figure 4.1a with $w_{ij} = 1,\ i = 1, 2, \ldots, 5$ and $\epsilon = 11.5$. The total simulation time is 3000 seconds. At $t = 1000$, the link between the nodes 1 and 3 is removed, and we have the network shown in Figure 4.7a. Then, at $t = 2000$, the link between the nodes 1 and 4 is removed and rewired to the nodes 1 and 3, and we get the network shown in Figure 4.10a. Note from the time waveform of the errors for $t \in [0, 1000]$ that the network achieves full synchronization since all the nodes synchronize. After applying the first control action, the network achieves the cluster pattern shown in Figure 4.7b for $t \in [1000, 2000]$. Moreover, after the second control action is applied, the cluster pattern of the network changes from Figure 4.7b to the one shown in Figure 4.10b. Hence, it is clear from the simulation results that the cluster pattern of the network can be controlled by controlling the topological structure of the network.

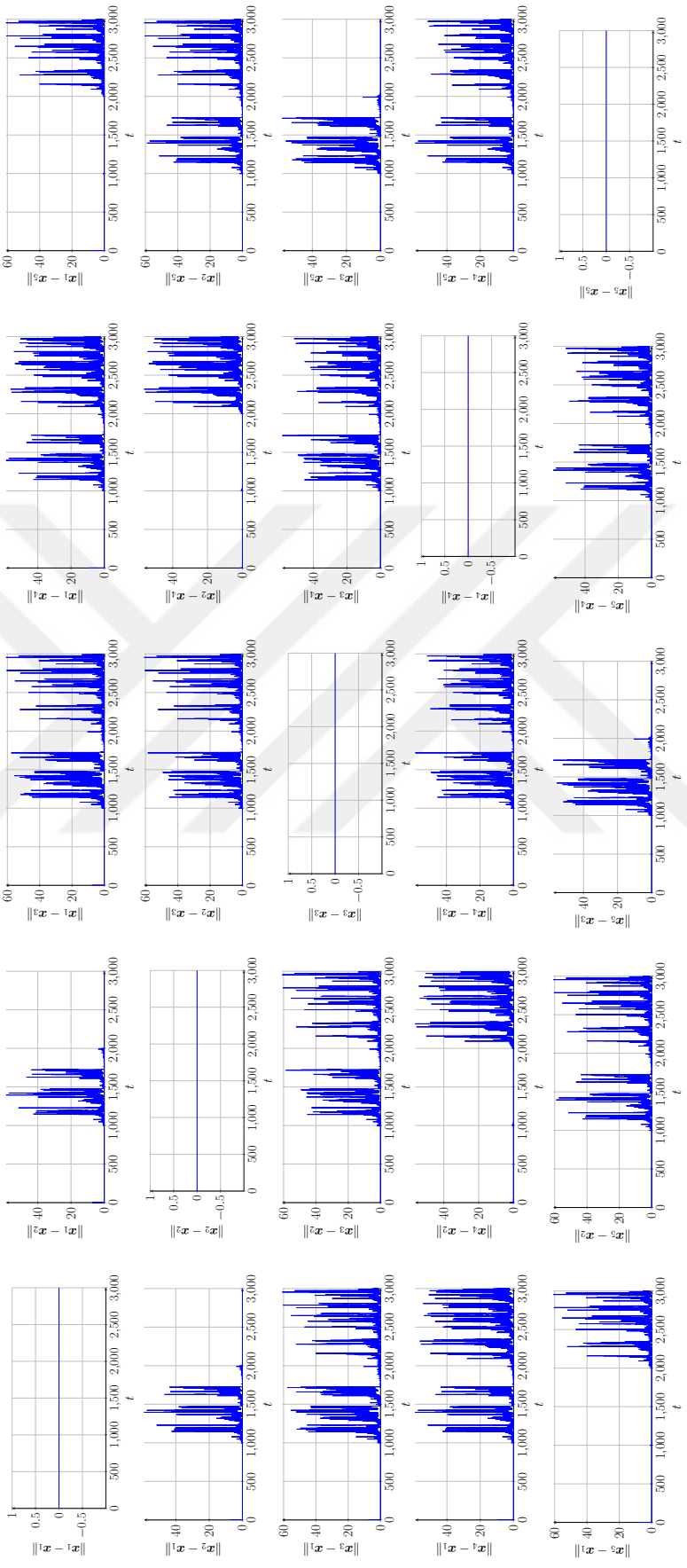

Figure 4.13 The simulation of the network in Figure 4.10.

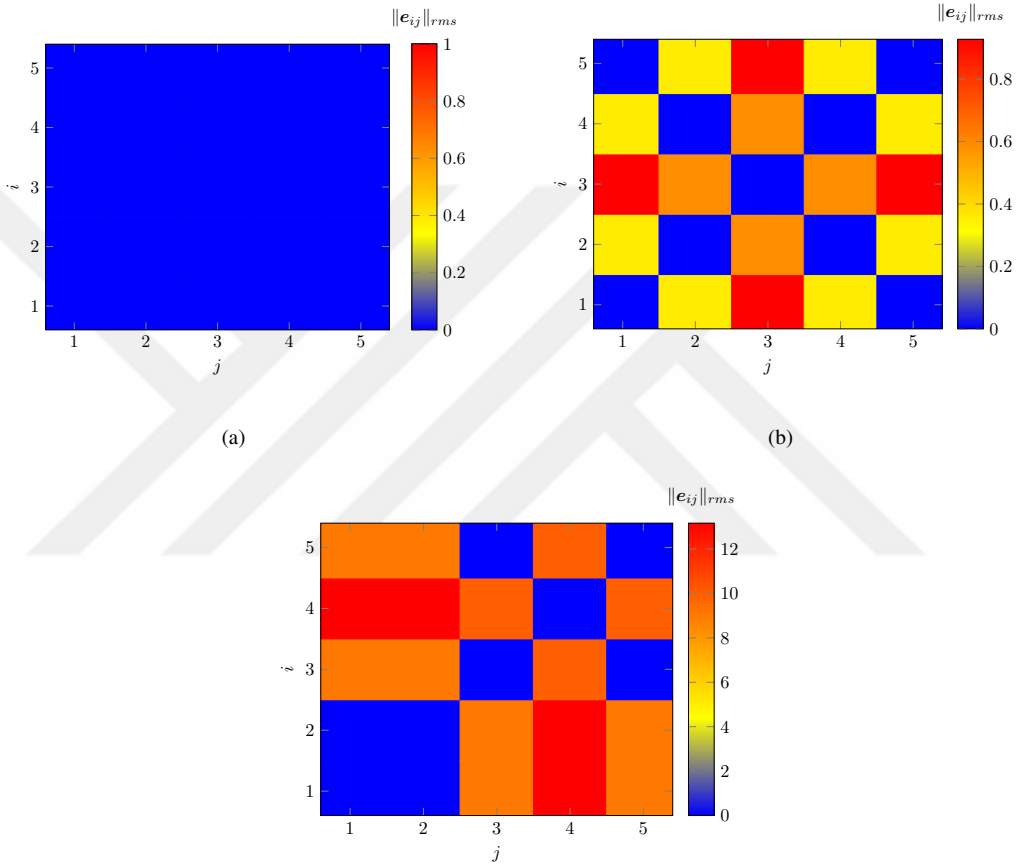

Figure 4.14 The spatiotemporal view of the network in Figure 4.11. $\epsilon = 11.5$ (a) $0 \leq t < 1000$, (b) $1000 \leq t < 2000$, (c) $2000 \leq t \leq 3000$.

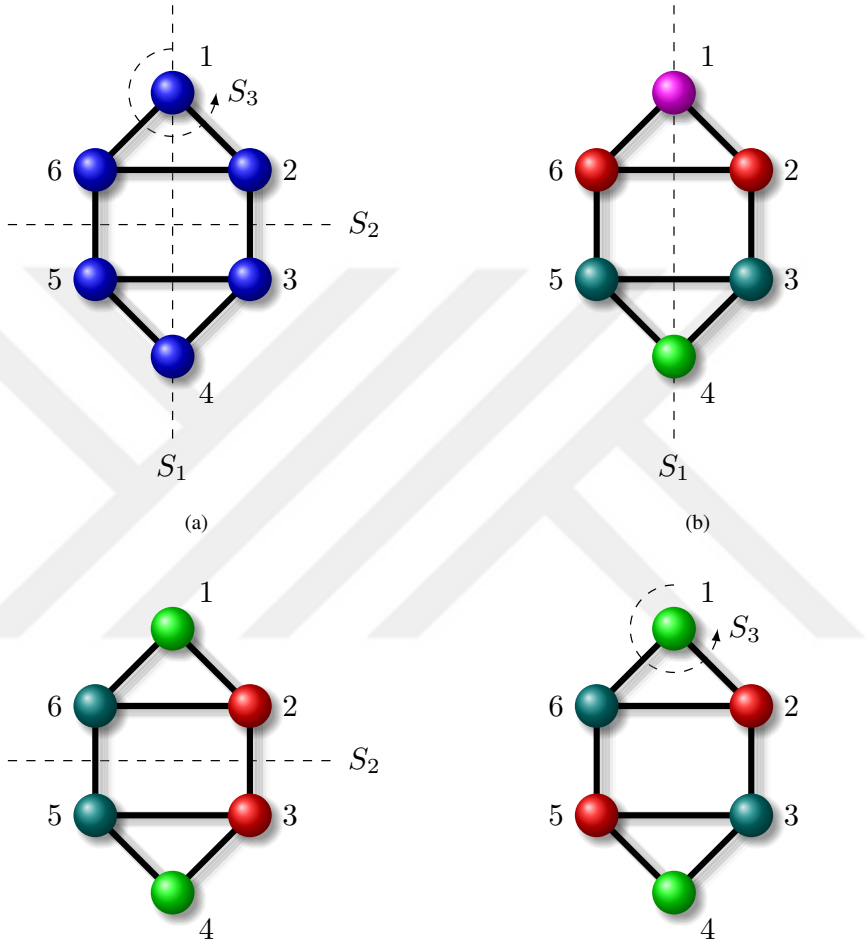

Figure 4.15 (a) An example network having the rotation symmetries (b) $\mathcal{S}_1$ and (c) $\mathcal{S}_2$, and (d) a rotation symmetry $\mathcal{S}_3$.

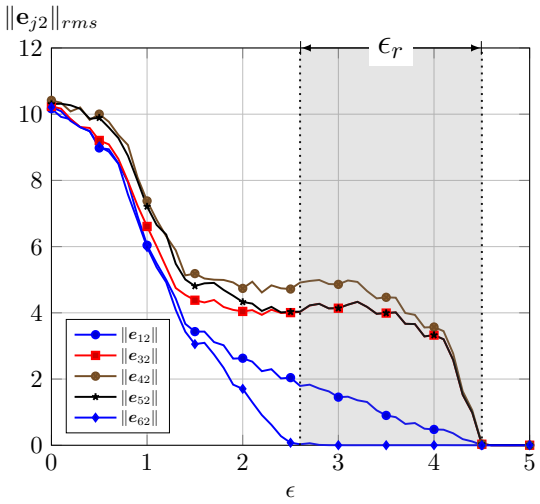

Figure 4.16 The change of the spatiotemporal status of the original (unpinned) network.

4.2.2 With Control Network

4.2.2.1 Inducing Cluster Synchronization

Consider the network shown in Figure 4.15 where $w_{14} = 0.8$ and $w = 1$ for the other connections. The individual node dynamics evolves by the Lorenz system given by

$$\begin{aligned} \dot{x} &= \alpha(y - x) \\ \dot{y} &= rx - y - xz \\ \dot{z} &= xy - bz \end{aligned} \tag{4.36}$$

where $\alpha = 10, r = 35$, and $b = 8/3$ are the parameters for which the individual nodes exhibit chaotic behavior. The inner coupling is chosen as

$$\boldsymbol{P} = \begin{bmatrix} 0 & 0 & 0 \\ 1 & 0 & 0 \\ 0 & 0 & 0 \end{bmatrix} \tag{4.37}$$

The threshold $\tilde{\eta}$ for which $\mu = g(\eta) < 0$ for $\eta < \tilde{\eta}$ is found to be $\tilde{\eta} \approx 8.3$ where g is the master stability function corresponding to Lorenz dynamics in (4.36) and the inner coupling matrix $\boldsymbol{P}$ in (4.37). The network in Figure 4.15 has the reflection symmetries $\mathcal{S}_1$ and $\mathcal{S}_2$ and the rotation symmetry $\mathcal{S}_3$.

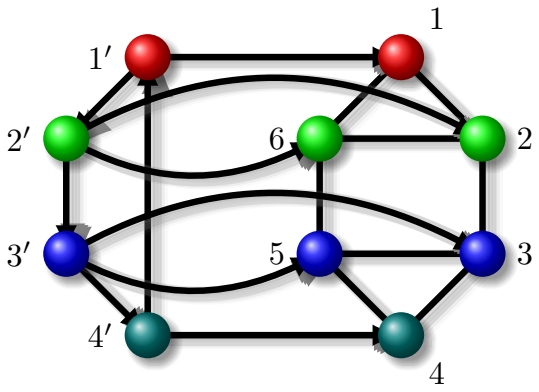

Figure 4.17 Controlled network.

Figure 4.16 shows the relation between the coupling strength ϵ and the synchronization status of the network. Figure 4.16 shows that when $2.6 < \epsilon < 4.5$, $\|e_6\| = 0, \|e_3\| = \|e_5\|$. Hence, the clusters $\mathcal{G}_1 = \{2, 6\}$ and $\mathcal{G}_2 = \{3, 5\}$ are achieved. The synchronized nodes satisfy the symmetry $\mathcal{S}_1$. For $\epsilon \approx 4.5$, full synchronization is achieved since $\|e_i\| = 0, i = 1, 2, \ldots, 6$. Although the network in Figure 4.15a has three symmetries, Figure 4.16 shows that only the cluster pattern $\mathscr{C}$ corresponding to $\mathcal{S}_1$ is observable for all values of ϵ. We need pinning control to observe the cluster pattern $\mathscr{C}_i$ corresponding to $\mathcal{S}_i$ for $i = 2, 3$.

Let $\epsilon = 1.0 < \epsilon_1$ for which all the nodes are out of synchronization, as seen from Figure 4.16. We know that although the cluster pattern $\mathscr{C}_1$ corresponding to $\mathcal{S}_1$ is topologically stable, it cannot be observed in the network due to the weak coupling for $\epsilon = 1.0$.

Corresponding to the clusters $\mathcal{G}_1 = \{1\}, \mathcal{G}_2 = \{2, 6\}, \mathcal{G}_3 = \{3, 5\}, \mathcal{G}_4 = \{4\}$, we have the control matrix $\boldsymbol{A} = [\omega_{ij}]$ and the outer coupling matrix $\boldsymbol{\Xi} = [\xi_{ij}]$ and the interlayer coupling matrix $\boldsymbol{C} = [\delta_{ij}]$

$$\boldsymbol{\Xi} = \begin{bmatrix} -2.8 & 1.0 & -0.0 & 0.8 & -0.0 & 1.0 \\ 1.0 & -3.0 & 1.0 & -0.0 & -0.0 & 1.0 \\ -0.0 & 1.0 & -3.0 & 1.0 & 1.0 & -0.0 \\ 0.8 & -0.0 & 1.0 & -2.8 & 1.0 & -0.0 \\ -0.0 & -0.0 & 1.0 & 1.0 & -3.0 & 1.0 \\ 1.0 & 1.0 & -0.0 & -0.0 & 1.0 & -3.0 \end{bmatrix} \tag{4.38}$$

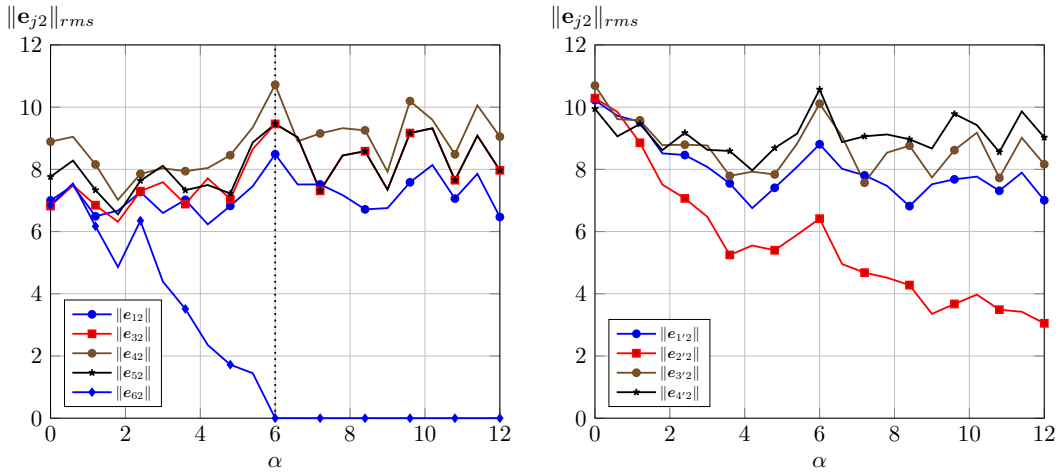

Figure 4.18 The change of spatiotemporal status of the network for changing control strength α.

$$\boldsymbol{A} = \begin{bmatrix} -2.8 & 2.0 & 0.0 & 0.8 \\ 1.0 & -2.0 & 1.0 & 0.0 \\ 0.0 & 1.0 & -2.0 & 1.0 \\ 0.8 & 0.0 & 2.0 & -2.8 \end{bmatrix} \tag{4.39}$$

$$\boldsymbol{C} = \begin{bmatrix} 1 & 0 & 0 & 0 \\ 0 & 1 & 0 & 0 \\ 0 & 0 & 1 & 0 \\ 0 & 0 & 0 & 1 \\ 0 & 0 & 1 & 0 \\ 0 & 1 & 0 & 0 \end{bmatrix} \tag{4.40}$$

The nodes l' of the control network are pinned to all the nodes of the clusters $\mathcal{G}_l$ for $l = 1, 2, \ldots, 4$, respectively. Although the unpinned network is undirected, the coupling from the control network to the unpinned network is directed.

The change of the spatiotemporal status of the network is shown in Figure 4.18, which shows clearly that at $\eta_1 \approx 6$, the synchronous pattern corresponding to $\mathcal{S}_1$ is successfully induced.

To derive the thresholds η_1 and η_2 theoretically, we have the permutation matrix corresponding to $\mathcal{S}_1$,

$$\boldsymbol{\Delta} = \begin{bmatrix} 1 & 0 & 0 & 0 & 0 & 0 \\ 0 & 0 & 0 & 0 & 0 & 1 \\ 0 & 0 & 0 & 0 & 1 & 0 \\ 0 & 0 & 0 & 1 & 0 & 0 \\ 0 & 0 & 1 & 0 & 0 & 0 \\ 0 & 1 & 0 & 0 & 0 & 0 \end{bmatrix}, \tag{4.41}$$

from which

$$\boldsymbol{\Psi} = \begin{bmatrix} 0.00 & 0.00 & 0.00 & 0.00 & 1.00 & 0.00 \\ 0.00 & -0.71 & 0.00 & 0.00 & 0.00 & 0.71 \\ 0.71 & 0.00 & 0.71 & 0.00 & 0.00 & 0.00 \\ 0.00 & 0.00 & 0.00 & 1.00 & 0.00 & 0.00 \\ -0.71 & 0.00 & 0.71 & 0.00 & 0.00 & 0.00 \\ 0.00 & 0.71 & 0.00 & 0.00 & 0.00 & 0.71 \end{bmatrix}. \tag{4.42}$$

After the transformation $\boldsymbol{\Theta} = \boldsymbol{\Psi}^{-1}\boldsymbol{\Xi}\boldsymbol{\Psi}$, $\boldsymbol{\Xi}$ has the blocked form

$$\boldsymbol{\Theta} = \begin{bmatrix} 0.00 & 0.00 & 0.00 & 0.00 & 1.00 & 0.00 \\ 0.00 & -0.71 & 0.00 & 0.00 & 0.00 & 0.71 \\ 0.71 & 0.00 & 0.71 & 0.00 & 0.00 & 0.00 \\ 0.00 & 0.00 & 0.00 & 1.00 & 0.00 & 0.00 \\ -0.71 & 0.00 & 0.71 & 0.00 & 0.00 & 0.00 \\ 0.00 & 0.71 & 0.00 & 0.00 & 0.00 & 0.71 \end{bmatrix}. \tag{4.43}$$

Thus,

$$\boldsymbol{\Omega} = \begin{bmatrix} -4.00 & -1.00 \\ -1.00 & -4.00 \end{bmatrix}, \tag{4.44}$$

and

$$\boldsymbol{\Phi} = \begin{bmatrix} -2.00 & 1.41 & 0.00 & 1.00 \\ 1.41 & -2.80 & 0.80 & 0.00 \\ 0.00 & 0.80 & -2.80 & 1.41 \\ 1.00 & 0.00 & 1.41 & -2.00 \end{bmatrix}. \tag{4.45}$$

The eigenvalues of $\mathbf{\Omega}$ and $\mathbf{\Phi}$ are $\lambda_{2,t} = -5, \lambda_{1,t} = -3$ and $\lambda_{4,s} = -4.74, \lambda_{3,s} = -3, \lambda_{2,s} = -1.85, \lambda_{1,s} = 0$, respectively. Hence, we have $\eta_1 = 5.3$ and $\eta_2 = 8.3$, which agree with the numerical results obtained in Figure 4.18.

4.2.2.2 Controlling Cluster Synchronization

Next, we will obtain the cluster pattern $\mathscr{C}_3$ corresponding to the symmetry $\mathcal{S}_3$. The cluster pattern $\mathscr{C}_3$ cannot be observed for any value of the coupling strength ϵ without the control network. Hence, the control network must be employed to observe $\mathscr{C}_3$.

For the clusters $\mathcal{S}_3$ are $\mathcal{G}_1 = \{1, 4\}, \mathcal{G}_2 = \{2, 5\}, \mathcal{G}_3 = \{3, 6\}$, we have

$$\mathbf{\Xi} = \begin{bmatrix} -2.8 & 1.0 & -0.0 & 0.8 & -0.0 & 1.0 \\ 1.0 & -3.0 & 1.0 & -0.0 & -0.0 & 1.0 \\ -0.0 & 1.0 & -3.0 & 1.0 & 1.0 & -0.0 \\ 0.8 & -0.0 & 1.0 & -2.8 & 1.0 & -0.0 \\ -0.0 & -0.0 & 1.0 & 1.0 & -3.0 & 1.0 \\ 1.0 & 1.0 & -0.0 & -0.0 & 1.0 & -3.0 \end{bmatrix}, \tag{4.46}$$

$$\boldsymbol{A} = \begin{bmatrix} -2 & 1 & 1 \\ 1 & -3 & 2 \\ 1 & 2 & -3 \end{bmatrix}, \tag{4.47}$$

$$\boldsymbol{C} = \begin{bmatrix} 1 & 0 & 0 \\ 0 & 1 & 0 \\ 0 & 0 & 1 \\ 1 & 0 & 0 \\ 0 & 1 & 0 \\ 0 & 0 & 1 \end{bmatrix}. \tag{4.48}$$

For the Lorenz system and the inner coupling matrix $\boldsymbol{P}$ in (4.37), the threshold η for which the master stability function g goes from instability to stability is found to be $\tilde{\eta} \approx 8.3$.

The permutation matrix corresponding to the symmetry $\mathcal{S}_3$ is

$$\mathbf{\Delta} = \begin{bmatrix} 0 & 0 & 0 & 1 & 0 & 0 \\ 0 & 0 & 0 & 0 & 1 & 0 \\ 0 & 0 & 0 & 0 & 0 & 1 \\ 1 & 0 & 0 & 0 & 0 & 0 \\ 0 & 1 & 0 & 0 & 0 & 0 \\ 0 & 0 & 1 & 0 & 0 & 0 \end{bmatrix}. \tag{4.49}$$

Using the (4.9), we have

$$\mathbf{\Theta} = \begin{bmatrix} -3.0 & 1.0 & 0 & 0 & 0 & 0 \\ 1.0 & -3.6 & -1.0 & 0 & 0 & 0 \\ 0 & -1.0 & -3.0 & 0 & 0 & 0 \\ 0 & 0 & 0 & -2.0 & 1.0 & 1.0 \\ 0 & 0 & 0 & 1.0 & -3.0 & 2.0 \\ 0 & 0 & 0 & 1.0 & 2.0 & -3.0 \end{bmatrix}. \tag{4.50}$$

Hence,

$$\mathbf{\Omega} = \begin{bmatrix} -3.0 & 1.0 & 0 \\ 1.0 & -3.6 & -1.0 \\ 0 & -1.0 & -3.0 \end{bmatrix} \tag{4.51}$$

and

$$\mathbf{\Phi} = \begin{bmatrix} -2 & 1 & 1 \\ 1 & -3 & 2 \\ 1 & 2 & -3 \end{bmatrix} \tag{4.52}$$

The eigenvalues of $\mathbf{\Omega}$ is $\lambda_{3,t} = -4.74, \lambda_{2,t} = -3, \lambda_{1,t} = -1.85$, and those of $\mathbf{\Phi}$ are $\lambda_{3,s} = -5, \lambda_{2,s} = -3, \lambda_{1,s} = 0$. Hence, we have $\lambda_{min} = 1.85$. Thus, the cluster pattern $\mathcal{S}_3$ is topologically unstable and cannot be generated by varying the coupling strength ϵ without using the control network.

However, applying the control network can generate the cluster pattern for an

arbitrary ϵ. For example, let $\epsilon = 1.0$. Then, we have $\eta_1 = (\tilde{\eta}/\epsilon) - \lambda_{min} = 6.44$ and $\eta_2 = \tilde{\eta}/\epsilon = 8.3$ which implies that the cluster pattern corresponding to $\eta \in [\eta_1, \eta_2]$. Figure 4.19 illustrates the network simulation results for $\epsilon = 7.0$, which shows that the cluster pattern corresponding to the symmetry $\mathcal{S}_3$ is observed.

From the numerical results in Figure 4.19, we conclude that

1. The cluster pattern corresponding to the symmetry $\mathcal{S}_3$ was originally unstable, which implies that the cluster pattern corresponding to $\mathcal{S}_3$ cannot be realized by changing only the global coupling strength ϵ.

2. However, we introduced a small size network consisting of the nodes $\{1', 2', 3'\}$ and induced the cluster pattern corresponding cluster pattern consisting of the clusters $\mathcal{G}_1 = \{1, 4\}, \mathcal{G}_2 = \{2, 5\}, \mathcal{G}_1 = \{3, 6\}$.

3. Here, the keyword inducing is very important. Because the driving, pinning, nodes $\{1', 2', 3'\}$ induces the required cluster synchronization without synchronizing with the nodes in their corresponding clusters. That is, the node $1'$, $2'$ and $3'$ do synchronize with the nodes in the clusters $\{1, 4\}$, $\{2, 5\}$ and $\{3, 6\}$ for $\eta \in [\eta_1, \eta_2]$.

4. The control network nodes are connected to the nodes in their corresponding clusters unidirectionally, and more importantly, the pinning and pinned nodes do not synchronize with each other. That is, we can divide the network nodes between the transmitter and receiver such that the pinning nodes reside in the transmitter and the pinned nodes remain on the receiver side.

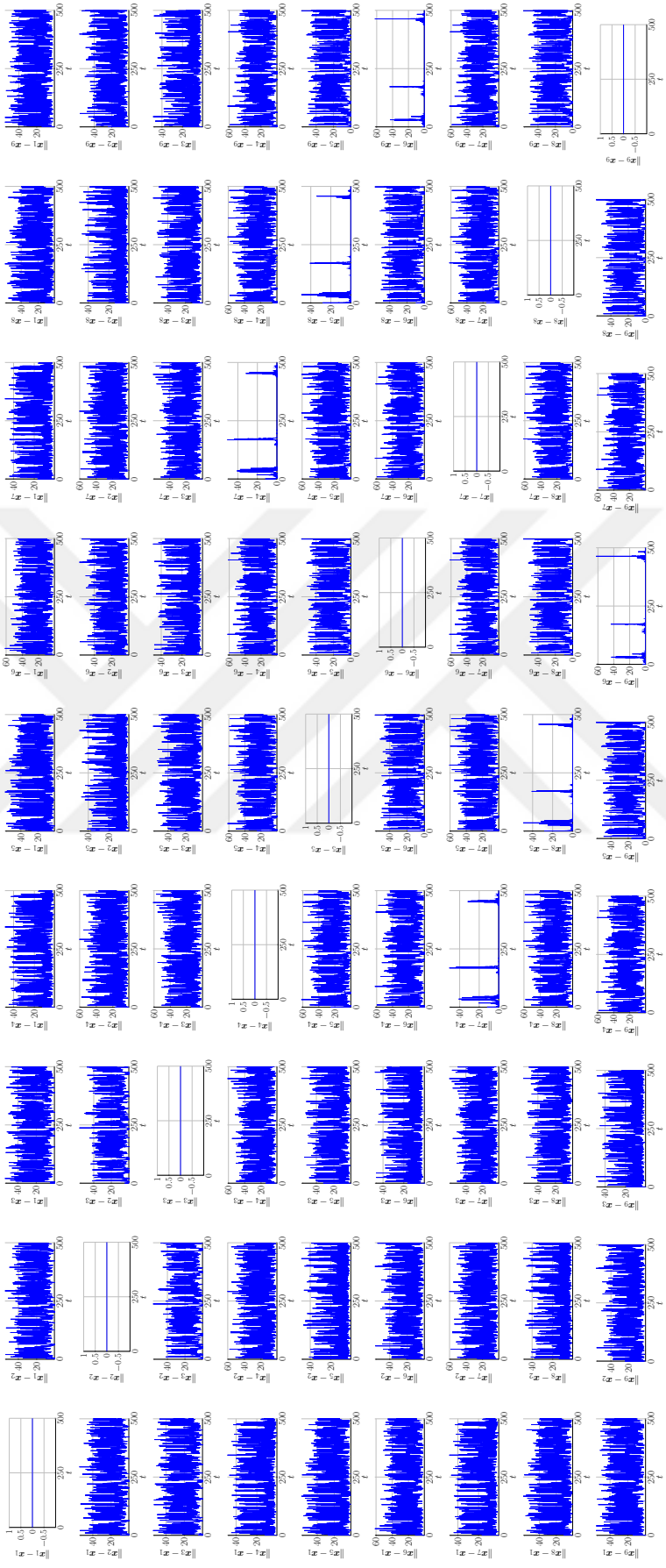

Figure 4.19 The numerical simulation of the network.

CHAPTER FIVE
CHAOTIC COMMUNICATION SYSTEMS

5.1 Spread Spectrum Communications

A communication system that transmits signals within a narrow frequency band is called a narrow-band communication system. One common issue experienced by such systems is jamming, wherein a deliberate injection of a high-energy sinusoidal signal disrupts the transmitted signal within the targeted frequency band. A possible solution is to spread the frequency band of the transmitted signal so that the information is concealed within the background noise. The frequency spectrum of the transmitted signals is spread over a broader range than their inherent bandwidths in a spread spectrum communication system (SSCS).

Apart from providing a means to hide information within the background noise, SSCSs also offer a certain level of security due to using encryption keys while spreading the frequency spectrum. Consequently, even if a third party eavesdrops on the communication channel, the information will only be available with prior knowledge of the decoding key. In addition to these security benefits, SSCSs also have the advantages of reducing the impact of multipath effects, enhancing signal quality in multi-user environments, lowering the required effort for frequency planning, and increasing the system's overall capacity (Tse & Lau, 2003).

SSCSs utilize two commonly used techniques: direct sequence and frequency hopping. The direct sequence technique involves multiplying the information sequence by a high frequency of the encoding sequence prior to modulation, effectively widening the transmitted signal's spectrum. On the other hand, the frequency hopping method entails the modulator's frequency changing within a broad frequency range, driven by an encoding sequence. Unlike the direct sequence approach, which employs a continuous spectrum, discrete frequencies are utilized in frequency hopping. The receiver uses the same encoding sequence the transmitter employs to decode the received information sequence.

5.2 Chaos Based Modulation Schemes

Wide frequency range signals are highly desirable in spread spectrum communications. Chaotic signals serve as suitable candidates for such communications. Chaotic dynamical systems, characterized by their sensitivity to initial conditions, generate uncorrelated, random-like, and aperiodic signals. These signals possess the advantage of uniform power distribution across a wide frequency band. The orthogonal signals are essential for expanding symbols in communication systems. Chaotic signals exhibit the desired property of being uncorrelated, thereby fulfilling the orthogonality requirement of digital communication systems. Moreover, different orthogonal chaotic signals can be easily generated by altering the initial conditions of chaotic oscillators.

Contrary to the advantages mentioned above, certain undesirable aspects are associated with chaotic communications. The chaotic communication systems, which rely on chaotic synchronization between the oscillators in both the transmitter and receiver, possess a slower data rate than conventional communication systems. The delay stems from the time required for the chaotic synchronization. Another drawback of chaotic synchronization is its vulnerability to channel impairments, such as noise and delay, which adversely impact the synchronization performance and consequently compromise the reliability of the communication. Shannon's theorem establishes a relation between the maximum data rate achievable for reliable transmission over a communication channel and factors such as bandwidth and noise level. Thus, knowledge of the bandwidth becomes necessary for determining the maximum data rate. Unfortunately, no analytical method is currently available to estimate the bandwidth of chaotic signals, leaving computer simulations as the sole viable approach.

Numerous chaotic modulation strategies have been devised following the concept that chaotic signals can be utilized in communication systems (Tse & Lau, 2003). These strategies can generally be clustered into analog and digital communication schemes. Analog chaotic communication systems include approaches such as chaotic

Table 5.1 Classification of chaotic communication systems

Class	Type	System	Coherent Detection Applicable
Coherent	Analog	Chaotic Masking	No
	Digital	Chaos Shift Keying (CSK)	No
		Chaotic Spreading Sequence	Yes
		Chaotic Digital CDMA	Yes
No	Analog	Chaotic Modulation	No
	Digital	Differential Chaos Shift Keying (DCSK)	Yes
		FM Differential Chaos Shift Keying (FM-DCSK)	Yes
		Chaotic On-Off Keying (COOK)	Yes
		Correlation Delay Shift Keying (CDSK)	Yes
		Quadrature CSK (QCSK)	Yes

masking and chaotic modulation. Chaotic masking involves combining the information-bearing message with a chaotic carrier signal. The information can be extracted in the receiver (Cuomo & Oppenheim, 1993) by exploiting the master-slave synchronization phenomenon of chaotic systems. Chaotic modulation, on the other hand, conceals the information within the parameters of the chaotic oscillators(Kennedy & Hasler, 1993). In the receiver, the information is retrieved by tracking which system parameter the oscillators are locked onto.

In chaotic digital communication, the detection can be coherent and non-coherent. Some chaotic modulation schemes are classified in Table 5.1. In the following subsections, we will look at two of the most intensively studied chaotic modulation schemes, namely the chaos shift keying (CSK) and differential chaos shift keying (DCSK), which form the comparison base for the proposed method.

5.2.1 Chaos Shift Keying

Figure 5.1 shows the block diagram of the chaos shift keying scheme (Tse & Lau, 2003). The transmitter utilizes two chaotic oscillators to transmit two outputs for a duration of T. The transmission is based on a binary sequence b_i. The transmitted signal for the interval $(i-1)T \leq t \leq iT$ can be represented as

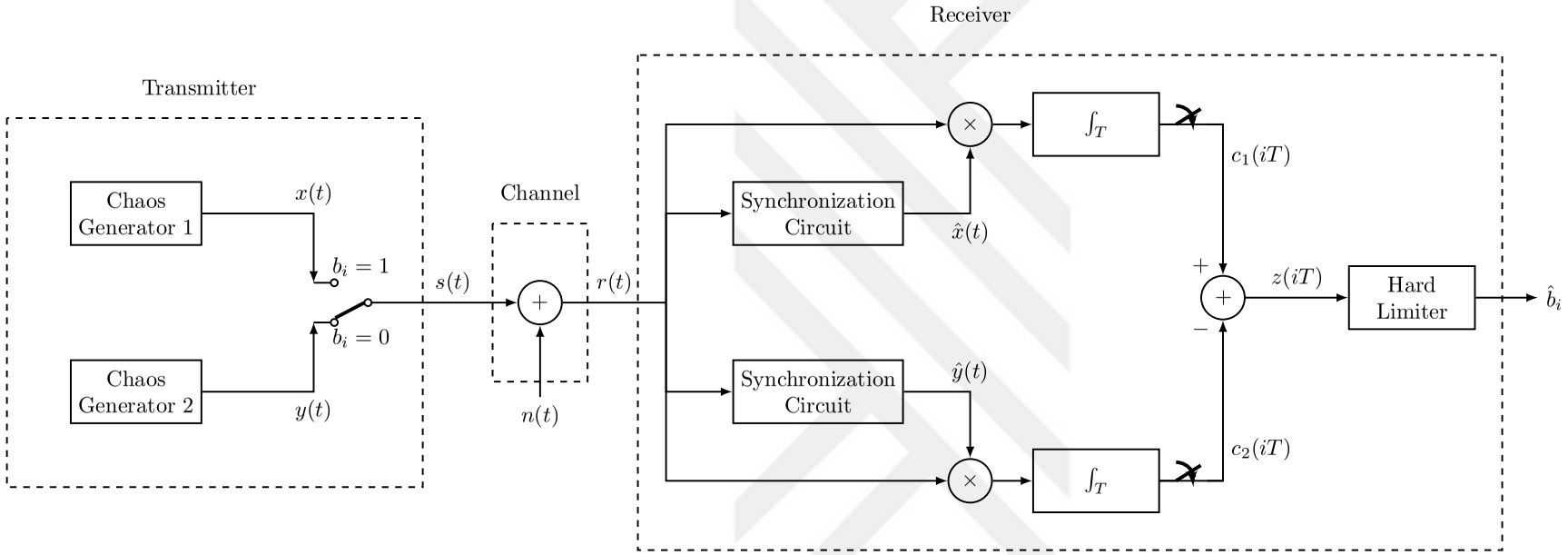

Figure 5.1 Block diagram for chaos shift keying.

$$s(t) = \begin{cases} x(t), & b_i = 0, \\ y(t) & b_i = 1, \end{cases} \tag{5.1}$$

where $b_i \in \{0, 1\}$ is the i^{th} binary symbol, and $x(t)$ and $y(t)$ represent the output of the first and second chaotic oscillator, respectively. The transmitted chaotic waveform $s(t)$ is affected by the channel noise $n(t)$, which is assumed to be a white Gaussian process with zero mean and a noise power spectral density of $\frac{N_0}{2}$. On the receiver side, the received corrupted signal $r(t) = s(t) + n(t)$ is cross-correlated with the replicated chaotic signals $\hat{x}(t)$ and $\hat{y}(t)$ that are generated using chaotic synchronization. The output of the correlator is sampled at intervals of duration T. Thus, the outputs of the correlators after the i^{th} symbol can be expressed as

$$\begin{aligned} c_1(iT) &= \int_{(i-1)T-T_s}^{iT} r(t)\hat{x}(t)dt, \\ c_2(iT) &= \int_{(i-1)T-T_s}^{iT} r(t)\hat{y}(t)dt, \end{aligned} \tag{5.2}$$

where T_s is the time it takes for the chaotic oscillators in the transmitter and the receiver to synchronize, the difference between the outputs of the correlator is passed through a hard limiter. The hard limiter implements the detection rule given by

$$\hat{b}_i = \begin{cases} 0 & z(iT) \leq 0, \\ 1 & z(iT) < 0, \end{cases} \tag{5.3}$$

where $\hat{b}_i$ is the detected binary value at time index i, and $z(iT)$ represents the input of the hard limiter at time $t = iT$.

The receiver requires reference signals, $\hat{x}(t)$ and $\hat{y}(t)$, in order to make a decision (Figure 5.1). The decision-making process relies on the phenomenon of chaotic synchronization. It is crucial to acknowledge that channel impairments, such as noise and delay, can disrupt this synchronization. A differential chaos shift keying scheme

has been proposed alternatively.

5.2.2 Differential Chaos Shift Keying

The block diagram depicting the structure of the differential chaos shift keying (DCSK) scheme is illustrated in Figure 5.2 (Tse & Lau, 2003). The reference signal is transmitted in the initial half of a symbol duration. The binary information determines the choice between transmitting the reference signal or its negation. Consequently, the transmitted signal during the transmission of the i^{th} symbol can be expressed as

$$s(t) = \begin{cases} x(t) & (i-1)T \le t \le (i-\frac{1}{2}T) \\ x(t-\frac{T}{2}) & (i-\frac{1}{2})T \le t \le iT) \quad \text{if } b_i = 0, \\ -x(t-\frac{T}{2}) & (i-\frac{1}{2})T \le t \le iT) \quad \text{if } b_i = 1. \end{cases} \tag{5.4}$$

At the receiver's end, the received signal $r(t)$ is correlated with a delayed replica of itself, with the delay equal to half the symbol duration. The output of the correlator is sampled at the end of each symbol duration T. Consequently, the input to the hard limiter at the end of the i^{th} symbol transmission is given by the integral expression

$$z(iT) = \int_{(i-1/2)T}^{iT} r(t) r\left(t - \frac{T}{2}\right) dt \tag{5.5}$$

The decision rule employed by the hard limiter is as follows:

$$\hat{b}_i = \begin{cases} 0, & z(iT) \ge 0 \\ 1, & z(iT) < 0 \end{cases} \tag{5.6}$$

Notably, the encoding of information in DCSK is differential in nature. In other words, the binary information determines the transition from the waveform transmitted during the first half of the symbol duration to the waveform transmitted during the second half of the symbol duration. This means that the reference signal is

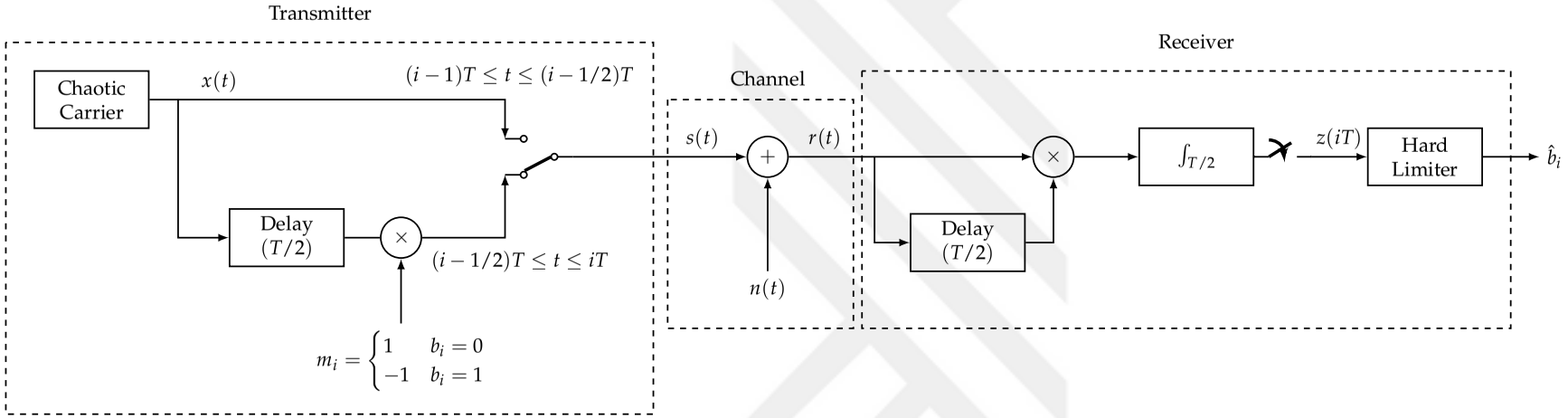

Figure 5.2 Block diagram for differential chaos shift keying.

transmitted during the first half of the symbol duration, followed by the information-carrying signal during the second half. Consequently, the receiver does not need to reproduce the reference signals, leading to the disappearance of synchronization between the chaotic oscillators in the transmitter and receiver. This noncoherent detection in DCSK results in a simplified receiver structure compared to the CSK technique. However, this simplification comes at the cost of halving the symbol transmission rate, as half of the symbol duration is wasted to transmit the reference signal.

The primary explanation of DCSK signaling provided here encompasses several variations, including chaotic on-off keying (COOK), frequency-modulated differential chaos shift keying (FM-DCSK), correlation delay shift keying (CDSK), and quadrature chaos shift keying (QCSK) (Tse & Lau, 2003). In COOK, a chaotic signal is transmitted during the first half of the symbol transmission, while no signal is transmitted through the channel during the second half. The FM-DCSK scheme generates chaotic basis signals through chaotic frequency modulation generators that employ a chaotic generator to feed an FM modulator. DCSK entails transmitting the sum of the chaotic signal and its delayed form. Consequently, there is no switching during DCSK signaling. Lastly, QCSK involves further phase shifting a replica of the delayed chaotic signal by $\pi/2$. Like DCSK, the chaotic reference signal is transmitted during the first half of the symbol transmission. Then, during the second half, a linear combination of the delayed and $\pi/2$-shifted signal is transmitted. Symbols determine the coefficients of the linear combination, each consisting of two bits.

5.3 Detection Performances

5.3.1 Detection Performance of Chaos Shift Keying

Consider the CSK scheme in Figure 5.3, which is the discrete-time equivalent of the CSK scheme in Figure 5.1. In particular, the relation between continuous time and discrete time signals are

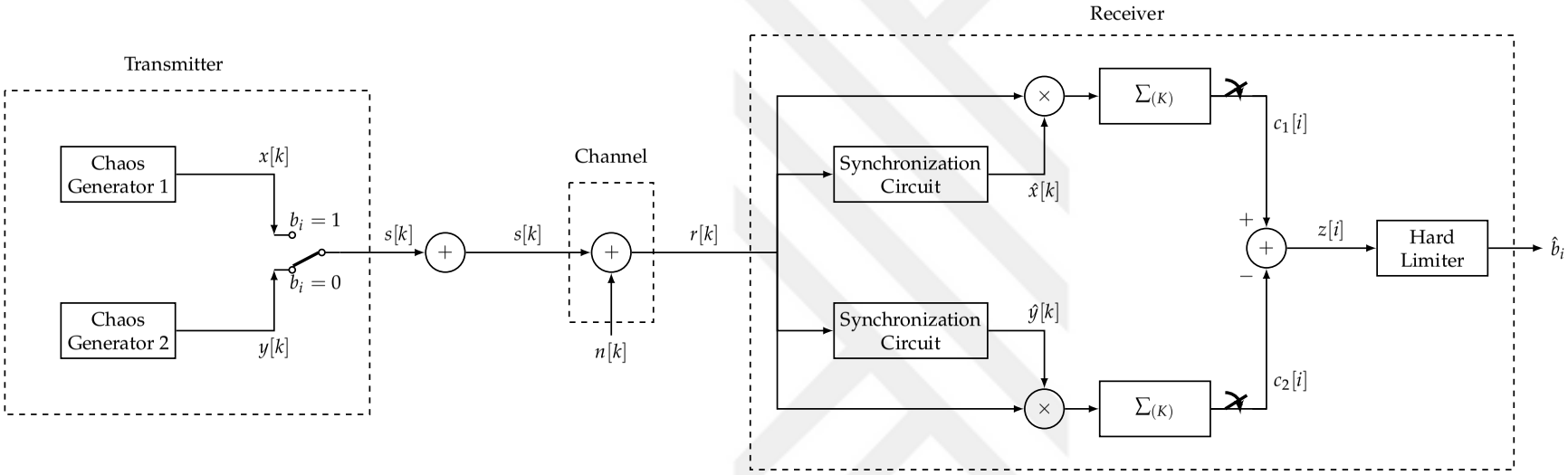

Figure 5.3 Block diagram of single user chaos shift keying.

$$x[k] = x(kT_s), \quad y[k] = y(kT_s), \quad s[k] = s(kT_s) \quad r[k] = r(kT_s) \quad n[k] = n(kT_s) \tag{5.7}$$

for $k = 1, 2, \ldots, K$, Here, T_s is the sampling period used to sample the continuous time signals K is the number of samples in a symbol duration. During the transmission of the symbol b_i, the transmitted signals are

$$s[k] = \begin{cases} x[k], & b_i = 1, \\ y[k], & b_i = 0, \end{cases} \tag{5.8}$$

for $(i-1)K \leq k \leq iK$. Assuming that the channel noise n_k is AWGN with power spectral density of $N_0/2$, the received signal is then

$$r[k] = s[k] + n[k] \tag{5.9}$$

The CSK receiver is a coherent receiver, i.e., the exact replicas $\hat{x}[k]$ and $\hat{y}[k]$ of $x[k]$ and $y[k]$, are constructed at the receiver using the drive-response type of chaotic synchronization. The replicas correlate the received signal as

$$\begin{aligned} c_1[i] &= \sum_{k=(i-1)K+1}^{K} \hat{x}[k] r[k], \\ c_2[i] &= \sum_{k=(i-1)K+1}^{K} \hat{y}[k] r[k], \end{aligned} \tag{5.10}$$

and the decision variable is obtained as

$$z[i] = c_1[i] - c_2[i], \tag{5.11}$$

with the decision rule

$$\hat{b}_i = \begin{cases} 1 & z[i] \geq 0, \\ 0 & z[i] < 0. \end{cases} \tag{5.12}$$

The generalization of a single user CSK to a multiple access CSK is shown in Figure 5.4 where N is the number of users (Tse & Lau, 2003). $x_j[k]$ and $y_j[k]$ are the output of the chaotic oscillators for the j^{th} user for $j = 1, 2, \ldots, N$ and $b_{ji} \in \{0, 1\}$ is the i^{th} symbol transmitted for j^{th} user. The channel has an AWGN $n[k]$ with a power spectral density of $N_0/2$. The transmitted signal is

$$s[k] = \sum_{j=1}^{N} s_j[k] \tag{5.13}$$

where

$$s_j[k] = \begin{cases} x_j[k] & b_{ji} = 1, \\ y_j[k] & b_{ji} = 0. \end{cases} \tag{5.14}$$

The received signal

$$r[k] = s[k] + n[k] \tag{5.15}$$

is correlated by the exact replicas $\hat{x}_j[k]$ and $\hat{y}_k$ of the $x_j[k]$ and $y_j[k]$ at the receiver and the decision variable

$$z_j[i] = \sum_{k=(i-1)K+1}^{iK} r[k]\hat{x}_j[k] - \sum_{k=(i-1)K+1}^{iK} r[k]\hat{y}_j[k] \tag{5.16}$$

is obtained for the j^{th} user during the transmission of i^{th} symbol. The detection of the symbol b_{ji} is done by

$$\hat{b}_{ji} = \begin{cases} 1 & z_{ij} \geq 0, \\ 0 & z_{ij} < 0, \end{cases} \tag{5.17}$$

where $\hat{b}_{ji}$ is the extracted symbol for the j^{th} user.

Theorem 5.3.1. *Let the N-user multiple access chaos shift keying (MA-CSK) scheme in Figure 5.4 has a zero mean additive white Gaussian noise with a power spectral density of $N_0/2$. Assume that*

$$\begin{aligned} E[x_i^2[k]] = E[y_j^2[k]] = P_s, \\ \text{cov}[x_j^2[k], x_j^2[m]] = 0, \ k \neq m, \\ E[x_j[k]x_j[m]] = 0, \ k \neq m \end{aligned} \tag{5.18}$$

for $i, j = 1, 2, \ldots, N$ where $E[\cdot]$ and $\text{cov}[\cdot]$ is the expectation and covariance operator, respectively. Let K be the number of samples in a symbol duration, $E_b = \sum_{k=1}^{K} x_k^2$ be the average energy per symbol and

$$\Omega_j = \frac{\text{var}[x_j^2[k]]}{P_s^2} = \frac{\text{var}[x_j^2[k]]}{E^2[x_j^2[k]]}. \tag{5.19}$$

Then, the probability of symbol error for the j^{th} user is

$$\begin{aligned} P_{e,j} &= \frac{1}{2}\,\text{erfc}\left(\left[\frac{2\Omega_j}{K} + \frac{2(2N-1)}{K} + \frac{2N_0}{KP_s}\right]^{-1/2}\right) \\ &= \frac{1}{2}\,\text{erfc}\left(\left[\frac{2\Omega_j}{K} + \frac{2(2N-1)}{K} + 2\left(\frac{E_b}{N_0}\right)^{-1}\right]^{-1/2}\right) \\ &= \frac{1}{2}\,\text{erfc}\left(\left[\frac{2\Omega_j}{K} + \frac{2(2N-1)}{K} + \frac{2}{\frac{E_b}{N_0}}\right]^{-1/2}\right) \end{aligned} \tag{5.20}$$

Proof. See (Tse & Lau, 2003). □

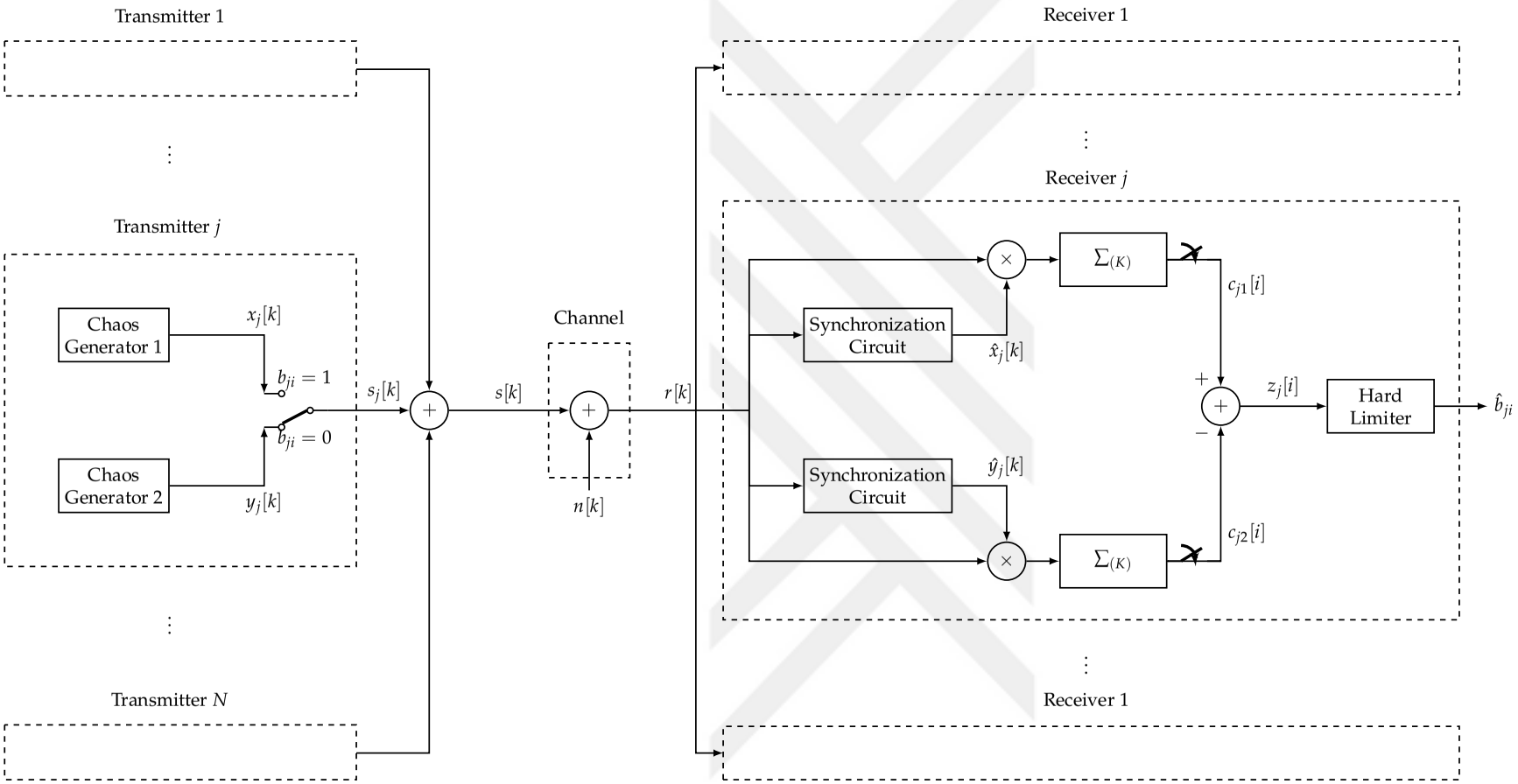

Figure 5.4 Block diagram of multiple access chaos shift keying.

The argument of the erfc function

$$\theta = \frac{2\Omega_j}{K} + \frac{2(2N-1)}{K} + \frac{2}{\dfrac{E_b}{N_0}}, \tag{5.21}$$

can be decomposed into three distinct terms. The first term is the variation of $x_j^2[k]$. The second term corresponds to interfering signals acting on the same correlator. The last term is the noise component. Since the erfc function is decreasing, the probability of symbol error increases with decreasing θ. Thus, for fixed average energy per symbol to noise power spectral density ratio, the communication system performance can be improved for the j^{th} user if the spreading factor K is increased, the variance of $x_j^2[k]$ for fixed P_s is minimized or the number of users N is decreased.

Corollary 5.3.2. *Given the assumptions in (5.32) and assuming that all users utilize a common chaotic oscillator (albeit with different initial conditions). The probability of symbol error for each user is*

$$P_e = \frac{1}{2}\,\mathrm{erfc}\left(\left[\frac{2\Omega}{K} + \frac{2(2N-1)}{K} + \frac{2}{\dfrac{E_b}{N_0}}\right]^{-1/2}\right) \tag{5.22}$$

where $\Omega = \dfrac{\mathrm{var}[x_i^2[k]]}{P_s^2} \quad i = 1, 2, \ldots, N.$

Proof. See (Tse & Lau, 2003). □

Just like in the previous case, to improve the performance (by decreasing the probability of symbol error) for a fixed symbol energy to noise spectral density ratio, we can increase the number of samples K, minimize the variance of $x[k]^2$ for fixed P_s and decrease the number of users N.

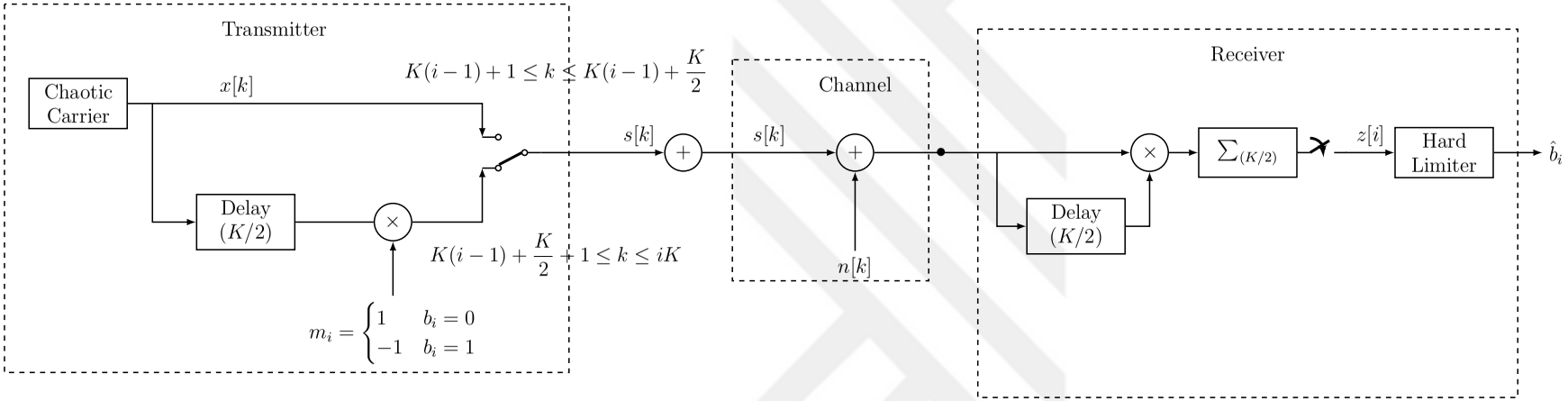

Figure 5.5 Block diagram of single user differential chaos shift keying.

5.3.2 *Detection Performance of Differential Chaos Shift Keying*

Figure 5.5 shows the discrete time equivalent of the DCSK system in Figure 5.2 (Tse & Lau, 2003). For the i^{th} symbol, the transmitted signal

$$s[k] = \begin{cases} x[k] & (i-1)K/2 + 1 \leq k \leq (i-1)K/2 + K/2 \\ b_i x[k] & (i-1)K/2 + K/2/1 \leq k \leq iK \end{cases} \tag{5.23}$$

is corrupted by the noise term $n[k]$ with a power spectral density of $N_0/2$ resulting in the received the signal $r[k] = s[k] + n[k]$. The decision variable for the i^{th} symbol is obtained by

$$z[i] = \sum_{k=(i-1)K+1}^{(i-1)K+K/2} r[k]r[k + K/2] \tag{5.24}$$

Then, the detection rule in (5.17) is applied to detect the i^{th} symbol b_i.

The multiple access differential chaos shift keying (MA-DCSK) scheme is shown in Figure 5.6 where N is the number of users, and $x_j[k]$ is the chaotic oscillator of the j^{th} user for $j = 1, 2, \ldots, N$. Like the case of MA-CSK, an MA-DCSK scheme consists of identical transmitter and receiver blocks each j^{th} user for $j = 1, 2, \ldots, N$.

$$s[k] = \sum_{j=1}^{N} s_j[k], \tag{5.25}$$

where

$$s_j[k] = \begin{cases} x_j[k] & (i-1)K/2 + 1 \leq k \leq (i-1)K/2 + K/2, \\ b_{ji} x_j[k] & (i-1)K/2 + K/2/1 \leq k \leq iK. \end{cases} \tag{5.26}$$

The channel $n[k]$ is assumed to be AWGN with a power spectral density of $N_0/2$. Hence, $r[k] = s[k] + n[k]$ is received at the receiver. The decision variable for the j^{th}

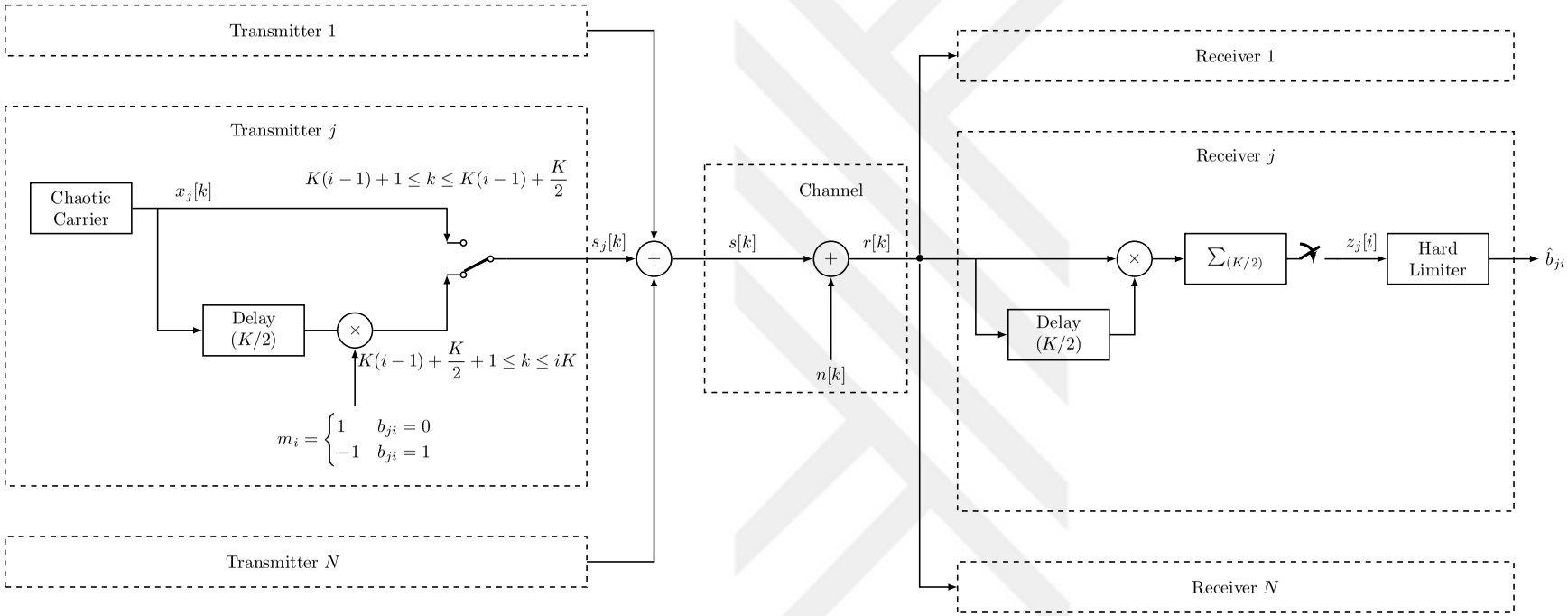

Figure 5.6 Block diagram of multiple access differential chaos shift keying (MA-DCSK)

user during the i^{th} symbol duration is

$$z[i] = \sum_{(i-1)K+1}^{(i-1)K+K/2} r[k]r[k + K/2]. \tag{5.27}$$

Denoting

$$\begin{aligned}
\boldsymbol{x}_i &= [x[(i-1)K+1], x[(i-1)K+2], \ldots, x[(i-1)K+\frac{K}{2}]] \\
\boldsymbol{n}_m &= [n[mK/2+1], n[mK/2+2], \ldots, n[mK/2+\frac{K}{2}]] \\
\boldsymbol{s}_i &= [s[(i-1)K+1], s[(i-1)K+2], \ldots, s[(i-1)K+\frac{K}{2}], \\
&\quad s[(i-1)K+\frac{K}{2}+1], s[(i-1)K+\frac{K}{2}+2], \ldots s[iK]] \\
\boldsymbol{r}_i &= [r[(i-1)K+1], r[(i-1)K+2], \ldots, r[(i-1)K+\frac{K}{2}], \\
&\quad r[(i-1)K+\frac{K}{2}+1], r[(i-1)K+\frac{K}{2}+2], \ldots r[iK]]
\end{aligned} \tag{5.28}$$

we have,

$$\boldsymbol{s}_i = [\boldsymbol{x}_i, b_i\boldsymbol{x}_i], \tag{5.29}$$

and

$$\boldsymbol{r}_i = [\boldsymbol{x}_i + \boldsymbol{n}_{2(i-1)}, b_i\boldsymbol{x}_i + \boldsymbol{n}_{2(i-1)+1}]. \tag{5.30}$$

Thus, the decision variable for the j^{th} user for the transmission of i^{th} symbol is

$$z_j[i] = [\boldsymbol{x}_i + \boldsymbol{n}_{2(i-1)}][b_i\boldsymbol{x}_i + \boldsymbol{n}_{2(i-1)+1}]^T, \tag{5.31}$$

and the decision rule is given as in (5.17).

Theorem 5.3.3. *Let the N-user multiple access differential chaos shift keying (MA-DCSK) scheme in Figure 5.6 have a zero mean additive white Gaussian noise with a power spectral density of $N_0/2$. Assume that*

- *The chaotic sequences $x_j[k],\ j = 1, 2, \ldots, N$ are independent of each other.*
- $E[x_j[k]] = 0,\ j = 1, 2, \ldots, N.$
- *$x_j[k],\ j = 1, 2, \ldots, N$ and $n[k]$ are stationary, and*

$$\begin{aligned} E[x_i^2[k]] &= P_s \\ \operatorname{cov}[x_i^2[k], x_i^2[m]] &= 0,\ k \neq m, \\ E[x_i[k]x_i[m]] &= 0,\ k \neq m \\ E[x_i[k]x_i[k+\kappa]x_i[k+\mu]x_i[k+\theta]] &= 0,\ \forall k, \mu, \theta \in I^+ \text{ and } 0 < k < \mu < \theta \end{aligned} \tag{5.32}$$

for $i, j = 1, 2, \ldots, N$ where $E[\cdot]$ and $\operatorname{cov}[\cdot]$ is the expectation and covariance operator, respectively. Let K be the number of samples in a symbol duration, $E_b = \sum_{k=1}^{K} x_k^2 = KP_s$ be the average energy per symbol and

$$\Omega_j = \frac{\operatorname{var}[x_j^2[k]]}{P_s^2} = \frac{\operatorname{var}[x_j^2[k]]}{E^2[x_j^2[k]]}. \tag{5.33}$$

Then, the probability of symbol error for the j^{th} user is

$$P_{e,j} = \frac{1}{2}\operatorname{erfc}\left(\left[\frac{4\Omega_j}{K} + \frac{4(N^2-1)}{K} + \frac{4N}{\dfrac{E_b}{N_0}} + \frac{K}{\left(\dfrac{E_b}{N_0}\right)^2}\right]^{-1/2}\right). \tag{5.34}$$

Proof. See (Tse & Lau, 2003) □

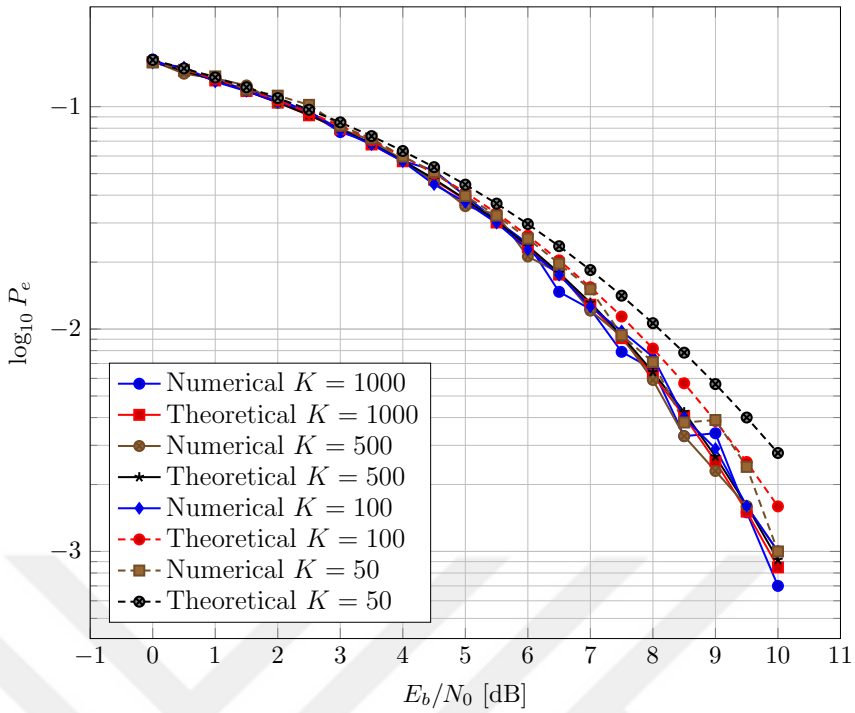

Figure 5.7 Detection performance of single user CSK with logistic map

5.4 Numerical Simulations

5.4.1 Chaos Shift Keying Performance

Figure 5.7 shows the detection performance curves of the CSK signaling for Logistic chaotic dynamics given as

$$x_{k+1} = 1 - 2x_k^2. \tag{5.35}$$

In Figure 5.7 are plotted both theoretically and numerically obtained performances obtained using (5.22) and Monte Carlo simulations, respectively. The results in Figure 5.7 illustrate that (5.22) approximates the detection performance better for large spreading factor K. However, for low K values, the difference between the numerical and theoretical approximation increases.

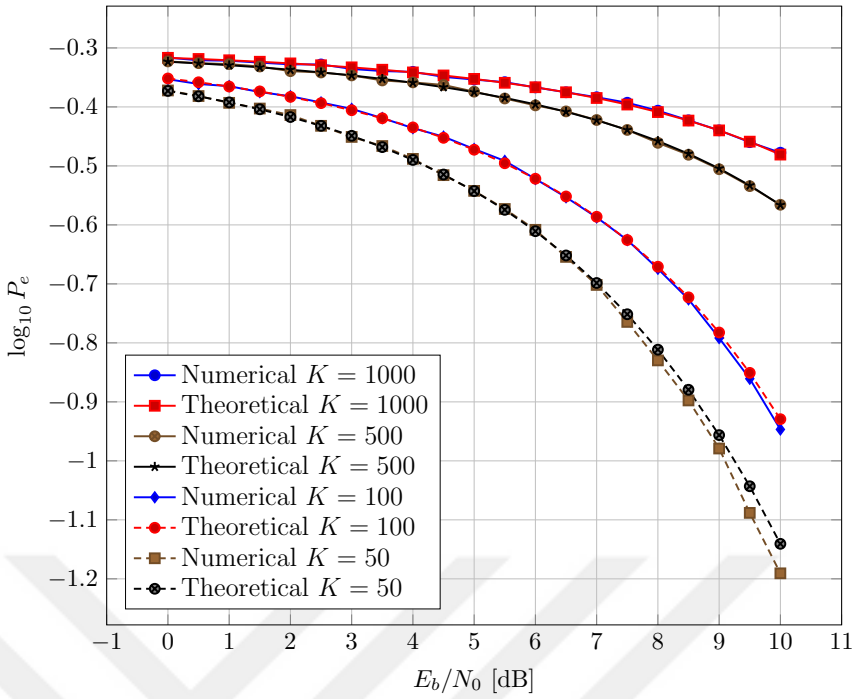

Figure 5.8 Detection performance of single user DCSK with logistic map

5.4.2 Differential Chaos Shift Keying Performance

Figure 5.7 shows the detection performance curves of the CSK signaling for Logistic chaotic dynamics given in (5.35). In Figure 5.7 are plotted both theoretically and numerically obtained performances obtained using (5.22) and Monte Carlo simulations, respectively. The results in Figure 5.7 illustrate that (5.22) approximates the detection performance better for large spreading factor K. However, for low K values, the difference between the numerical and theoretical approximation increases.

The comparison of CSK and DSCK signaling is depicted in Figure 5.9 using the Logistic map system in (5.35). CSK, being a coherent signaling, outperforms the non-coherent DCSK system.

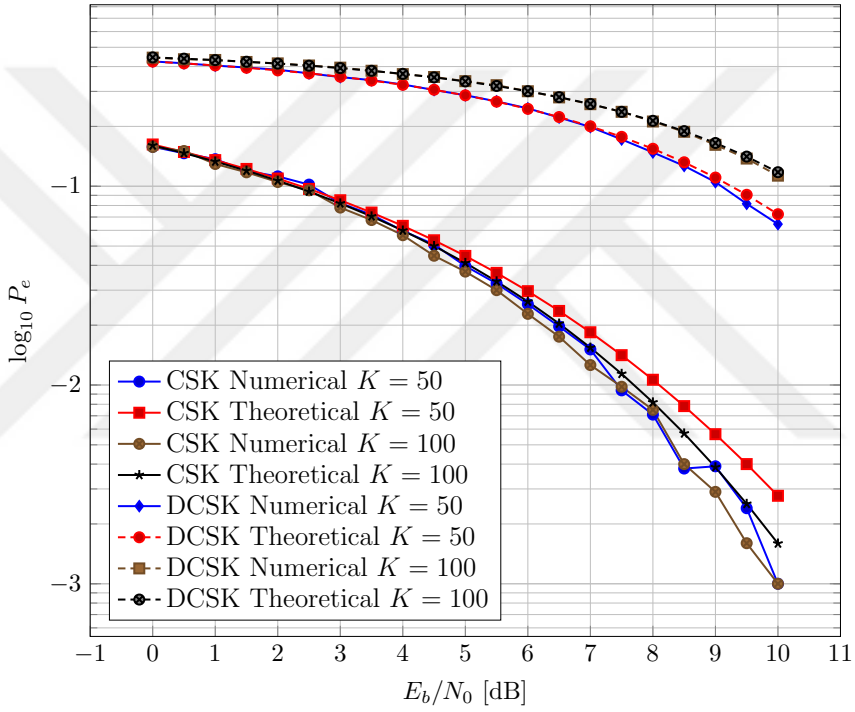

Figure 5.9 Comparison of detection performances of single user CSK and DCSK with logistic map.

CHAPTER SIX
NETWORK DESIGN

In the study context, we want to employ cluster synchronization in a communication system in which the symbols to be transmitted are encoded by different cluster patterns. Since we have multiple symbols for the transmission, we need different cluster patterns, naturally. The network should be designed such that switching between different cluster patterns is possible by controlling network parameters such as the coupling between some specified nodes. In other words, the network should be programmable to exhibit different cluster patterns.

In the proposed system, the network is divided into the transmitter and the receiver. The network can achieve different cluster patterns, and the cluster pattern of the whole network is controlled without any change in the receiver subnetwork. Thus, the cluster pattern of the whole network can be controlled through suitable adjustment of coupling strengths between the nodes of the network or gains of the negative feedback controllers. On the other hand, the nodes connecting the transmitter and receiver must not be in the same cluster so that the signals transmitted through the channel remain chaotic during the transmission to provide covertness.

We studied the conditions to design the networks capable of achieving the desired cluster patterns employing the pinning and the topological control in Chapters 3 and 4, respectively. This chapter is devoted to the design of *programmable* networks in which different cluster patterns can be achieved for different values of the control parameters. In the sequel, we will design networks using both the pinning and the topological control and present the weaknesses and strengths of the corresponding network design method.

6.1 Network Design Using Pinning Control

Let us start with the network in Figure 6.1. We will use the pinning control approach presented in Chapter 3 to design the clusters $\mathcal{G}_1 = \{1, 2, 3\}$ and $\mathcal{G}_2 = \{4, 5, 6\}$ corresponding to pinning nodes $1'$, and $2'$, respectively. The preliminary condition is

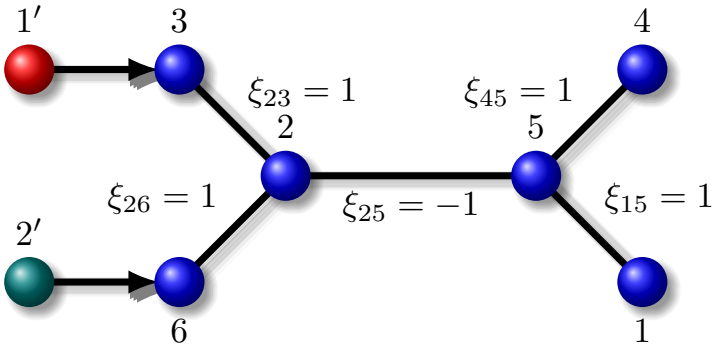

Figure 6.1 An example network.

that the outer coupling matrix of the network must be partitioned into block matrices, which are all zero-row-sum. The network in Figure 6.1 does not satisfy this condition since its outer coupling matrix is

$$\Xi = \left[\begin{array}{c|c} \Xi_{11} & \Xi_{12} \\ \hline \Xi_{21} & \Xi_{22} \end{array}\right] = \left[\begin{array}{ccc|ccc} 0 & 0 & 0 & 0 & 1 & 0 \\ 0 & -1 & 1 & 0 & -1 & 1 \\ 0 & 1 & -1 & 0 & 0 & 0 \\ \hline 0 & 0 & 0 & -1 & 1 & 0 \\ 1 & -1 & 0 & 1 & -1 & 0 \\ 0 & 1 & 0 & 0 & 0 & 0 \end{array}\right]. \tag{6.1}$$

The problem here is that the sums of the rows of the sub-blocks Ξ_{11} and Ξ_{22} are not equal to zero. To satisfy the zero-row-sum property, one may add an edge between nodes 1 and 6 whose weight is -1 as shown in Figure 6.2. The outer coupling matrix

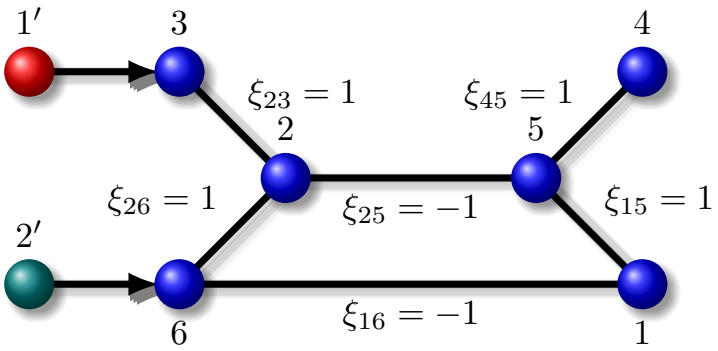

Figure 6.2 The network in Figure 6.1 with the nodes 1 and 6 are coupled to each other.

of the network in Figure 6.2 is

$$\Xi = \left[\begin{array}{c|c} \Xi_{11} & \Xi_{12} \\ \hline \Xi_{21} & \Xi_{22} \end{array}\right] = \left[\begin{array}{ccc|ccc} 0 & 0 & 0 & 0 & 1 & -1 \\ 0 & -1 & 1 & 0 & -1 & 1 \\ 0 & 1 & -1 & 0 & 0 & 0 \\ \hline 0 & 0 & 0 & -1 & 1 & 0 \\ 1 & -1 & 0 & 1 & -1 & 0 \\ -1 & 1 & 0 & 0 & 0 & 0 \end{array}\right]. \tag{6.2}$$

However, the problem is that off-diagonal elements of the sub-blocks cannot be negative. One can solve this problem by deleting the link between node 1 and 6 and rewiring it between the nodes 1 and 4 as shown in Figure 6.3. The coupling matrix of

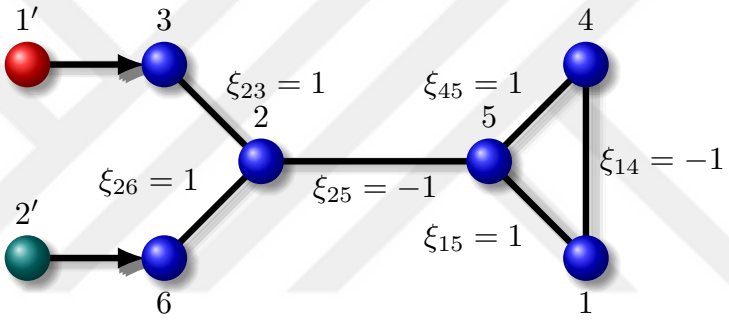

Figure 6.3 The network in Figure 6.2 with nodes 1 and 6 are decoupled, and the nodes 1 and 4 are coupled.

the network shown in Figure 6.3 is

$$\Xi = \left[\begin{array}{c|c} \Xi_{11} & \Xi_{12} \\ \hline \Xi_{21} & \Xi_{22} \end{array}\right] = \left[\begin{array}{ccc|ccc} 0 & 0 & 0 & -1 & 1 & 0 \\ 0 & -1 & 1 & 0 & -1 & 1 \\ 0 & 1 & -1 & 0 & 0 & 0 \\ \hline -1 & 0 & 0 & -1 & 1 & 0 \\ 1 & -1 & 0 & 1 & -1 & 0 \\ 0 & 1 & 0 & 0 & 0 & 0 \end{array}\right]. \tag{6.3}$$

Again, the sub-blocks Ξ_{12} and Ξ_{21} are not zero-row-sum matrices. One can add a link between nodes 3 and 4 to have a zero-row-sum in the first row of Ξ_{21} as shown in Figure 6.4. The outer coupling matrix of the network in Figure 6.4 is

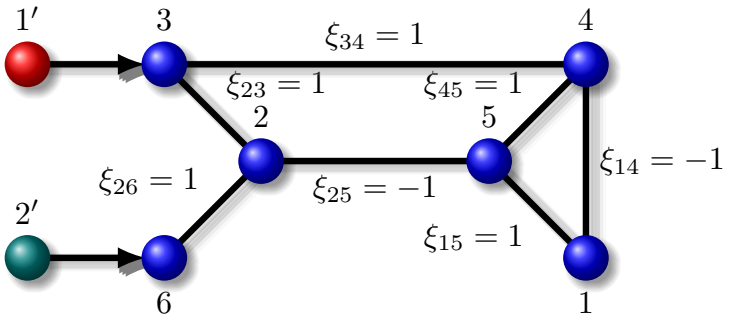

Figure 6.4 The network in Figure 6.3 with the nodes 3 and 4 are coupled.

$$\Xi = \left[\begin{array}{c|c} \Xi_{11} & \Xi_{12} \\ \hline \Xi_{21} & \Xi_{22} \end{array}\right] = \left[\begin{array}{ccc|ccc} 0 & 0 & 0 & -1 & 1 & 0 \\ 0 & -1 & 1 & 0 & -1 & 1 \\ 0 & 1 & -1 & 1 & 0 & 0 \\ \hline -1 & 0 & 1 & -1 & 1 & 0 \\ 1 & -1 & 0 & 1 & -1 & 0 \\ 0 & 1 & 0 & 0 & 0 & 0 \end{array}\right] \tag{6.4}$$

Again, we have some nonzero rows, so we add one more link between nodes 3 and 6 as shown in Figure 6.5. Now, we have the coupling matrix with all zero-row-sum

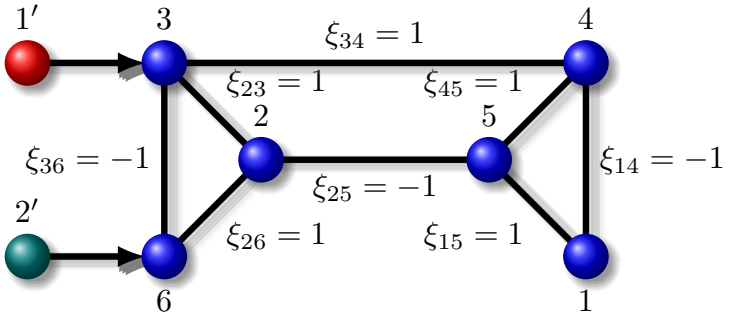

Figure 6.5 The network in Figure 6.4 with the nodes 3 and 4 are coupled.

sub-blocks as given in (6.5)

$$\Xi = \begin{bmatrix} \Xi_{11} & \Xi_{12} \\ \Xi_{21} & \Xi_{22} \end{bmatrix} = \left[\begin{array}{ccc|ccc} 0 & 0 & 0 & -1 & 1 & 0 \\ 0 & -1 & 1 & 0 & -1 & 1 \\ 0 & 1 & -1 & 1 & 0 & -1 \\ \hline -1 & 0 & 1 & -1 & 1 & 0 \\ 1 & -1 & 0 & 1 & -1 & 0 \\ 0 & 1 & -1 & 0 & 0 & 0 \end{array}\right]. \tag{6.5}$$

At this point, if the strengths of the feedback controllers satisfy the condition given in Theorem 3.2.4, the clusters $\mathcal{G}_1 = \{1, 2, 3\}$ and $\mathcal{G}_2 = \{4, 5, 6\}$ (corresponding to pinning nodes $1'$, and $2'$, respectively) can be observed as shown in Figure 6.6.

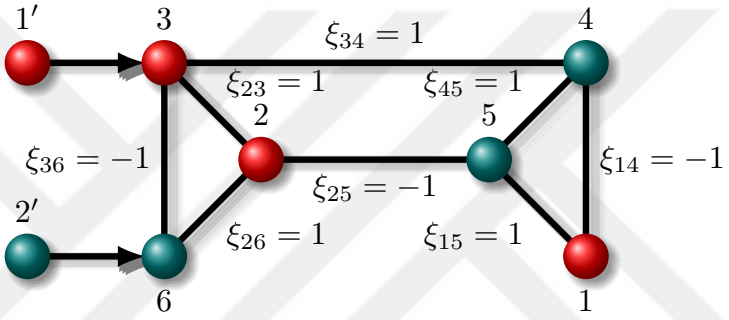

Figure 6.6 The first cluster pattern with the clusters $\mathcal{G}_1 = \{1, 2, 3\}$ and $\mathcal{G}_2 = \{4, 5, 6\}$. The nodes in the same cluster is shown with the same color.

If the node indices are rearranged, the cluster pattern in Figure 6.7 can be observed. Note the spatial change of the link between nodes 3 and 4 and the corresponding spatial change of cluster pattern in the whole network.

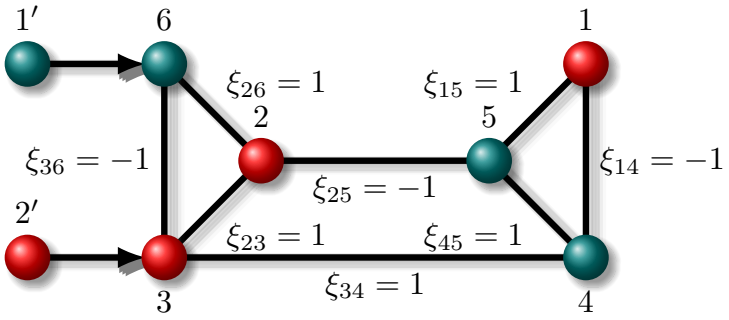

Figure 6.7 The second cluster pattern with the clusters $\mathcal{G}_1 = \{1, 2, 3\}$ and $\mathcal{G}_2 = \{4, 5, 6\}$.

In an attempt to use this network can be used in a binary communication system, consider the network shown in Figure 6.8. The cluster pattern of the network is controlled with the parameters ξ_{34} and ξ_{56}. Consider that the symbols of the binary communication system are denoted as $b_0 = 0$ and $b_1 = 1$.

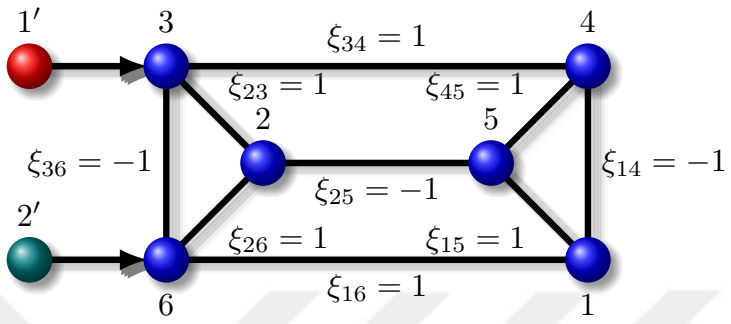

Figure 6.8 The network to be used in the proposed communication system.

Now divide the network into the receiver and transmitter as shown in Figure 6.9. During symbol b_0 transmission, the strength of the upper control link is 1 while that of the lower control link is 0, so the network achieves the cluster pattern shown in 6.10. Similarly, during b_1 transmission, the strength of the upper control link is 0 while that of the lower control link is 1, so the network achieves the cluster pattern shown in 6.11. Regardless of the transmitted symbol, the nodes connecting the receiver and the transmitter are in different clusters. However, we have two problems with the design.

1. The signals flowing through the channel are not always chaotic because during the transmission of b_0, the signal flowing through the channel link between the node pair $(1, 6)$ is zero. Similarly, the signal on the channel link between the node pair $(3, 4)$ is zero during the transmission of b_1. Hence, the signals flowing in the channel carry information, which is to be avoided in the communication system proposed in this study.

2. The links between the node pairs $(3, 4)$ and $(6, 1)$ are in the channel, not entirely on the transmitter side. Once the network is divided between the transmitter and receiver, we do not have access to the control parameters from the transmitter side only.

Because of the above two problems, this network design is unsuitable for the proposed communication system.

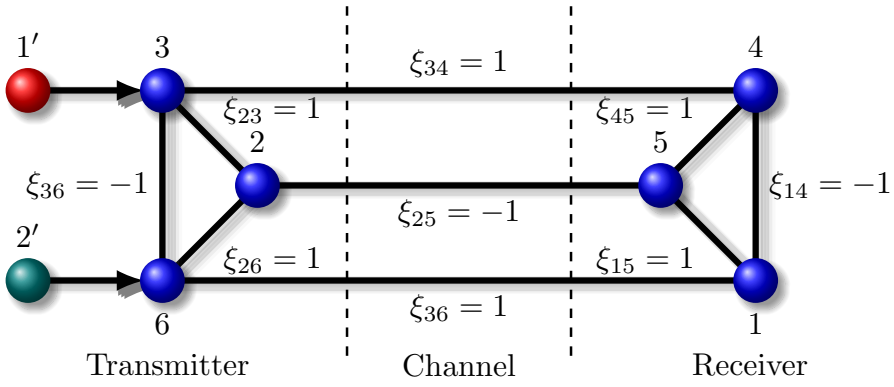

Figure 6.9 The distribution of the nodes in the network in Figure 6.8 between the transmitter and the receiver.

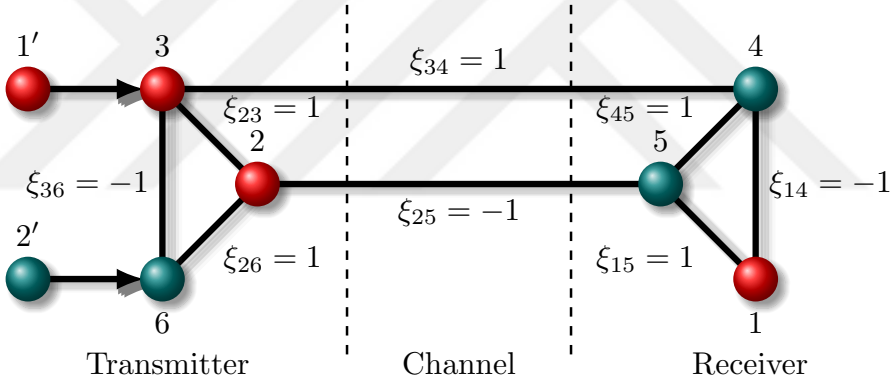

Figure 6.10 The cluster pattern of the network during symbol 0 transmission.

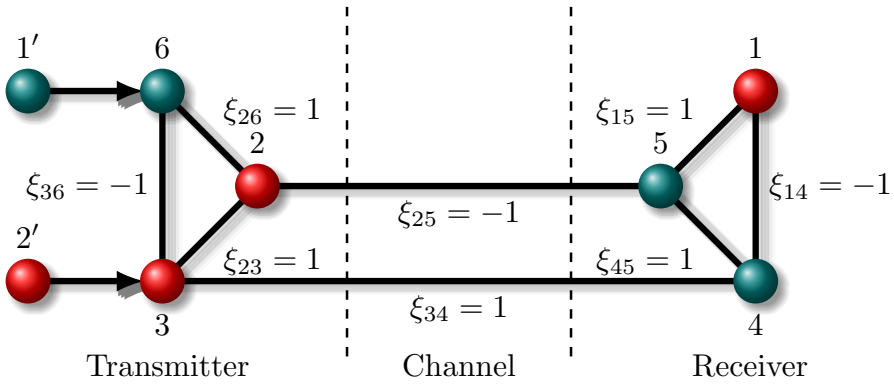

Figure 6.11 The cluster pattern during symbol 1 transmission.

6.2 Network Design Using Topological Control

We have presented the network design based on topological control with and without an auxiliary control network in Chapter 4. We will design networks using these two techniques individually in this section.

6.2.1 Design without Control Network

If we recall from Chapters 3 and 4, a network design capable of achieving multiple clusters is possible with various methods, such as pinning control. The challenge here is not the programmable network design but dividing the network into the transmitter and receiver. This division must be carried out such that the nodes connecting the transmitter and the receiver are not in the same cluster, regardless of the transmitted symbol. Additionally, we want all the control parameters to reside on the transmitter side only. This is because, during the transmission, we do not have any access to the subnetwork on the receiver side.

In the previous chapter, we have seen that the network shown in Figure 6.12a exhibits different cluster synchronization patterns for different values of the control parameters. The control parameters are the weights of the coupling between different nodes. The network in Figure 6.12a is unweighted, i.e., $w_{ij} = 1,\ i = 1, 2, \ldots, 5$. If the weight between the nodes 2 and 5 exceeds 1, then the cluster pattern in Figure 6.12b is observed. If the link between the nodes 1 and 3 is removed, the pattern in Figure 6.12c is obtained. Moreover, if the link between the nodes 1 and 5 is removed and rewired between the nodes 1 and 3, the pattern in Figure 6.12d is observed. So, if we choose the weights of w_{25}, w_{13}, w_{14} as the control parameters [2], we can program the network in Figure 6.12a to exhibit cluster patterns the Figure 6.12b-6.12d. However, although the network is programmable, it is useless in the communication system since we cannot divide the network into two, satisfying the constraints of the communication system. This is because the control parameters do not reside in the

[2] Beware that adding(removing) a link between the nodes i and j is actually changing the weight w_{ij} from 0(1) to 1(0)

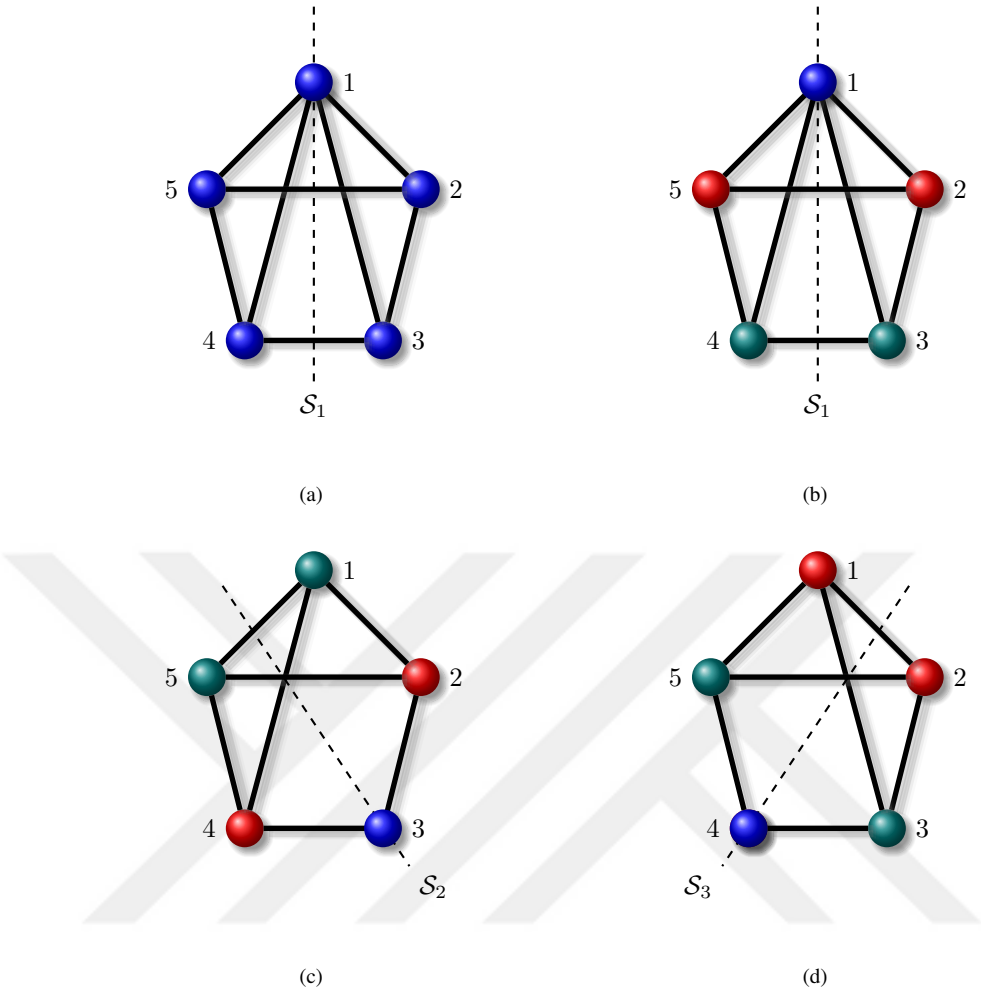

Figure 6.12 (a) A network that can be programmed to exhibit three different cluster patterns. (b) The pattern corresponding to the symmetry $\mathcal{S}_1$. (c) The pattern corresponding to the symmetry $\mathcal{S}_2$. (d) The pattern corresponding to the symmetry $\mathcal{S}_3$.

transmitter. To see this, let us divide the nodes into two tr: transmitter and receiver nodes. Since w_{25} is a control parameter, the nodes 2 and 5 must be in the transmitter. Next, consider the cluster pattern in Figure 6.12c. Since the nodes 1 and 5, 2, and 4 are in the same cluster, the nodes 1 and 4 must also be in the transmitter because the nodes connecting the transmitter and receiver must not be in the same cluster. Similarly, for the cluster pattern in Figure 6.12d, the nodes 3 and 5 are in the same cluster, and the node 3 must also be in the transmitter because the nodes connecting the transmitter and receiver must not be in the same cluster. Therefore, it turned out that all the nodes must be in the transmitter, which is meaningless.

Consider a completely different network shown in Figure 6.13a. The network

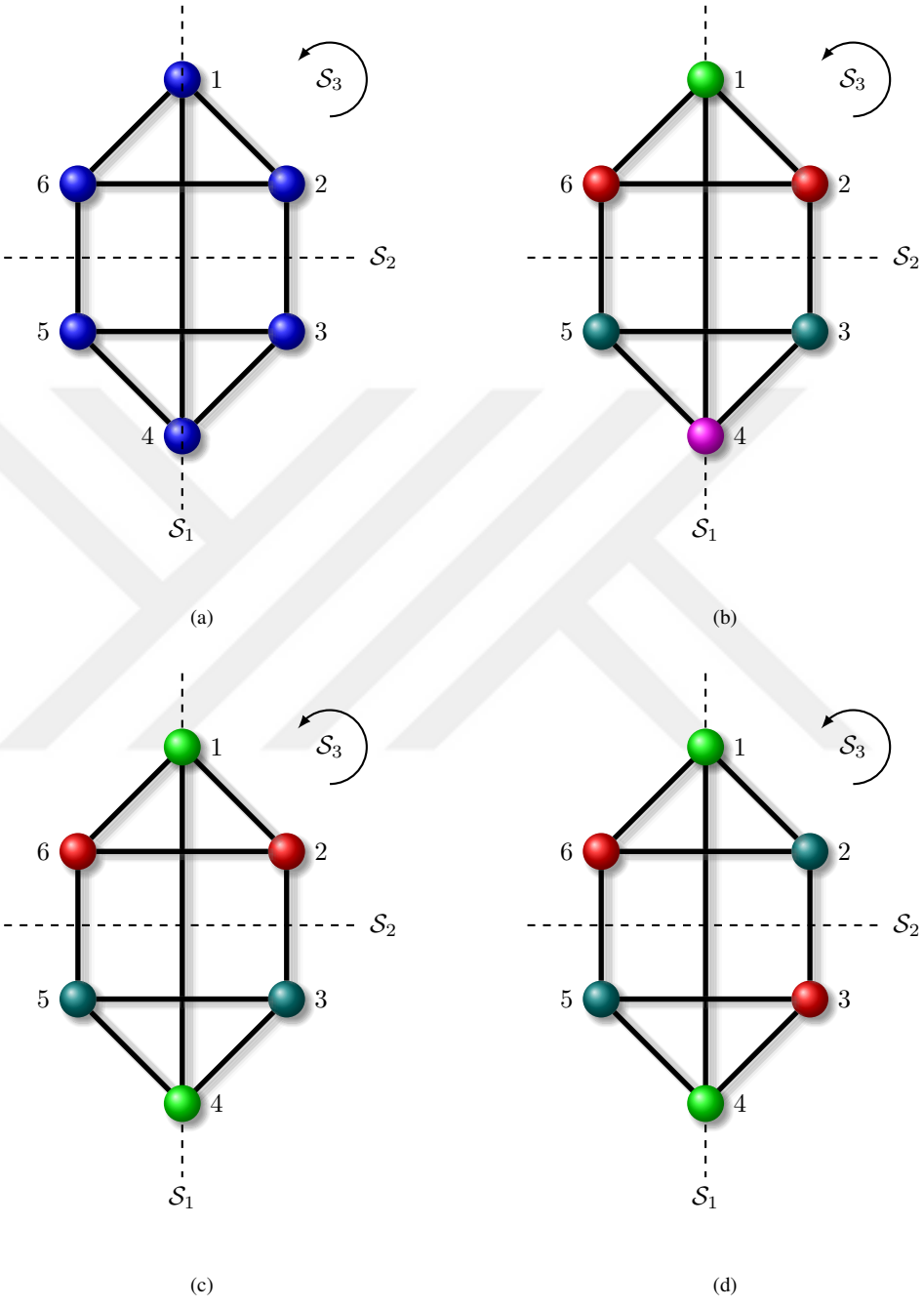

Figure 6.13 (a) A network that can be programmed to exhibit three different cluster patterns. (b) The pattern corresponding to the symmetry $\mathcal{S}_1$. (c) The pattern corresponding to the symmetry $\mathcal{S}_2$.(d) The pattern corresponding to the symmetry $\mathcal{S}_3$.

exhibits three symmetries in Figure 6.13b-6.13d. The symmetries $\mathcal{S}_1$ and $\mathcal{S}_2$ are reflection symmetries, while the symmetry $\mathcal{S}_3$ is a rotation symmetry. Therefore, the network in Figure 6.13a is capable of exhibiting three different cluster patterns corresponding to the symmetries $\mathcal{S}_1, \mathcal{S}_2, \mathcal{S}_3$. To investigate the stabilities of these cluster patterns, we will start with the analysis by checking if the eigenvalue condition in (4.1) is satisfied. If the network is unweighted, i.e., $w_{ij} = 1, \ , i = 1, 2, \ldots, 6$, The permutation matrix $\mathbf{\Delta}_1$ corresponding to the symmetry $\mathcal{S}_1$ is

$$\mathbf{\Delta}_1 = \begin{bmatrix} 1 & 0 & 0 & 0 & 0 & 0 \\ 0 & 0 & 0 & 0 & 0 & 1 \\ 0 & 0 & 0 & 0 & 1 & 0 \\ 0 & 0 & 0 & 1 & 0 & 0 \\ 0 & 0 & 1 & 0 & 0 & 0 \\ 0 & 1 & 0 & 0 & 0 & 0 \end{bmatrix}. \tag{6.6}$$

The transformation matrix $\mathbf{\Psi}_1$ corresponding to $\mathbf{\Delta}_1$ is

$$\mathbf{\Psi}_1 = \begin{bmatrix} 0.00 & 0.00 & 0.00 & 0.00 & 1.00 & 0.00 \\ 0.00 & -0.71 & 0.00 & 0.00 & 0.00 & 0.71 \\ 0.71 & 0.00 & 0.71 & 0.00 & 0.00 & 0.00 \\ 0.00 & 0.00 & 0.00 & 1.0 & 0.00 & 0.00 \\ -0.71 & 0.00 & 0.71 & 0.00 & 0.00 & 0.00 \\ 0.00 & 0.71 & 0.00 & 0.00 & 0.00 & 0.71 \end{bmatrix}. \tag{6.7}$$

When the outer coupling matrix

$$\mathbf{\Xi} = \begin{bmatrix} 1.00 & -0.33 & 0.00 & -0.33 & 0.00 & -0.33 \\ -0.33 & 1.00 & -0.33 & 0.00 & 0.00 & -0.33 \\ 0.00 & -0.33 & 1.00 & -0.33 & -0.33 & 0.00 \\ -0.33 & 0.00 & -0.33 & 1.00 & -0.33 & 0.00 \\ 0.00 & 0.00 & -0.33 & -0.33 & 1.00 & -0.33 \\ -0.33 & -0.33 & 0.00 & 0.00 & -0.33 & 1.00 \end{bmatrix} \tag{6.8}$$

is transformed by $\mathbf{\Psi}_1$, we have

$$\boldsymbol{\Theta}_1 = \begin{bmatrix} 1.33 & 0.33 & 0.00 & 0.00 & 0.00 & 0.00 \\ 0.33 & 1.33 & 0.00 & 0.00 & 0.00 & 0.00 \\ 0.00 & 0.00 & 0.67 & -0.47 & 0.00 & -0.33 \\ 0.00 & 0.00 & -0.47 & 1.00 & -0.33 & 0.00 \\ 0.00 & 0.00 & 0.00 & -0.33 & 1.00 & -0.47 \\ 0.00 & 0.00 & -0.33 & 0.00 & -0.47 & 0.67 \end{bmatrix}, \tag{6.9}$$

which implies

$$\boldsymbol{\Omega}_1 = \begin{bmatrix} 1.33 & 0.33 \\ 0.33 & 1.333 \end{bmatrix}, \tag{6.10}$$

and

$$\boldsymbol{\Phi}_1 = \begin{bmatrix} 0.67 & -0.47 & 0.00 & -0.33 \\ -0.47 & 1.00 & -0.33 & 0.00 \\ 0.00 & -0.33 & 1.00 & -0.47 \\ -0.33 & 0.00 & -0.47 & 0.666667 \end{bmatrix}. \tag{6.11}$$

The eigenvalues of $\boldsymbol{\Omega}_1$ and $\boldsymbol{\Phi}_1$ are found to be $\lambda_1^t = 1 < \lambda_2^t = 1.67$ and $\lambda_s^1 = 0 < \lambda_2^s = 0.67 < \lambda_3^s = 1 < \lambda_4^s = 1.67$. Since $\lambda_1^t > \lambda_2^s$, the eigenvalue condition is satisfied for the symmetry $\mathcal{S}_1$.

When the similar steps are performed by the symmetry $\mathcal{S}_2$, we have

$$\boldsymbol{\Delta}_2 = \begin{bmatrix} 0 & 0 & 0 & 1 & 0 & 0 \\ 0 & 0 & 1 & 0 & 0 & 0 \\ 0 & 1 & 0 & 0 & 0 & 0 \\ 1 & 0 & 0 & 0 & 0 & 0 \\ 0 & 0 & 0 & 0 & 0 & 1 \\ 0 & 0 & 0 & 0 & 1 & 0 \end{bmatrix}, \tag{6.12}$$

$$\mathbf{\Psi}_2 = \begin{bmatrix} 0.00 & -0.71 & 0.00 & 0.71 & 0.00 & 0.00 \\ 0.71 & 0.00 & 0.00 & 0.00 & 0.71 & 0.00 \\ -0.71 & 0.00 & 0.00 & 0.00 & 0.71 & 0.00 \\ 0.00 & 0.71 & 0.00 & 0.71 & 0.00 & 0.00 \\ 0.00 & 0.00 & 0.71 & 0.00 & 0.00 & 0.71 \\ 0.00 & 0.00 & -0.71 & 0.00 & 0.00 & 0.71 \end{bmatrix}, \tag{6.13}$$

$$\mathbf{\Theta}_2 = \begin{bmatrix} 1.33 & 0.33 & 0.33 & 0.00 & 0.00 & 0.00 \\ 0.33 & 1.33 & -0.33 & 0.00 & 0.00 & 0.00 \\ 0.33 & -0.33 & 1.33 & 0.00 & 0.00 & 0.00 \\ 0.00 & 0.00 & 0.00 & 0.67- & 0.33 & -0.33 \\ 0.00 & 0.00 & 0.00 & -0.33 & 0.67 & -0.33 \\ 0.00 & 0.00 & 0.00 & -0.33- & 0.33 & 0.67 \end{bmatrix}, \tag{6.14}$$

$$\mathbf{\Omega}_2 = \begin{bmatrix} 1.33 & 0.33 & 0.33 \\ 0.33 & 1.33 & -0.33 \\ 0.33 & -0.33 & 1.33 \end{bmatrix}, \tag{6.15}$$

$$\mathbf{\Phi}_2 = \begin{bmatrix} 0.67 & -0.33 & -0.33 \\ -0.33 & 0.67 & -0.33 \\ -0.33 & -0.33 & 0.67 \end{bmatrix}. \tag{6.16}$$

The eigenvalues of $\mathbf{\Omega}_2$ and $\mathbf{\Phi}_2$ are found to be $\lambda_1^t = 0.67 < \lambda_2^t = 1.67 = \lambda_3^t = 1.67$ and $\lambda_s^1 = 0 < \lambda_2^s = 1 < \lambda_3^s = 1$. Since $\lambda_1^t < \lambda_2^s$, the eigenvalue condition is not satisfied for the symmetry $\mathcal{S}_2$.

However, we can see that the eigenvalue condition can be satisfied if the weight of the link between the nodes w_{14} is changed. The change of the distribution of the eigenvalues corresponding to the symmetries for $\mathcal{S}_1$ and $\mathcal{S}_2$ are shown in Figure 6.14. From Figure 6.14a, it is clear that the change of the weight of the link between the nodes 1 and 4 does not affect the stability of the cluster pattern corresponding to the symmetry $\mathcal{S}_1$. The eigenvalue condition $\lambda_1^t > \lambda_2^s$ satisfies all w_{14}, and the cluster pattern is always stable. However, as shown in Figure 6.14b, the cluster pattern corresponding

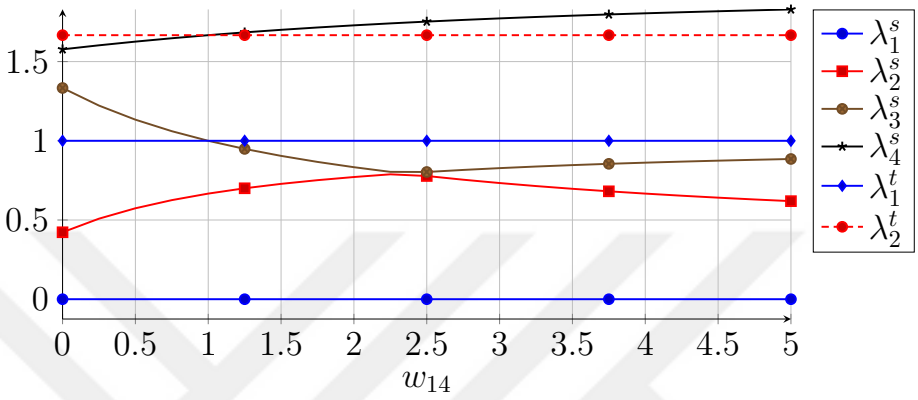

(a)

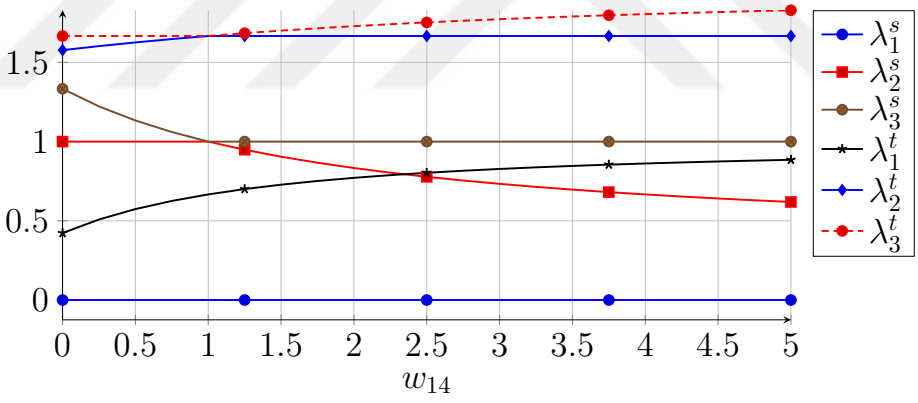

(b)

Figure 6.14 The change of eigenvalues in response to the change of the weight between the nodes 1 and 4. (a) The change of the eigenvalue distribution for the symmetry $\mathcal{S}_1$. (b) The change of the eigenvalue distribution for the symmetry $\mathcal{S}_2$.

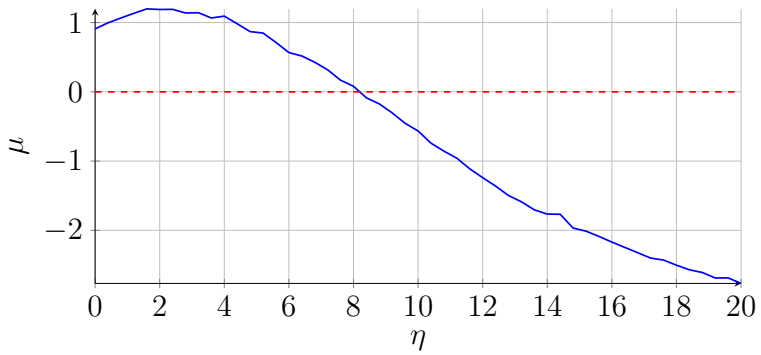

Figure 6.15 Plot of the master stability function for the Lorenz dynamics given in (4.22) and the inner coupling matrix $\boldsymbol{P} = [p_{ij}]$ with only nonzero element $p_{21} = 0$

to the symmetry $\mathcal{S}_2$ goes from instability to stability as the weight w_{14} passes through $w_{14}^* \approx 2.4$. Therefore, the cluster pattern of the network can be changed from the pattern shown in Figure 6.13b to the pattern shown in Figure 6.13c. To observe this, let us choose a uniform coupling strength ϵ such that it suffices to change the weight between the nodes 1 and 4. From Figure 6.14, for $w_{14} = 0.8$, the cluster pattern corresponding to the symmetry $\mathcal{S}_1$ is stable, and the one corresponding to the symmetry $\mathcal{S}_2$ is unstable. And, for $w_{14} = 3$, both of the cluster patterns corresponding to the symmetries $\mathcal{S}_1, \mathcal{S}_2$ are stable.

We need to find threshold $\eta^* = \epsilon\lambda$ to determine the range for ϵ, where λ is an eigenvalue of outer coupling matrix $\boldsymbol{\Xi}$, through which the master stability function $\mu = g(\eta)$ changes its sign from positive (which implies instability of the mode corresponding to λ) to negative (which implies stability). The threshold η^* depends on the individual node dynamics f and the inner coupling matrix $\boldsymbol{P}$. g is plotted in Figure 6.15 for the Lorenz dynamics defined in (4.22) and the inner coupling matrix

$$\boldsymbol{P} = \begin{bmatrix} 0 & 0 & 0 \\ 1 & 0 & 0 \\ 0 & 0 & 0 \end{bmatrix}. \tag{6.17}$$

From Figure 6.15, η^* is found to be $\eta^* \approx 8.4$. For $w_{14} = 0.8$, the eigenvalues of $\boldsymbol{\Omega}_1$ and $\boldsymbol{\Phi}_1$ is found to be $\lambda_1^t = 1 < \lambda_2^t = 1.67$ and $\lambda_1^s = 0 < \lambda_2^s = 0.63 < \lambda_3^s = 1.05 < \lambda_4^s = 1.65$. The range for ϵ is $\epsilon_{r1} = [\epsilon_{l1}, \epsilon_{h1}]$ where $\epsilon_{l1} = \eta^*/\lambda_1^t = 8.4, \epsilon_{h1} = \eta^*/\lambda_2^s = 13.24$. For

$w_{14} = 3$, the eigenvalues of $\mathbf{\Omega}_2$ and $\mathbf{\Phi}_2$ is found to be $\lambda_1^t = 0.83 < \lambda_2^t = 1.67 < \lambda_3^t = 1.77$ and $\lambda_1^s = 0 < \lambda_2^s = 0.73 < \lambda_3^s = 1$. The range for ϵ is $\epsilon_{r2} = [\epsilon_{l2}, \epsilon_{h2}]$ where $\epsilon_{l2} = \eta^*/\lambda_1^t = 10.15, \epsilon_{h1} = \eta^*/\lambda_2^s = 11.45$. To control the cluster pattern of the network without changing the whole coupling strengths but changing just the weight w_{14}, the uniform coupling strength ϵ must satisfy $\epsilon \in \epsilon_{r1}$ and $\epsilon \in \epsilon_{r2}$.

Figure 6.16 shows the errors between the network nodes in Figure 6.13a for $\epsilon = 10.5$. The total simulation time is 2000 seconds. The weight $w_{25} = 0.8$ for the time interval $\mathcal{I}_1 = [0, 1000]$ and $w_{25} = 3$ for the time interval $\mathcal{I}_2 = [1000, 2000]$. It is apparent from Figure 6.16 that the cluster pattern in Figure 6.13b is achieved for the time interval $\mathcal{I}_1$. However, for the time interval $\mathcal{I}_2$, the cluster in Figure 6.13c is not achieved. Instead, the cluster pattern in Figure 6.13d is achieved. This situation may seem inconsistent and surprising at first glance. However, recall that the time interval $\mathcal{I}_1$ only the cluster pattern in Figure 6.13b is stable; while for the time interval both of the cluster patterns in Figure 6.13b and Figure 6.13c are stable. The stability of both the patterns in Figure 6.13b and Figure 6.13c implies the stability of the cluster pattern in Figure 6.13d, which is the combination of the patterns in Figure 6.13b and Figure 6.13c.

Hence, the network in Figure 6.13a can be programmed to exhibit the cluster patterns in Figure 6.13b and Figure 6.12d. To use the network in the proposed communication system, the next step is to divide the network between the transmitter and the receiver. Note from Figure 6.13b and Figure 6.13d that the nodes 1 and 4 do not reside in the same cluster patterns with their neighbors. So, the links connecting nodes 1 and 4 to their neighbors may stay in the channel. Besides, the cluster pattern of the network is controlled by the link weight between the nodes 1 and 4. Thus, the nodes 1 and 4 must stay on the transmitter side. All the remaining nodes, i.e., the nodes $2, 3, 5, 6$, are elements of the receiver. The spatiotemporal status of the subnetwork consisting of the nodes $2, 3, 5, 6$ can be controlled by the transmitter by the weight of the link connecting the nodes 1 and 4. Since the network can be programmed such that two different cluster patterns can be observed in the subnetwork residing in the receiver, the network can be used in a binary

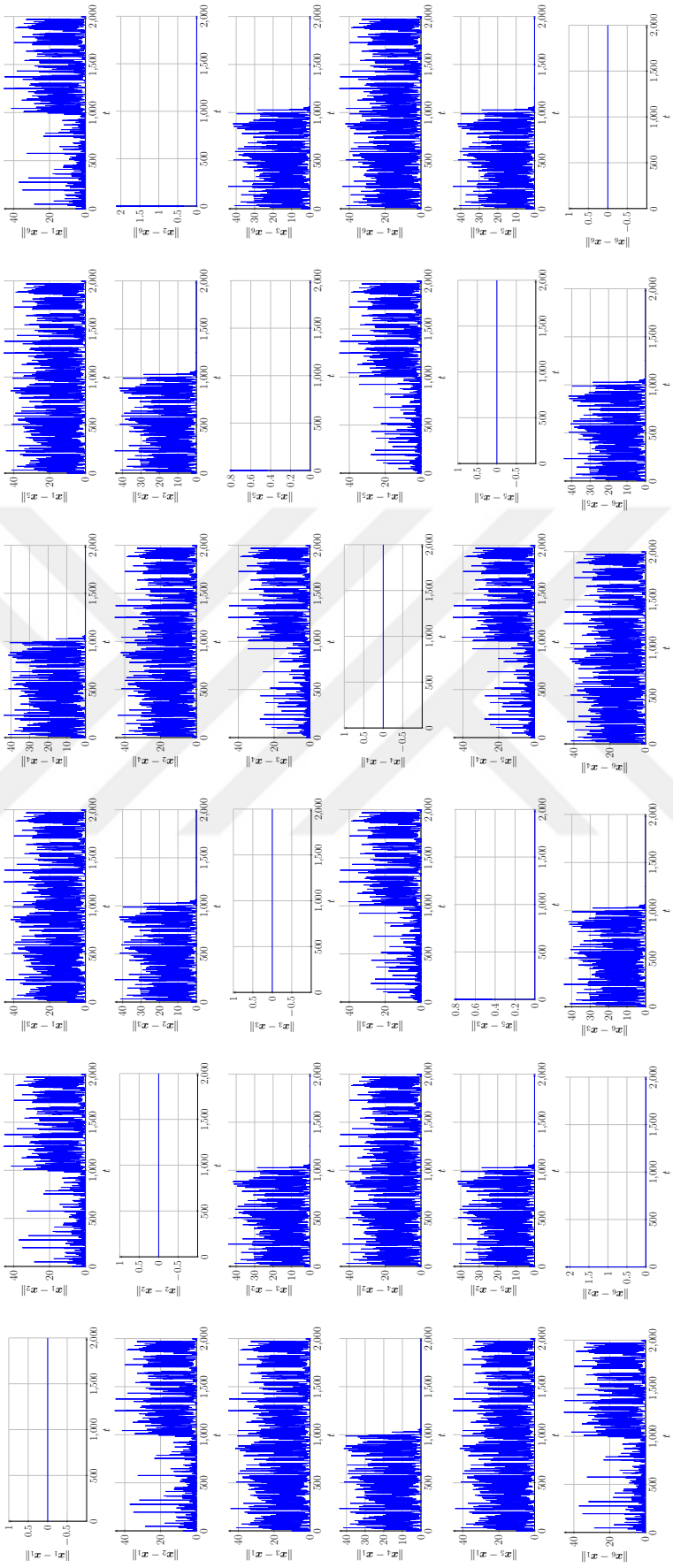

Figure 6.16 The simulation of the network in Figure 6.13a. $e_{ij} = |x_i - x_j|$ where $\boldsymbol{x}_i = [x_i, y_i, z_i]$.

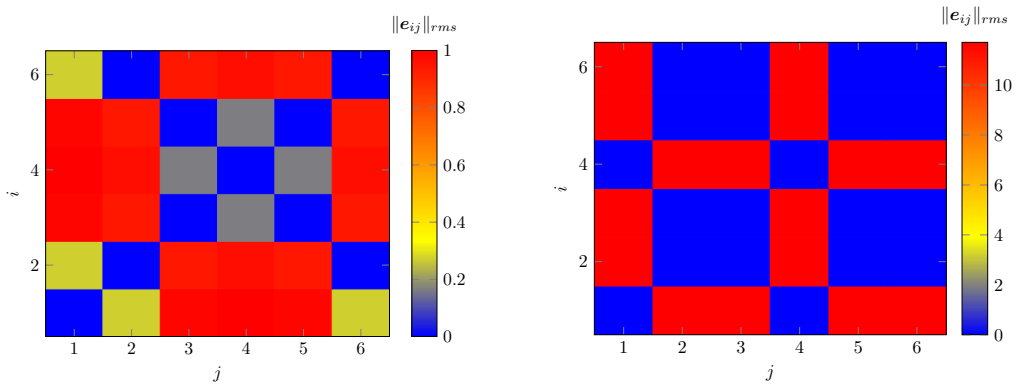

(a) (b)

Figure 6.17 The spatiotemporal view of the network in Figure 6.13. $\epsilon = 10.5$ (a) $0 \leq t < 1000$, (b) $1000 \leq t < 2000$,

communication system. As shown in Figure 6.18a, during b_0 transmission the pattern in the subnetwork in the receiver is $\mathcal{G}_1 = \{2, 6\}, \mathcal{G}_1 = \{3, 5\}$. And, as shown in Figure 6.18b, during b_1 transmission the pattern in the receiver is the single pattern $\mathcal{G}_3 = \{2, 3, 5, 6\}$. The nodes connecting the transmitter and receiver are always out of synchronization regardless of the symbol being sent.

As illustrated in Figure 6.18, we designed a network exhibiting different cluster patterns in response to a particular link's weight change. The network in Figure 6.18 is equivalent to that in Figure 6.13. A tiny problem with the network in Figure 6.13 is that both of the cluster patterns corresponding to the symmetries $\mathcal{S}_1$ and $\mathcal{S}_2$ are stable at the same time. This dual stability results in that the cluster pattern corresponding to symmetry $\mathcal{S}_2$ cannot be observed independently. Instead, we observe the cluster pattern corresponding to the symmetry $\mathcal{S}_3$. Although the network can be employed in the desired communication system, we may want to observe the cluster pattern corresponding to the symmetry $\mathcal{S}_2$. However, this is not possible with these configurations, and this is all we get from the network in Figure 6.13. To go further, we need to design a completely different network.

Consider the network shown in Figure 6.19. The networks in Figure 6.19a and Figure 6.19c are equivalent. The network possesses the symmetries $\mathcal{S}_1$ and $\mathcal{S}_2$, shown in Figure 6.19b and Figure 6.19d, respectively. If the network is unweighted, i.e.,

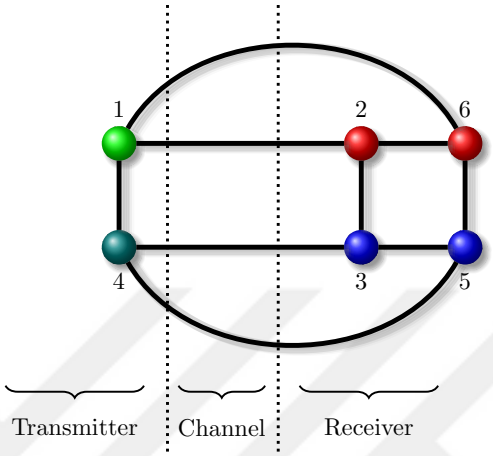

(a) $w_{14} = 0.8$.

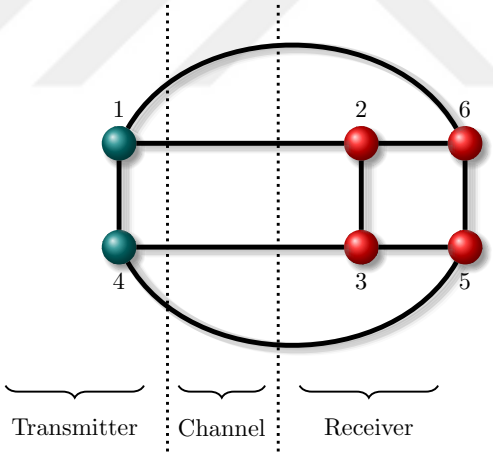

(b) $w_{14} = 3$

Figure 6.18 Using the network in Figure 6.13a in a binary communication system in which the symbols are s_1, s_2. The cluster pattern is controlled via the weight w_{14}. (a)Spatiotemporal status of the network during s_1 transmission. (b) Spatiotemporal status of the network during s_2 transmission. $\epsilon = 10.5$

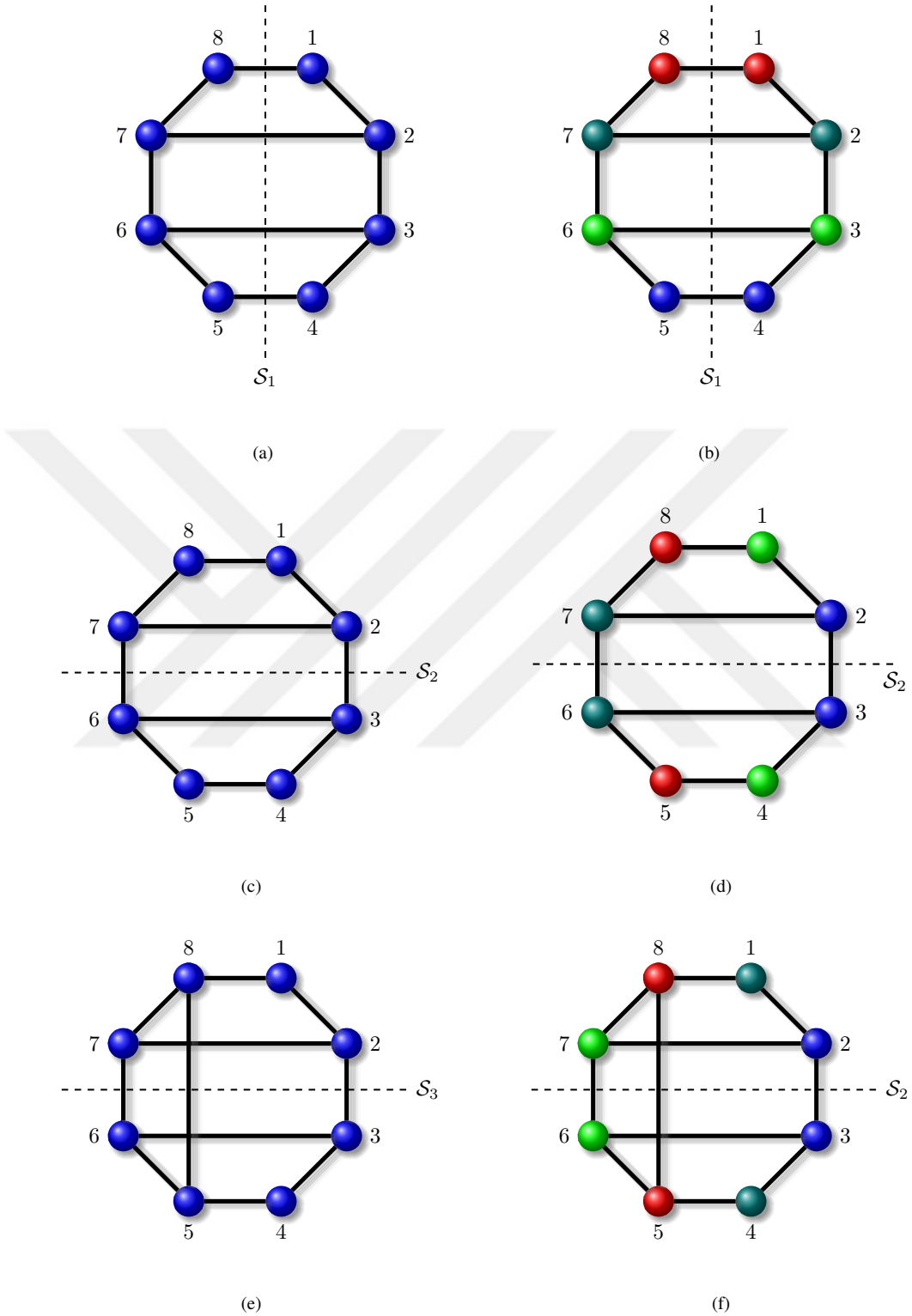

Figure 6.19 A network that can be programmed to possessing different topological symmetries. (a), (c) The symmetry $\mathcal{S}_1$ its corresponding pattern, respectively. (c), (d) The symmetry $\mathcal{S}_2$ its corresponding pattern, respectively.(e), (f) The symmetry $\mathcal{S}_3$ its corresponding pattern, respectively.

$w_{ij} = 1,\ i = 1, 2, \ldots, 8$, the outer coupling matrix is

$$\boldsymbol{\Xi} = \begin{bmatrix} 1.00 & -0.50 & 0.00 & 0.00 & 0.00 & 0.00 & 0.00 & -0.50 \\ -0.33 & 1.00 & -0.33 & 0.00 & 0.00 & 0.00 & -0.33 & 0.00 \\ 0.00 & -0.33 & 1.00 & -0.33 & 0.00 & -0.33 & 0.00 & 0.00 \\ 0.00 & 0.00 & -0.50 & 1.00 & -0.50 & 0.00 & 0.00 & 0.00 \\ 0.00 & 0.00 & 0.00 & -0.50 & 1.00 & -0.50 & 0.00 & 0.00 \\ 0.00 & 0.00 & -0.33 & 0.00 & -0.33 & 1.00 & -0.33 & 0.00 \\ 0.00 & -0.33 & 0.00 & 0.00 & 0.00 & -0.33 & 1.00 & -0.33 \\ -0.50 & 0.00 & 0.00 & 0.00 & 0.00 & 0.00 & -0.50 & 1.00 \end{bmatrix}. \tag{6.18}$$

If we perform the eigenvalue analysis for the symmetry $\mathcal{S}_1$, we get

$$\boldsymbol{\Delta}_1 = \begin{bmatrix} 0 & 0 & 0 & 0 & 0 & 0 & 0 & 1 \\ 0 & 0 & 0 & 0 & 0 & 0 & 1 & 0 \\ 0 & 0 & 0 & 0 & 0 & 1 & 0 & 0 \\ 0 & 0 & 0 & 0 & 1 & 0 & 0 & 0 \\ 0 & 0 & 0 & 1 & 0 & 0 & 0 & 0 \\ 0 & 0 & 1 & 0 & 0 & 0 & 0 & 0 \\ 0 & 1 & 0 & 0 & 0 & 0 & 0 & 0 \\ 1 & 0 & 0 & 0 & 0 & 0 & 0 & 0 \end{bmatrix}, \tag{6.19}$$

$$\boldsymbol{\Psi}_1 = \begin{bmatrix} 0.00 & 0.00 & 0.00 & -0.71 & 0.00 & 0.00 & 0.00 & 0.71 \\ 0.71 & 0.00 & 0.00 & 0.00 & 0.71 & 0.00 & 0.00 & 0.00 \\ 0.00 & 0.00 & -0.71 & 0.00 & 0.00 & 0.71 & 0.00 & 0.00 \\ 0.00 & 0.71 & 0.00 & 0.00 & 0.00 & 0.00 & 0.71 & 0.00 \\ 0.00 & -0.71 & 0.00 & 0.00 & 0.00 & 0.00 & 0.71 & 0.00 \\ 0.00 & 0.00 & 0.71 & 0.00 & 0.00 & 0.71 & 0.00 & 0.00 \\ -0.71 & 0.00 & 0.00 & 0.00 & 0.71 & 0.00 & 0.00 & 0.00 \\ 0.00 & 0.00 & 0.00 & 0.71 & 0.00 & 0.00 & 0.00 & 0.71 \end{bmatrix}, \tag{6.20}$$

$$\mathbf{\Theta}_1 = \begin{bmatrix} 1.33 & 0.00 & 0.33 & 0.33 & 0.00 & 0.00 & 0.00 & 0.00 \\ 0.00 & 1.50 & 0.50 & 0.00 & 0.00 & 0.00 & 0.00 & 0.00 \\ 0.33 & 0.33 & 1.33 & 0.00 & 0.00 & 0.00 & 0.00 & 0.00 \\ 0.50 & 0.00 & 0.00 & 1.50 & 0..0 & 0.00 & 0.00 & 0.00. \\ 0.00 & 0.00 & 0.00 & 0.00 & 0.67 & -0.33 & 0.00 & -0.33 \\ 0.00. & 0.00. & 0.00 & 0.00 & -0.33 & 0.67 & -0.33 & 0.00 \\ 0.00 & 0.00 & 0.00 & 0.00 & 0.00 & -0.50 & 0.50 & 0.00 \\ 0.00. & 0.00 & 0.00 & 0.00 & -0.50 & 0.00 & 0.00 & 0.50 \end{bmatrix}, \tag{6.21}$$

$$\mathbf{\Omega}_1 = \begin{bmatrix} 1.33 & 0.00 & 0.33 & 0.33 \\ 0.00 & 1.50 & 0.50 & 0.00 \\ 0.33 & 0.33 & 1.33 & 0.00 \\ 0.50 & 0.00 & 0.00 & 1.50 \end{bmatrix}, \tag{6.22}$$

$$\mathbf{\Phi}_1 = \begin{bmatrix} 0.67 & -0.33 & 0.00 & -0.33 \\ -0.33 & 0.67 & -0.33 & 0.00 \\ 0.00 & -0.50 & 0.50 & 0.00 \\ -0.50 & 0.00 & 0.00 & 0.50 \end{bmatrix}. \tag{6.23}$$

The eigenvalues of $\mathbf{\Omega}_1$ and $\mathbf{\Phi}_1$ are found to be $\lambda_1^t = 0.77 < \lambda_2^t = 1.17 = \lambda_3^t = 1.73 < \lambda_4^t = 2$ and $\lambda_s^1 = 0 < \lambda_2^s = 0.27 < \lambda_3^s = 0.83 < \lambda_4^s = 1.22$. Since $\lambda_1^t > \lambda_2^s$, the eigenvalue condition is satisfied for the symmetry $\mathcal{S}_1$. Hence, the cluster pattern corresponding to the symmetry $\mathcal{S}_1$ is stable. For the symmetry $\mathcal{S}_2$, we get

$$\mathbf{\Delta}_2 = \begin{bmatrix} 0 & 0 & 0 & 1 & 0 & 0 & 0 & 0 \\ 0 & 0 & 1 & 0 & 0 & 0 & 0 & 0 \\ 0 & 1 & 0 & 0 & 0 & 0 & 0 & 0 \\ 1 & 0 & 0 & 0 & 0 & 0 & 0 & 0 \\ 0 & 0 & 0 & 0 & 0 & 0 & 0 & 1 \\ 0 & 0 & 0 & 0 & 0 & 0 & 1 & 0 \\ 0 & 0 & 0 & 0 & 0 & 1 & 0 & 0 \\ 0 & 0 & 0 & 0 & 1 & 0 & 0 & 0 \end{bmatrix}, \tag{6.24}$$

$$\boldsymbol{\Psi}_2 = \begin{bmatrix} 0.00 & -0.71 & 0.00 & 0.00 & 0.00 & 0.00 & 0.71 & 0.00 \\ 0.71 & 0.00 & 0.00 & 0.00 & 0.71 & 0.00 & 0.00 & 0.00 \\ -0.71 & 0.00 & 0.00 & 0.00 & 0.71 & 0.00 & 0.00 & 0.00 \\ 0.00 & 0.71 & 0.00 & 0.00 & 0.00 & 0.00 & 0.71 & 0.00 \\ 0.00 & 0.00 & 0.00 & -0.71 & 0.00 & 0.00 & 0.00 & 0.71 \\ 0.00 & 0.00 & 0.71 & 0.00 & 0.00 & 0.71 & 0.00 & 0.00 \\ 0.00 & 0.00 & -0.71 & 0.00 & 0.00 & 0.71 & 0.00 & 0.00 \\ 0.00 & 0.00 & 0.00 & 0.71 & 0.00 & 0.00 & 0.00 & 0.71 \end{bmatrix}, \tag{6.25}$$

$$\boldsymbol{\Theta}_2 = \begin{bmatrix} 1.33 & 0.33 & 0.33 & 0.00 & 0.00 & 0.00 & 0.00 & 0.00 \\ 0.50 & 1.00 & 0.00 & 0.50 & 0.00 & 0.00 & 0.00 & 0.00 \\ 0.33 & 0.00 & 1.33 & 0.33 & 0.00 & 0.00 & 0.00 & 0.00 \\ 0.00 & 0.50 & 0.50 & 1.00 & 0.00 & 0.00 & 0.00 & 0.00 \\ 0.00 & 0.00 & 0.00 & 0.00 & 0.67 & -0.33 & 0.00 & 0.00 \\ 0.00 & 0.00 & 0.00 & 0.00 & -0.33 & 0.67 & 0.00 & -0.33 \\ 0.00 & -0.00 & 0.00 & 0.00 & -0.50 & 0.00 & 1.00 & -0.50 \\ 0.00 & 0.00 & 0.00 & 0.00 & 0.00 & -0.50 & -0.50 & 1.00 \end{bmatrix}, \tag{6.26}$$

$$\boldsymbol{\Omega}_2 = \begin{bmatrix} 1.33 & 0.33 & 0.33 & 0.00 \\ 0.50 & 1.00 & 0.00 & 0.50 \\ 0.33 & 0.00 & 1.33 & 0.33 \\ 0.00 & 0.50 & 0.50 & 1.00 \end{bmatrix}, \tag{6.27}$$

$$\boldsymbol{\Phi}_2 = \begin{bmatrix} 0.67 & -0.33 & -0.33 & 0.00 \\ -0.33 & 0.67 & 0.00 & -0.33 \\ -0.50 & 0.00 & 1.00 & -0.50 \\ 0.00 & -0.50 & -0.50 & 1.00 \end{bmatrix}. \tag{6.28}$$

The eigenvalues of $\boldsymbol{\Omega}_2$ and $\boldsymbol{\Phi}_2$ are found to be $\lambda_1^t = 0.27 < \lambda_2^t = 1.17 = \lambda_3^t = 1.23 < \lambda_4^t = 2$ and $\lambda_s^1 = 0 < \lambda_2^s = 0.77 < \lambda_3^s = 0.83 < \lambda_4^s = 1.73$. Since $\lambda_1^t < \lambda_2^s$, the eigenvalue condition is not satisfied for the symmetry $\mathcal{S}_2$. This implies that the cluster pattern in Figure 6.19d corresponding to the symmetry $\mathcal{S}_2$ cannot be observed with this configuration.

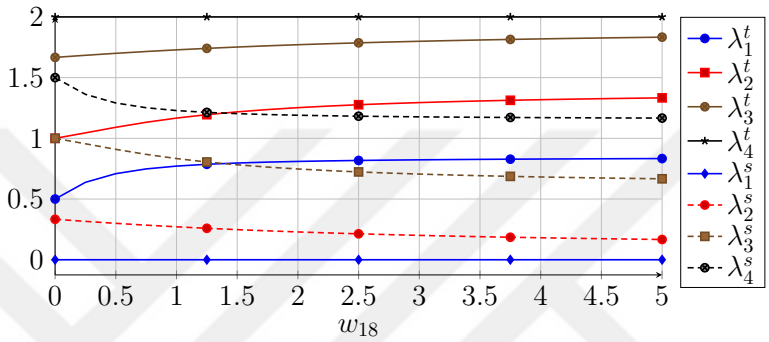

(a)

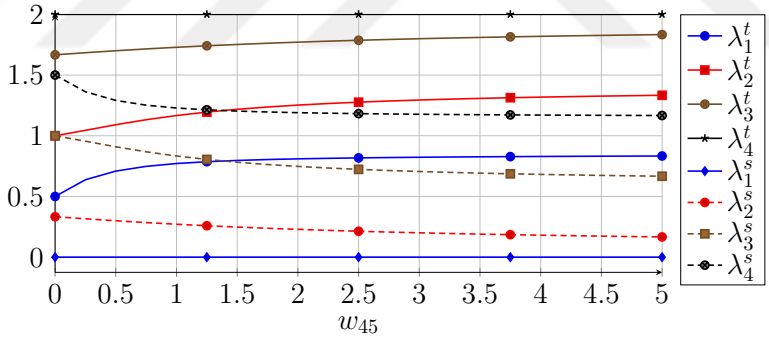

(b)

Figure 6.20 The change of eigenvalues for the symmetry $\mathcal{S}_1$

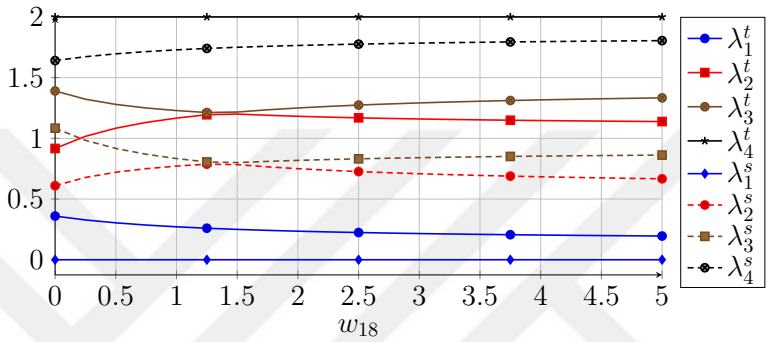

(a)

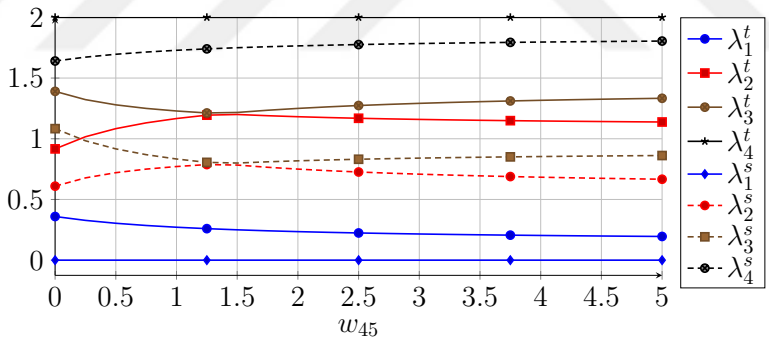

(b)

Figure 6.21 The change of eigenvalues for the symmetry $\mathcal{S}_2$

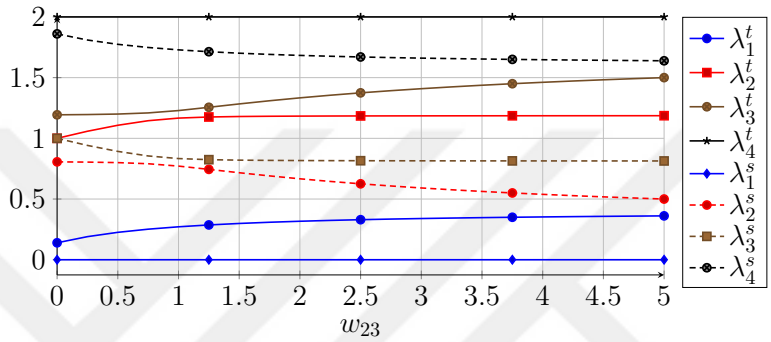

(a)

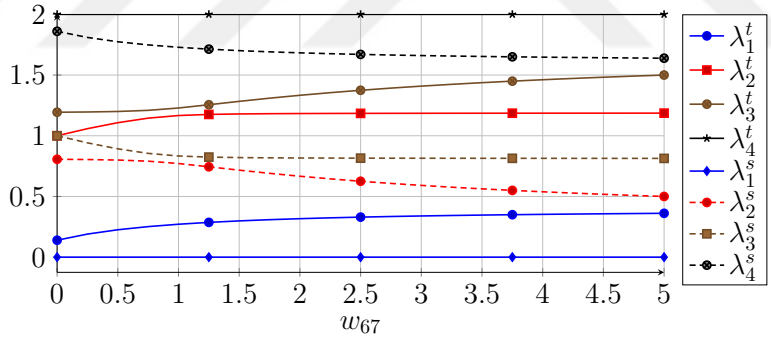

(b)

Figure 6.22 The change of eigenvalues for the symmetry $\mathcal{S}_2$

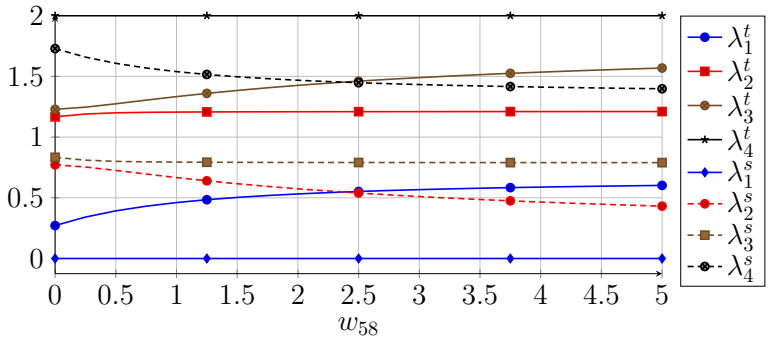

(a)

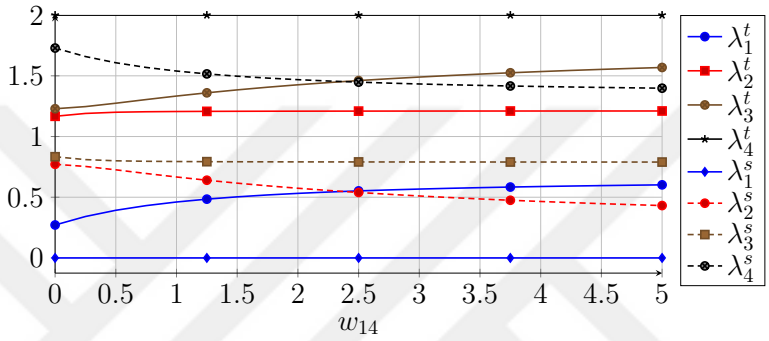

(b)

Figure 6.23 The change of eigenvalues for the symmetry $\mathcal{S}_3$

Changing the weights of some particular links can stabilize the cluster pattern in Figure 6.13d corresponding to the symmetry $\mathcal{S}_2$. For this purpose, the distribution of the eigenvalues of the outer coupling matrix with respect to the changes in the weights w_{18} and w_{45} for symmetries $\mathcal{S}_1$ and $\mathcal{S}_2$ are shown in Figure 6.20 and Figure 6.21, respectively. Note from Figure 6.20 that the changes in the weights w_{18} and w_{45} do not have any effect on the stability of the cluster pattern corresponding to the symmetry $\mathcal{S}_1$, since the eigenvalue condition $\lambda_1^t > \lambda_2^s$ is satisfied for all values of w_{14} and w_{45}. Similarly, it is apparent from Figure 6.21 that the changes in the weights w_{18} and w_{45} do not have any effect on the stability of the cluster pattern corresponding to the symmetry $\mathcal{S}_2$, as the eigenvalue condition $\lambda_1^t > \lambda_2^s$ is not satisfied for all values of w_{14} and w_{45}. In Figure 6.22, the weights w_{23} and w_{67} are chosen as the control parameters. However, as can be seen from the change of the eigenvalue distribution in Figure 6.22, the cluster pattern corresponding to the symmetry $\mathcal{S}_2$ cannot be stabilized by changing the weights between the nodes 2 and 3, and the nodes 6 and 7.

To form the cluster pattern corresponding to the symmetry $\mathcal{S}_2$, we can modify the network in Figure 6.19c without changing its symmetry. For this purpose, we can insert a link between the nodes 5 and 8. This insertion modifies the network's topological structure, affecting the eigenvalue distribution, and does not change topological symmetry $\mathcal{S}_2$. However, to distinguish the networks with and without the coupling between the nodes 5 and 8, we will call the new symmetry $\mathcal{S}_3$. In Figure 6.23 are shown the changes of the eigenvalue distribution with respect to the changes in the weights w_{58} and w_{14}. From Figure 6.23a, it is clear that when weight w_{58} passes through the threshold $w^* \approx 2.5$, the eigenvalue condition $\lambda_1^t > \lambda_2^s$ is satisfied and the pattern in Figure 6.19f corresponding to the symmetry $\mathcal{S}_3$ becomes stable.

After the eigenvalue condition is satisfied, the next step is to determine the uniform coupling strength ϵ such that both of the cluster patterns in Figure 6.19b and Figure 6.19f are stable. When this requirement is satisfied, the cluster pattern of the network can be controlled by just controlling the weight between the nodes 5 and 8. For the unweighted network in Figure 6.19b, the range for ϵ is $\epsilon_{r_1} = [\epsilon_{l_1}, \epsilon_{h_1}]$ where $\epsilon_{l_1} = \eta^*/\lambda_1^t$ and $\epsilon_{h_1} = \eta^*/\lambda_2^s$. For the Lorenz dynamics defined in (4.22) and the inner coupling matrix $\boldsymbol{P} = \text{diag}(1, 0, 0)$, the threshold $\eta^* \approx 10$. Thus, for the cluster pattern in Figure 6.19b, we find $\epsilon_{l_1} = 10/0.77 = 12.96, \epsilon_{h_1} = 10/0.27 = 36.86$. For the weighted network in Figure 6.19f, where all the links have weights 1 apart from the link between the nodes 5 and 8 which has weight $w_{58} = 5$, the range for ϵ is $\epsilon_{r_2} = [\epsilon_{l_2}, \epsilon_{h_2}]$ where $\epsilon_{l_2} = \eta^*/\lambda_1^t = 10/0.60 = 16.81$ and $\epsilon_{h_2} = \eta^*/\lambda_2^s = 10/0.43 = 23.18$.

Having chosen $\epsilon = 20$, the network in Figure 6.19 is simulated for a total simulation duration of 2000 seconds. The weight w_{58} of the link between the nodes 5 and 8 is chosen as the control parameter to switch between the cluster patterns in Figure 6.19b and Figure 6.19f. During the time interval $\mathcal{I}_1 = [0, 1000]$, the link between the nodes 5 and 8 is removed, i.e., $w_{58} = 0$. For the interval $\mathcal{I}_2 = [1000, 2000]$, the link between the nodes 5 and 8 is inserted with a weight of $w_{58} = 5$. The uniform scaling is fixed during the transmission, and $\epsilon = 20$. From the time waveforms of the errors shown in Figure 6.24, it is clear that for the time duration $\mathcal{I}_1$ the cluster pattern in Figure 6.13b is observed while for the time duration $\mathcal{I}_2$ the cluster pattern shown in Figure 6.19f is

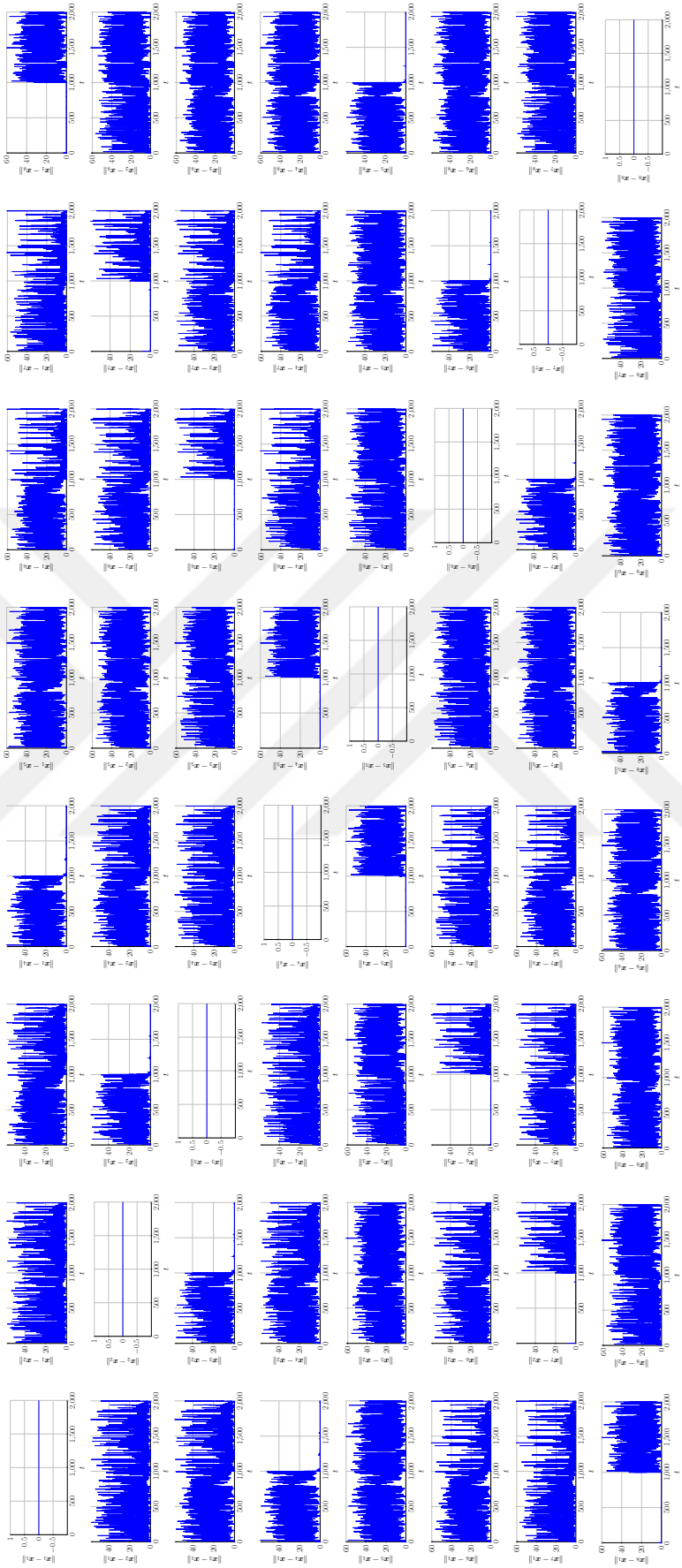

Figure 6.24 The simulation of the network in Figure 6.19. $e_{ij} = |x_i - x_j|$ where $\boldsymbol{x}_i = [x_i, y_i, z_i]$.

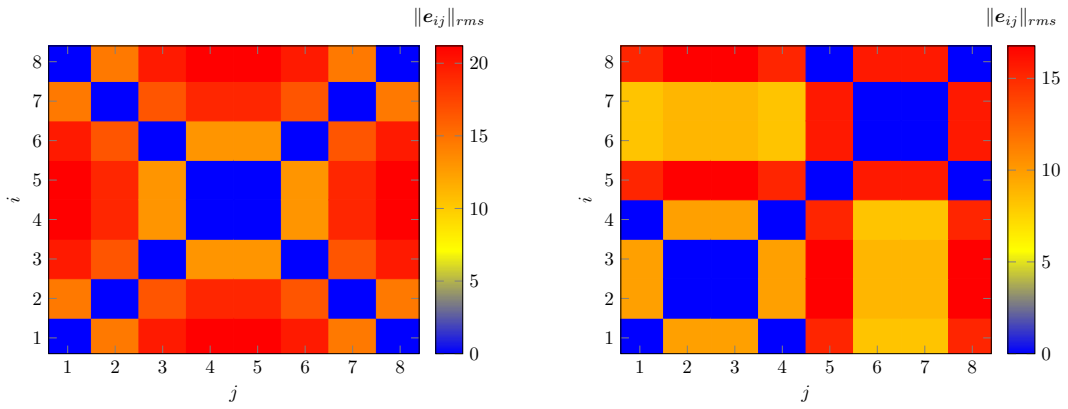

(a) (b)

Figure 6.25 The spatiotemporal view of the network in Figure 6.19. $\epsilon = 15$. (a) $0 \leq t < 1000$, ()b) $1000 \leq t < 2000$,

observed.

Since the network in Figure 6.19 can be programmed to exhibit two different cluster patterns in Figures 6.19a and Figure 6.19f, it is inherently possible for it to be employed in the desired communication system. The number of cluster patterns observed from the network is two, which implies that the network can be used in a binary communication system. Let the symbols in the communication system be $b_0 = 0$ and $b_1 = 1$. We can encode the cluster patterns in Figure 6.19b and Figure 6.19f to the symbols b_0 and b_1, respectively. The next step is to separate the transmitter and the receiver sides. Let ℓ_{ij} link the nodes i and j. With the requirements of the communication system in mind, we can start with $\ell_{12}, \ell_{78}, \ell_{34}, \ell_{56}$ since the nodes of these are not in the same clusters for both the cluster patterns in Figure 6.19b and Figure 6.19f. Hence, we can put these links on the channel. This implies that the nodes $1, 4, 5, 8$ and the nodes $2, 3, 6, 7$ must be on the opposite sides of the communication system. Since the cluster pattern of the network is controlled with the weight of the link ℓ_{58}, we must have access to the nodes 5 and 8, so they must be on the transmitter side. Since the nodes 1 and 4 are in the same clusters with the nodes 8 and 5, respectively, in the cluster pattern in Figure 6.19b, the nodes 1 and 4 must be on the transmitter side. As the nodes $1, 4, 5, 8$ are on the transmitter side, the nodes $2, 3, 6, 7$ must be on the receiver side. The resulting network is shown in Figure 6.26.

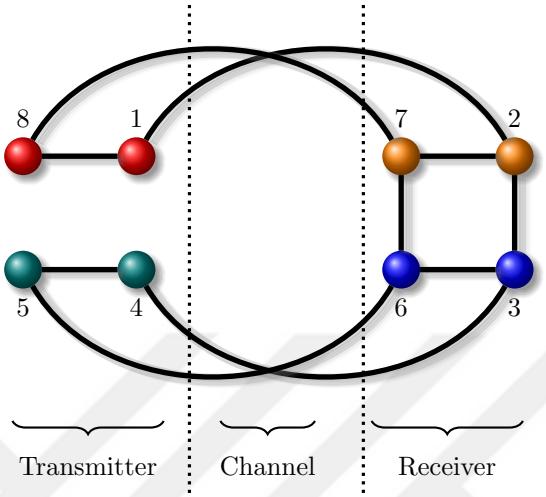

(a) $w_{58} = 0$.

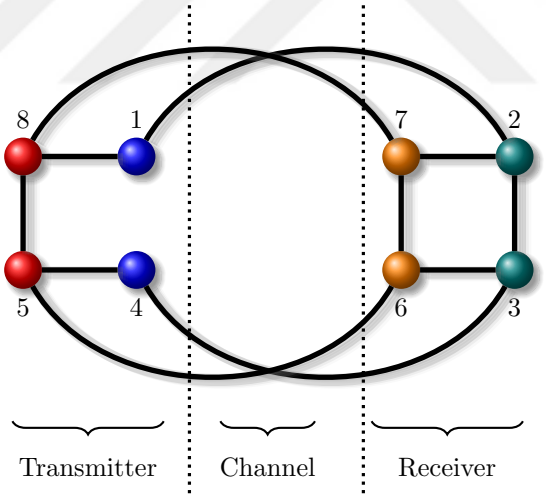

(b) $w_{58} = 5$

Figure 6.26 Using the network in Figure 6.19 in a binary communication system in which the symbols are s_1, s_2. The cluster pattern is controlled via the weight w_{58}. (a) Spatiotemporal status of the network during s_1 transmission. (b) Spatiotemporal status of the network during s_2 transmission. $\epsilon = 20$

The cluster patterns in Figure 6.26a and Figure 6.26b are associated with the symbols s_1 and s_2, respectively.

The resulting configuration shown in Figure 6.26 fulfills all the requirements of the communication system that can be outlined as follows:

1. A network of chaotic dynamical systems has been designed.
2. The network can be programmed to ensure different cluster patterns for different control parameters.
3. The network can be separated into two to be used in the receiver sides such that the nodes connecting the transmitter and receiver sides are out of synchronization during the transmission, so the signals transmitted through the channel always remain chaotic.
4. The control parameters are on the transmitter side only.
5. Encoding the symbols with the spatiotemporal status of the network provides covertness and security against malicious third-party activities.

6.2.2 Design with Control Network

6.2.2.1 Conceptual Design

In Section 4.2.2.1, we investigated how to induce cluster patterns in a network of chaotic oscillators. The technique exploits network symmetry in addition to the pinning control technique. The technique constructs a small-sized control network first. Then, it pins each control network node to all the nodes of their corresponding clusters. The nodes of the original network form the cluster pattern specified by the topological symmetry under this configuration. The point is that the control, i.e., pinning nodes, do not synchronize with their controlled nodes.

We have three striking remarks in this configuration that are useful for the network design in the proposed communication system.

1. The control network controls the cluster pattern of the original network.

2. The coupling from the control network to the original network is *unidirectional*.

3. There is no synchronization between the nodes of the control network and the original networks' nodes.

Hence, a programmable network useful for the communication system can be designed as follows.

1. In the receiver, we have $2N$ nodes. These nodes will be the control nodes to control nodes to control the cluster pattern of nodes in the receiver.

2. We associate each node pair in the receiver to one of the nodes in the transmitter as seen in Figure 6.27

3. We couple the nodes in the receiver in pairs as

   $graph \leftarrow Network\ of\ 2N nodes\ without\ edges$

   $i \leftarrow 1$

   while $i \leq 2N - 1$ **do**

   add edge between the nodes i *and* $i + 1$

   $i+ = 2$

4. Couple the node pairs on the transmitter side such that the node pairs in the receiver are synchronized. For example,

   (a) To synchronize the node groups $1, 2, 3, 4$ in the receiver, we need to couple the nodes $1'$ and $2'$.

   (b) For the synchronization of the node groups $1, 2, 5, 6$, we need to couple the nodes $1'$ and $3'$.

   (c) To synchronize the nodes groups $1, 2, 3, 4, 5, 6$, the nodes $1'$ and $2'$ and $3'$ must be coupled.

   (d) By changing the coupled node groups in the transmitter, the corresponding node groups in the receiver are synchronized, changing the topology.

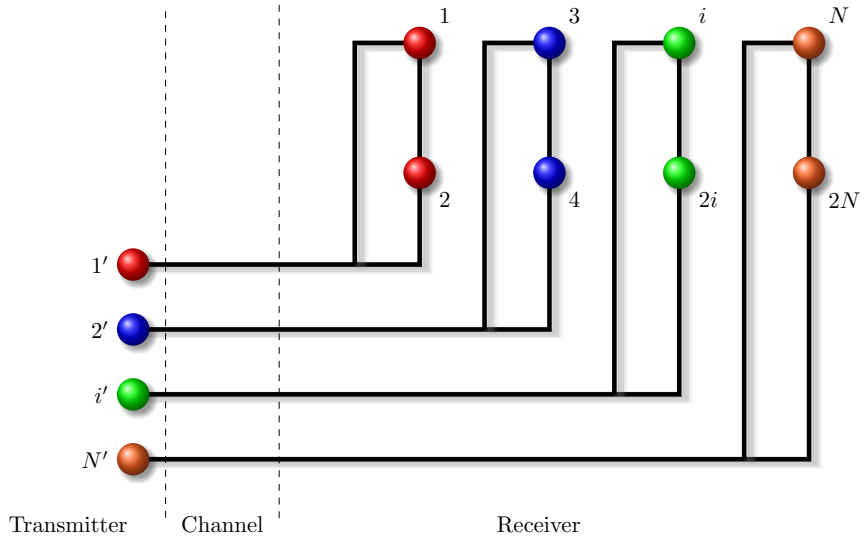

Figure 6.27 Conceptual network design.

5. We have the following implications for this design.

   (a) The cluster pattern of the node groups in the receiver is controlled from the transmitter side only.

   (b) There is no synchronization among the nodes connecting the transmitter and receiver. The signals flowing through the channel are always chaotic.

   (c) The coupling between the transmitter and receiver sides is unidirectional. This property is significant since we can model the noise in the channel as additive, as the noise only affects the dynamics of the receiver side, not those on the transmitter side.

   (d) The symbol capacity of the network is simple: the $M = \binom{N}{2}$ evaluated only using the synchronized node pairs on the receiver side. This simple result indicated that we can design networks having theoretically infinite symbol capacity.

6.2.2.2 *Network Design Approach Disconnected Subnetworks*

Consider the cluster pattern shown in Figure 6.28 where we want only one single cluster at the receiver node groups consisting of the node groups $\mathcal{G}_1 = \{1, 2, \ldots, 6\}$. We

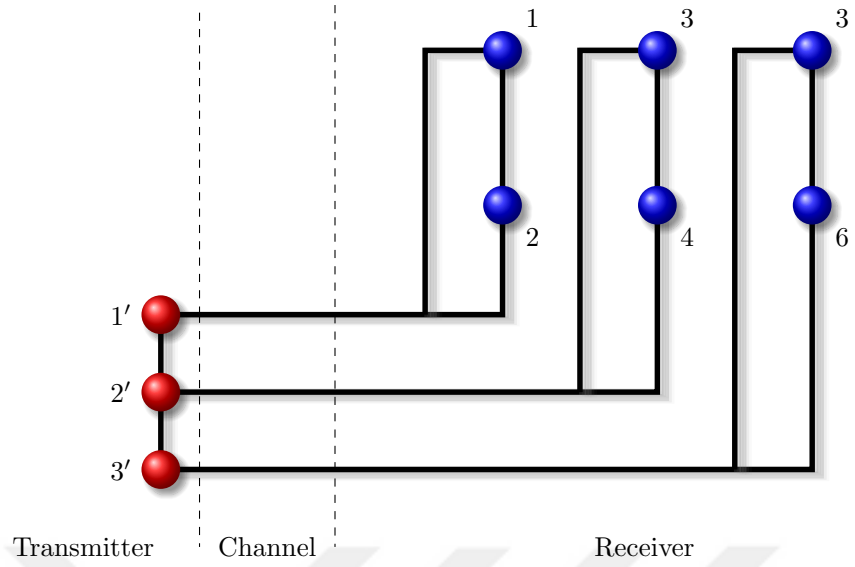

Figure 6.28 The cluster pattern 1.

have one cluster in the receiver consisting of the nodes $1, 2, \ldots, 6$. The control matrix for this cluster pattern is

$$\boldsymbol{A} = \begin{bmatrix} -20 & 10 & 10 \\ 10 & -20 & 10 \\ 10 & 10 & -20 \end{bmatrix}. \tag{6.29}$$

The nodes $1', 2', 3'$ are all connected. Figure 6.29 shows the synchronization errors between the node pairs. The occurrence of the cluster pattern in Figure 6.28 can be observed from Figure 6.29.

Let us delete the links between the nodes $1'$ and $2'$, and the nodes $2'$ and $3'$ to get the cluster pattern in Figure 6.31 The control matrix takes the form

$$\boldsymbol{A} = \begin{bmatrix} -10 & 10 & 0 \\ 10 & -10 & 0 \\ 0 & 0 & 0 \end{bmatrix} \tag{6.30}$$

Hence, we want the clusters $(1, 2, 3, 4)$ and $(5, 6)$ in the receiver side. The simulation results in Figure 6.32 show that the cluster pattern in Figure 6.31 is achieved.

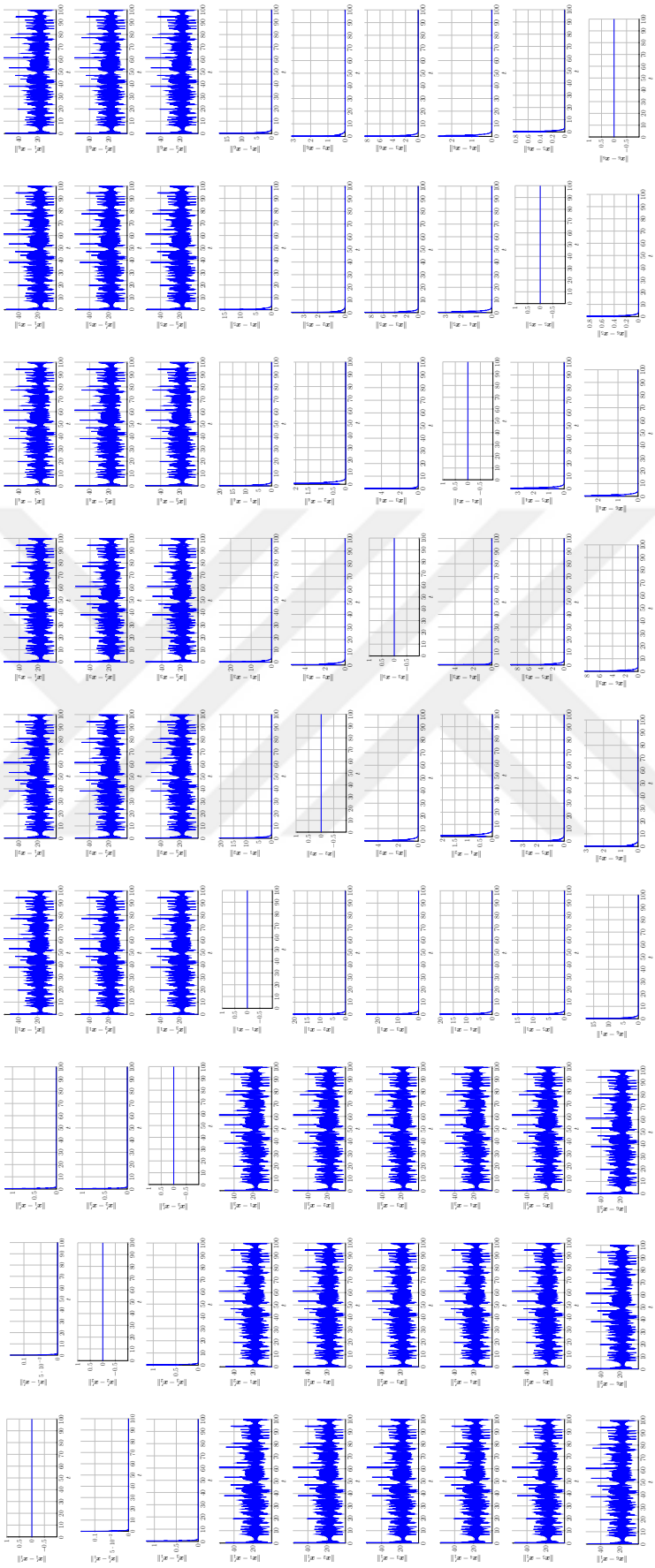

Figure 6.29 Error waveforms $e_{ij}(t)$ for $i, j = 1, 2, \ldots, 9$.

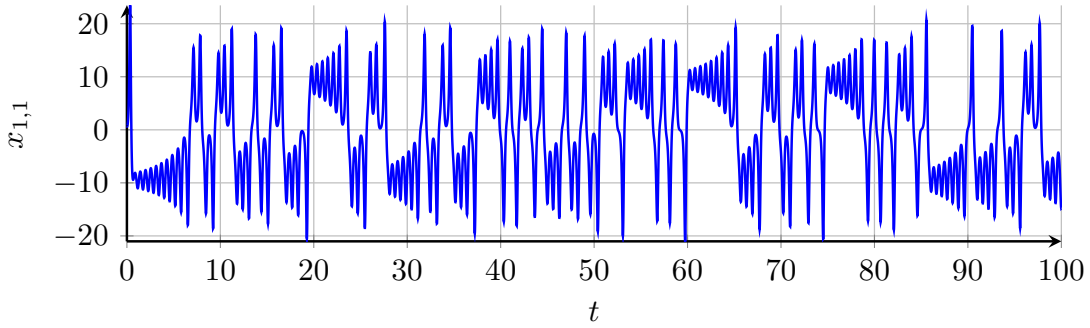

(a)

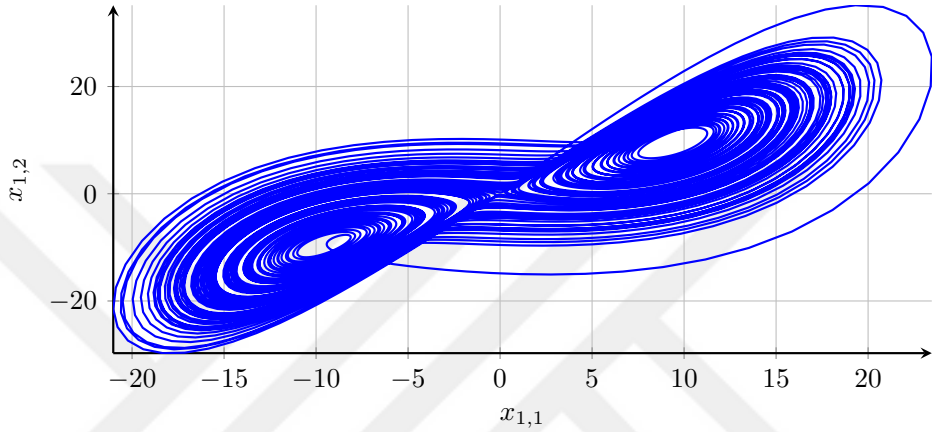

(b)

Figure 6.30 (a) Time waveform and (b) the chaotic attractor of the node 1.

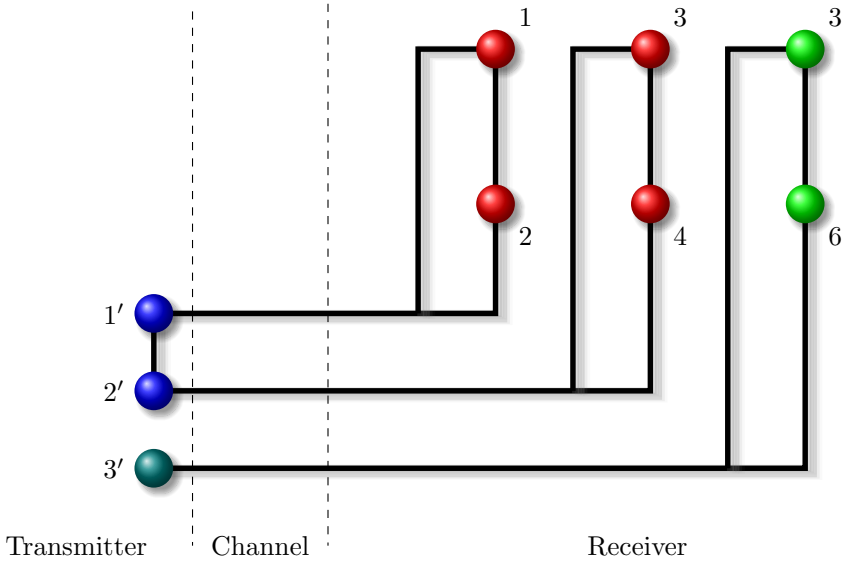

Figure 6.31 The cluster pattern 2

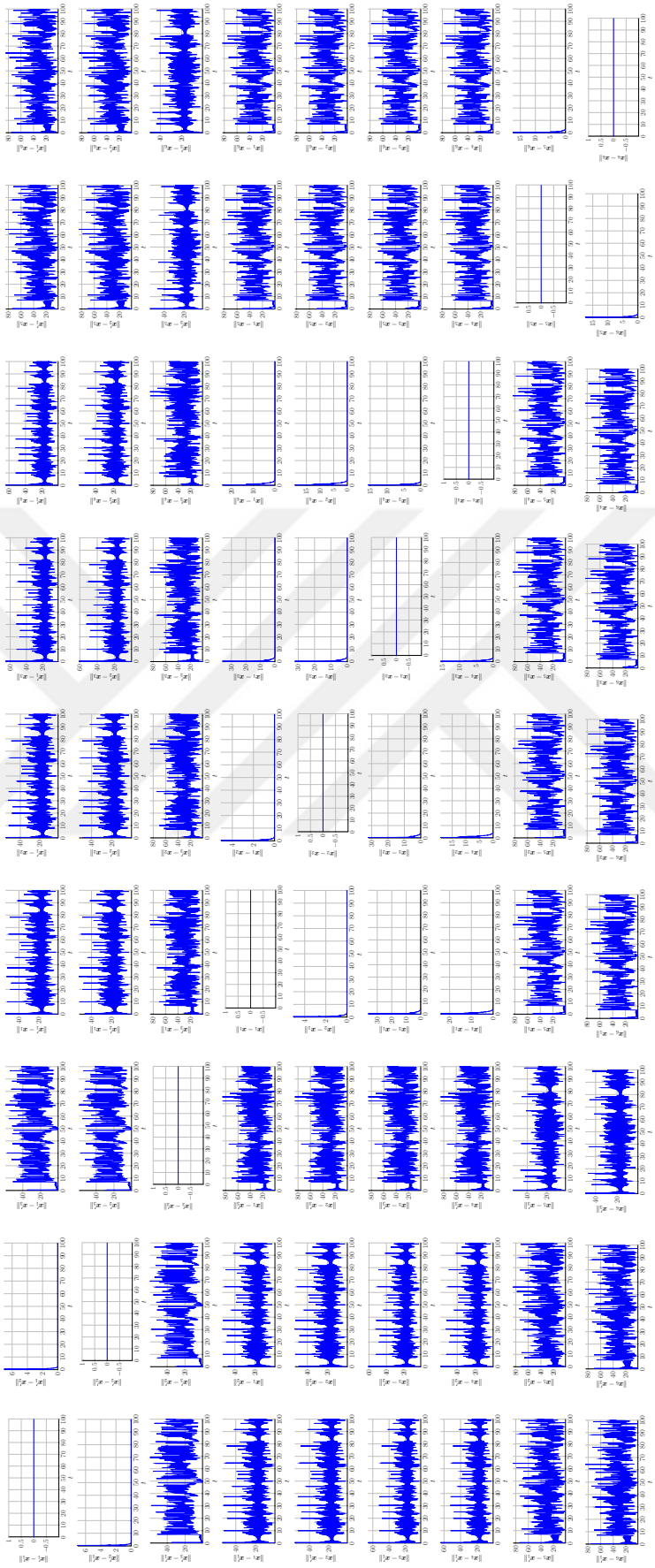

Figure 6.32 Error waveforms $e_{ij}(t)$ for $i, j = 1, 2, \ldots, 9$.

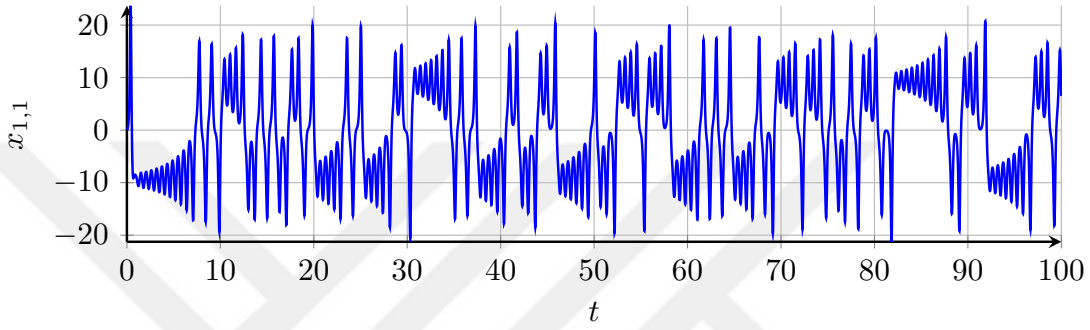

(a)

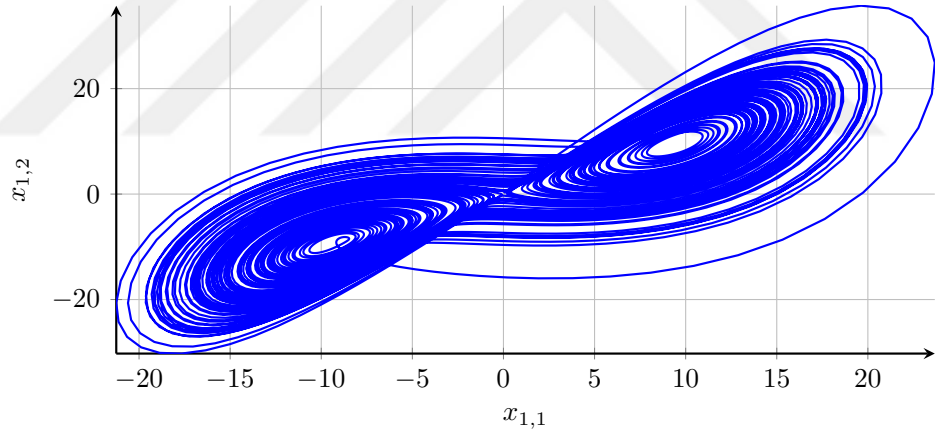

(b)

Figure 6.33 (a)Time waveform and (b)the chaotic attractor of the node 1.

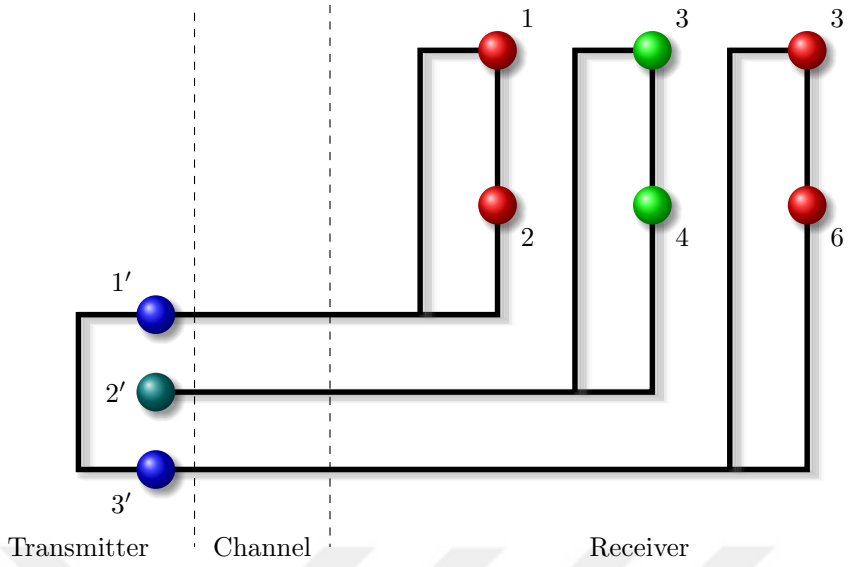

Figure 6.34 The cluster pattern 3

If we change the coupling such that only the nodes $1'$ and $3'$ are connected, we get the network shown in Figure 6.34. That is, we want the clusters $\mathcal{G}_1 = \{1, 2, 5, 6\}$ and $\mathcal{G}_2 = \{3, 4\}$ in the receiver side. Figure 6.35 shows the simulation results corresponding to this topology.

As the last example, let us construct the cluster pattern $\mathcal{G}_1 = \{1, 2\}, \mathcal{G}_2 = \{3, 4\}, \mathcal{G}_3 = \{5, 6\}$ by choosing

$$\boldsymbol{A} = \begin{bmatrix} 0 & 0 & 0 \\ 0 & 0 & 0 \\ 0 & 0 & 0 \end{bmatrix}, \tag{6.31}$$

that is, all the nodes $1', 2', 3'$ are disconnected. Figure 6.37 shows the corresponding cluster pattern. The simulation results in Figure 6.38 justify the occurrence of the cluster pattern in Figure 6.37.

We have the following remarks with this network design

1. One of the drawbacks of this scheme is that the number of links in the channel is directly equal to the number of clusters in the network. Therefore, the larger the

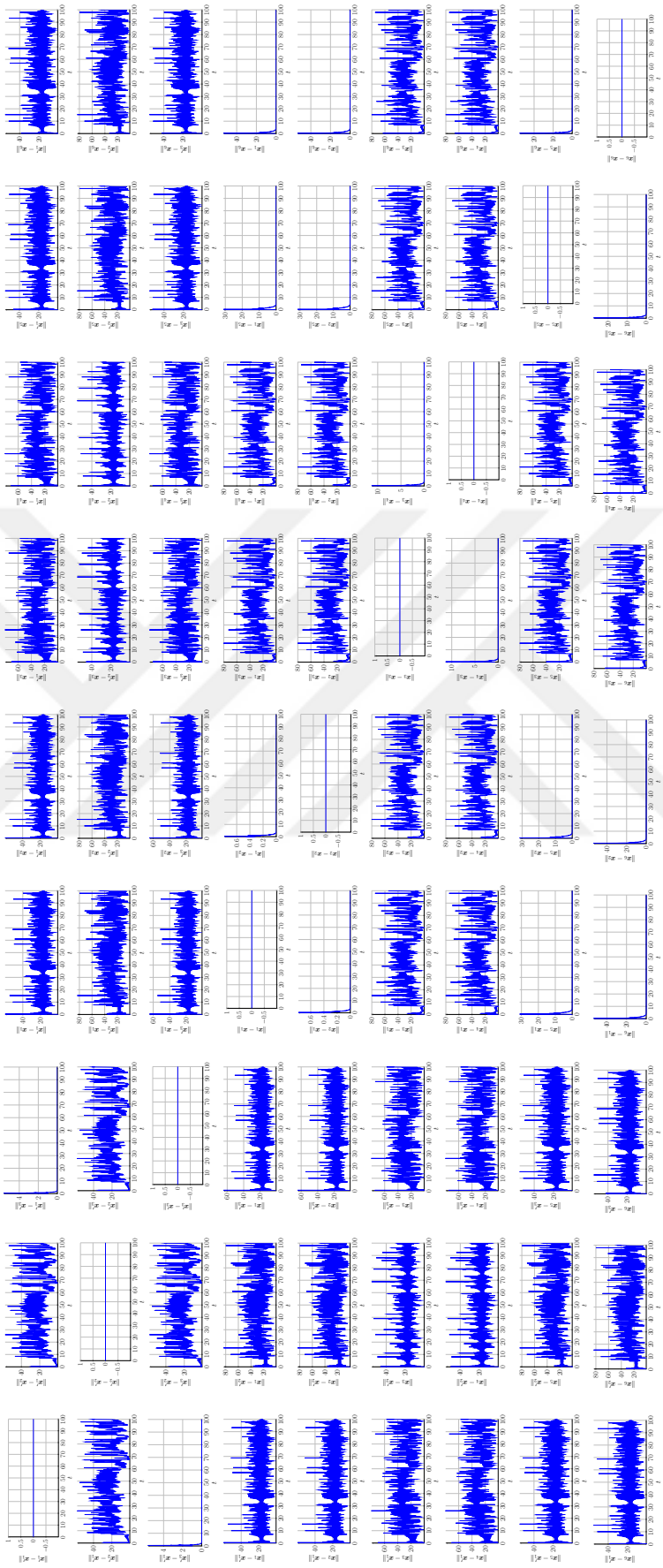

Figure 6.35 Error waveforms $e_{ij}(t)$ for $i, j = 1, 2, \ldots, 9$.

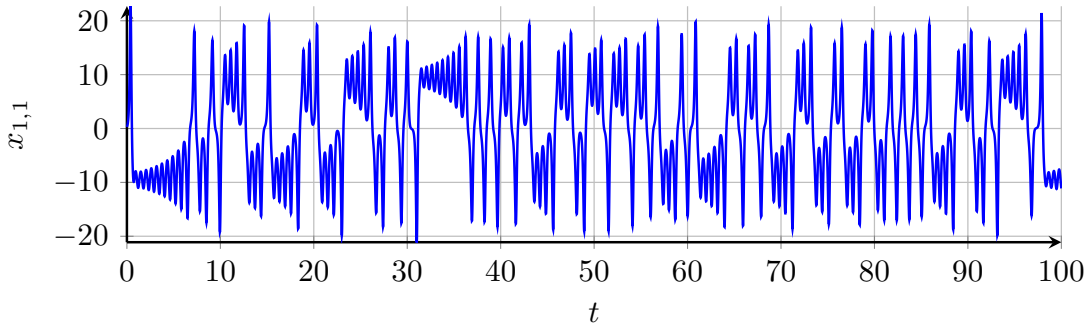

(a)

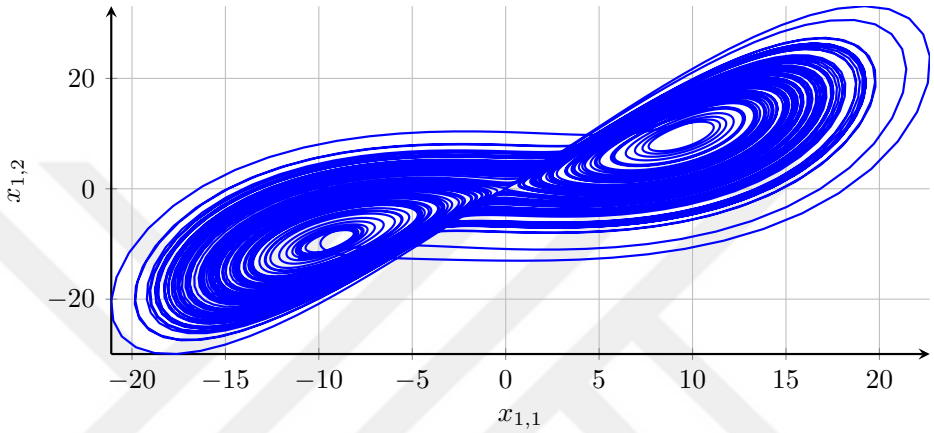

(b)

Figure 6.36 (a) Time waveform and (b) the chaotic attractor of the node 1.

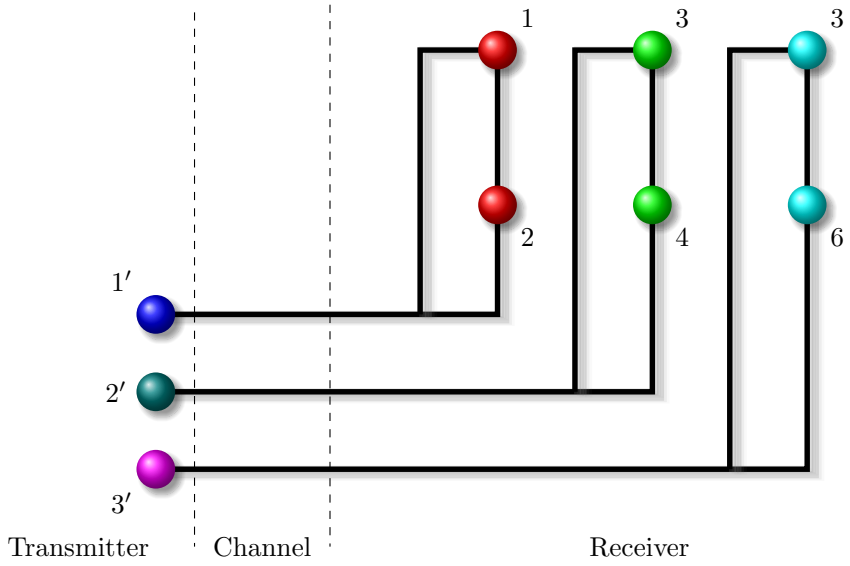

Figure 6.37 The cluster pattern 4

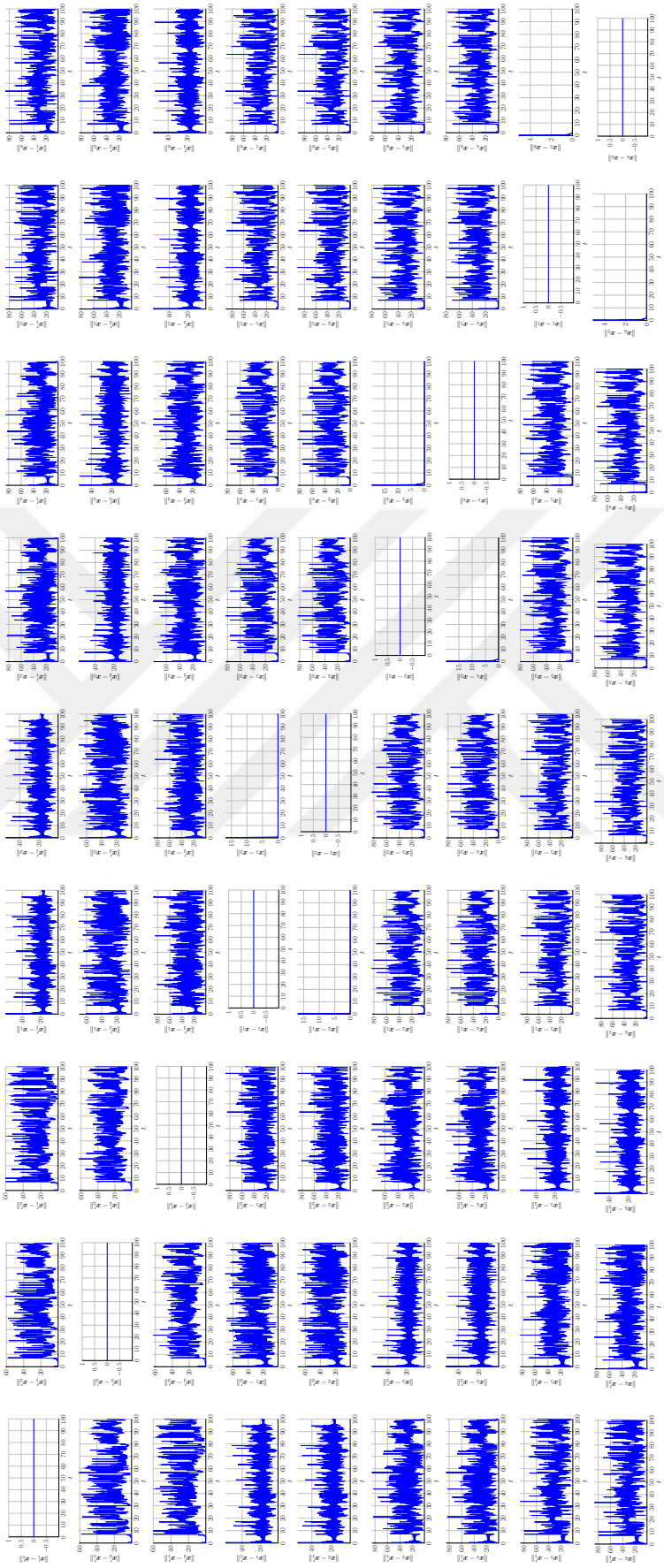

Figure 6.38 Error waveforms $e_{ij}(t)$ for $i, j = 1, 2, \ldots, 6$.

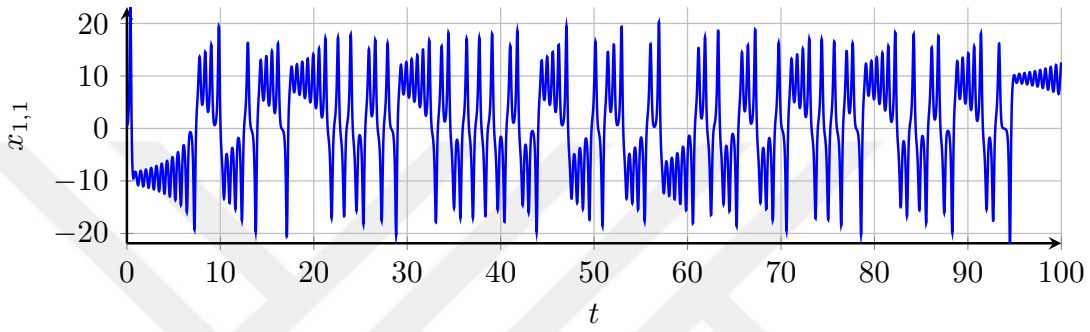

(a)

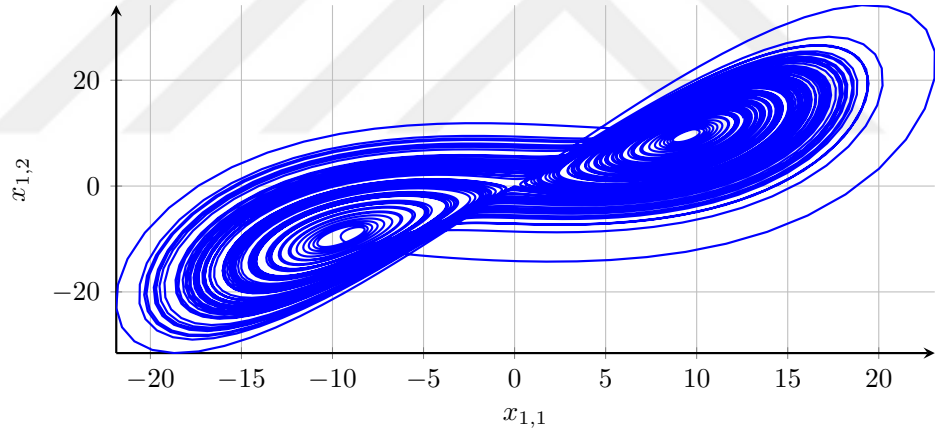

(b)

Figure 6.39 (a) Time waveform and (a) the chaotic attractor of the node 1.

number of symbols in the alphabet of the communication system, the larger the number of links in the channel.

2. Since the nodes on the receiver side drive the nodes on the receiver side, the signal flow is unidirectional from the transmitter side to the receiver side. This fact helps us quantify the amount of noise in the channel.

3. In contrast to our previous designs in which the number of nodes and topology of the subnetworks are the same on the transmitter and receiver sides, the number of nodes and the topology of the subnetworks in the transmitter and receiver can be different.

4. The symbol capacity of the network can be increased as many as we want by adding new node pairs in the receiver and a control node at the receiver.

5. Since the signal flow is unidirectional from the transmitter to the receiver, the non-idealities of the channel, such as filtering, delay, attenuation, etc., can be analyzed much more easily when compared to our previous network design approach in which the signal flow is bi-directional in the channel.

6.2.2.3 Network Design Approach Connected Subnetworks

To use the designed network in the proposed communication system, we divide the network such that the control network stays in the transmitter while the original network stays in the receiver. In our previous attempt, we designed such networks, however, the network in the receiver is not simply-connected. A network is simply-connected if there exists a link from node i to node j and a directed link from node j to i for every pair of nodes i and j.

Recall also that we determined a symmetry axis and then placed nodes on both sides of this symmetry axis (we assumed reflection symmetry). The nodes on both sides of the symmetry axis are then coupled in pairs. Then, we assigned a control node for each pair of nodes on the receiver side. The problem is that the receiver network's node pairs are not connected. To make the network simply-connected, we can add nodes on the

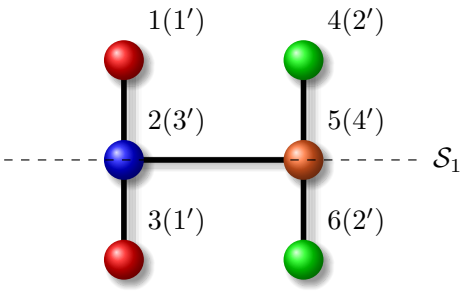

Figure 6.40 A simply-connected network with the clusters $\mathcal{G}_1 = \{1, 3\}, \mathcal{G}_2 = \{4, 6\}, \mathcal{G}_3 = \{2\}, \mathcal{G}_3 = \{5\}$. The nodes $1, 2, \ldots, 6$ and $1', 2', \ldots, 4'$ are the controlled and the control nodes, respectively. The control node of each controlled node is written in the parenthesis next to it.

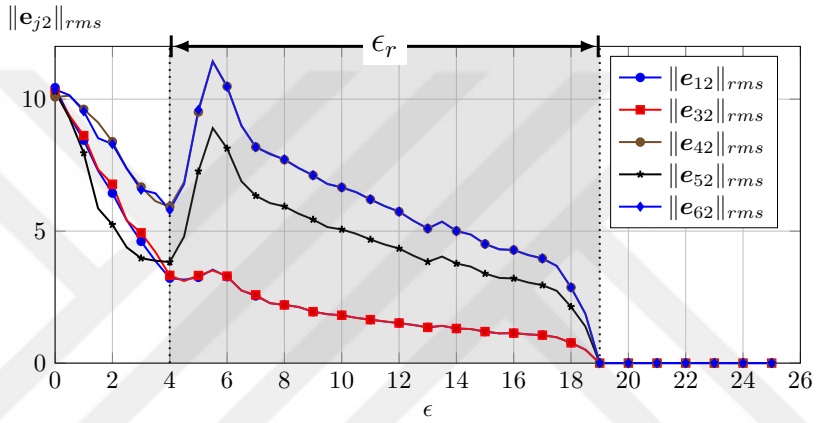

Figure 6.41 The change of the spatiotemporal status of the original (unpinned) network.

symmetry axis and add connections from these nodes to the remaining nodes. Figure 6.40 illustrates such a case.

The symmetry axis in the network is a horizontal line passing through the nodes 2 and 5. The desired clusters in this network are $\mathcal{G}_1 = \{1, 3\}, \mathcal{G}_2 = \{4, 6\}, \mathcal{G}_3 = \{2\}, \mathcal{G}_4 = \{5\}$. To get the cluster pattern, we need to use the control nodes i' and connect them to the nodes of $\mathcal{G}_i$ for $i = 1, 2, 3, 4$ (Figure 6.40).

Before implementing the pinning control, let us check the network status as the coupling strength ϵ changes. Figure 6.41 illustrates the change of the cluster pattern of the original network for changing ϵ. Note from Figure 6.41 that for $\epsilon \in [5, 18]$, the cluster pattern in Figure 6.40 is stable. However, by changing ϵ, we only have a single pattern shown in Figure 6.40. We need one more pattern to use the network in a binary communication system.

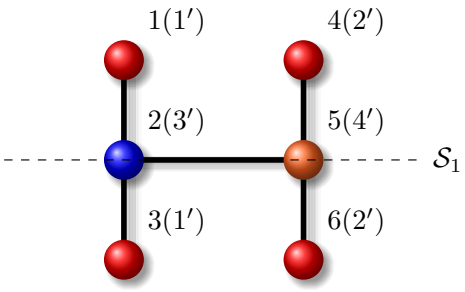

Figure 6.42 The network in Figure 6.40 with the clusters $\mathcal{G}_1 = \{1, 3, 4, 6\}, \mathcal{G}_2 = \{2\}, \mathcal{G}_3 = \{5\}$

Consider that we want the cluster pattern shown in Figure 6.42. Note from Figure 6.41 that the pattern in Figure 6.42 cannot be realized for any value of ϵ. Therefore, we must apply the control network and change the control strength α for $\epsilon = 3$. The control matrix $\boldsymbol{A}$ and the matrix $\boldsymbol{C}$ that couples the control network to the original network and the outer coupling matrix $\boldsymbol{\Xi}$ of the original network found as

$$\boldsymbol{\Xi} = \begin{bmatrix} -1 & 1 & 0 & 0 & 0 & 0 \\ 1 & -3 & 1 & 0 & 1 & 0 \\ 0 & 1 & -1 & 0 & 0 & 0 \\ 0 & 0 & 0 & -1 & 1 & 0 \\ 0 & 1 & 0 & 1 & -3 & 1 \\ 0 & 0 & 0 & 0 & 1 & -1 \end{bmatrix}, \tag{6.32}$$

$$\boldsymbol{A} = \begin{bmatrix} -1 & 0 & 1 & 0 \\ 0 & -1 & 0 & 1 \\ 2 & 0 & -3 & 1 \\ 0 & 2 & 1 & -3 \end{bmatrix}, \tag{6.33}$$

$$\boldsymbol{C} = \begin{bmatrix} 1 & 0 & 0 & 0 \\ 0 & 0 & 1 & 0 \\ 1 & 0 & 0 & 0 \\ 0 & 1 & 0 & 0 \\ 0 & 0 & 0 & 1 \\ 0 & 1 & 0 & 0 \end{bmatrix}. \tag{6.34}$$

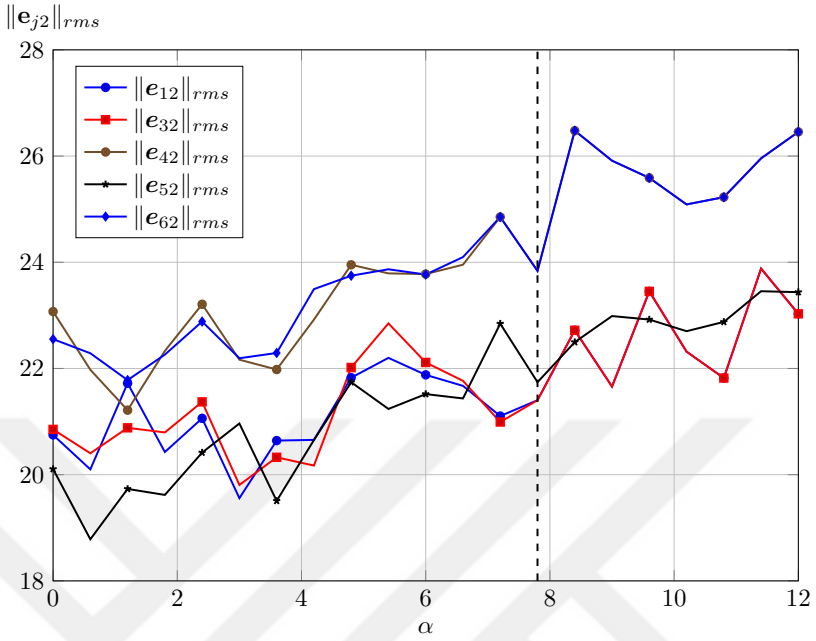

(a)

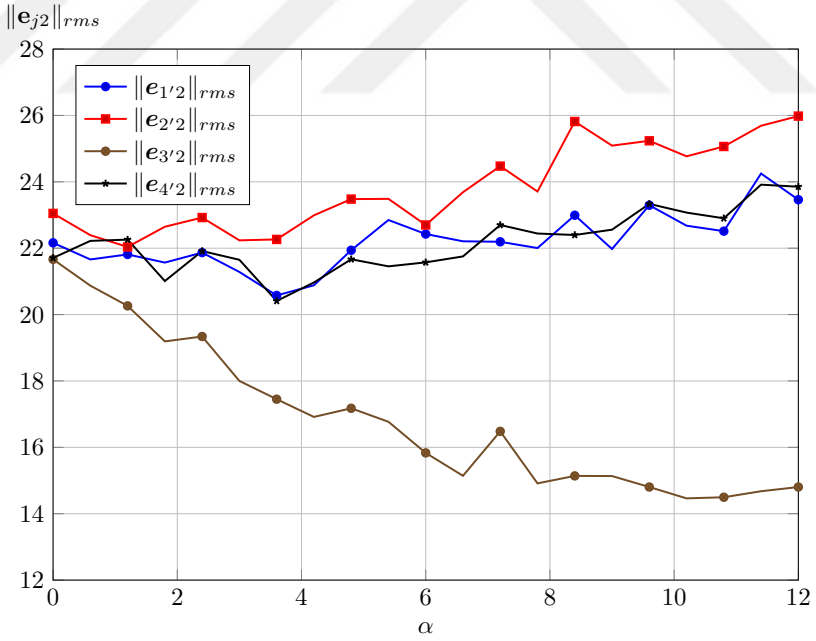

(b)

Figure 6.43 The spatiotemporal status of the network for changing control strength. The dashed line at $\alpha \approx 7.8$ shows the threshold above which the cluster pattern in Figure 6.40 is achieved.

Figure 6.43 shows the change in the spatiotemporal status of the network for changing α. Note from Figure 6.43 that for $\alpha > 8$, the cluster pattern in Figure 6.40 is stable. However, the cluster pattern in Figure 6.42 is neither stable for any α values. To stabilize the cluster pattern in Figure 6.42, we can couple the control nodes $1'$ and $2'$ to make them synchronize. We expect that the synchronized nodes $1'$ and $2'$ make the nodes $1, 2, 3, 4$ synchronized. Since we defined the clusters as $\mathcal{G}_1 = \{1, 3\}, \mathcal{G}_2 = \{4, 6\}, \mathcal{G}_3 = \{2\}, \mathcal{G}_4 = \{5\}$, and we want the nodes $1'$ and $2'$ to be synchronized, we define the control matrix as

$$\boldsymbol{A} = \begin{bmatrix} -20 & 20 & 0 & 0 \\ 20 & -20 & 0 & 0 \\ 0 & 0 & 0 & 0 \\ 0 & 0 & 0 & 0 \end{bmatrix}. \tag{6.35}$$

Figure 6.44 illustrates the simulation results. Note from Figure 6.44 that for changing values of α, the network achieves the cluster pattern in Figure 6.40 while the pattern in Figure 6.42 could not be achieved. The coupling for $\epsilon = 1$ is purposefully chosen in the results presented in Figure 6.44 to make the cluster pattern in Figure 6.40 unstable. However, the network cannot be used in the proposed communication system.

In the previous network design, our primary concern was designing the network as simply connected. Therefore, we can delete one of the nodes on the symmetry axis in Figure 6.40 and consider the second network design as shown in Figure 6.45, which is also simply-connected.

First, let us check the topological stability of the network without pinning control. The results are shown in Figure 6.46; the network directly undergoes from complete desynchronization to full synchronization without achieving any cluster synchronization pattern. We have to apply pinning control to the network to achieve the cluster pattern in Figure 6.45. The control matrix for the cluster pattern in Figure 6.45 is

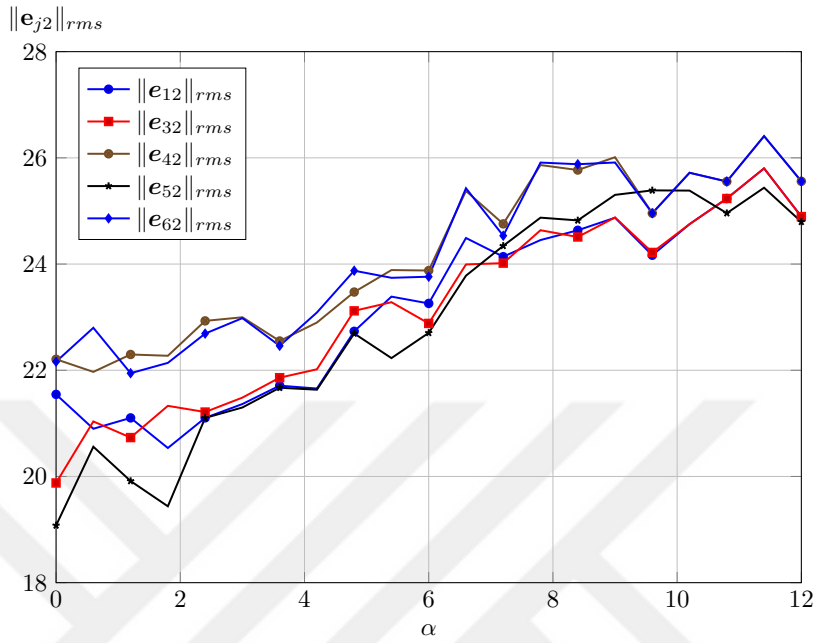

(a)

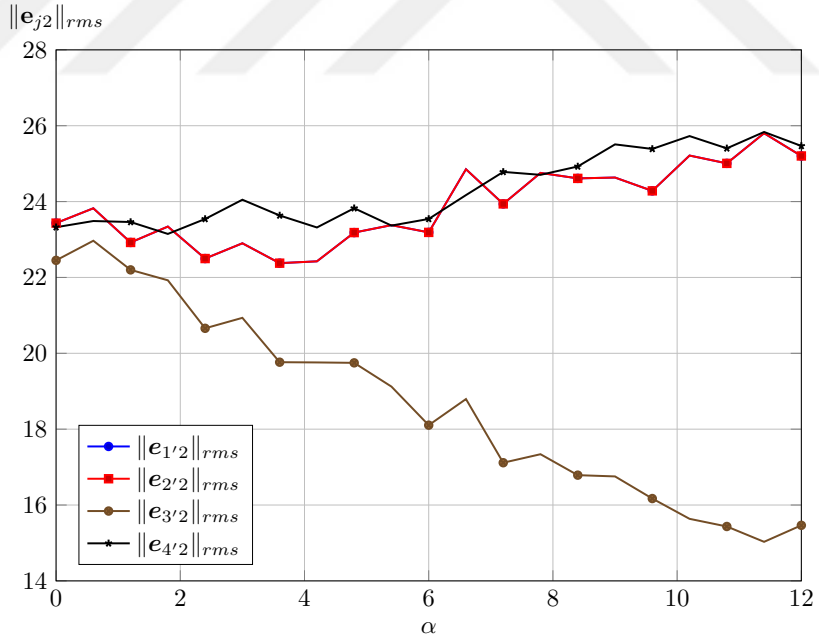

(b)

Figure 6.44 The spatiotemporal status of the network for changing control strength α.

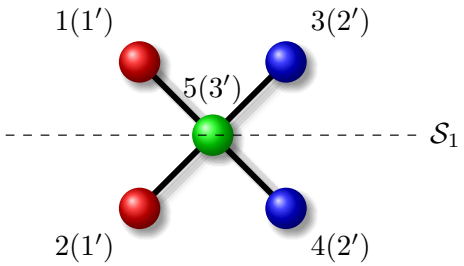

Figure 6.45 A simply-connected network with the clusters $\mathcal{G}_1 = \{1, 2\}, \mathcal{G}_2 = \{3, 4\}, \mathcal{G}_3 = \{5\}$. The nodes $1, 2, \ldots, 5$ and $1', 2', 3'$ are the controlled and the control nodes, respectively. The control node of each controlled node is written in the parenthesis next to it.

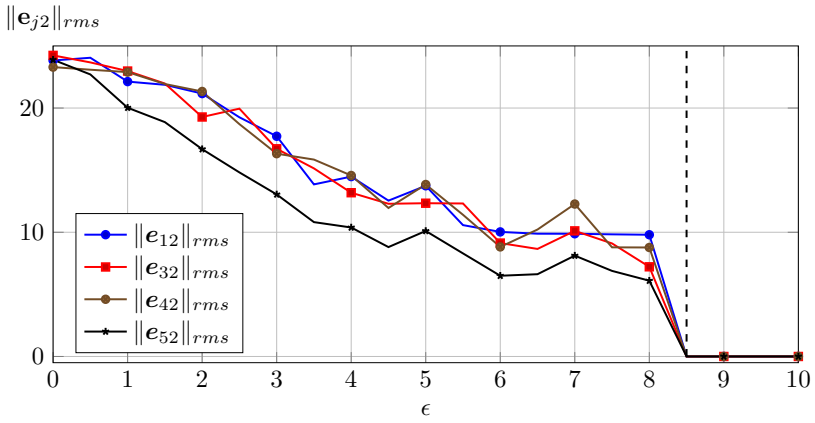

Figure 6.46 The change of the spatiotemporal status of the original (unpinned) network.

$$\Xi = \begin{bmatrix} -1 & 0 & 0 & 0 & 1 \\ 0 & -1 & 0 & 0 & 1 \\ 0 & 0 & -1 & 0 & 1 \\ 0 & 0 & 0 & -1 & 1 \\ 1 & 1 & 1 & 1 & -4 \end{bmatrix} \tag{6.36}$$

$$\boldsymbol{A} = \begin{bmatrix} -1 & 0 & 1 \\ 0 & -1 & 1 \\ 2 & 2 & -4 \end{bmatrix} \tag{6.37}$$

$$\boldsymbol{C} = \begin{bmatrix} 1 & 0 & 0 \\ 1 & 0 & 0 \\ 0 & 1 & 0 \\ 0 & 1 & 0 \\ 0 & 0 & 1 \end{bmatrix} \tag{6.38}$$

The change of spatiotemporal status of the network with respect to the change of the control strength is shown in Figure 6.47. From the results in Figure 6.47 it is seen that the cluster pattern shown in Figure 6.45 is achieved for $\alpha > 8$. Note also that the pinned nodes $1'$, $2'$ and $3'$ do not synchronize with any of the nodes in their corresponding clusters.

We only have one stable cluster pattern shown in Figure 6.45. We need at least one stable cluster pattern to use the network in a binary communication system. Let us use the cluster pattern in Figure 6.48. The results in Figure 6.47 show that the cluster pattern in Figure 6.48 cannot be achieved without the pinning control. We want the nodes $1, 2, 3, 4$ to be synchronized. So, we expect that if the control nodes $1'$ and $2'$ synchronize, then we can achieve the cluster pattern shown in Figure 6.48. The control pattern corresponding to the cluster pattern is

$$\boldsymbol{A} = \begin{bmatrix} -20 & 20 & 0 \\ 20 & -20 & 0 \\ 0 & 0 & 0 \end{bmatrix}. \tag{6.39}$$

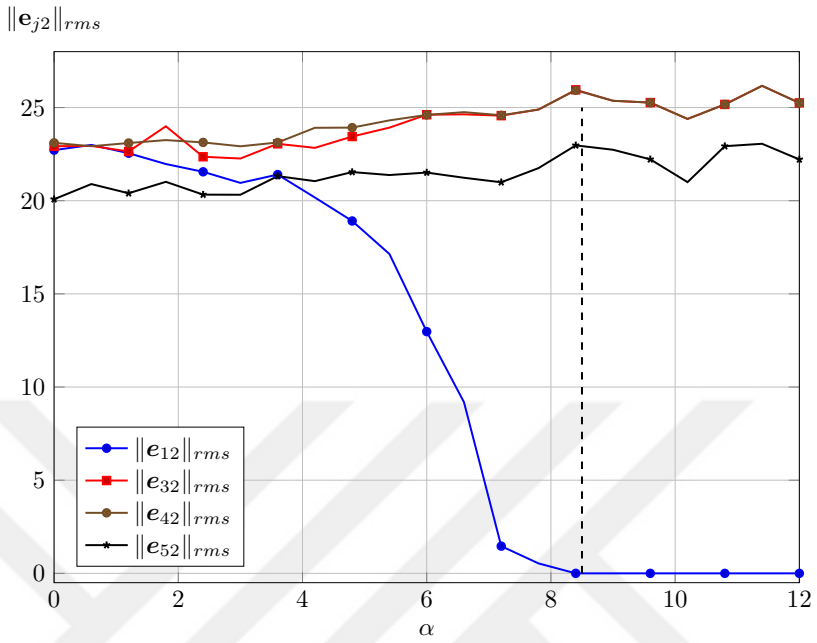

(a)

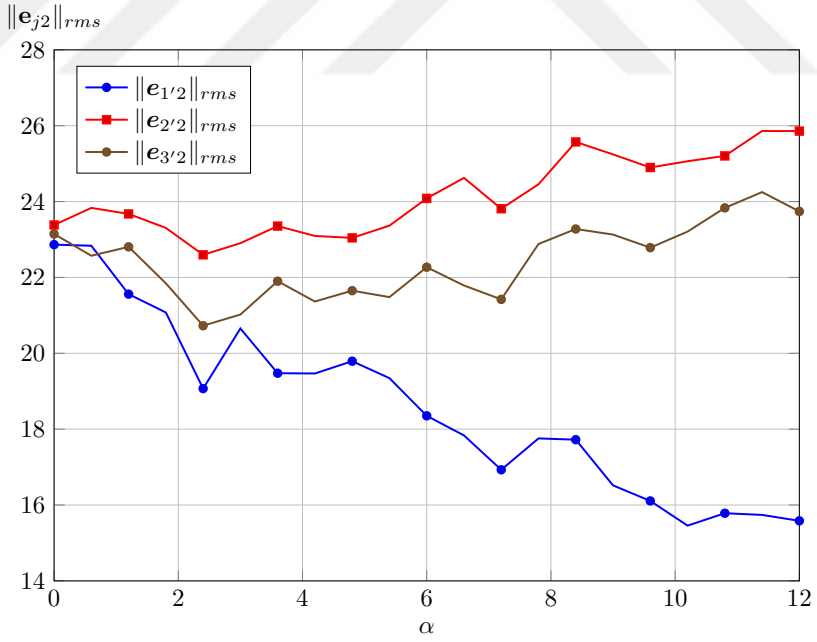

(b)

Figure 6.47 The change of spatiotemporal status of the network for changing control strength.

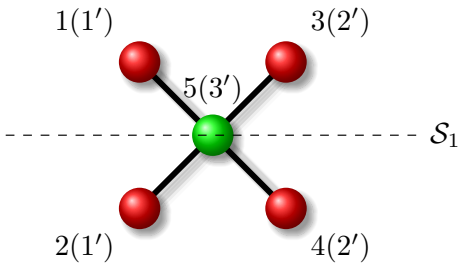

Figure 6.48 The network in Figure 6.45 with the clusters $\mathcal{G}_1 = \{1, 2, 3, 4\}, \mathcal{G}_2 = \{5\}$.

The change of the spatiotemporal status of the network with respect to the changing values of the control strength α is given in Figure 6.49. Note from Figure 6.49 that the cluster pattern shown in Figure 6.48 is achievable for $\alpha > 10$. As we have achieved two different cluster patterns that can be used to encode the symbols 0 and 1 of the communication system, the next step is to split the network nodes between the transmitter and the receiver parts.

6.2.2.4 Splitting Nodes

As the network can achieve the cluster patterns shown in Figure 6.40 and in Figure 6.48, we can split the nodes as shown in Figure 6.50 and Figure 6.51. We can encode the symbol to the cluster pattern in Figure 6.50 and the symbol to the cluster pattern in Figure 6.51. We couple the node $1'$ to node $2'$ during the symbol 1 transmission, and we decouple $1'$ and $2'$ during symbol 0 transmission. We split the network nodes such that the control nodes, i.e., the pinning nodes, stay on the transmitter side while those of the original network stay on the receiver side. In this way, we can control the cluster pattern of the network in the receiver from the transmitter. During the transmission of both symbols, the pinning nodes do not synchronize with the nodes in the receiver. Therefore, the signals in the channel are always chaotic.

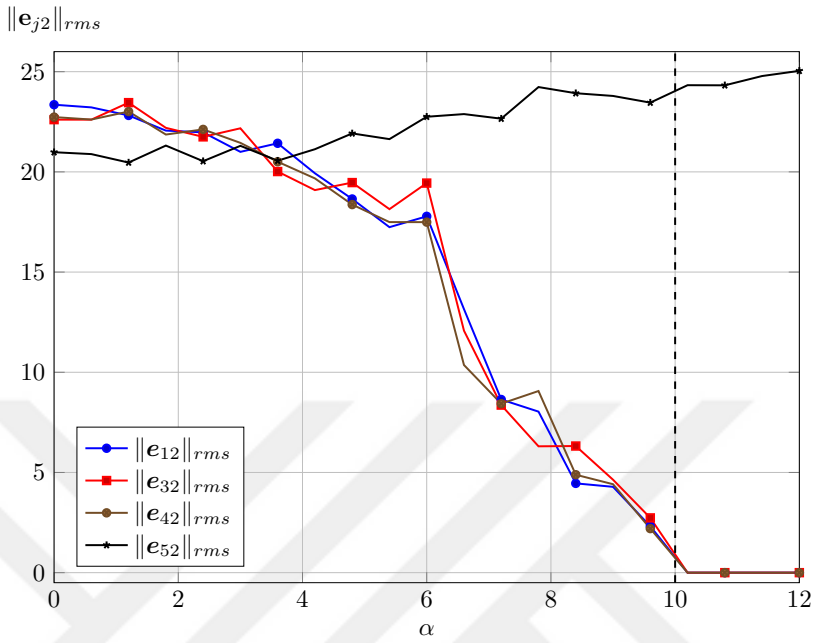

(a)

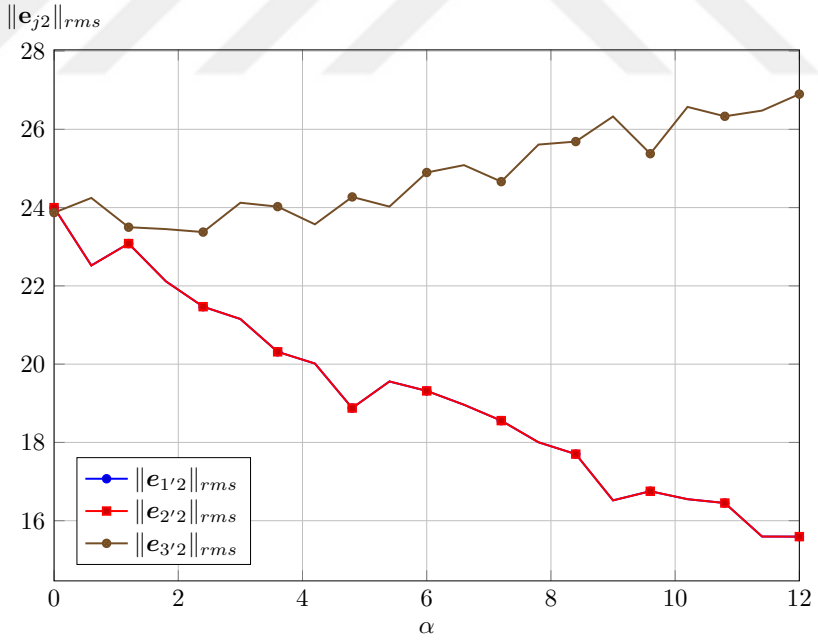

(b)

Figure 6.49 The change of spatiotemporal status of the network for changing control strength α.

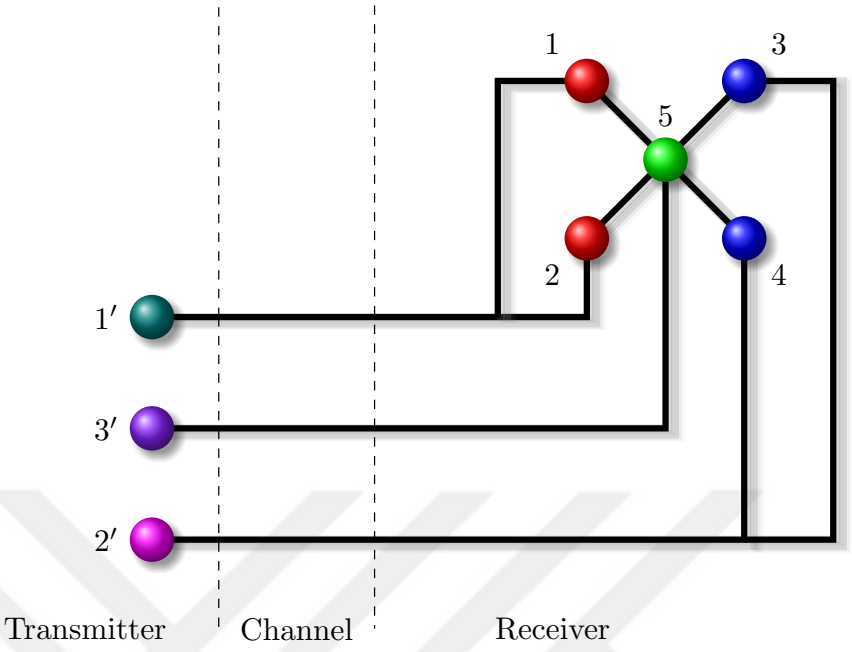

Figure 6.50 Symbol 0 transmission

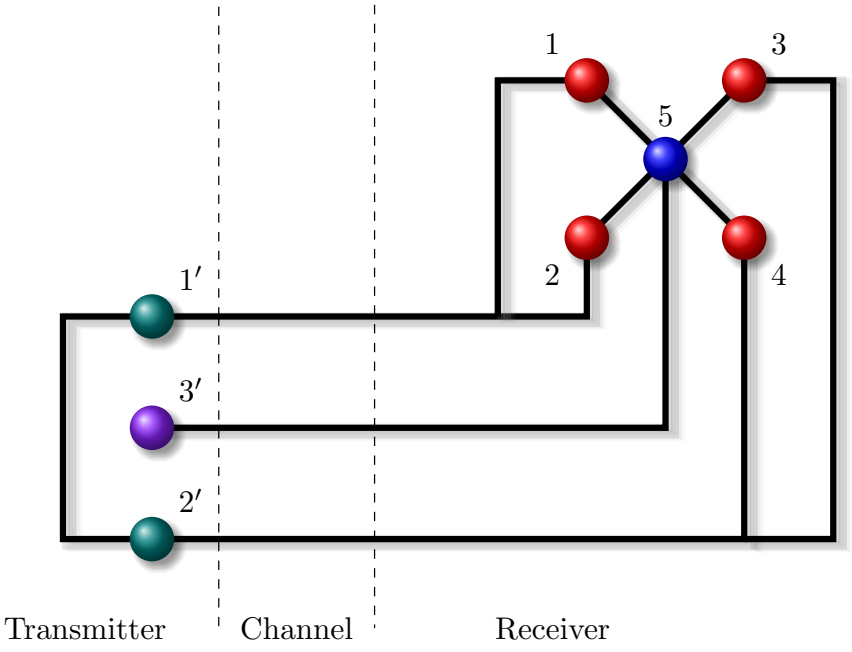

Figure 6.51 Symbol 1 transmission

CHAPTER SEVEN
CLUSTER SHIFT KEYING

In Chapters 3 and 4, we have studied the programmable network design techniques. Moreover, we designed networks capable of achieving different controllable clusters and meeting the requirements of the proposed communication system in the previous chapter. We also studied briefly some chaos communication methods in Chapter 5. We are ready to obtain the detection performance of the communication system and compare the method proposed in this thesis with the available chaos communication schemes. In this chapter, we will first quantify the channel noise and investigate the effect of unidirectional and bidirectional couplings in the links on the system modeling. Then, we will study the conceptual design and basics of the proposed communication system. We will obtain the detection performance of the proposed method and compare it with available counterparts.

7.1 Quantifying Noise

7.1.1 Quantifying Noise in terms of E_b/N_0

In contrast to analog communication systems, in which signal-to-noise ratio (SNR) is defined as the ratio of signal power to noise power in the receiver, E_b/N_0 defined as the ratio of the average symbol energy to noise power spectral density is used to compare the performance

There are some significant differences between CSK signaling and CLSK. The first one is that in CSK signaling, the information is directly buried into the channel signals, while in CLSK, the channel signals are not modulated by the information directly. Besides, the CSK uses master-slave type chaotic synchronization to generate the replicas of transmitted signals in the receiver. In master-slave type chaotic synchronization, the master chaotic system drives the slave system. The critical point of the master-slave chaotic synchronization is that the coupling is unidirectional, i.e., the dynamics of the master system are not affected by the dynamics of the slave system. This implies that the transmitted signals $x(t)$ and $y(t)$ (Figure 5.1) are

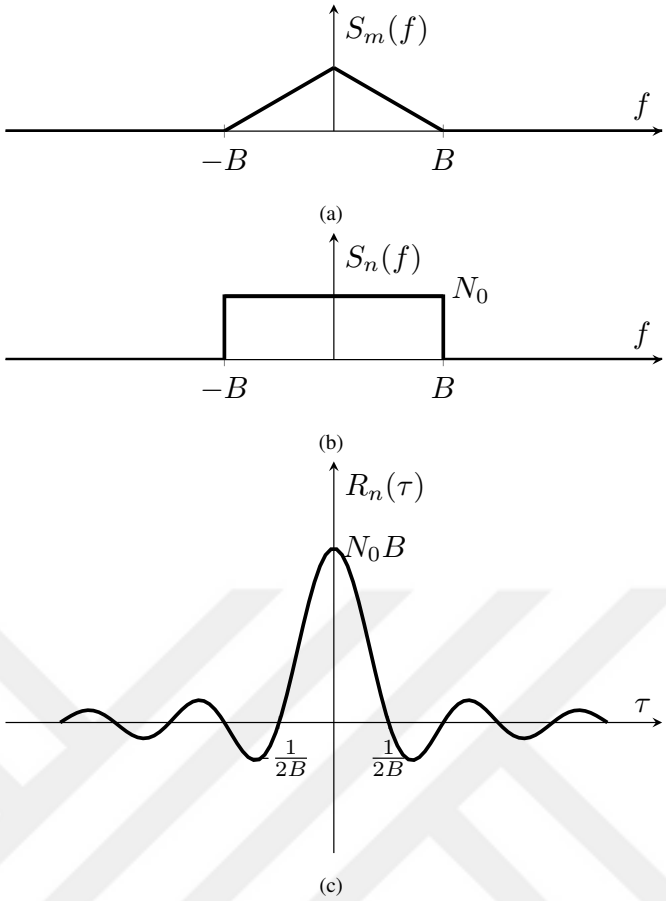

Figure 7.1 Signal spectrum (a) Frequency spectrum of the transmitted signal $s_m(t)$. (b) Power spectral density of noise $n(t)$. (c) Autocorrelation function of noise $n(t)$.

independent of the dynamics of the systems in the receiver. The corruption of the received signal in the channel affects the synchronization of the slave systems, thus causing bit errors. However, in the CLSK, the coupling may be bidirectional, i.e., the dynamics of the connected nodes affect their dynamics equally. This makes the signals flowing through the channel dependent on the dynamics of the nodes, not only in the transmitter but also in the receiver. Thus, the transmitted signals cannot be generated in isolation from the nodes in the receiver; the noise affects not only the dynamics of the nodes in the receiver but also those of the nodes in the transmitter. As the noise is injected into the dynamics of the network nodes, the noise is not additive in our case. Consequently, a challenge arises when attempting to measure the noise level in the channel necessary to obtain the noise performance of the communication system. We will try to define the noise differently than the one adopted commonly to quantify the noise level.

The additive nature of the channel noise provides the well-defined noise level in terms of E_b/N_0, defined as the average energy per bit to the power spectral density of the noise in the channel. Let us assume a baseband communication system in Figure 5.1 i.e.; there is no modulation to shift the frequency spectrum of the message signals to higher frequencies. Furthermore, let us assume that we have a baseband information signal $s_m(t)$ as shown in Figure 7.1a. We assume zero-mean Gaussian distributed noise $n(t)$ with a double-sided power spectral density of N_0 as shown in Figure 7.1b. The power spectral density of the noise is band-limited since it is the baseband equivalent (lowpass filtered having bandwidth B) of the white noise. We assume that the noise process is broad sense stationary, i.e. its autocorrelation function $R_n(t_1, t_2) = E[n(t_1)n(t_2)]$ is just a function of the time difference $\tau = t_2 - t_1$, i.e. $R_n(\tau) = E[n(t)n(t + \tau)]$. Since the autocorrelation function $R_n(\tau)$ is the inverse Fourier transform of the power spectral density function $S_n(f)$, we have

$$R_n(\tau) = N_0 B \,\mathrm{sinc}(2B\tau). \tag{7.1}$$

Thus, the variance of the noise $n(t)$ is

$$\sigma^2 = R_n(\tau = 0) = N_0 B. \tag{7.2}$$

Since computer simulations obtain the BER performance of the communication systems, discrete-time equivalents $s_m[k], n[k], r[k]$ of the continuous time signals $s_m(t), n(t)$ and $r(t)$ are used in the simulations. Thus, we must define the noise level E_b/N_0 for discrete-time signals. Let us assume that the continuous time signals are sampled with a sampling period of T_s and $t = kT_s, k = 0, 1, 2, \ldots$. Let $\tau = t_2 - t_1 = (k + m)T_s - kT_s = mT_s$. Then, the autocorrelation function of the discrete-time noise process $n[k]$ is

$$R_n[m] = R_n(mT_s) = N_0 B \,\mathrm{sinc}(2BmT_s). \tag{7.3}$$

If the sampling period T_s is chosen such that

$$T_s = \frac{l}{2B}, \quad l = 1, 2, \ldots \tag{7.4}$$

we have $R_n[m] = 0, m = 1, 2, \ldots$. This choice makes the discrete-time noise process uncorrelated with each other. We can choose

$$T_s = \frac{1}{2B}. \tag{7.5}$$

E_b/N_0 can be computed using the discrete time signals. Let $s_m[k], m = 0, 1$ is transmitted during the transmission of symbol m. Then, the energy of $s_m[k]$ is

$$E_m = \sum_{k=1}^{L} s_m[k]^2 T_s, \tag{7.6}$$

where L, the spreading factor, is the number of samples in $s_m[k]$. The problem here is that the waveforms of the transmitted signals $s_{m_1}[k] \neq s_{m_2}[k]$ even if $m_1 = m_2$ because the changes in the initial conditions may result in completely different waveforms. Thus, we compute the average energy per bit statistically. We can perform a complete simulation for M number of bits, then compute the waveform energies for each symbol and take the average of energies as the average energy per bit. That is

$$E_b = \frac{1}{M} \sum_{m=1}^{M} E_m = \frac{T_s}{M} \sum_{m=1}^{M} \sum_{k=1}^{L} s_m[k]^2. \tag{7.7}$$

From (7.5), we have

$$B = \frac{f_s}{2}, \tag{7.8}$$

where f_s is the sampling frequency. Using (7.7), (7.8) and (7.2), we have

$$\frac{E_b}{N_0} = \frac{\frac{T_s}{M}\sum_{m=1}^{M}\sum_{k=1}^{L} s_m[k]^2}{2T_s\sigma^2} = \frac{\frac{1}{M}\sum_{m=1}^{M}\sum_{k=1}^{L} s_m[k]^2}{2\sigma^2} = \frac{E_{b_0}}{2\sigma^2} \tag{7.9}$$

The noise level E_b/N_0 is generally given in units of decibel (dB) defined as

$$\left(\frac{E_b}{N_0}\right)_{dB} = 10\log_{10}\left(\frac{E_b}{N_0}\right) \tag{7.10}$$

Following are the steps to obtain the BER performance of a chaos-based communication system

1. For a given number of bits M, obtain the noise free transmitted signal $s_m[k]$.
2. Compute average energy per bits E_{b_0}.
3. For a given noise level E_b/N_0, compute the variance σ^2 of the discrete time noise process $n[k]$. Generate the discrete-time noise $n[k] = \sigma\eta[k]$ where $\eta[k]$ is the discrete time random process having Normal distribution with zero mean and unity variance.
4. Corrupt the noise-free transmitted signals $s_m[k]$ by adding the noise term $n[k]$ to compute $r[k] = s_m[k] + n[k]$.
5. Perform the detection using the received signals $r[k]$.
6. Compute the probability of making an incorrect decision as $P_b \approx L/M$ where L is the number of incorrectly-detected bits.
7. Repeat the steps for different noise levels E_b/N_0.

7.1.2 SNR

The signal-to-noise ratio (SNR), defined as the ratio of the signal power S to the noise power N, is another way of quantifying noise level with respect to the signal level. Like E_b/N_0, SNR is generally given in units of decibels as

$$SNR_{dB} = 10 \log_{10} \frac{S}{N} \tag{7.11}$$

SNR is primarily preferred in analog communication systems, while E_b/N_0 is the commonly used term in digital communication systems. However, there is a strong relation between these terms. Let $R_b = 1/T_b$ be the symbol rate, where T_b is the symbol duration. $S = E_b/R_b$ is the average power per bit. Let $N_0/2$ be the two-sided power spectral density of the noise over the frequency range $[-B, B]$. Then the total noise power $N = (N_0/2)2B = N_0B$. Thus, we have

$$SNR = \frac{S}{N} = \frac{E_bR_b}{N_0B} = \frac{E_b}{N_0}\gamma. \tag{7.12}$$

Here, the term γ is called the spectral efficiency, which refers to the information transmission rate over a given bandwidth. Hence, E_b/N_0 is the normalized SNR, i.e., SNR normalized by the spectral efficiency. E_b/N_0 is also called SNR per bit. In the dB scale, we have

$$SNR_{dB} = \left(\frac{E_b}{N_0}\right)_{dB} + 10 \log_{10} \frac{R_b}{B} \tag{7.13}$$

7.2 The Type of Coupling

The signal flow in the channel may be unidirectional and bi-directional in the proposed method. In other words, the channel may be half-duplex or full-duplex. We have designed networks in the previous chapter with help-duplex or full-duplex

channels.

For E_n/N_0 and SNR to be used as a measure for noise compared to the signal energy or power, the noise signal and transmitted signal must be well-separated. That is, the transmitted signal must not depend on the channel noise or dynamics of the systems in the receiver. We call such communication system channels additive since noise is directly added to the transmitted signal. In the upcoming two subsections, it will be shown that in the case of chaotic communications, the noise is additive if the coupling between the systems in the transmitter and the receiver is unidirectional. In the case of bidirectional coupling, however, the definition of E_n/N_0 becomes ambiguous.

7.2.1 Unidirectional Coupling

Electronic implementation of CSK signaling is shown in Figure 7.2 (Kennedy & Hasler, 1993). We have binary signaling in which the symbols are $b_0 = 0$ and $b_1 = 1$. A single Chua circuit is used in the transmitter. For 0 and 1 transmission, the switch S is closed and opened for symbol duration of T_b, respectively. The voltage of the capacitor C_1 is transmitted to drive the circuits in the receiver. The receiver circuits are implemented in two stages. The first stage generates the replica of the voltage υ_{C21}. In the second stage, each circuit generates the replica of the υ_{C_1} corresponding to 0 or 1 transmission.

The dynamics of the transmitter circuit during 1 transmission is given as

$$\begin{aligned} C_1\frac{d\upsilon_{C_1}(t)}{dt} &= \frac{1}{R}\left(\upsilon_{C_2}(t)-\upsilon_{C_1}(t)\right)-h(\upsilon_{C_1}(t)) \\ C_2\frac{d\upsilon_{C_2}(t)}{dt} &= -\frac{1}{R}\left(\upsilon_{C_2}(t)-\upsilon_{C_1}(t)\right)+i_{L_1}(t) \\ L_1\frac{di_{L_1}(t)}{dt} &= -\upsilon_{C_2}(t) \end{aligned} \tag{7.14}$$

where

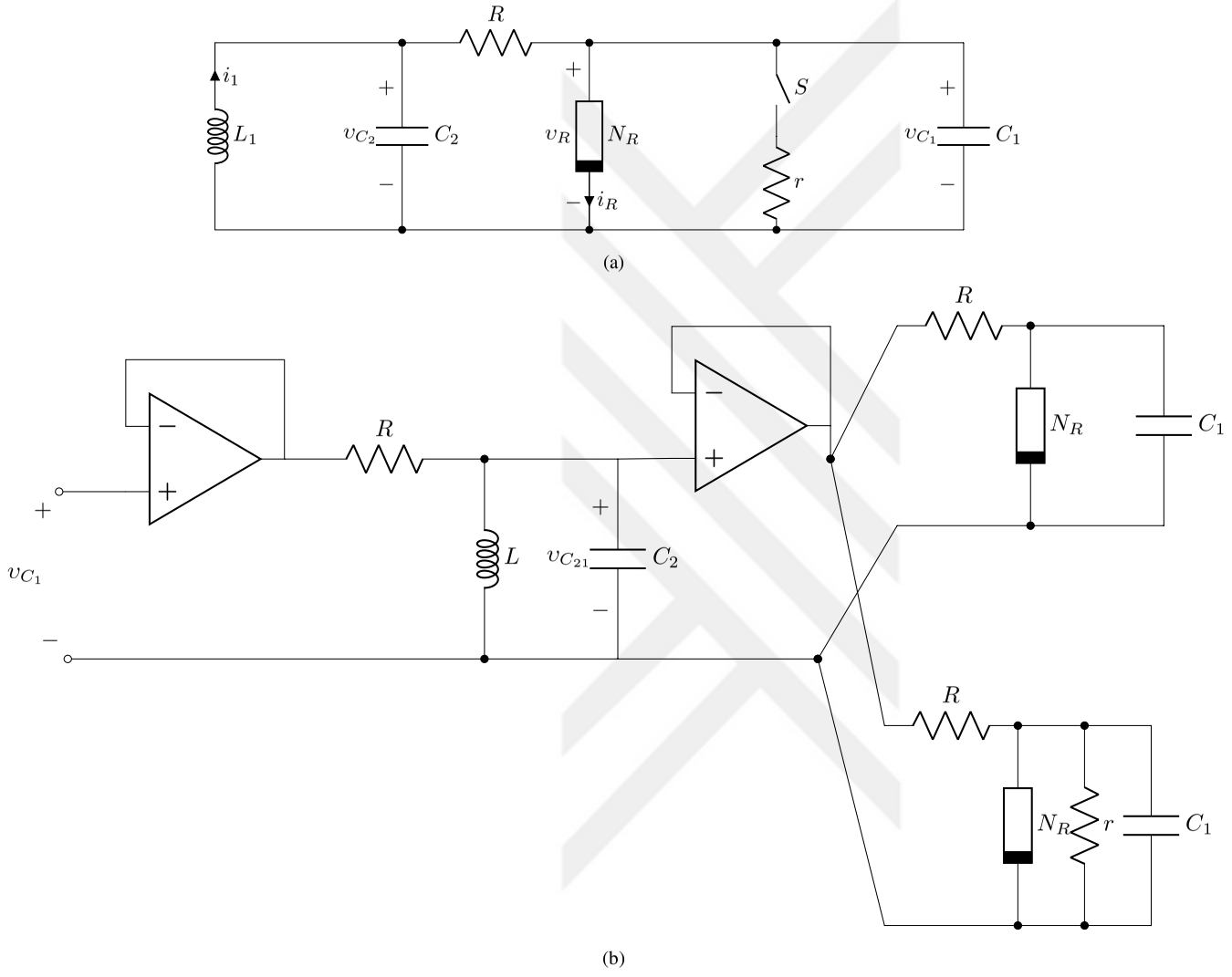

Figure 7.2 Transmitter and receiver circuit in CSK. (a) Transmitter circuit (b) Receiver circuit

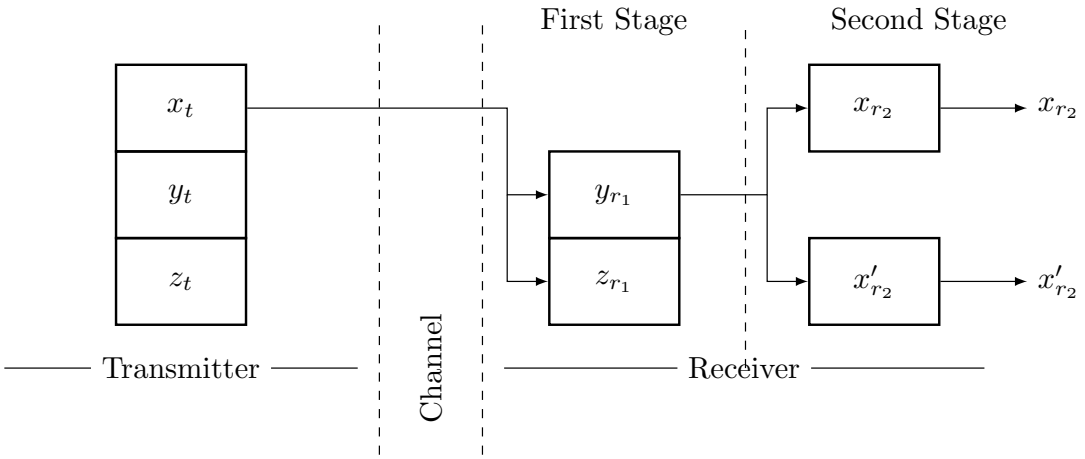

Figure 7.3 Master-slave type synchronization applied in CSK.

$$h(v_{C_1}) = \begin{cases} m_0 v_{C_1} + m_1 - m_0, & 1 < v_{C_1}, \\ m_1 v_{C_1}, & -1 \le v_{C_1} \le 1, \\ m_0 v_{C_1} + m_0 - m_1, & v_{C_1} < -1. \end{cases} \tag{7.15}$$

is the nonlinear resistor. During 0 transmission, we have the same dynamics in (7.14) where the nonlinear resistor h' takes the form

$$h'(v_{C_1}) = \begin{cases} (m_0 + 1/r) v_{C_1} + m_1 - m_0, & 1 < v_{C_1}, \\ (m_1 + 1/r) v_{C_1}, & -1 \le v_{C_1} \le 1, \\ (m_0 + 1/r) v_{C_1} + m_0 - m_1, & v_{C_1} < -1. \end{cases} \tag{7.16}$$

For the parameter values

$$1/C_1 = 9, \quad 1/C_2 = 1, \quad 1/L = 7, \quad 1/R = 0.7, \quad m_0 = -0.5, \quad m_1 = -0.8, \quad B_p = 1, \tag{7.17}$$

the system exhibits chaotic dynamics (Kennedy & Hasler, 1993).

The dynamics of the circuit in the first stage of the receiver is

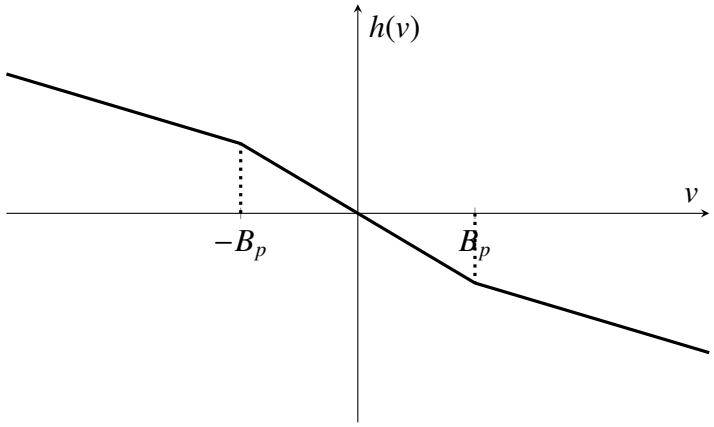

Figure 7.4 Piecewise linear resistor

$$\begin{aligned} C_2 \frac{d\upsilon_{C_{21}}(t)}{dt} &= -\frac{1}{R}\left(\upsilon_{C_1}(t) - \upsilon_{C_{21}}(t)\right) + i_{L_2}(t) \\ L_2 \frac{di_{L_2}(t)}{dt} &= -\upsilon_{C_{21}}(t), \end{aligned} \tag{7.18}$$

and the dynamics of the circuits in the second stage of the receiver circuit is

$$\begin{aligned} C_1 \frac{d\upsilon_{C_{12}}(t)}{dt} &= \frac{1}{R}\left(\upsilon_{C_{21}}(t) - \upsilon_{C_{12}}(t)\right) - h_+(\upsilon_{C_{12}}(t)) \\ C_1 \frac{d\upsilon'_{C_{12}}(t)}{dt} &= \frac{1}{R}\left(\upsilon_{C_{21}}(t) - \upsilon'_{C_{12}}(t)\right) - h_-(\upsilon'_{C_{12}}(t)). \end{aligned} \tag{7.19}$$

Receiver circuits do not load the dynamics of the transmitter circuit since the unidirectional coupling is implemented via voltage buffers. Similarly, circuits at the second stages of the receiver do not load the circuit at the first stage of the receiver. We get the signal flow diagram shown in Figure 7.3 by choosing the state variables as

$$x_t = \upsilon_{C_1} \quad y_t = \upsilon_{C_1} \quad z_t = i_{L_1} \quad y_{r_1} = \upsilon_{C_{21}} \quad z_{r_1} = i_{L_2} \quad x_{r_2} = \upsilon_{C_{12}} \quad x'_{r_2} = \upsilon'_{C_{12}}. \tag{7.20}$$

x_t is transmitted from the transmitter to drive the subsystems in the receiver, and the replicas x_{r_1} and x'_{r_2} corresponding to symbol 0 and 1, respectively, of x_t signal is generated in the receiver. The signal flow is always from the transmitter to the

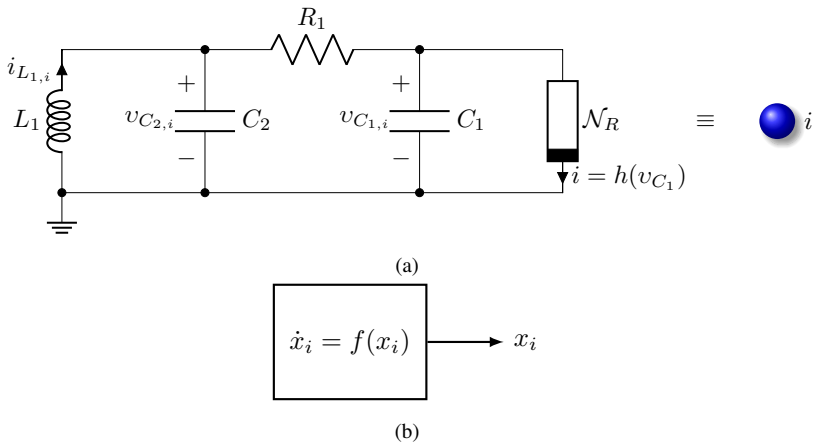

Figure 7.5 Circuit schematics of Chua system.

receiver. The channel noise is added to the transmitted signal v_{C_1} and degrades the synchronization performance, causing detection errors.

7.2.2 Bidirectional Coupling

Consider the network in the communication system illustrated in Figure 4.15. We split the nodes of the network between the transmitter and the receiver. The nodes $1, 4, 5, 8$ and $2, 3, 6, 7$ reside in the transmitter and the receiver side, and the link connecting the node pairs $(1, 2), (3, 4), (5, 6), (7, 8)$ connects the transmitter and the receiver side.

We assume the noise is only present on the channel following the general approach adopted in conventional communication systems. The noise corrupts the signals flowing through the links residing on the channel. We assume that independent and identically distributed Gaussian noise with zero mean and variance σ^2 corrupts each signal flowing through the channel's links. We need to identify the type of signal (electronically or physically) flowing through the nodes of the network.

The nodes in the network are linearly coupled continuous time dynamical systems having chaotic behavior. Without loss of generality, let us assume that the nodes in the network are Chua systems whose circuit schematics are given in Figure 7.5.

The dynamics of the Chua circuit given in Figure 7.5 is given in (7.14). With the

change of variables

$$\begin{aligned} x_i &= \upsilon_{C_{1,i}}/B_p \quad y_i = \upsilon_{C_{2,i}}/B_p \quad z_i = i_{L_{1,i}}/(B_p G) \\ \tau &= tG/C_2 \quad a = m_1/G \quad b = m_0/G \\ \alpha &= C_2/C_1 \quad \beta = C_2/(LG^2) \end{aligned} \tag{7.21}$$

where $G = 1/R_1$, the (7.14) can be transformed into

$$\begin{aligned} \dot{x}_i &= \alpha(y_i - x_i - \tilde{h}(x_i)) \\ \dot{y}_i &= x_i - y_i + z_i \\ \dot{z}_i &= -\beta y_i \end{aligned} \tag{7.22}$$

where

$$\tilde{h}(x) = \begin{cases} bx + a - b, & x \geq 1 \\ ax, & -1 \leq \nu \leq 1 \\ bx - a + b, & x \leq -1. \end{cases} \tag{7.23}$$

The individual nodes are autonomous systems, i.e., there is no input to the node as shown in Figure 7.5b.

The network given in Definition 2.1.3 is undirected; we have bidirectional coupling between the nodes, implying that the nodes interact equally. When the nodes i and j are coupled through their $\upsilon_{C_{k,1}}, k = i, j$, the dynamics of the coupled system evolves by

$$
\begin{aligned}
C_1\frac{d\upsilon_{C_{i,1}}(t)}{dt} &= \frac{1}{R_1}\Big(\upsilon_{C_{i,2}}(t)-\upsilon_{C_{i,1}}(t)\Big) - h(\upsilon_{C_{i,1}}(t)) + \frac{1}{R_c}(\upsilon_{C_{j,1}}(t)-\upsilon_{C_{i,1}}(t))\\
C_2\frac{d\upsilon_{C_{i,2}}(t)}{dt} &= -\frac{1}{R_1}\Big(\upsilon_{C_{i,2}}(t)-\upsilon_{C_{i,1}}(t)\Big) + i_{L_{i,1}}(t)\\
L_1\frac{di_{L_{i,1}}(t)}{dt} &= -\upsilon_{C_{i,2}}(t)\\
C_1\frac{d\upsilon_{C_{j,1}}(t)}{dt} &= \frac{1}{R_1}\Big(\upsilon_{C_{j,2}}(t)-\upsilon_{C_{j,1}}(t)\Big) - h(\upsilon_{C_{j,1}}(t)) + \frac{1}{R_c}(\upsilon_{C_{i,1}}(t)-\upsilon_{C_{j,1}}(t))\\
C_2\frac{d\upsilon_{C_{j,2}}(t)}{dt} &= -\frac{1}{R_1}\Big(\upsilon_{C_{j,2}}(t)-\upsilon_{C_{j,1}}(t)\Big) + i_{L_{j,1}}(t)\\
L_1\frac{di_{L_{j,1}}(t)}{dt} &= -\upsilon_{C_2}(t)
\end{aligned}
\tag{7.24}
$$

Using the transformations in (7.21), (7.24) can be transformed into

$$
\begin{aligned}
\dot{x}_{i,1} &= \alpha(x_{i,2}-x_{i,1}-h(x_{i,1})) + \epsilon(x_{i,1}-x_{i,1})\\
\dot{x}_{i,2} &= x_{i,1}-x_{i,2}-x_{i,3}\\
\dot{x}_{i,2} &= -\beta x_{i,2}\\
\dot{x}_{j,1} &= \alpha(x_{j,2}-x_{j,1}-h(x_{j,1})) + \epsilon(x_{i,1}-x_{j,1})\\
\dot{x}_{j,2} &= x_{j,1}-x_{j,2}-x_{j,3}\\
\dot{x}_{j,3} &= -\beta x_{j,2}
\end{aligned}
\tag{7.25}
$$

where $\epsilon = 1/(R_cC_1)$ is the coupling strength between the nodes i and j. The state variables $x_{i,1}$ and $x_{j,1}$ are the voltages while the terms $\dot{x}_{i,1}$ and $\dot{x}_{j,1}$ are the currents of the capacitors $C_{i,1}$ and $C_{j,1}$, respectively. The coupling terms $\epsilon(x_{i,1}-x_{j,1})$ and $\epsilon(x_{j,1}-x_{i,1})$ are currents since are added up to the terms $\dot{x}_{i,1}$ and $\dot{x}_{j1}$. The coupling term affecting the node i is the opposite of that affecting the node j. Thus, the nodes i and j are coupled to each other via the current signals.

Figure 7.6 illustrates the coupling of the nodes. As illustrated in Figure 7.6a, the coupling current signals u_i and u_j can be obtained if we connect the two circuits via a simple resistor $R_c = 1/\epsilon$, where ϵ is the coupling strength. As illustrated in Figure 7.6b, the individual nodes become non-autonomous systems when coupled. The states of each node affect the input to the individual nodes. The coupling resistor R_c can be replaced by a current source $u_j = -u_i$ as shown in Figure 7.6c.

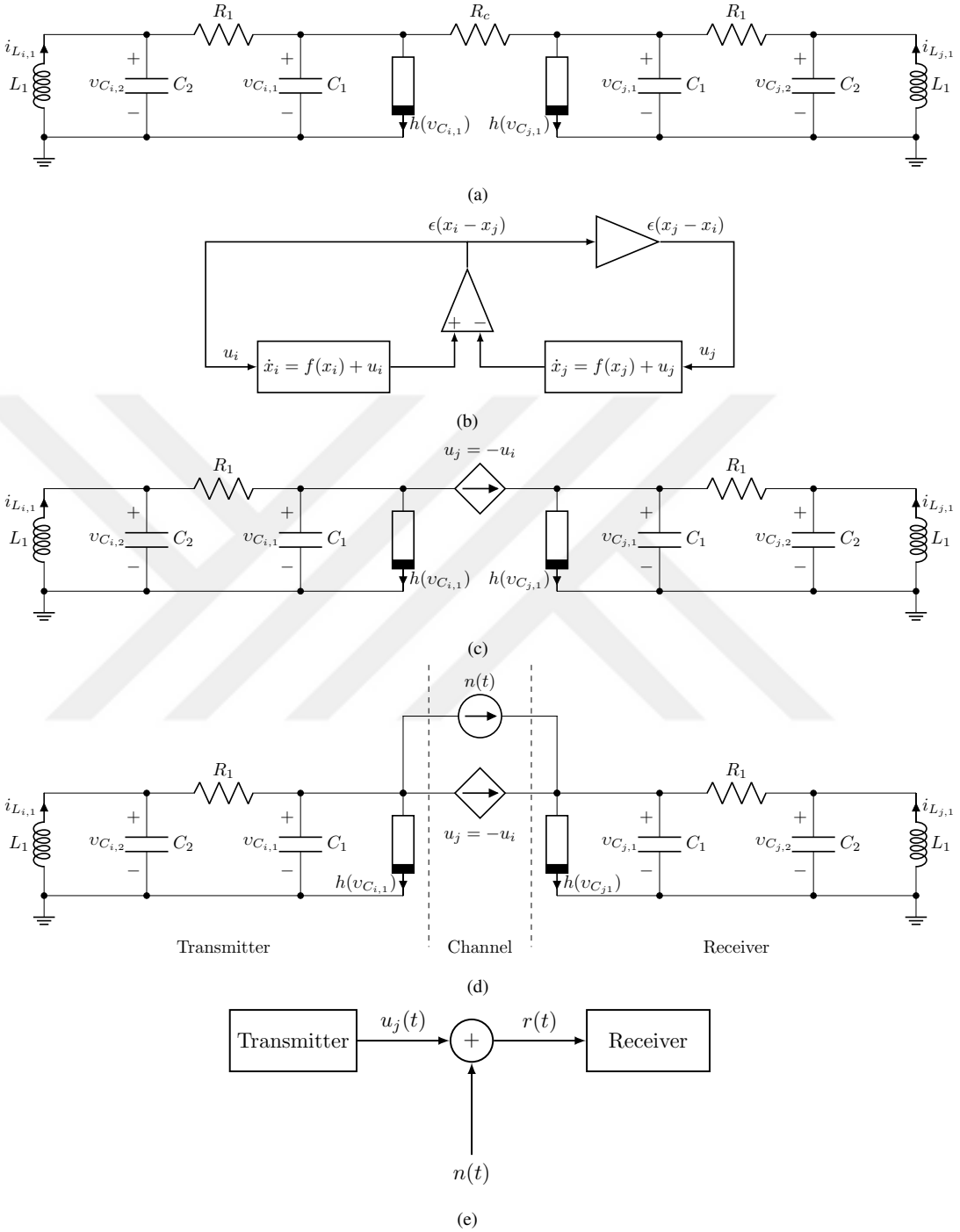

Figure 7.6 Coupling of Chua circuits in node *i* and *j*. (a) Coupling node *i* and *j* via resistor. (b) Block diagram of the coupled nodes *i* and *j*. (c) Coupling of node *i* and *j* by a dependent current source. (e) Simplified communication system signal flow.

Consider that we split the nodes i and j such that node i stays on the transmitter side and node j stays on the receiver side. As such, the current signal u_j connecting both nodes resides at the channel. Assume that zero-mean Gaussian distributed noise process $n(t)$ is present on the channel. Since the signal flowing through the channel is a current signal, and we assume additive noise at the channel, we model the noise as an independent current source $n(t) = \sigma\eta(t)$ where σ is the strength of the noise and $\eta(t)$ has a Normal distribution with zero mean and unity variance. Then, we can have the signal flow shown in Figure 7.6e between the transmitter, channel, and receiver.

In conventional communication systems, the signals received by the receiver are assumed to be formed as $r(t) = u_j(t) + n(t)$. The noise power can well be separated from the signal power, which makes us able to compare the signal power to the noise power using quantities such as the signal-to-noise (SNR) ratio of average energy per bit to noise power spectral density (E_b/N_0) ratio.

On the contrary, however, if the coupling is bi-directional in the proposed communication system, the transmitted signal flowing from the transmitter to the receiver affects the receiver system and the transmitter system. Let us consider the node i in particular. If noise is not present on the channel, its dynamics are given by

$$\begin{aligned}
\dot{x}_{i,1} &= \alpha(x_{i,2} - x_{i,1} - h(x_{i,1})) + \epsilon(x_{i,1} - x_{i,1}) \\
\dot{x}_{i,2} &= x_{i,1} - x_{i,2} - x_{i,3} \\
\dot{x}_{i,2} &= -\beta x_{i,2}
\end{aligned} \tag{7.26}$$

If noise is present, from Kirchhoff's current law, the noise term is added on the right-hand side of the equation, which makes the equation

$$\begin{aligned}
\dot{x}_{i,1} &= \alpha(x_{i,2} - x_{i,1} - h(x_{i,1})) + \epsilon(x_{i,1} - x_{i,1}) + \sigma\eta(t) \\
\dot{x}_{i,2} &= x_{i,1} - x_{i,2} - x_{i,3}i, 3 \\
\dot{x}_{i,2} &= -\beta x_{i,2}.
\end{aligned} \tag{7.27}$$

For node j we have,

$$\begin{aligned}
\dot{x}_{j,1} &= \alpha(x_{j,2} - x_{j,1} - h(x_{j,1})) + \epsilon(x_{i,1} - x_{j,1}) - \sigma\eta(t) \\
\dot{x}_{j,2} &= x_{j,1} - x_{j,2} - x_{j3} \\
\dot{x}_{j3} &= -\beta x_{j,2}.
\end{aligned} \tag{7.28}$$

However, the presence of the noise term $\eta(t)$ on the right-hand side transforms ordinary differential equations (7.27) and (7.28) to stochastic differential equations of the form

$$\begin{aligned}
dx_{i,1} &= (\alpha(x_{i,2} - x_{i,1} - h(x_{i,1})) + \epsilon(x_{j,1} - x_{i,1}))dt + \sigma dW(t) \\
dx_{i,2} &= (x_{i,1} - x_{i,2} - x_{i3})dt \\
dx_{i,2} &= (-\beta x_{i,2})dt,
\end{aligned} \tag{7.29}$$

and

$$\begin{aligned}
dx_{j,1} &= (\alpha(x_{j,2} - x_{j,1} - h(x_{j,1})) + \epsilon(x_{i,1} - x_{j,1}))dt - \sigma dW(t) \\
dx_{j,2} &= (x_{j,1} - x_{j,2} - x_{j,3})dt \\
dx_{j,3} &= (-\beta x_{j,2})dt,
\end{aligned} \tag{7.30}$$

respectively, where $W(t)$ is the Wiener process corresponding to the noise process $\eta(t)$. Since the noise process affects the transmitter system's dynamics, the noise is not additive in nature. Let $u_{j0}(t)$ and $u_j(t)$ denote the transmitted signal when the noise $n(t)$ is not present and present, respectively. Then, because of the stochastic dynamics, we have $u_j(t) \neq u_{j0}(t) + n(t)$, which implies that noise is not additive.

7.3 Noise Model

We need a programmable network in the proposed scheme. Consider a network as in Definition 2.1.2. $\mathcal{N}$ can be partitioned such that $\mathcal{N} = \mathcal{N}_T \cup \mathcal{N}_R$ where $\mathcal{N}_T = \{i_1, i_2, \ldots, i_{N_T}\}$ and $\mathcal{N}_R = \{j_1, j_2, \ldots, j_{N_R}\}$ are the sets of node indices in the transmitter and receiver, respectively. Let $\mathcal{L}_T = \{\ell_{ij} \mid i, j \in \mathcal{N}_T\} \cap \mathcal{L}$ and $\mathcal{L}_R = \{\ell_{ij} \mid i, j \in \mathcal{N}_R\} \cap \mathcal{L}$ be the sets of links in the transmitter and receiver, respectively. Then, the set of the links in the channel is $\mathcal{L}_C = \mathcal{L} \backslash (\mathcal{L}_T \cup \mathcal{L}_R)$.

Although not strictly necessary, the couplings between the nodes can be bidirectional in the proposed scheme. The bi-directionality of the couplings implies that the noise acting on the channel links affects both the transmitter and receiver symmetrically. For most of the cases, the noise is more pronounced on the links in $\mathcal{L}_C$, and it may be safe to assume the noise is not present on the links $\ell_{ij} \notin \mathcal{L}_C$. In the presence of Gaussian distributed noise affecting the links in the channel, the coupled network can be represented with a stochastic differential equation (SDE)

$$d\boldsymbol{x}_i = \left(f(\boldsymbol{x}_i) + \epsilon \sum_{j=1}^{N} \xi_{ij} \boldsymbol{P} \boldsymbol{x}_j + \alpha\epsilon \sum_{k=1}^{L} \delta_{ik} \boldsymbol{P} \tilde{\boldsymbol{x}}_k \right) dt + \alpha\epsilon\sigma \sum_{k=1}^{L} \delta_{ik} \boldsymbol{P} d\boldsymbol{W}_k, \tag{7.31}$$

where $\boldsymbol{W}_k$ is the Wiener process acting on the link $\ell_{ik} \in \mathcal{L}_C$. $\sigma > 0$ is the noise strength. Denoting $\boldsymbol{x} = [\boldsymbol{x}_1^T, \boldsymbol{x}_2^T, \ldots, \boldsymbol{x}_N^T]^T$, $\tilde{\boldsymbol{x}} = [\tilde{\boldsymbol{x}}_1^T, \tilde{\boldsymbol{x}}_2^T, \ldots, \tilde{\boldsymbol{x}}_L^T]^T$, $F(\boldsymbol{x}) = [f(\boldsymbol{x}_1)^T, f(\boldsymbol{x}_2)^T, \ldots, f(\boldsymbol{x}_N)^T]^T$, $F(\tilde{\boldsymbol{x}}) = [f(\tilde{\boldsymbol{x}}_1)^T, f(\tilde{\boldsymbol{x}}_2)^T, \ldots, f(\tilde{\boldsymbol{x}}_L)^T]^T$, $d\boldsymbol{W} = [d\boldsymbol{W}_1^T, d\boldsymbol{W}_2^T, \ldots, d\boldsymbol{W}_L^T]^T$, the network in 7.31 can be represented more compactly as

$$\begin{aligned} \begin{bmatrix} d\tilde{\boldsymbol{x}} \\ d\boldsymbol{x} \end{bmatrix} = & \left\{ \begin{bmatrix} F(\tilde{\boldsymbol{x}}) \\ F(\boldsymbol{x}) \end{bmatrix} + \left(\begin{bmatrix} \boldsymbol{A} & \boldsymbol{0} \\ \alpha\epsilon\boldsymbol{C} & \epsilon\boldsymbol{\Xi} \end{bmatrix} \otimes \boldsymbol{P} \right) \begin{bmatrix} \tilde{\boldsymbol{x}} \\ \boldsymbol{x} \end{bmatrix} \right\} dt \\ & + \left(\begin{bmatrix} \boldsymbol{0} \\ \sigma\alpha\epsilon\boldsymbol{C} \end{bmatrix} \otimes \boldsymbol{P} \right) d\boldsymbol{W} \end{aligned} \tag{7.32}$$

The noise in (7.32) is not additive as it is directly injected into the network dynamics. Unfortunately, the non-additive nature of the noise avoids direct comparison of noise performance to conventional communication schemes.

7.4 Detection Rule

Let $T_b \in \mathbb{R}^+$ be the symbol duration. We detect n-th symbol $s[n] \in \{s_1, s_2, \ldots, s_M\}$, during the time frame $nT_b \leq t \leq (n+1)T_b$, $n = 0, 1, \ldots$ by detecting the corresponding cluster pattern $\mathscr{C}[n] \in \mathscr{P}$ in the receiver. The energy of the synchronization error

between the nodes i and $j \in \mathcal{N}_R$ when transmitting $s[n]$ is

$$E_{ij}[n] = \int_{nT_b}^{(n+1)T_b} \|\boldsymbol{e}_{ij}(t)\|^2 dt \ . \tag{7.33}$$

We decide that the node pair (i, j) is synchronized if $E_{ij}[n] \leq \gamma_n$ given some threshold $\gamma_n > 0$. Specifically,

$$\gamma_n = \frac{1}{N_R^2} \sum_{i=1}^{N_R} \sum_{j=1}^{N_R} E_{ij}[n] \ . \tag{7.34}$$

We represent $\mathscr{C}[n]$ by a synchronization matrix $\boldsymbol{A}[n] = [\alpha_{ij}[n]] \in \mathbb{R}^{N_R \times N_R}$ where

$$\alpha_{ij}[n] = \begin{cases} 1, & E_{ij}[n] \leq \gamma_n, \\ 0, & E_{ij}[n] > \gamma_n, \end{cases} \quad \forall i, j \in \mathcal{N}_R. \tag{7.35}$$

Let $\boldsymbol{B}_m = [\beta_{m,ij}] \in \mathbb{R}^{N_R \times N_R}, m = 1, 2, \ldots, M$ be the reference matrices corresponding to the cluster patterns $\mathscr{C}_m$, where

$$\beta_{m,ij} = \begin{cases} 1, & i, j \in \mathcal{G}_{p,m} \\ 0, & i \in \mathcal{G}_{p,m}, \ j \in \mathcal{G}_{q,m}, p \neq q, \end{cases} \tag{7.36}$$

$p, q = 1, 2, \ldots, L_m$ and $i, j \in \mathcal{N}_R$. Then, we use the detection rule

$$\hat{s}[n] = \underset{m=1,2,\ldots,M}{\arg\max} [h(\boldsymbol{A}[n] \odot \boldsymbol{B}_m)] \tag{7.37}$$

where $\hat{s}[n]$ is the n-th detected symbol, $h(\boldsymbol{Z}) = \sum_{i=1}^{N} \sum_{j=1}^{N} \zeta_{ij}$ for $\boldsymbol{Z} = [\zeta_{ij}] \in \mathbb{R}^{N \times N}$, and $\odot$ denotes the Hadamard product of two matrices.

We are not concerned about the exact waveforms of the chaotic signals transmitted over $\mathcal{L}_C$ in detection. In other words, the received signals, which do not carry any

directly modulated information, are essentially not used in the detection process. The signals on $\mathcal{L}_C$ indirectly interact between the transmitter's control parameters and the receiver's subnetwork. The control parameters are adjusted for the symbol to be sent. The corresponding cluster pattern of the subnetwork in the receiver is checked through the signals over the links in $\mathcal{L}_R$, from which the transmitted information is extracted.

7.5 Illustrative Examples

7.5.1 Example I: Design without Control Network

7.5.1.1 The Network

Consider the networks in 7.7a and 7.7b consist of the classical Chen systems

$$\dot{\boldsymbol{x}}_i = f(\boldsymbol{x}_i) = \begin{bmatrix} a(x_{i,2} - x_{i,1}) \\ x_{i,1}(c - a - x_{i,3}) + cx_{i,2} \\ x_{i,1}x_{i,2} - bx_{i,3} \end{bmatrix}, \quad i = 1, 2 \ldots, 8. \tag{7.38}$$

where $\boldsymbol{x}_i = [x_{i,1}, x_{i,2}, x_{i,3}]^T, a = 35, b = 8/3, c = 28$, with inner coupling matrix

$$\boldsymbol{P} = \begin{bmatrix} 0 & 0 & 0 \\ 1 & 0 & 0 \\ 0 & 0 & 0 \end{bmatrix}. \tag{7.39}$$

The networks have the coupling matrices

$$\Xi_1 = \begin{bmatrix} -2 & 1 & 0 & 0 & 0 & 0 & 0 & 1 \\ 1 & -3 & 1 & 0 & 0 & 0 & 1 & 0 \\ 0 & 1 & -3 & 1 & 0 & 1 & 0 & 0 \\ 0 & 0 & 1 & -2 & 1 & 0 & 0 & 0 \\ 0 & 0 & 0 & 1 & -2 & 1 & 0 & 0 \\ 0 & 0 & 1 & 0 & 1 & -3 & 1 & 0 \\ 0 & 1 & 0 & 0 & 0 & 1 & -3 & 1 \\ 1 & 0 & 0 & 0 & 0 & 0 & 1 & -2 \end{bmatrix} \tag{7.40}$$

and

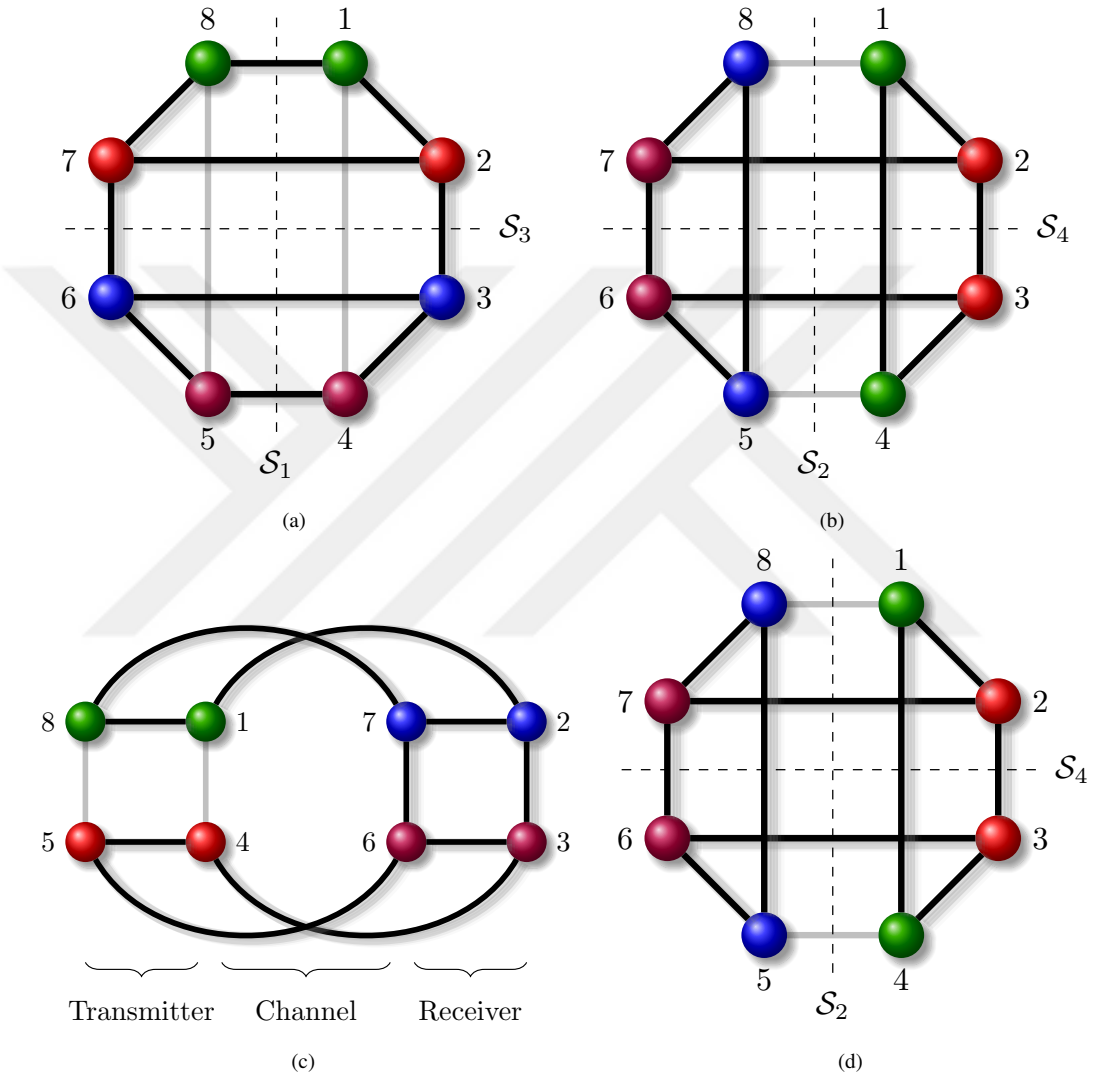

Figure 7.7 (a) and (b) are the cluster patterns in the illustrative network. (c) and (d) are the split of the nodes of the network in (a) and (b) between the transmitter and receiver, respectively.

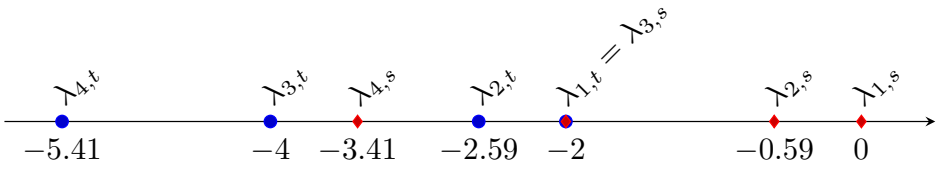

(a)

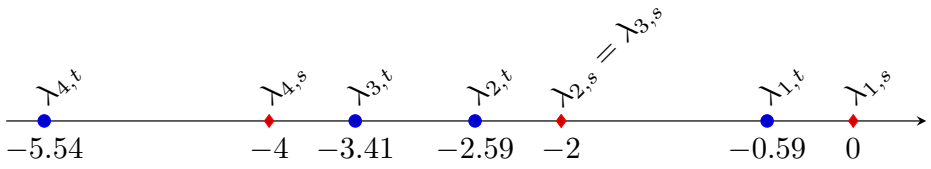

(b)

Figure 7.8 The distribution of eigenvalues with respect to (a) $\mathcal{S}_{11}$ and $\mathcal{S}_{22}$, and (b) $\mathcal{S}_{12}$ and $\mathcal{S}_{21}$.

$$\Xi_2 = \begin{bmatrix} -2 & 1 & 0 & 1 & 0 & 0 & 0 & 0 \\ 1 & -3 & 1 & 0 & 0 & 0 & 1 & 0 \\ 0 & 1 & -3 & 1 & 0 & 1 & 0 & 0 \\ 1 & 0 & 1 & -2 & 0 & 0 & 0 & 0 \\ 0 & 0 & 0 & 0 & -2 & 1 & 0 & 1 \\ 0 & 0 & 1 & 0 & 1 & -3 & 1 & 0 \\ 0 & 1 & 0 & 0 & 0 & 1 & -3 & 1 \\ 0 & 0 & 0 & 0 & 1 & 0 & 1 & -2 \end{bmatrix} \tag{7.41}$$

and the cluster patterns $\mathscr{C}_1 = \{\{1,8\},\{2,7\},\{3,6\},\{4,5\}\}$ and $\mathscr{C}_2 = \{\{1,4\},\{2,3\},\{5,8\},\{6,7\}\}$ corresponding to the symmetries $\mathcal{S}_1$ and $\mathcal{S}_2$, respectively. The permutation matrices corresponding to $\mathcal{S}_1$ and $\mathcal{S}_2$ are

$$\Delta_1 = \begin{bmatrix} 1 & 0 & 0 & 0 & 0 & 0 & 0 & 1 \\ 0 & 1 & 0 & 0 & 0 & 0 & 1 & 0 \\ 0 & 0 & 1 & 0 & 0 & 1 & 0 & 0 \\ 0 & 0 & 0 & 1 & 1 & 0 & 0 & 0 \\ 0 & 0 & 0 & 1 & 1 & 0 & 0 & 0 \\ 0 & 0 & 1 & 0 & 0 & 1 & 0 & 0 \\ 0 & 1 & 0 & 0 & 0 & 0 & 1 & 0 \\ 1 & 0 & 0 & 0 & 0 & 0 & 0 & 1 \end{bmatrix} \tag{7.42}$$

and

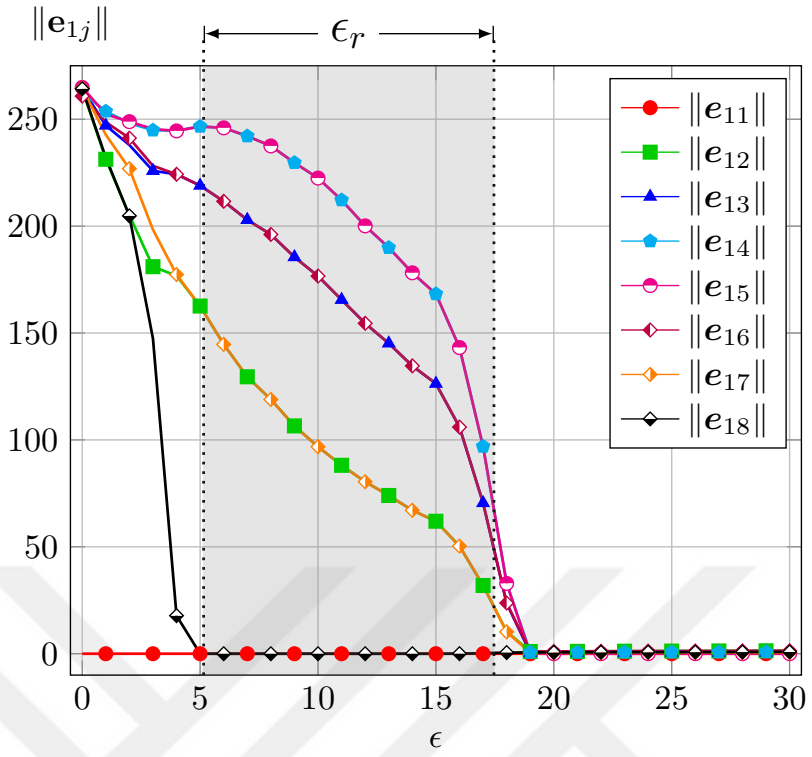

(a)

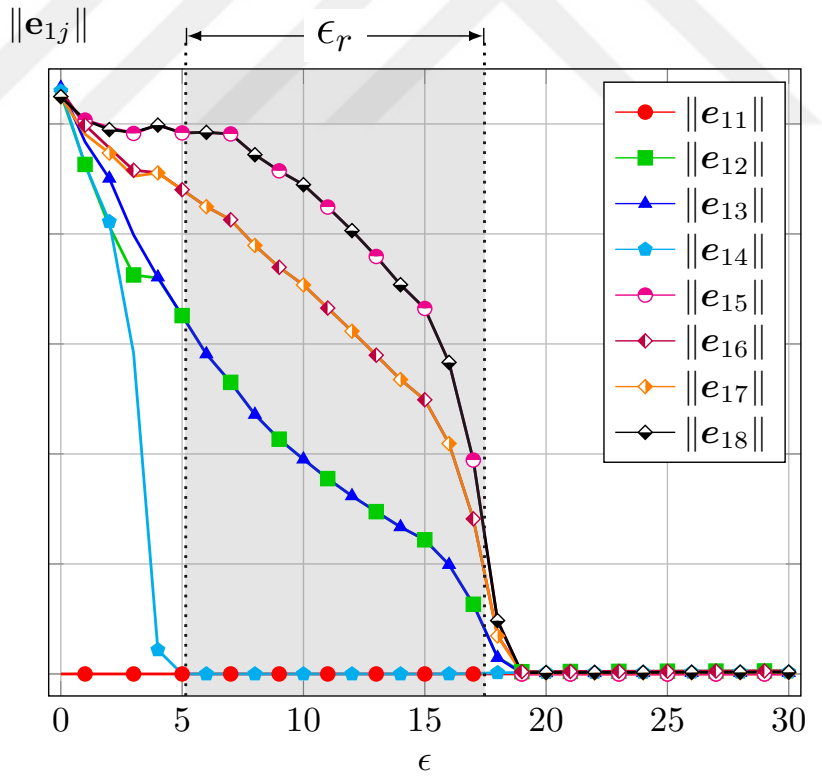

(b)

Figure 7.9 (a) The spatiotemporal status of the network when $s_k = s_1 = 0$ (7.7c) (b) and when $s_k = s_2 = 1$ (7.7d) with respect to coupling strength ϵ. The range $\epsilon_r = [5.15, 17.46]$ is the guaranteed cluster synchronization range.

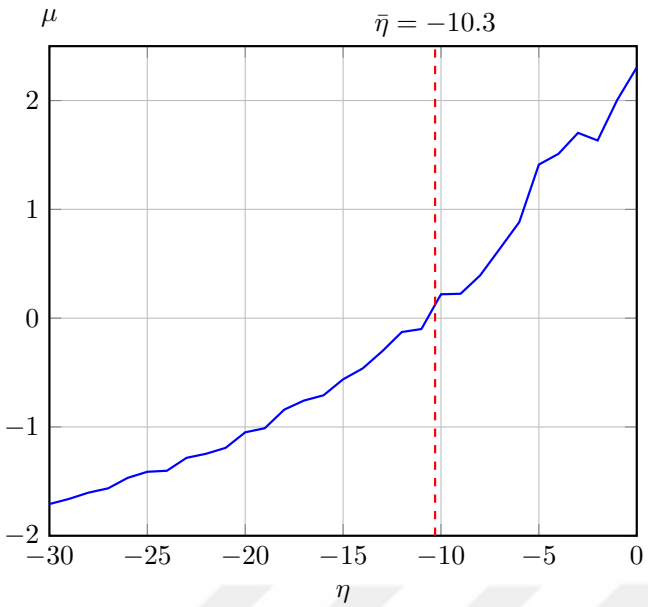

Figure 7.10 The master stability function calculated numerically for 7.38 using 2.43. The stability threshold $\bar{\eta} \approx -10.3$ for which $\mu = g(\eta) < 0, \eta \leq \bar{\eta}$ is indicated by dashed vertical line.

$$\mathbf{\Delta}_2 = \begin{bmatrix} 1 & 0 & 0 & 1 & 0 & 0 & 0 & 0 \\ 0 & 1 & 1 & 0 & 0 & 0 & 0 & 0 \\ 0 & 1 & 1 & 0 & 0 & 0 & 0 & 0 \\ 1 & 0 & 0 & 1 & 0 & 0 & 0 & 0 \\ 0 & 0 & 0 & 0 & 1 & 0 & 0 & 1 \\ 0 & 0 & 0 & 0 & 0 & 1 & 1 & 0 \\ 0 & 0 & 0 & 0 & 0 & 1 & 1 & 0 \\ 0 & 0 & 0 & 0 & 1 & 0 & 0 & 1 \end{bmatrix} \tag{7.43}$$

The distribution of the eigenvalues corresponding to $\mathcal{S}_1$ and $\mathcal{S}_2$ is shown in 7.8a. Since $|\lambda_2^s| < \lambda_{min}$, the eigenvalue condition is satisfied for both $\mathcal{S}_1$ and $\mathcal{S}_2$. 7.10 depicts the master stability function $g(\cdot)$ calculated for 7.38 using 2.43. We have $\bar{\eta} \approx -10.3$ for 7.38. Thus, $\epsilon_r = [5.15, 17.46]$ is the range for ϵ to realize both $\mathscr{C}_1$ and $\mathscr{C}_2$. 7.9 depicts the change of the spatio-temporal status of the networks in 7.7c and 7.7b. The nodes are de-synchronized for $\epsilon < \epsilon_l \approx 4.5$, while all the nodes are completely synchronized (full synchronization) for $\epsilon > \epsilon_h \approx 19$. We have the cluster patterns $\mathscr{C}_1$ and $\mathscr{C}_2$ in the networks 7.7c and 7.7d, respectively, for $\epsilon \in [\epsilon_l, \epsilon_h] \supset \epsilon_r$,

The network in 7.7b is obtained from the network in 7.7a by removing the links between the node pairs $(1, 8)$ and $(4, 5)$ and connecting the node pairs $(1, 4)$ and $(5, 8)$.

Hence, if we choose $\epsilon \in \epsilon_r$, it is possible to switch between $\mathscr{C}_1$ and $\mathscr{C}_2$ by controlling only the links $\ell_{14}, \ell_{45}, \ell_{58}, \ell_{18}$ without touching the remaining links.

The networks in 7.7a and 7.7b have also $\mathcal{S}_3$ and $\mathcal{S}_4$ symmetries, respectively. However, from the eigenvalue distribution illustrated in 7.8b, the eigenvalue condition in (4.1) is not satisfied. Thus, the cluster patterns corresponding to $\mathcal{S}_3$ and $\mathcal{S}_4$ cannot be observed in the networks in 7.7a and 7.7b.

7.5.1.2 Signalling

We divide the nodes of the networks in Figure 7.7a and Figure 7.7b between the transmitter and receiver as shown in Figure 7.7c and Figure 7.7d, respectively. As the cluster pattern capacity of the network in Figure 7.7 is $M = 2$, we can use the network in a binary communication system in which the symbols $s_1 = 0, s_2 = 1$ are encoded with $\mathscr{C}_1$ and $\mathscr{C}_2$, respectively.

We assume that the channel noise is present only on the links $\ell_{12}, \ell_{34}, \ell_{56}, \ell_{78} \in \mathcal{L}_C$. Figure 7.11 illustrates the signaling of the communication system 7.38 with $\epsilon = 7$ and $\sigma = 0.25$. The error waveforms in Figure 7.11 illustrate $\mathscr{C}_k$ during the transmission of s_k for $k = 1, 2$. By construction, the nodes of the links in the channel do not synchronize with each other regardless of the symbol being sent during the whole transmission.

If the signals flowing through the channel are eavesdropped, the transmitted information cannot be extracted without knowing the network topologies and symbol-to-cluster-pattern encoding. The spectrogram given in Figure 7.12 shows that the frequency content of the transmitted signals is independent of the symbols sent. The signals transmitted through the channel do not carry information about the transmitted information directly; instead, the information is distributed over the network. This very property of the proposed approach provides the covertness.

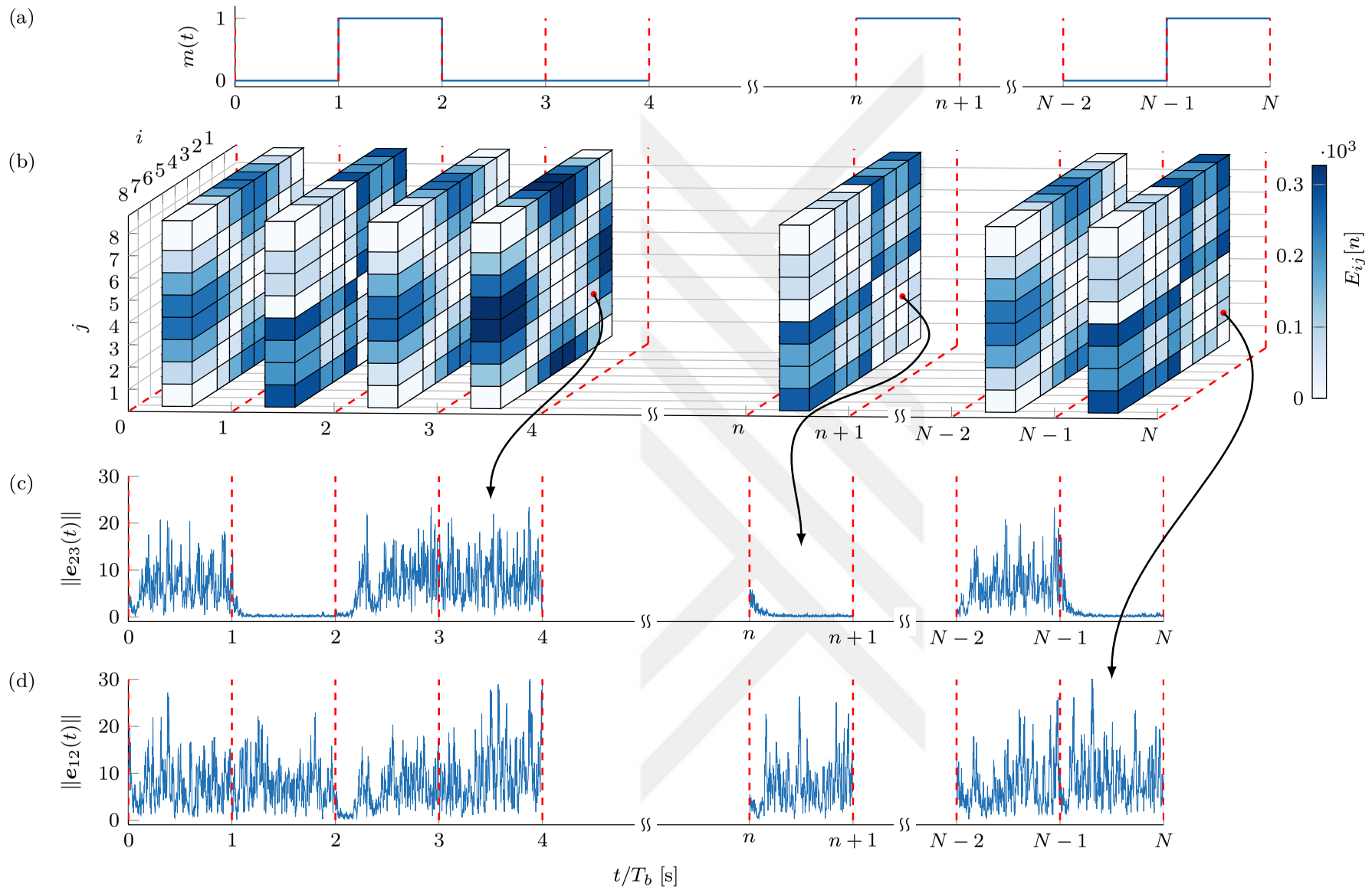

Figure 7.11 Transmission of symbols $s[n] \in \{0, 1\}, n = 0, 2, \ldots, N$. (a) Time waveform of message signal $m(t) = s[n], nT_b \leq t \leq (n + 1)T_b$, where T_b is the symbol duration. (b) The cluster patterns $\mathscr{C}[n]$. (c) Time waveform, $\|e_{23}(t)\|$, in the receiver. (d) Time waveform, $\|e_{12}(t)\|$, over a channel link.

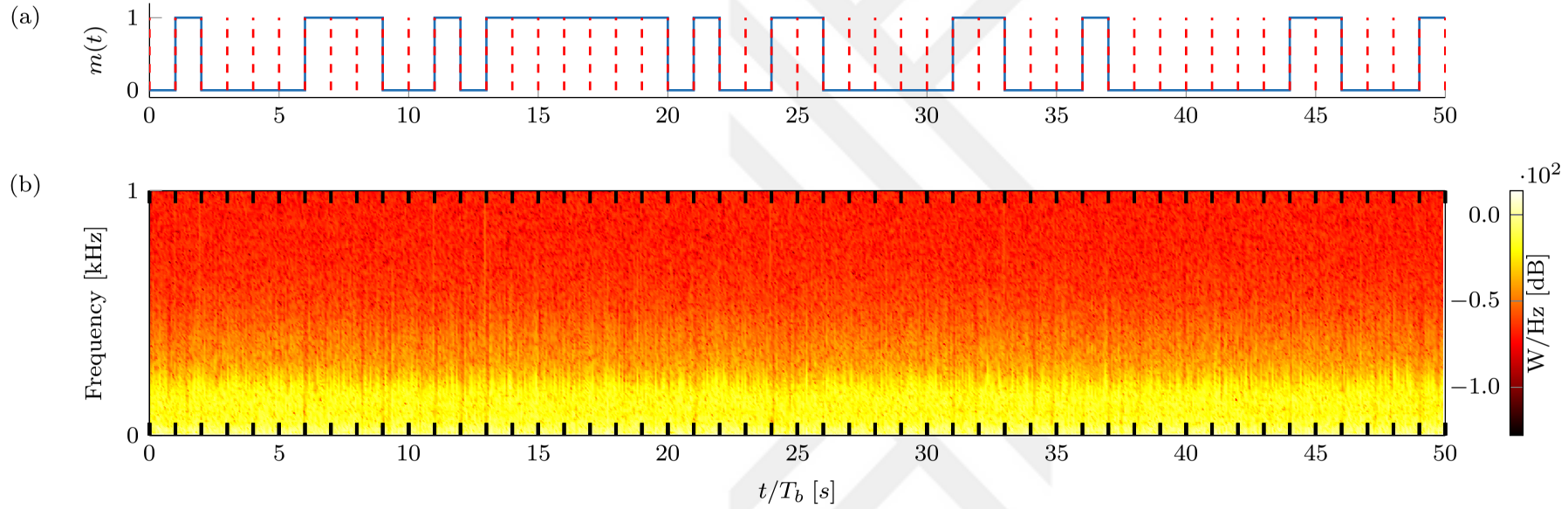

Figure 7.12 (a) The time waveform of message signal $m(t) = s[n]$, where T_b is the symbol duration (b) The spectrogram of $\|e_{12}\|$ during the transmission of symbols $s[n] \in \{0, 1\}$.

7.5.1.3 Detection Performance

The performance of the proposed scheme is degraded by synchronization errors as well as the noise acting on the channel. Occasionally, the error energy during the bit duration is not small/large enough, although the corresponding receiver nodes tend to synchronize/desynchronize in reality for a larger bit duration because of the asymptotic nature of the synchronization. Therefore, T_b must be chosen large enough to allow the network to settle on the synchronization manifolds for the respective symbols. The second source of detection errors is the diffusive term in 4.5. Obviously, the dominant dynamics cannot be considered chaotic anymore and the synchronization manifolds are destroyed completely when the noise amplitude is large enough.

We solved 7.32 using Order 1.5 strong Stochastic Runge-Kutta (SRK) method with weak order 2 to demonstrate the noise performance (Rößler, 2010). The simulation results have been obtained for 7.38 and a spreading factor (the number of samples in one symbol duration) of 200. The transmitted bits have been chosen randomly with equal probabilities. The number of bits transmitted has been adapted to the noise levels as in Table 7.1. We assumed reliable transmission is possible when the probability of making an incorrect decision at the receiver given the noise level σ and coupling strength $\epsilon \in \epsilon_r$ in 7.32, i.e., $P_e(\sigma; \epsilon)$, is smaller than 10^{-6}. 7.13 depicts the bit error rate (BER) performances of the system in the worst case. Clearly, the BER performance depends on the coupling strength ϵ.

$P_e(\sigma; \epsilon = 7) < P_e(\sigma; \epsilon = 15) < P_e(\sigma; \epsilon = 17)$ for $0 < \sigma < 7$. In comparison, the network undergoes complete desynchronization to cluster synchronization followed by full synchronization for increasing values of ϵ as suggested by Figure 7.9. The distribution of the synchronization error energies between the node pairs does not change uniformly with ϵ. The average synchronization error energies between the node pairs converge as ϵ approaches its lower and upper limits. The network is on the verge of complete desynchronization and complete synchronization for $\epsilon = 5$ and $\epsilon = 17$ respectively. The detection of the correct cluster pattern is more unlikely for both cases. We get lower detection error probabilities if the synchronization error

Table 7.1 Number of bits used for different noise levels in 7.13.

σ range	$[0, 4]$	$[5, 10]$	$[11, 15]$	$[16, 20]$
Number of bits	$2 \cdot 10^7$	$1 \cdot 10^6$	$5 \cdot 10^5$	$1 \cdot 10^5$

energies between the intra-cluster nodes are more dispersed for both symbols. In Figure 7.7, we can see that the difference between cluster to non-cluster error energies are maximum around $\varepsilon \approx 7$ for both symbols (Figure 7.9) at which BER performance is better (Figure 7.13).

Basically, we have two trends in the BER performance. The asymptotic nature of the stability of synchronization manifolds causes bit errors when switching from one manifold to the other. The bit errors occur when the time required for synchronization is longer than the selected bit duration. For the low noise levels ($\sigma < 2$), the errors due to manifold switching are dominant, and the network needs more time to form the required cluster synchronization patterns for obtaining lower error probabilities. As we increase the noise to moderate levels ($2 < \sigma < 5$), the presence of the noise helps the desynchronization of the nodes that are not synchronized in the newly switched pattern, yielding better BER performance compared to zero noise level. No bit errors observed for $\epsilon = 7$ and $\sigma = 3$ or $\sigma = 4$ in the numerical simulations. Hence, $P_e(\sigma; \epsilon = 7) \leq 5 \cdot 10^{-8}$ can be assumed safely in this range $\sigma \in (3, 4)$. For higher noise levels ($\sigma > 7$), the dynamics of the system dominated by the diffusion term in (7.32) cannot be considered chaotic anymore. The channel noise destroys the cluster patterns eventually, and becomes the primary cause of the detection errors.

7.5.2 Example II: Design with Control Network

7.5.2.1 The Network

Consider the network and desired cluster patterns $\mathscr{C}_1$ and $\mathscr{C}_2$ illustrated in Figure 7.14. The control node of each node has been written in the parentheses next to it. Figure 7.15a illustrates the change in the spatiotemporal status of the network without the control. The network directly transitions from complete de-synchronization to full synchronization without achieving any cluster synchronization pattern. Hence, to

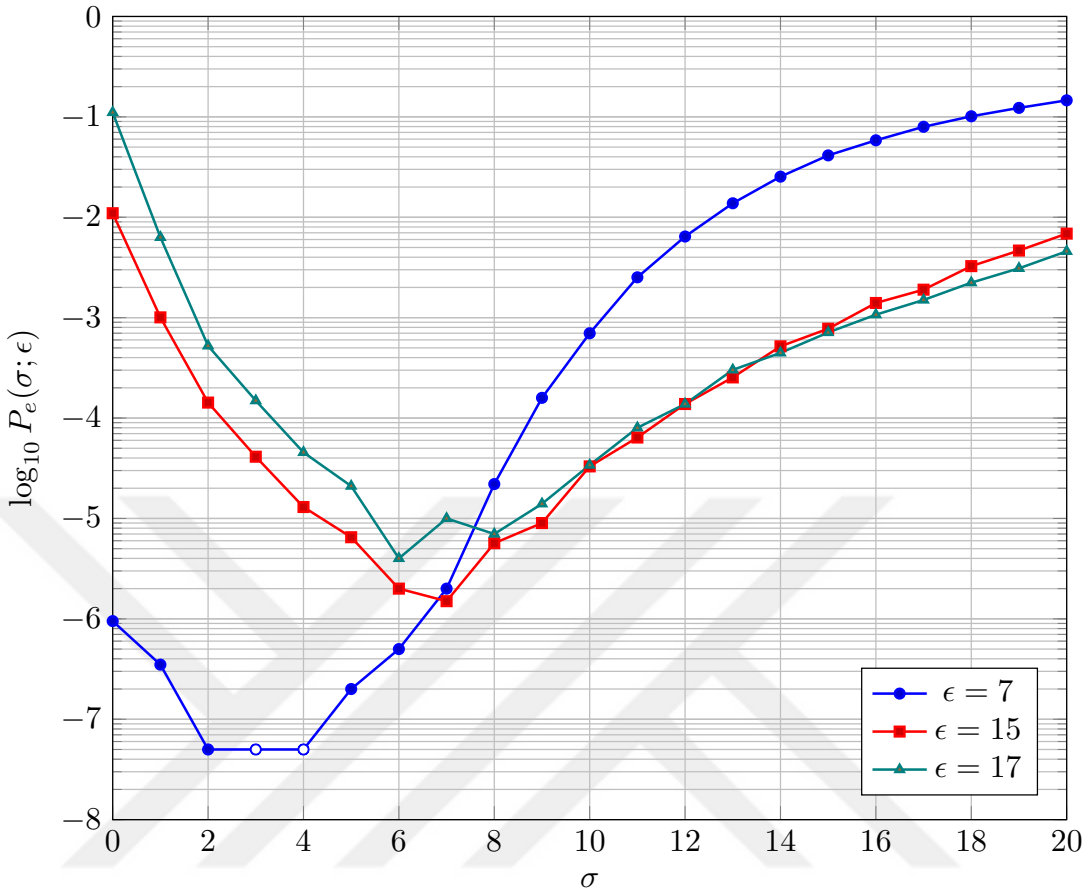

Figure 7.13 BER performance in terms of noise level σ and coupling strength ϵ in 7.32. The points marked with ○ presents the cases with no bit errors, for which the worst case is assumed in calculation of P_e.

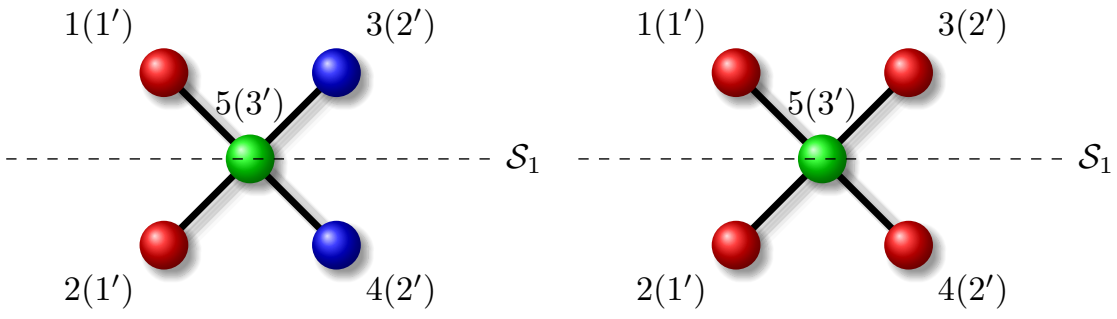

(a) (b)

Figure 7.14 The cluster patterns (a) $\mathscr{C}_1$ and (b) $\mathscr{C}_2$

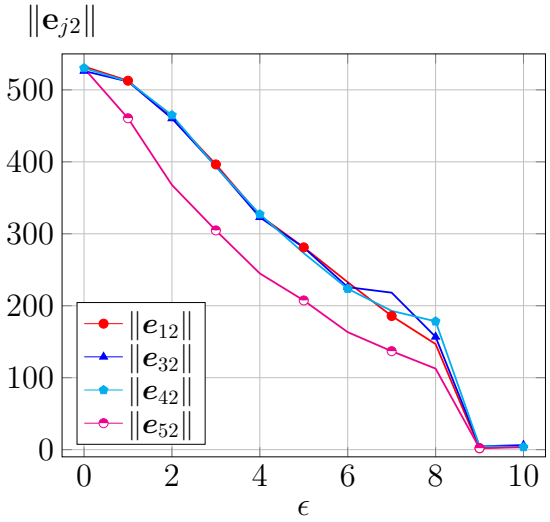

(a)

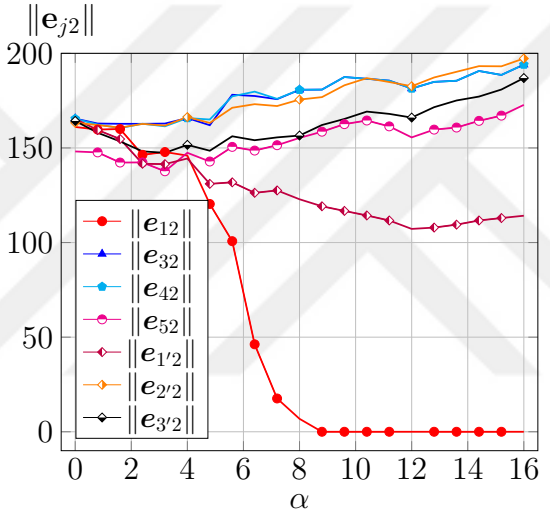

(b)

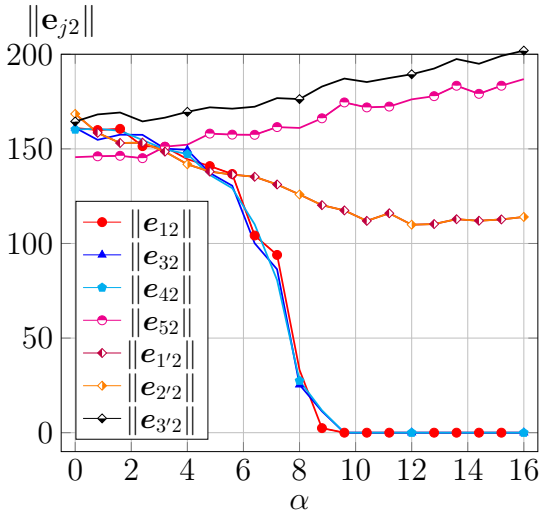

(c)

Figure 7.15 The change of spatiotemporal status of the network with respect to a coupling strength ϵ, and b and c control strength α corresponding to the cluster patterns in 7.14a and 7.14b, respectively.

achieve the cluster patterns $\mathscr{C}_1$ and $\mathscr{C}_2$ in Figure 7.14, we have to apply control to the network. We have the coupling and control matrix for the network in Figure 7.14a.

$$\Xi = \begin{bmatrix} -1 & 0 & 0 & 0 & 1 \\ 0 & -1 & 0 & 0 & 1 \\ 0 & 0 & -1 & 0 & 1 \\ 0 & 0 & 0 & -1 & 1 \\ 1 & 1 & 1 & 1 & -4 \end{bmatrix}, \quad \boldsymbol{A} = \begin{bmatrix} -1 & 0 & 1 \\ 0 & -1 & 1 \\ 2 & 2 & -4 \end{bmatrix}, \tag{7.44}$$

respectively, and the interconnection matrix

$$\boldsymbol{C} = \begin{bmatrix} 1 & 0 & 0 \\ 1 & 0 & 0 \\ 0 & 1 & 0 \\ 0 & 1 & 0 \\ 0 & 0 & 1 \end{bmatrix} \tag{7.45}$$

that connects the control and controlled network. The change of spatiotemporal status of the network with respect to the change of the control strength α is shown in Figure 7.15b. It is seen that the cluster pattern shown in Figure 7.14a is achieved for $\alpha > 8$, and the control nodes $1'$, $2'$ and $3'$ do not synchronize with any of the nodes in their corresponding clusters.

The results in Figure 7.15b show that the cluster pattern in Figure 7.14b cannot be achieved without applying a control network. For the cluster pattern $\mathscr{C}_2$ in Figure 7.15c, we want the nodes $1, 2, 3, 4$ to be synchronized. Since the control nodes $1'$ and $2'$ control the node pairs $(1, 2)$ and $(3, 4)$, respectively, if the control nodes $1'$ and $2'$ synchronize to each other, then we can achieve the cluster pattern shown in 7.14b. The nodes $1'$ and $2'$ synchronize for the control matrix

$$\boldsymbol{A} = \begin{bmatrix} -20 & 20 & 0 \\ 20 & -20 & 0 \\ 0 & 0 & 0 \end{bmatrix}. \tag{7.46}$$

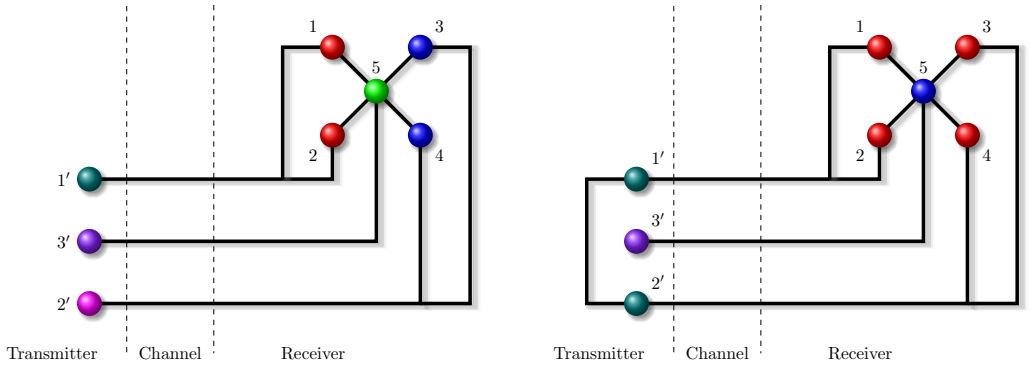

(a) (b)

Figure 7.16 (a) and (b) The split of nodes of the network in Figure 7.14a and Figure 7.14b, respectively.

The change of the spatiotemporal status of the network with respect to the changing values of the control strength α is given in Figure 7.15c. Note from Figure 7.15c that the cluster pattern shown in Figure 7.14b is achieved for $\alpha > 10$. As we have achieved two different cluster patterns, we can encode the symbols 0 and 1 of the communication system by these cluster patterns.

We can split the nodes as shown in Figure 7.16a and Figure 7.16b, and encode the symbols 0 and 1 to the cluster patterns in Figure 7.16a and Figure 7.16b, respectively. The node $1'$ is coupled to node $2'$ during symbol 0 transmission, and we decouple $1'$ and $2'$ during symbol 1 transmission. The nodes are split such that the control nodes stay on the transmitter side while the nodes of the original network stay on the receiver side. In this way, we can control the cluster pattern of the whole network from the transmitter. The control nodes do not synchronize to the receiver's nodes during the transmission. Since the coupling between the control and controlled nodes is unidirectional, and the nodes are always in their chaotic regimes, the signals transmitted through the channel are always chaotic.

7.5.2.2 Signalling

Figure 7.17 illustrates the successful transmission and detection of a symbol stream. The formation of the cluster pattern in Figure 7.14a during the symbol 0 transmission. Also, there is no synchronization between the controlling and

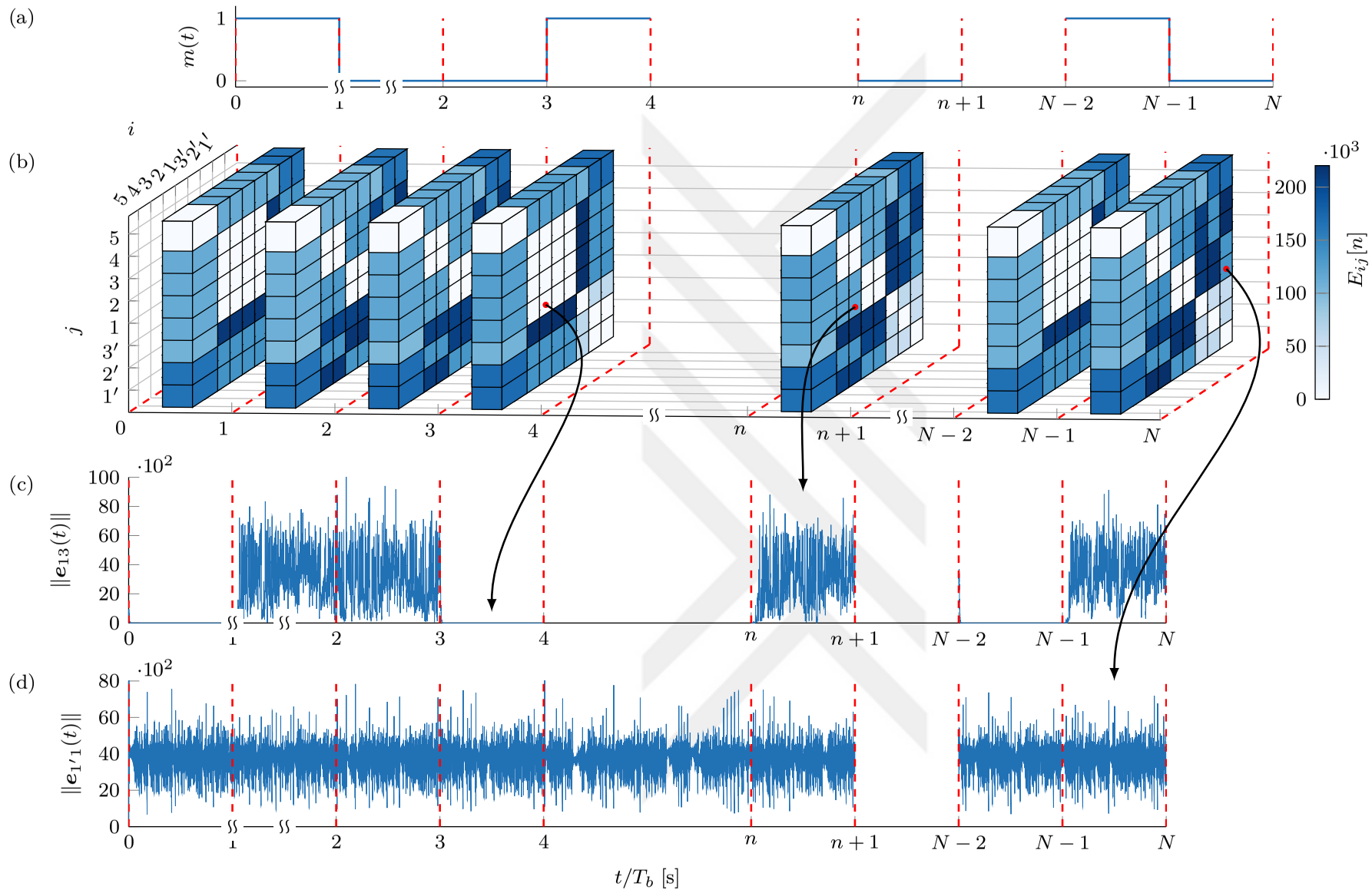

Figure 7.17 Transmission of symbols $s[n] \in \{0, 1\}, n = 0, 2, \ldots, N$. (a) Time waveform of message signal $m(t) = s[n], nT_b \leq t \leq (n + 1)T_b$, where T_b is the symbol duration. (b) The cluster patterns $\mathscr{C}[n]$. (c) Time waveform, $\|\boldsymbol{e}_{23}(t)\|$, in the receiver. (d) Time waveform, $\|\boldsymbol{e}_{12}(t)\|$, over a channel link.

Table 7.2 Number of bits used for different values of σ, α and s_f in Figure 7.18.

α	s_f	σ range	Number of bits
20	500	[0, 0.15]	$1 \cdot 10^7$
		[0.2, 0.65]	$5 \cdot 10^6$
		[0.7, 1.0]	$1 \cdot 10^5$
20	1000	[0, 0.15]	$1 \cdot 10^7$
		[0.2, 0.65]	$7 \cdot 10^6$
		[0.7, 1.0]	$1 \cdot 10^6$
10	1000	[0, 0.6]	$1 \cdot 10^7$
		[0.65, 1]	$1 \cdot 10^6$
		[1, 1.5]	$1 \cdot 10^5$

controlled nodes. Once the nodes $1'$ and $2'$ are synchronized, the nodes $1, 2, 3, 4$ are all synchronized as expected. The transmission of information from the transmitter to the receiver is apparent from the waveforms.

7.5.2.3 Detection Performance

The noise performance of the network in Figure 7.16 is given in Figure 7.18 in terms of σ in (7.32) versus the probability of making a detection error P_e. Table 7.2 shows the adaptation of the number of bits used in the simulation in Figure 7.18 for different values of α, σ, and s_f defined as the number of samples in the transmitted signals within a symbol duration. We have two different trends in noise performance. The ambient noise is the primary source of symbol detection error for a fixed network where the coupling and control strengths are kept constant. Once the noise strength decreases and passes through a threshold dependent on the network parameters, the simulation errors are the leading cause of the symbol detection errors.

The cluster synchronization defined in (2.4) assumes asymptotic synchronization, where the synchronization errors between the nodes in the same clusters decay to zero as the time approaches infinity. However, practically, we have to specify a specific finite symbol duration. During the symbol transmission, the nodes in the same cluster may need more time to be decided as synchronized. The detection decision given in the specified symbol duration results in detection errors. This simulation error can be overcome using finite-time synchronization techniques in which the nodes are guaranteed to be synchronized within a specified time. This observation is justified

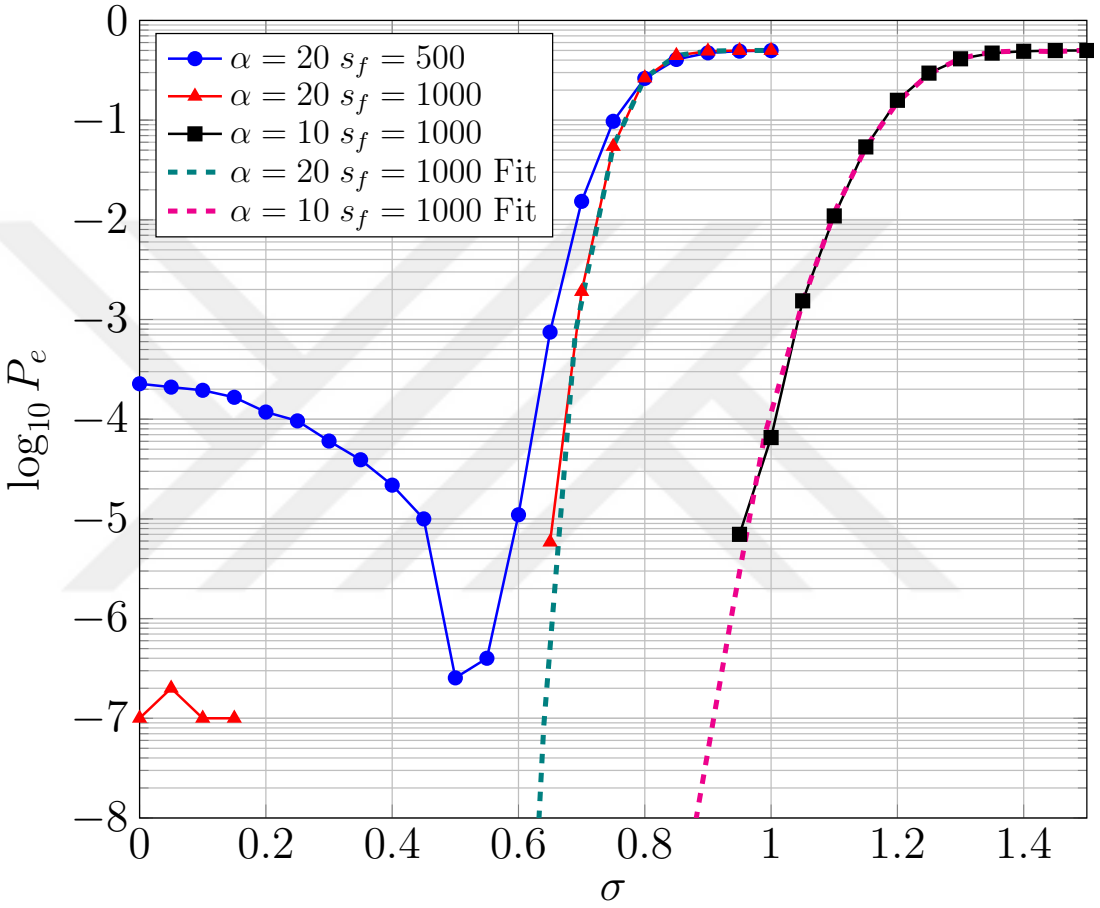

Figure 7.18 BER performances (plotted by solid lines with markers) obtained by numerical simulations and curves (plotted by dashed lines) fitted to the BER performances to represent the trends of the noise performances. BER performances in terms of noise level σ and probability of making a detection error P_e of the network in Figure 7.16 for $\epsilon = 3$ and different values of α and s_f.

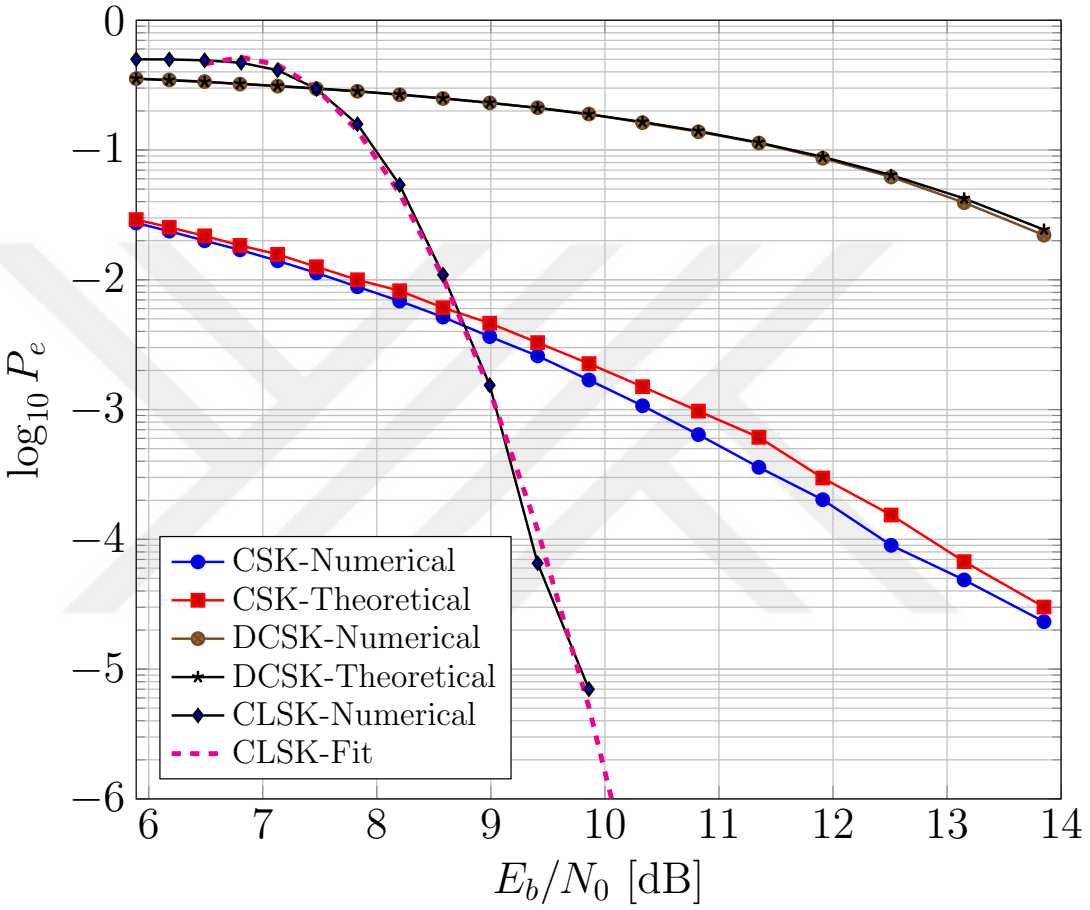

Figure 7.19 BER performances (plotted by solid lines with markers) obtained by numerical simulations and curves (plotted by dashed lines) fitted to the BER performances to represent the trends of the noise performances. BER performances of a single user CSK, DCSK, and CLSK scheme for $\epsilon = 3, \alpha = 10, s_f = 1000$ in terms of the ratio of average symbol energy to noise power spectral density E_b/N_0 versus the probability of making a detection error P_e.

numerically in Figure 7.18. Doubling the symbol duration, i.e., doubling the spreading factor s_f, lowers the probability of detection errors for the same amount of noise.

The formation and deformation of the cluster patterns of the network are controlled by the control strength α. It is the networks' not being able to deform a synchronized cluster pattern that causes the simulation errors. Hence, for excessive values of control strength, it becomes harder to deform a synchronized cluster pattern. Figure 7.18 shows the effect of the control strength on the noise performance. Decreasing the control strength from $\alpha = 20$ to $\alpha = 10$ improves the noise performance dramatically and removes the numerical errors for deficient noise levels.

$\chi = \sigma\alpha\epsilon$ is the noise's total strength in the equation's diffusion term in (7.32). For $\epsilon = 3, \gamma = 20$ and $\sigma \in [0, 1]$, the range of the total noise strength that drives the receiver nodes is $\chi = [0, 60]$. Compared to the amplitudes of the outputs of the receiver nodes, such noise amplitudes can drive the receiver nodes out of their chaotic dynamics and even make them unstable.

Figure 5.1 depicts the block diagram of a CSK scheme in which the signals $\hat{x}(t)$ and $\hat{y}(t)$ are *assumed* to be the *exact* replicas of $x(t)$ and $y(t)$, respectively, relying on the drive-response synchronization phenomenon. The noise performances of a CSK system are shown in Figure 7.19 where the simulation is performed by solving numerically the ordinary differential equations that result in chaotic signals $x(t)$ and $y(t)$. $r(t)$ is obtained by *directly adding* $n(t)$ to $s(t)$. Although the theoretical and numerical results are in good agreement in Figure 7.19, this approach does not reflect the physical reality that $s(t)$ is injected into the dynamics of the synchronization circuits in the receiver to generate the $\hat{x}(t)$ and $\hat{y}(t)$. Hence, the dynamics of the systems must be represented by stochastic differential equations (SDEs) instead of ODEs. We have seen in our simulations that in the case of SDEs used to model the system dynamics, the driven chaotic systems in the receiver go out of their chaotic regimes and become unstable, even for small values of $\sigma \approx 0.0083$. Hence, a CSK system is not always physically robust under noise. Figure 7.19 compares the

performance of the CLSK obtained by solving numerically the SDE in (7.32) to those of a single-user CSK and differential chaos shift keying (DCSK). The curve $\log_{10} P_e(x) = ax^2 + b^x + c$, where $a = -0.5354, b = 7.2835, c = -25.05$, plotted by a dashed line in Figure 7.19, can be fit to the numerical noise performance data of the CLSK. Even under unfair comparison, although the performance of the CLSK lags behind that of CSK for high noise levels, the CLSK outperforms DCSK and CSK for noise levels greater than $E_b/N_0 \approx 7.5$ dB and $E_b/N_0 \approx 8.75$ dB, respectively. Note, in particular, the drastic differences in the CSK, DCSK, and CLSK performances as E_b/N_0 increases.

CHAPTER EIGHT
CONCLUSION

In this thesis, we have proposed a new covert communication scheme based on cluster synchronization in networks of chaotic oscillators. In this scheme, the symbols are encoded to the spatio-temporal state of the network as synchronous cluster patterns. We have illustrated how existing cluster synchronization design techniques could construct the network to achieve different clusters for different values of control parameters. We ensure that the transmitted signals are always chaotic by construction, regardless of the transmitted symbol. The information is distributed over the network in contrast to its counterparts in which the information is modulated onto the transmitted signals. Therefore, the transmitted signals do not carry information directly. The transmitted information cannot be extracted without knowing which symbols are encoded into which cluster patterns, even if the channel is eavesdropped.

Unlike the available communication systems in which the modulation is in the time-frequency domain, the proposed method performs the modulation in the spatiotemporal domain, where the neighborhood of the nodes' neighborhood determines the detected symbol spatially.

The noise in the channel is assumed to be additive in the analysis of chaotic communication systems, and the signal flow is conventionally from the transmitter to the receiver. In the proposed approach, we consider that the noise directly affects the systems' dynamics at receiver subnetworks. The injection of noise directly into the dynamics of the receiver subnetworks causes the noise to be non-additive due to the diffusion terms in the stochastic model. Consequently, an analytical approach to determining the noise performance is not straightforward. Nevertheless, we have illustrated the typical performances of the specifically designed networks of chaotic systems and obtained the BERs of the proposed scheme via extensive simulations assuming binary signaling. The results indicate that the system is robust to noise at the channel and outperforms some well-known chaotic communication schemes for E_b/N_0 values greater than certain thresholds. The performance also depends on

channel filtering, transmission delay, jamming, and parameter mismatches between the nodes and the links. The basic stochastic model has to be extended beyond the presented to analyze how performance is affected in these conditions.

The proposed cluster shift keying scheme offers a pertinent way for covert signaling. The scheme can be combined with existing cryptographic techniques and error-correcting codes to provide an additional layer of protection against eavesdropping on a physical level.

Finally, the thesis combines the chaotic network construction and communication techniques, providing a new application for chaotic systems.

The study can be extended further to answer the following open questions.

1. An essential limitation of the approach is that the number of achievable cluster patterns determines the symbol capacity, which depends on the network graph's topological symmetries. Determining all the symmetries in the graph of a network with complex topology can be quite involved, which leads us to use networks with regular topologies. However, more flexible network design methods (Fan et al., 2023; Gambuzza et al., 2020) having no dependency on topological symmetries can be used to overcome this limitation. One important direction of further research is to determine the symbol capacity of large networks to allow M-ary communication with large M. On the other hand, as the number of nodes in the network increases, additional concerns affecting the communication performance may arise. For example, an increased number of nodes results in delays in the synchronization practically, resulting in detection errors or reduced bit rates in the system.

2. We have used the conditions that guarantee asymptotic synchronization in which the synchronization errors decay to zero as time approaches infinity. However, the detection done in finite symbol duration may result in detection errors. Finite-time synchronization techniques can overcome such errors and improve the noise performance further (Liu & Chen, 2016; Yu et al., 2021).

3. Additionally, the required communication bandwidth is proportional to the number of links in the channel. Hence, the links connecting the transmitter and the receiver subnetwork should be minimized for more efficient bandwidth use. On the other hand, the required number of links in the channel may not be decreased as desired in the case of M-ary communication because of the constraints on the network topology imposed by synchronization requirements. However, this is a relatively small price in exchange for the covertness.

4. The design of a reliable detector to detect whether a given cluster is synchronized constitutes a crucial part of the study since the detector's performance directly affects the overall performance of the communication system. Studies on synchronization detection from available data are rare in the literature and generally establish criteria for offline data (Liu et al., 2014; Tokuda & Herzel, 2005; Allefeld & Bialonski, 2007). As such, these criteria appear inadequate for synchronization detection in a real-time system. The energies of error signals in the clusters exceeding a particular threshold within one symbol duration can be associated with desynchronization, and the opposite case can be associated with synchronization. A synchronization detector based on the energies of the error signals between the nodes has been designed in this study. The results showed that this detector may suffer from numerical errors for symbol detection. Thus, detectors based on more reliable measures, such as mutual information from information theory or maximum Lyapunov exponents from nonlinear systems theory, can be among the further research of the study.

5. The claim that the data being sent is not decipherable by any third party in case the signals transmitted through the channel are known has been justified. For this purpose, the spectrograms of the signals on the channel have been computed. It has been observed from the spectrograms that there is no apparent correlation between the signals on the channel and the data being sent. However, the proposed system must be checked thoroughly against known cryptologic attacks.

6. The only non-ideality of the channel has been the additive white Gaussian noise.

Investigation of other channel non-idealities such as noise other than additive white Gaussian noise, delay, or filtering are among the further research of this study.

REFERENCES

Abarbanel, H. D. I. (1996). *Analysis of Observed Chaotic Data*. Institute for Nonlinear Science, New York, U.S.A: Springer New York, ISBN 978-0-387-98372-1.

Abel, A., & Schwarz, W. (2002). Chaos communications - Principles, schemes, and system analysis. *Proceedings of the IEEE*, *90*(5), 691–710.

Allefeld, C., & Bialonski, S. (2007). Detecting synchronization clusters in multivariate time series via coarse-graining of Markov chains. *Physical Review E - Statistical, Nonlinear, and Soft Matter Physics*. 0707.2479.

Amigó, J. M. (2009). Chaos-Based Cryptography. In *Intelligent Computing Based on Chaos*, vol. 184, 291–313, Berlin, Heidelberg: Springer Berlin Heidelberg, ISBN 9783540959717.

Belykh, I., Belykh, V., & Hasler, M. (2006). Generalized connection graph method for synchronization in asymmetrical networks. *Physica D: Nonlinear Phenomena*, *224*(1-2), 42–51.

Belykh, I., Belykh, V., Nevidin, K., & Hasler, M. (2003). Persistent clusters in lattices of coupled nonidentical chaotic systems. *Chaos*, *13*(1), 165–178.

Belykh, V. N., Belykh, I. V., & Hasler, M. (2000). Hierarchy and stability of partially synchronous oscillations of diffusively coupled dynamical systems. *Physical Review E*, *62*(5), 6332–6345.

Bhatia, R. (2013). *Matrix analysis*, vol. 169. Springer Science & Business Media.

Bohme, F., & Schwarz, W. (1986). The Chaotizer-Dechaotizer-Channel. *IEEE Transactions on Circuits and Systems I: Fundamental Theory and Applications*, *43*(7), 596–599.

Cai, X., Xu, W., Hong, S., Wang, L., & Zhang, L. (2021). General carrier index aided dual-mode differential chaos shift keying with full mapping: Design and optimization. *IEEE Transactions on Vehicular Technology*, *70*(11), 11665–11677.

Cai, X., Xu, W., Zhang, R., & Wang, L. (2019). A multilevel code shifted differential chaos shift keying system with M-ary modulation. *IEEE Transactions on Circuits and Systems II: Express Briefs*, *66*(8), 1451–1455.

Chen, G. (2014). Pinning control and synchronization on complex dynamical networks. *International Journal of Control, Automation and Systems*, *12*(2), 221–230.

Chen, L., Chai, Y., Wu, R., Sun, J., & Ma, T. (2012). Cluster synchronization in fractional-order complex dynamical networks. *Physics Letters, Section A: General, Atomic and Solid State Physics*, *376*(35), 2381–2388.

Chen, T., Liu, X., & Lu, W. (2007). Pinning complex networks by a single controller. *IEEE Transactions on Circuits and Systems I: Regular Papers*, *54*(6), 1317–1326.

Christine, J., Näslund, M., Mattson, J., & Smeets, B. (2015). Cryptography in an all encrypted world. *Ericsson Technology Review*, *92*(10), 1–13.

Chua, L. (1997). Impulsive stabilization for control and synchronization of chaotic systems: theory and application to secure communication. *IEEE Transactions on Circuits and Systems I: Fundamental Theory and Applications*, *44*(10), 976–988.

Cook, C. E. (1983). *Spread-spectrum communications*. U.S.A.: IEEE Press, ISBN 0879421703.

Cuomo, K. M., & Oppenheim, A. V. (1993). Circuit implementation of synchronized chaos with applications to communications. *Physical Review Letters*, *71*(1), 65–68.

Dachselt, F., Kelber, K., & Schwarz, W. (1997). Chaotic coding and cryptoanalysis. In *IEEE International Symposium on Circuits and Systems,*, 1061–1064, ISBN 078033583X.

Dachselt, F., & Schwarz, W. (2001). Chaos and cryptography. *IEEE Transactions on Circuits and Systems I: Fundamental Theory and Applications*, *48*(12), 1498–1509.

Fan, H., Wang, Y., & Wang, X. (2023). Eigenvector-based analysis of cluster synchronization in general complex networks of coupled chaotic oscillators. *Frontiers of Physics*, *18*(4), 45302.

Feldmann, U., Hasler, M., & Schwarz, W. (1996). Communication by chaotic signals: The inverse system approach. *International journal of circuit theory and applications*, *24*(5), 551–579.

Fu, C., Deng, Z., Huang, L., & Wang, X. (2013). Topological control of synchronous patterns in systems of networked chaotic oscillators. *Physical Review E - Statistical, Nonlinear, and Soft Matter Physics*, *87*(3).

Fu, C., Lin, W., Huang, L., & Wang, X. (2014). Synchronization transition in networked chaotic oscillators: The viewpoint from partial synchronization. *Physical Review E - Statistical, Nonlinear, and Soft Matter Physics*, *89*(5), 1–11.

Gambuzza, L. V., Frasca, M., Sorrentino, F., Pecora, L. M., & Boccaletti, S. (2020). Controlling symmetries and clustered dynamics of complex networks. *IEEE Transactions on Network Science and Engineering*, *8*(1), 282–293.

Gambuzza, L. V., Frasca, M., Sorrentino, F., Pecora, L. M., & Boccaletti, S. (2021). Controlling Symmetries and Clustered Dynamics of Complex Networks. *IEEE Transactions on Network Science and Engineering*, *8*(1), 282–293. 2011.11122.

Geist, K., Parlitz, U., & Lauterborn, W. (1990). Comparison of Different Methods for Computing Lyapunov Exponents. *Progress of Theoretical Physics*, *83*(5), 875–893.

Herceg, M., Vranjes, D., Kaddoum, G., & Soujeri, E. (2018). Commutation code index dcsk modulation technique for high-data-rate communication systems. *IEEE Transactions on Circuits and Systems II: Express Briefs*, *65*, 1954–1958.

Hillier, D., Günel, S., Suykens, J. A., & Vandewalle, J. (2006). Learning partial synchronization regimes with imposed qualitative behavior on an array of chua's oscillators. In *Proc. Int. Symp. Nonlinear Theory and its Applications (NOLTA)*, 983.

Huang, L., Chen, Q., Lai, Y. C., & Pecora, L. M. (2009). Generic behavior of master-stability functions in coupled nonlinear dynamical systems. *Physical Review E - Statistical, Nonlinear, and Soft Matter Physics*, *80*(3), 036204.

Jalan, S., & Singh, A. (2014). Cluster Synchronization in Multiplex Networks. *arXiv preprint arXiv:1412.5261*, *30002*, 6. 1412.5261.

Kennedy, M. P., & Hasler, M. (1993). Chaos Shift Keying: Modulation and Demodulation of a Chaotic Carrier Using Self-Synchronizing Chua's Circuits. *IEEE Transactions on Circuits and Systems II: Analog and Digital Signal Processing*, *40*(10), 634–642.

Khanra, P., Ghosh, S., Alfaro-Bittner, K., Kundu, P., Boccaletti, S., Hens, C., & Pal, P. (2022). Identifying symmetries and predicting cluster synchronization in complex networks. *Chaos, Solitons & Fractals*, *155*, 111703. 2102.06957.

Kocarev, L. (2001). Chaos-Based Cryptography: A Brief Overview. *Circuits and Systems Magazine, IEEE*, *1*(3), 6–21.

Kolumban, G., Vizvki, B., Schwarz, W., & Abel, A. (1996). Differential chaos shift keying : A robust coding for chaotic communication. In *Nonlinear Dynamics of Electronic Systems*, 87–92.

Li, W., Liu, Z., & Miao, J. (2009). Pinning synchronization of a general complex dynamical network. *2009 Chinese Control and Decision Conference, CCDC 2009*, *44*, 3340–3344.

Lin, W., Fan, H., Wang, Y., Ying, H., & Wang, X. (2016a). Controlling synchronous patterns in complex networks. *Physical Review E*, *93*(4), 1–13. 1511.00892.

Lin, W., Li, H., Ying, H., & Wang, X. (2016b). Inducing isolated-desynchronization states in complex network of coupled chaotic oscillators. *Physical Review E*, *94*(6), 1–9.

Liu, H., Wang, X., & Tan, G. (2014). Adaptive cluster synchronization of directed complex networks with time delays. *PLoS ONE*, *9*(4), 1–8.

Liu, X., & Chen, T. (2011). Cluster synchronization in directed networks via intermittent pinning control. *IEEE Transactions on Neural Networks*, *22*(7), 1009–1020.

Liu, X., & Chen, T. (2016). Finite-time and fixed-time cluster synchronization with or without pinning control. *IEEE transactions on cybernetics*, *48*(1), 240–252.

Lü, J., Yu, X., & Chen, G. (2004). Chaos synchronization of general complex dynamical networks. *Physica A: Statistical Mechanics and its Applications*, *334*(1-2), 281–302.

Lu, W., Liu, B., & Chen, T. (2010). Cluster synchronization in networks of coupled nonidentical dynamical systems. *Chaos*, *20*.

Lu, Y., Miao, M., Wang, L., & Xu, W. (2020). A Multilevel Code-Shifted Differential Chaos Shift Keying System with Reference Diversity. *IEEE Transactions on Circuits and Systems II: Express Briefs*, *67*(11), 2462–2466.

Ma, Q., & Lu, J. (2013). Cluster synchronization for directed complex dynamical networks via pinning control. *Neurocomputing*, *101*, 354–360.

Ma, Z., Liu, Z., & Zhang, G. (2006). A new method to realize cluster synchronization in connected chaotic networks. *Chaos*, *16*(2).

Parlitz, U., Chua, L. O., Kocarev, L., Halle, K. S., & Shang, A. (1992). Transmission of Digital Signals By Chaotic Synchronization. *International Journal of Bifurcation and Chaos*, *02*(04), 973–977.

Pecora, L., & Carroll, T. L. (1990). Synchronization in chaotic systems. *Physical Review Letters*, *64*(8), 821–824.

Pecora, L. M., & Carroll, T. L. (1998). Master stability functions for synchronized coupled systems. *Physical Review Letters*, *80*(10), 2109–2112. 0811.0649.

Pecora, L. M., & Carroll, T. L. (2015). Synchronization of chaotic systems. *Chaos*, *25*(9).

Pecora, L. M., Sorrentino, F., Hagerstrom, A. M., Murphy, T. E., & Roy, R. (2014). Cluster synchronization and isolated desynchronization in complex networks with symmetries. *Nature Communications*, *5*(May).

Porfiri, M., & di Bernardo, M. (2008). Criteria for global pinning-controllability of complex networks. *Automatica*, *44*(12), 3100–3106.

Rosenblum, M., Pikovsky, A., & Kurths, J. (1997). From Phase to Lag Synchronization in Coupled Chaotic Oscillators. *Physical Review Letters*, *78*(22), 4193–4196.

Rosenblum, M. G., Pikovsky, a. S., & Kurths, J. (1996). Phase synchronization of chaotic oscillators. *Physical Review Letters*, *76*(11), 1804–1807. 1108.6117.

Rößler, A. (2010). Runge–kutta methods for the strong approximation of solutions of stochastic differential equations. *SIAM Journal on Numerical Analysis*, *48*(3), 922–952.

Rulkov, N. F., Sushchik, M. M., Tsimring, L. S., & Abarbanel, H. D. I. (1995). Generalized synchronization of chaos in directionally coupled chaotic systems. *Physical Review E*, *51*(2), 980–994.

Schaub, M. T., O'Clery, N., Billeh, Y. N., Delvenne, J. C., Lambiotte, R., & Barahona, M. (2016). Graph partitions and cluster synchronization in networks of oscillators. *Chaos*, *26*(9). arXiv:1608.04283v2.

Sevilla-Escoboza, R., Sendiña-Nadal, I., Leyva, I., Gutiérrez, R., Buldú, J. M., & Boccaletti, S. (2016). Inter-layer synchronization in multiplex networks of identical layers. *Chaos*, *26*, from http://dx.doi.org/10.1063/1.4952967.

Shilnikov, L. P., Shilnikov, A. L., Turaev, D. V., & Chua, L. O. (1998). *Methods of qualitative theory in nonlinear dynamics (Part I)*. New Jersey, U.S.A.: World Scientific, ISBN 9810233825.

Simon, M. K. (2002). *Spread spectrum communications handbook*. New York,U.S.A: McGrawHill, ISBN 9780071382151.

Singh, A., Jalan, S., & Boccaletti, S. (2017). Interplay of delay and multiplexing: Impact on cluster synchronization. *Chaos*, *27*(4).

Sorrentino, F., Pecora, L. M., Hagerstrom, A. M., Murphy, T. E., & Roy, R. (2016). Complete characterization of the stability of cluster synchronization in complex dynamical networks. *Science Advances*, *2*(4). 1507.04381.

Strogatz, S. H. (2001). Exploring complex networks. *Nature*, *410*(6825), 268–276.

Tan, Y., Xu, W., Hu, W., & Wang, L. (2019). Efficient and robust M-ary differential chaos shift keying scheme with code index modulation. *IET Communications*, *13*(2), 232–242.

Tan, Y., Xu, W., Huang, T., & Wang, L. (2018). A Multilevel Code Shifted Differential Chaos Shift Keying Scheme with Code Index Modulation. *IEEE Transactions on Circuits and Systems II: Express Briefs*, *65*(11), 1743–1747.

Tokuda, I., & Herzel, H. (2005). Detecting synchronizations in an asymmetric vocal fold model from time series data. *Chaos*, *15*(1).

Tse, C., & Lau, F. (2003). Chaos-based digital communication systems. *Operating Principles, Analysis Methods and Performance Evaluation (Springer Verlag, Berlin, 2004)*.

Voss, H. (2000). Anticipating chaotic synchronization. *Physical Review E*, *61*(5), 5115–5119.

Wang, Y., Wang, L., Fan, H., & Wang, X. (2019). Cluster synchronization in networked nonidentical chaotic oscillators. *Chaos*, *29*(9), 093118.

Wiggins, S. (2003). *Introduction to applied nonlinear dynamical systems and chaos*, vol. 2. Springer Science & Business Media.

Wu, W., Zhou, W., & Chen, T. (2009). Cluster synchronization of linearly coupled complex networks under pinning control. *IEEE Transactions on Circuits and Systems I: Regular Papers*, *56*(4), 829–839.

Wu, X., & Lu, H. (2011). Cluster synchronization in the adaptive complex dynamical networks via a novel approach. *Physics Letters, Section A: General, Atomic and Solid State Physics*, *375*(14), 1559–1565.

Xiang-Jun, W. (2006). A new chaotic communication scheme based on adaptive synchronization. *Chaos*, *16*, 43118.

Yang, H., Tang, W. K., Chen, G., & Jiang, G. P. (2017). Multi-Carrier Chaos Shift Keying: System Design and Performance Analysis. *IEEE Transactions on Circuits and Systems I: Regular Papers*, *64*(8), 2182–2194.

Yu, T., Cao, J., & Huang, C. (2021). Finite-time cluster synchronization of coupled dynamical systems with impulsive effects. *Discrete & Continuous Dynamical Systems-Series B*, *26*(7).

Yu, W., Chen, G., & Lü, J. (2009). On pinning synchronization of complex dynamical networks. *Automatica*, *45*(2), 429–435.

Zhang, B., Xu, W., Wu, Y., & Wang, L. (2019). Design and Performance Analysis of Multilevel Code-Shifted M-Ary Differential Chaos Shift Keying System. *IEEE Transactions on Circuits and Systems II: Express Briefs*, *66*(7), 1257–1261.

Zhang, F. (2006). *The Schur complement and its applications*, vol. 4. Springer Science & Business Media.